Translational Control of Epidermal Growth Factor Receptor in Neurodegenerative Diseases

Daniel S. Smalley, BSc.

Thesis submitted to the University of Nottingham for the degree of Doctor of Philosophy

February 2017

Abstract

Epidermal Growth Factor Receptor (EGFR) is a key modulator of a number of cellular processes such as cell fate, proliferation, migration, and apoptosis. The *EGFR* gene is commonly amplified in a number of cancers and EGFR has been implicated in Alzheimer's disease, but its role in this context is uncertain. An internal ribosome entry site (IRES) within the EGFR 5'untranslated region (UTR) has been previously discovered which maintains EGFR expression under hypoxic conditions and has a high requirement for the eukaryotic initiation factor (eIF) 4A helicase. Requirement for eIF4A suggests that the structure of the IRES is important in its regulation. Identifying the structure of the IRES and the conditions in which the IRES is active could lead to the development of therapeutics targeting the IRES.

The IRES was investigated using bicistronic luciferase vectors. The IRES was found to be active in serum starvation stress but this activation appeared to be cell type specific, suggesting the IRES may depend upon tissue specific trans-acting factors for function. The EGFR IRES appears to not be modular, drawing similarities to the L-myc IRES. Structural data was used to improve prediction models for the IRES, which identified a structural switch that may be regulated by trans-acting factors. Targeting the IRES with anti-sense oligonucleotides proved moderately successful in inhibiting cap-independent translation. To study translational control in an environment closer to those found in Alzheimer's disease, a 3-dimensional model was developed. Although the

model was not spherical and could not be used as intended, it may be useful as a model for studying stress gradients. The effects that EGF stimulation has on translational regulation is poorly understood, yet may be a significant mediator in disease. RNA-seq allows for the quantification of the entire transcriptome for a given condition, whilst polysome profiling fractions mRNA based on ribosomal association. Through polysome profiling, RNA-seq and ontological clustering, it was revealed that EGF increased the translational efficiency of genes associated with Alzheimer's disease aetiology. Some of these genes were found to be directly connected to the production and oligomerisation of the amyloid beta protein.

Acknowledgements

I would first like to thank my supervisor, Keith Spriggs, for his immense patience, encouragement, and enthusiasm, which got me through this project. Thanks also go to Catherine Jopling and Cornelia de Moor for their generosity and advice, to Hilary Collins for always finding time to help me with the confocal microscope and to Graeme Thorn for the crash course in Linux.

I'd also like to thank the members of the MRC Toxicology Unit for their support during my time there, in particular David Piñeiro for the introduction to RNA structure analysis.

A thank you to all the members of the RNA Biology and Gene Regulation Group who have helped and supported me during my studies. Particular thanks go to Alex Hughes for showing me the ropes, Aimée Parsons for cat chats, Raj Gandhi, Hannah Parker and Jialiang Lin for the laughs, Kathyrn Williams for being my bioinformatics buddy and Heba Al-Masmoum for keeping me sane.

Finally, a thank you to my partner Samantha who has supported me all the way. I would not have started, or finished, this without all your encouragement.

Table of Contents

List of Figures

List of Tables

List of Abbreviations

2'OMe	2'OMethyl
4E-BP	eIF4E- binding protein
ACADS	Acyl-CoA dehydrogenease
AD	Alzheimer's disease
ALOX5AP	5-lipoxygenase activating protein
Apaf-1	apoptotic protease-activating factor 1
APP	Amyloid Precursor Protein
AQP4	aquaporin 4
Aβ	Amyloid Beta
BACE1	β-site APP-cleaving enzyme 1/β-secretase
Bcl-2	B-cell lymphoma 2
CAPN3	Calpain 3
CCL2	chemokine ligand 2
cDNA	Complementary DNA
CPEB	cytoplasmic polyadenylation element binding protein
CSFV	classical swine fever virus
CST3	cystatin C
dATP	Deoxyadenosine triphosphate
dCTP	Deoxycytidine triphosphate
dGTP	Deoxyguanosine triphosphate
DFX	Deforoxamine
DMEM	Dulbecco's modified eagle's medium
DMS	Dimethyl sulphide
DMSO	Dimethyl sulfoxide
DNA	Deoxyribonucleic acid
DNase	Deoxyribonuclease
dNTP	Deoxynucleoside triphosphate
DSE	Downstream sequence element
DTT	Dithiothreitol
DTTP	Deoxythymidine triphosphate
ECM	Extracellular matrix
EDTA	Ethylenediaminetetraacetic acid
eEF	Eukaryotic elongation factor
EGF	Epidermal growth factor
EGFR	Epidermal growth factor receptor
eIF	Eukaryotic initiation factor
eIF2-TC	eIF2- ternary complex
EMCV	Encephalomyocarditis virus
EOAD	Early onset Alzheimer's disease

ER	Endoplasmic reticulum
eRF	Eukaryotic release factor
FACS	Fluorescence-activated cell sorting
FAD	Familial Alzheimer's disease
FBS	Fetal bovine serum
FPKM	Fragments per kilobase of transcript per million mapped reads
FTD	Fronto-temporal dementia
G418	Geneticin Sulphate
GAP	GTPase activating protein
GDP	Guanosine diphosphate
GFP	Green fluorescent protein
GO	Gene ontology
GTP	Guanosine triphosphate
HCV	Hepatitis C virus
HDL	High density-like lipoprotein
HEPES	4-(2-hydroxyethyl)-1-piperazineethanesulfonic acid
HIF	Hypoxia induced factor
HIV1	Human immunodeficiency virus
hnRNP	Heterogeneous ribonucleoprotein particle
HS	Horse serum
icSHAPE	*In vivo* click selective 2'hydroxyl acylation analysed by primer extension
IL-18	Interleukin-18
IR	Insulin receptor
IRE	Iron response element
IRES	Internal ribosome entry site
IRP1	Iron response protein 1
IRP2	Iron response protein 2
ITAF	IRES trans-acting factor
KE	Kethoxal
LB	Lysogeny broth
LOAD	Late-onset Alzheimer's disease
LRP	Lipoprotein receptor related proteins
L-VGCC	L-type voltage gated calcium channels
MAPK	Mitogen activated protein kinase
miR	MicroRNA
MM	Multiple myeloma
MMP9	Matrix metallopeptidase 9
mRNA	Messenger RNA
mRNP	Messenger ribonucleoprotein

MTT	3-(4,5-dimethylthiazol-2-yl)-2,5-diphenyltetrazolium bromide
NHE	Na+/H+ exchange pumps
NMDA	N-methyl-D-aspartate
NMIA	N-methylisotoic anhydride
NSCLC	Non-small cell lung cancer
nt	Nucleotide
OD	Optical density
ORF	Open reading frame
PBS	Phosphate buffered saline
PEG	polyethylene glycol
PERK	protein kinase RNA-like endoplasmic reticulum kinase
PI3K	Phosphoinositide 3-kinase
PINK1	PTEN-induced putative kinase-1
PKC	Protein kinase C
PLEK	Pleckstrin
PNK	Polynucleotide kinase
Poly(A)	Polyadenylated
PTB	polypyrimidine tract-binding protein
RMB4	RNA-binding motif protein 4
RBP	RNA binding protein
RHA	RNA helicase A
RISC	RNA-induced silencing complex
RNA	Ribonuceic acid
RNase	Ribonuclease
rRNA	Ribosomal RNA
ROS	Reactive oxygen species
rNTP	Ribonucleoside triphosphate
RYR	Ryanodine receptor
SDS	Sodium dodecyl sulphate
SERCA	sarcoplasmic/endoplasmic reticulum Ca2+ ATPase
SH2	Sarc homology 2
SHAPE	Selective 2'hydroxyl acylation analysed by primer extension
SNARF-4F	Seminaphthorhodafluor-4F 5-(and-6)-carboxylic acid, acetoxymethyl ester, acetate
SREBP-1	sterol-regulatory-element-binding protein 1
TACE	Tumour necrosis factor-α-converting enzyme
TAE	Tris-acetate-EDTA buffer
Tau	Microtubule-associated protein tau
TBE	Tris/Borate/EDTA buffer
TCP80	Translational control protein 80

TEMED	Tetramethylethylenediamine
TNF	Tumour necrosis factor
ULA	Ultra-low attachment
uORF	Upstream open reading frame
UPR	Unfolded protein response
UTR	Untranslated region
UV	Ultra-violet light
VEGF	Vascular endothelial growth factor
XIAP	X-linked inhibitor of apoptosis protein
Yn Tract	Oligo-pyrimidine tract

1. Introduction

The epidermal growth factor receptor (EGFR) is an important mediator in a number of processes and in disease. Overexpression of EGFR is common in many cancers, yet genetic mutations account for a small proportion of cases. Translational control has been identified as a potential source of EGFR overexpression, thus studying the mechanisms which control its expression is valuable in the development of therapeutics.

1.1 Alzheimer's Disease

1.1.1 Amyloid Beta and Microtubule-Associated Protein Tau

The leading cause of dementia in the elderly, Alzheimer's disease (AD) is rapidly becoming one of the most damaging diseases of the 21st Century; one in eight over 65s suffer from the disease and it is the 6th most common cause of death (Alzheimer's 2015). It is estimated that by 2050 the incidence of AD will have reached a hundred million and that currently, in the US alone, the disease costs $180 billion a year. Yet despite these figures the cause(s) of Alzheimer's disease remains elusive, with treatments transient and palliative (Ferreira and Klein 2011). It is becoming apparent that, like cancer, AD may not have a single cause or even a common pathology; rather AD may be a collection of diseases with common symptoms, the most prevalent of which is memory loss (Ferreira and Klein 2011).

AD is a neurodegenerative disease that is characterised by the presence of protein plaques and neurofibrillary tangles within neuronal cells. These proteinaceous aggregations are primarily composed of the proteins amyloid beta

(Aβ) and MAPT, often referred to as 'tau' (Glenner and Wong 1984; Grundkeiqbal et al. 1986). Aβ is a small, ~4.5kDa peptide that can form insoluble fibrillar polymers.

Aβ is a product of the cleavage of APP, the membrane-bound Amyloid Precursor Protein, by two proteases: β-secretase (also known as β-site APP-cleaving enzyme 1 (BACE1)) and γ-secretase. Cleavage by α-secretase does not produce Aβ, cleaving within the fragment sequence and producing APPsα. APPsα is thought to be neuroprotective and be involved in synaptic plasticity (Hick et al. 2015). The α-secretase pathway is the predominant APP processing pathway and is the non-amyloidogenic pathway of APP processing. BACE1 is a type 1 membrane aspartic protease that cleaves at the Asp^{+1} residue of the Aβ sequence to form the N-terminus of Aβ (Vassar 2004). The two fragments of this cleavage are the C-terminal fragment C99, which remains membrane bound, and APPsβ, a secreted ectodomain (Hussain et al. 1999). A second cleavage event is required to create Aβ. This is performed by γ-secretase, a multi-subunit protease that cleaves C99, generating an AICD and Aβ (Edbauer et al. 2003). The cleavage is imprecise and this leads to Aβ variants, most notably $Aβ_{40}$ and $Aβ_{42}$ (Hardy 1997). APP processing is shown in figure 1.1. The subunits of γ-secretase have not been fully characterised but consists of at least presenilin, nicastrin, APH-1 and PEN-2 (Takasugi et al. 2003; Edbauer et al. 2003). BACE1 is highly active within neural tissue and is expressed highly in the brain (Vassar et al. 1999). The proportion of $Aβ_{42}$ to $Aβ_{40}$ formed is important as $Aβ_{42}$ is more prone to aggregation into oligomers and plaques. Whilst production of Aβ is a normal

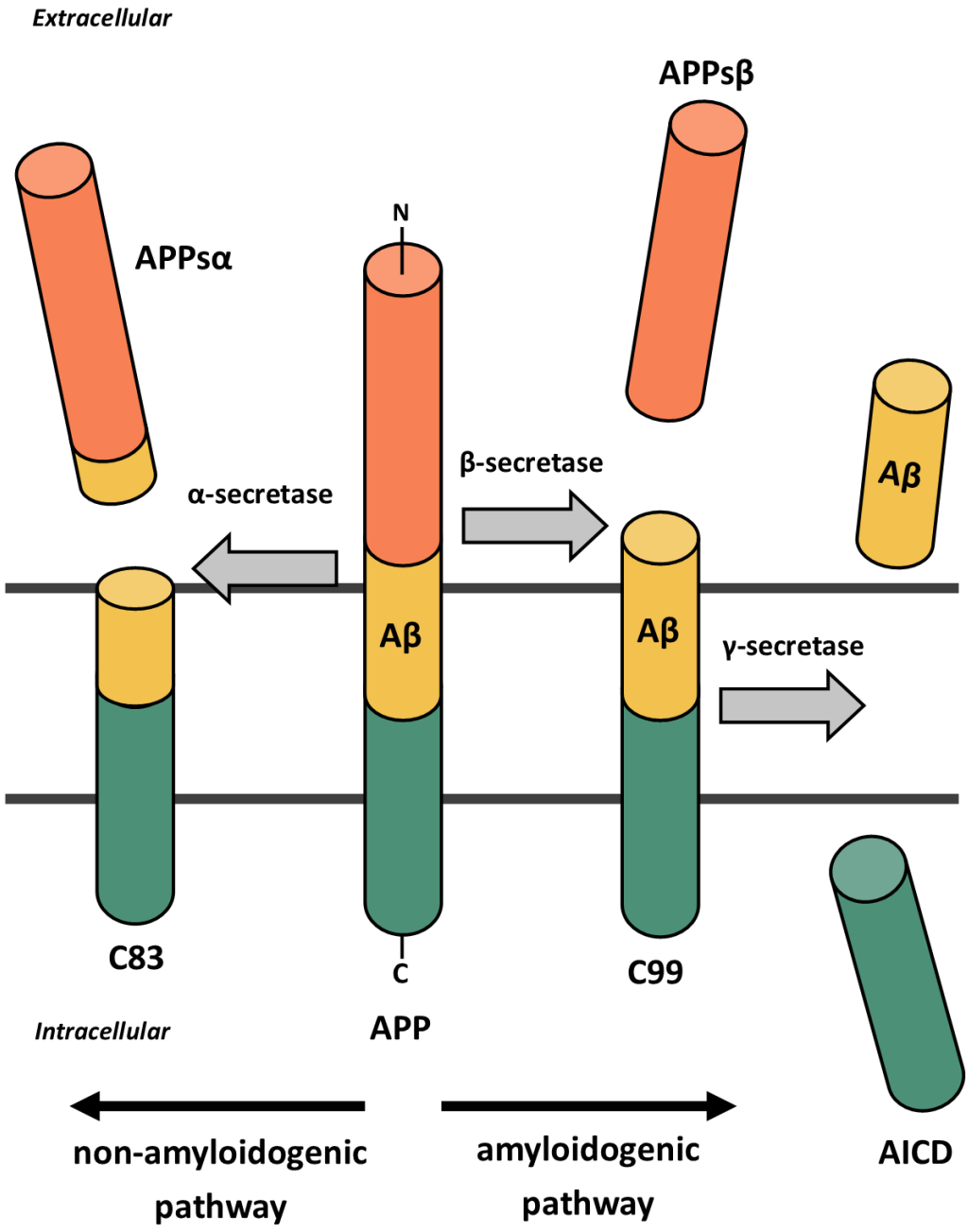

Figure 1.1 Amyloid Precursor Protein (APP) Processing by Secretases. In the non-amyloidogenic pathway, APP is cleaved by α-secretase to produce APPsα, a neuroprotective protein. Cleavage by β-secretase produces the membrane bound C99 fragment and a secreted APPsβ protein. Further cleavage of C99 by γ-secretase produces AICD and the amyloidogenic Aβ protein.

process, it is the overproduction of $A\beta_{42}$ which has been proposed to cause early-onset Alzheimer's disease. Production of Aβ is often portrayed as negative but its deletion from neuronal cells results in cell death, a characteristic unique to neuronal cells (Plant et al. 2003). Reintroduction of $A\beta_{40}$, restores cell survival, but the $A\beta_{25-35}$ fragment, which retains most of the toxic effects of $A\beta_{42}$, had little effect on survival. The mechanism by which $A\beta_{40}$ protects cells remains elusive, but may involve regulating K^+ channel expression (Yu 2003).

Tau is a microtubule binding protein that, in its hyperphosphorylated form, forms the core of neurofibrillary tangles in AD (Tolnay and Probst 1999). Although tangles and Aβ plaques are seen together in post-mortem examination of AD sufferers, the prevailing theory of AD development (until recently) largely ignores the possibility of tau tangles causing AD, and this for a number of reasons. Firstly, genetic studies on the early onset form of AD (EOAD), or familial Alzheimer's disease (FAD) due to its inherited, genetic basis, showed that mutations in the APP and presenilin 1 and 2 genes, that create the peptides of gamma secretase, caused EOAD through an increase in Aβ production (Goate et al. 1991). Secondly, mutations in tau do not cause AD but rather display a different form of dementia, fronto-temporal dementia (FTD) (Hutton et al. 1998). This is despite EOAD presenting the same histological profile as AD: plaques and tangles. This hypothesis, known as the Amyloid Cascade Hypothesis, links dementia to nerve cell death through the toxicity of large, insoluble amyloid fibrils. The hypothesis had great weight at its time of inception. The causative effect of the plaques drew parallels with other degenerative studies, such as Parkinson's and the prion diseases (Ferreira,

Vieira, and De Felice 2007). However, it is likely that late onset Alzheimer's disease (LOAD) is more complex and not monogenic and comparisons between LOAD and EOAD should only be used lightly in the understanding of LOAD. Often citing the failures of drugs developed for the cascade hypothesis, some studies suggest tau has a part to play in LOAD development in a 'dual-pathways hypothesis' (Small and Duff 2008). However, one of the leading hypotheses for the cause of AD is the oligomer hypothesis, which suggests that instead of large fibrillar aggregations of Aβ causing AD, it is the smaller soluble oligomers of Aβ that cause neuronal degeneration, with the plaques causing a secondary toxic effect (Ferreira and Klein 2011). Emerging in the 70s with the discovery that individuals with dementia showed considerable deterioration of dendritic projections (Scheibel et al. 1975), further advanced by plaque load correlating poorly with cognitive function (Terry, Katzman, and Bick 1994) and synaptic loss providing the best correlation with AD (Terry et al. 1991), the oligomer hypothesis proposes that loss of synaptic plasticity, rather than cell death, is the leading cause of senility. The oligomer hypothesis presents a molecular basis for AD. For example, Lambert et al showed that clusterin, a protein upregulated in AD and found within amyloid deposits, could promote the accumulation of soluble oligomers and that Aβ oligomers were neurotoxic; inhibiting synaptic plasticity and long-term potentiation without affecting baseline excitability (Lambert et al. 1998). This means that interference of signalling, rather than cellular degeneration, is the method through which Aβ oligomers causes memory loss. The conclusion of these data is that memory loss is caused by disruption of synaptic plasticity through the action of Aβ oligomers. The oligomer hypothesis is supported by recent findings that increased clusterin

levels are associated with higher levels of fibrillary Aβ (Thambisetty et al. 2010). The idea that interference of signalling pathways may be a cause of Alzheimer's has brought attention to receptors whose hyperactivity may lead to AD, including EGFR, which is activated by Aβ oligomers as discussed in section 1.4.4 (Wang et al. 2012).

1.1.2 Conditions and Risk Factors

There are a number of conditions which are thought to exacerbate Aβ production, deposition and oligomerisation. Inflammation is thought to be one of these. As part of the amyloid cascade hypothesis, it was once thought inflammation occurred after Aβ deposition (Hardy and Selkoe 2002). However in mild cognitive impairment, a state which often precedes AD, cytokine levels are elevated (Brosseron et al. 2014). Diseases of the CNS are almost always involves the immune system; traditional neuroinflammatory diseases such as encephalitis or multiple sclerosis invoke T and B lymphocytes as part of the adaptive immune response (Griffin et al. 1992; Hoglund and Maghazachi 2014). Activation of the adaptive immune system has not been observed in AD, rather the inflammatory reaction seen in AD is consistent with the activation of the innate immune system, produced by CNS-resident immune cells such as microglia and reactive astrocytes (Prinz et al. 2011). Anti-inflammatory drugs have been found to reduce the risk of AD when taken over a long period, before onset of the disease (Etminan, Gill, and Samii 2003), yet inflammation as a promoter of AD progression is not as clear as it would seem. Some inflammatory

mechanisms are thought to clear Aβ. One hypothesis suggests that binding of Aβ to microglial receptors activates the cells, causing expression of chemokines, growth factors and complement anaphylatoxins, causing proliferation or chemotaxis of microglial cells (Rogers et al. 2002). This position is strengthened by the presence of large numbers of reactive glial cells surrounding Aβ plaques (Thomason et al. 2013) Complement opsonins bind Aβ and allow Aβ to be taken into microglia by phagocytosis leading to clearance of Aβ (Frackowiak et al. 1992). In AD brains it is clear that this clearance is unsuccessful, but there is evidence that plaques are resolved over the course of the disease, suggesting that clearance does occur but not at a sufficiently rapid rate to combat aggregation (Hyman, Marzloff, and Arriagada 1993).

High levels of metal ions, such as iron, copper and zinc can mediate the aggregation of Aβ (Atwood et al. 1998; Bush et al. 1994; Atwood et al. 2000). Zinc binds readily to Aβ at neutral pH to form insoluble aggregates, whilst copper induces a soluble conformation (Miura et al. 2000). The mildly acidic pH often found in AD brains as well as the presence of inflammation, alters copper's effect on Aβ, inducing the formation of insoluble aggregates (Atwood et al. 1998). Dysregulation of metal ions can also induce oxidative stress through reactions between O_2 and metal ions, creating more ROS (Maynard et al. 2005). There is overwhelming evidence that oxidative stress occurs in AD (Christen 2000). High levels of ROS causes tissue damage and lipid peroxidation, a prominent feature in degeneration (Markesbery 1997).

The calcium hypothesis of AD suggests that calcium plays a key role in the deficits in memory and learning (Khachaturian 1987). As neurons age,

inefficient energy metabolism and accumulation of oxidative stress compromises their ability to tightly regulate Ca^{2+} gradients across the plasma and endoplasmic reticulum membrane, leading to sustained increases in Ca^{2+} concentration in the cytoplasm (Toescu and Verkhratsky 2007). Dysregulation of calcium signalling has been documented in mouse models of the disease, as well as in high risk groups of humans (Larson et al. 1999; Leissring et al. 2000). In the former, the disruption is found months before extracellular Aβ is detected (Etcheberrigaray et al. 1998).

Much evidence points to an increase in stored Ca^{2+} in the endoplasmic reticulum (ER). A polymorphism of the calcium channel CALHM1, a protein found on both the plasma membrane and ER membrane which acts as leak channel, increases the risk of AD and has a reduced Ca^{2+} permeability, resulting in higher stored calcium in the ER (Dreses-Werringloer et al. 2008; Cui et al. 2010). Presenilins also disrupt intracellular Ca^{2+} homeostasis through IP_3-gated channels, causing enhanced filling of calcium stores (Stutzmann et al. 2004). Further, $A\beta_{40}$ and $A\beta_{42}$ can form Ca^{2+} permeable pores in the plasma membrane leading to increased Ca^{2+} concentration in the cytoplasm (Arispe, Rojas, and Pollard 1993). There is conflicting data as to whether increased calcium levels affect Aβ production. Early reports suggest treatment of embryonic kidney cells that express APP with the Ca^{2+} ionophore A23187 increased Aβ production (Querfurth and Selkoe 1994). The same was true following caffeine treatment – caffeine is a known agonist of the ryanodine receptor, suggesting that influx of Ca^{2+} and release from stores enhanced Aβ production (Querfurth et al. 1997). Yet treatment with thapsigargin, irreversibly blocking the sarco/endoplasmic

reticulum Ca^{2+} -ATPASE (SERCA) activity and increasing intracellular Ca^{2+}, actually reduced Aβ production (Buxbaum et al. 1994). Contrary to this is the demonstration that influx of calcium through L-type voltage gated calcium channels (L-VGCC) increased $A\beta_{42}$ production in neurons, but release of calcium from the ER was not adequate for Aβ production (Pierrot et al. 2004). The general consensus appears to be that calcium dysregulation is important in AD progression, but the exact mechanisms and effects of calcium fluxes need further examination.

A number of genetic polymorphisms have been discovered which increase the risk of developing AD. The most recognised of these is the ApoE4 allele. ApoE4 homozygotes have between an 8 and 12-fold increase in the risk of developing Alzheimer's disease (Strittmatter et al. 1993; Roses 1996). The incidence of at least one copy of the ApoE4 allele in AD patients is 40-65%. ApoE is a 299aa glycoprotein, expressed in several organs with the highest expression in the liver followed by the brain. Astrocytes and microglia are the main expressors in the brain, although neurons do produce ApoE under certain conditions (Grehan, Tse, and Taylor 2001; Xu et al. 2006). ApoE is involved in endocytosis of lipoprotein particles. In the brain, ApoE is mainly associated with high density-like lipoprotein (HDL) particles and is the predominant apolipoprotein of HDL in the central nervous system, which deliver cholesterol to neurons (Fagan et al. 1999; Pitas et al. 1987). The released cholesterol support synaptogenesis and maintenance of synaptic connections (Pfrieger 2003). The three most common polymorphisms of ApoE are ApoE2, E3 and E4, and differ by just one or two amino acid residues. Yet these differences profoundly alter the structure and

function (Mahley, Weisgraber, and Huang 2006). For instance the more common ApoE3 is involved in clearance of Aβ, but ApoE4 does not clear Aβ effectively (Yang et al. 1999), yet ApoE4 still accumulates in plaques (Strittmatter et al. 1993). It is generally accepted that any of the ApoE polymorphisms aid in clearance of Aβ, but two studies have shown that removing one copy of either ApoE3 or E4 isoforms actually reduces Aβ levels (Kim et al. 2011; Bien-Ly et al. 2012). Yet the majority of published literature suggests ApoE aids in clearance either through proteolytic degradation (Jiang et al. 2008) or more recently by indirect means through receptor binding (Zlokovic et al. 2010; Verghese et al. 2013). As to why the E4 allele is so prevalent despite its association with disease, it can be noted that ApoE4 is positively associated with higher levels of vitamin D (Huebbe et al. 2011).

Aside from age and genetic risk factors, metabolic disorders such as diabetes, obesity and hypertension significantly increases the risk of developing AD. Type II diabetes has been reported as increasing the risk of dementia by 50-150% (Li, Song, and Leng 2015). The exact mechanism by which type II diabetes modulates AD progression is not known, but it has been proposed that insulin resistance or deficiency is involved. Insulin abnormalities have been observed in AD (de la Monte and Wands 2005), and defective insulin signalling results in increased Aβ production, through an impairment of the non-amyloidogenic pathway of APP processing and increased expression of BACE1, (Wang et al. 2010) Insulin deficiency in mice reduces insulin receptor (IR) phosphorylation, downregulating the insulin/IR signalling pathway but enhances the activity of GSK3 and JNK, both of which have been found to be involved in the formation

of Aβ plaques, hyperphosphorylated tau and neuronal cell death (Kim et al. 2006; Savage et al. 2002; Liu et al. 2003). Dysregulation of insulin signalling also increased Aβ fibrillisation and aggregation through an increase in GM1 ganglioside levels and clustering (Yamamoto et al. 2012). The GM1 ganglioside is a glycosphingolipid found on the outer layer of the plasma membrane and is involved in cell viability and differentiation, but appears to also serve as a scaffold for Aβ fibrillisation (Yamamoto et al. 2007). Type II diabetes may also contribute to the inflammatory environment that is a hallmark of AD; chronic inflammation through overexpression of TNF-α, is often seen in diabetes and in obesity (Hotamisligil, Shargill, and Spiegelman 1993). Oxidative stress is also found in both diseases, and in diabetes is often the reason for diabetes-induced vascular disease. Oxidative stress in diabetes may be caused by hyperglycaemic activation of nuclear factor- kappaB and NH2-terminal Jun kinases/stress-activated protein kinases pathways (Evans et al. 2002). High cholesterol levels are often seen in obesity and diabetes. Cholesterol has been shown to increase Aβ synthesis through APP processing by modulating gamma secretase activity (Cole et al. 2005).

1.1.3 Translational Control in Alzheimer's Disease

There is emerging evidence that mRNA translation is highly important in the disease process of many neurological diseases. The mRNA of both APP and MAPT, which codes for the 'tau' protein contain internal ribosome entry sites (IRESs), which may allow these proteins to be expressed during the conditions found in Alzheimer's disease (Beaudoin, Poirel, and Krushel 2008; Veo and Krushel 2009). Other mechanisms of translational control have also been

observed in AD related genes. An iron response element (IRE) can be found in the 5'UTR of APP, whilst BACE1 mRNA contains three upstream open reading frames (uORFs) (Cho et al. 2010) (O'Connor et al. 2008). Targeting these mechanisms could lead to potential therapeutics. These mechanisms are discussed further in section 1.2.5.

1.2 Translation

Proteins are fundamental to life, performing a vast array of functions within cells, ranging from metabolic catalysis, replication of DNA, cell signalling and providing extracellular and intracellular structures. Proteins account for approximately 44% of a human's dry weight (Davidson 1973). The production of this biomass requires a huge amount of resources to in terms of the translational machinery, ribosomes, tRNAs, and enzymes. This highly intensive system requires a high degree of control and regulation, not only to ensure resources are not wasted, but also that the cell responds to its environment appropriately. Translation is the process by which a messenger RNA (mRNA) transcript is read and used as a template for the synthesis of a specific protein. Translation consists of three separate stages; initiation, elongation and termination. Initiation describes the formation of the 80S ribosome on an mRNA transcript, aided by RNA-binding proteins, at the 'start codon', usually AUG, (Kozak 1983) which is base-paired to the anticodon of the Met-$tRNA_i$ in the peptidyl (P) site of the ribosome (Cigan, Feng, and Donahue 1988). Initiation requires the small, 40S and large, 60S ribosomal subunits and at least 12 eukaryotic initiation factors, (eIFs) each of which contributes to one or more of the steps of initiation. Elongation is the extension of the polypeptide chain, where the 80S ribosome reads the mRNA sequence and allows the base pairing of mRNA codons with their complementary anticodon on the amino acid bearing tRNA molecule followed by peptide bind formation between the two (Moore PB, Steiz, 2003). Elongation continues until a stop codon in the mRNA is

reached, where upon the ribosome detaches from the mRNA transcript, a process called termination.

1.2.1 Structure and Processing of mRNA

mRNA is an inherently unstable form of RNA; its quick degradation is key to regulation of expression, as one mRNA transcript can, in theory, be translated by hundreds of ribosomes indefinitely unless the mRNA is removed. Eukaryotic mRNA is more stable than prokaryotic mRNA due to the addition of several modifications to eukaryotic mRNA structure. Prokaryotic mRNA is translatable as soon as it is transcribed (Yanofsky 1981), unlike eukaryotic mRNA, which must be processed through modifications, splicing and editing as well as transported out of the nucleus. Due to the absence of a nuclear compartment, prokaryotic mRNA is transcribed in the cytoplasm, thus ribosomes can begin translating the mRNA whilst the latter part of it is still being transcribed (Yanofsky 1981). The co-transcriptional nature of prokaryotic mRNA endows the ability to be translated quickly, but degraded fast due to an unstable structure. This mechanism probably aids the bacteria to respond to its environment quickly (Sarkar 1997).

Before leaving the nucleus, pre-mRNA must first be processed in order to become mature mRNA. Two modifications to eukaryotic pre-mRNA protect the mRNA from the exonucleases that degrade it, as well as being essential to the mechanism of translation initiation. These modifications are the 5' cap and the 3' polyadenylated (Poly(A)) tail. The 5' terminal cap consists of a guanine nucleotide, methylated at the 7 position bound to the next nucleotide by an

unusual triphosphate 5’ to 5’ linkage (Reddy et al. 1974). First described in 1974, (Reddy et al. 1974) the 5’ cap is added to the pre-mRNA by the action of three enzymes and guanosine triphosphate (GTP), as reviewed in: (Banerjee 1980). In short, the 5’ terminal phosphate of the RNA is removed by hydrolysis, through the action of a phosphatase, leaving a diphosphate group (Venkatesan, Gershowitz, and Moss 1980). Guanylyl transferase catalyses the addition of GTP to the diphosphate, with GTP losing two of its phosphates in the process, creating the triphosphate, 5’ to 5’ linkage (Martin and Moss 1975). Methyl transferase methylates the nitrogen at the 7 position in the ring of guanine, finishing the cap structure (Martin and Moss 1975). The 5’ cap plays an essential role in the vast majority of translation initiation, as will be discussed later. The 3’ Poly(A) tail is also essential to cap-dependent translation initiation. To add the tail, part of the pre-mRNA transcript is cleaved. Most pre-mRNAs have the cleavage site between a heavily conserved AAUAAA hexamer, which acts as a polyadenylation signal sequence, and a GU- or U- rich downstream sequence element (DSE) (Proudfoot, Furger, and Dye 2002). The pre-mRNA is also spliced, a process where sequences are removed from pre-mRNA, termed introns, and the remaining sequences (exons) are ligated together. Once processed, mature mRNA is transported out of the nucleus through nuclear pores. mRNA is packaged into messenger ribonucleoprotein (mRNP) complexes which bind to export receptors. The receptors dock at the nuclear pore where the mRNA is translocated to the cytoplasm (Rodriguez, Dargemont, and Stutz 2004)

The cytoplasmic mRNA transcript does not merely code for its corresponding protein, it also contains regions that regulate the translation of the downstream coding sequence. The 5' untranslated region (UTR) holds various features that are important in the translation and regulation of initiation of the mRNA. These include upstream open reading frames (uORFs), Internal ribosome entry sites (IRESes), sites for RNA binding proteins (RBPs) and secondary structures (Araujo et al. 2012). The average length of the 5' UTR is between 100 and 200 nucleotides (nt) across many species whilst the 3' UTR has more striking differences, ranging between 200 and 1000nts (Pesole et al. 2001). In vertebrates, the length of the 5' UTR appears to be dependent on the function of the protein; growth and transcription factors, protooncogenes and growth factor receptors all tend to have longer UTRs (Davuluri et al. 2000). This allows for the regulation of translation of these genes through the structures mentioned previously. mRNAs that have longer UTRs tend to be translated through the cap-dependent mechanism requiring eIF4E to bind the cap. Secondary structures positioned close to the cap are very effective at inhibiting translation. Hairpins close to the cap require free energy of -30 kcal/mol if they are to block the helicase activity of eIF4A (Kozak 1989). Those structures further downstream require free energy stronger than -50 kcal/mol to block translation (Pickering and Willis 2005). Overexpression of eIF4A and its enhancer eIF4B can partially overcome this barrier (Rozen et al. 1990).

1.2.2 Initiation of Translation

Translation is a cyclical process, with ribosomes and eIFs recycled from previous rounds of translation through the dissociation of the subunits and ribosomal binding proteins. The 40S and 60S ribosome subunits are prevented from reassociation by the reattachment of eIF3 to the 40S ribosome (Freienstein and Blobel 1975), along with eIF1 and eIF1a (Kolupaeva et al. 2005), occluding the 60S binding site. The 40S ribosome is then ready for the next stage – the binding of the ternary complex. The process of translation initiation is shown in figure 1.2.

The formation of the ternary complex, an assembly of eIF2, GTP and the initiator tRNA, Met-$tRNA_i$, marks the beginning of a new round of translation initiation. The ternary complex delivers the $tRNA_i$ to the 40S subunit. eIF2 is a heterotrimeric GTP dependent protein (Lloyd et al. 1980), and must bind GTP in order for the initiator tRNA, Met-$tRNA_i$ to bind (Walton and Gill 1975). GTP binding causes conformational change in the switch 1 and 2 regions of eIF2 that allows Met-$tRNA_i$ to bind with a much greater affinity (Yatime et al. 2006). After formation, the ternary complex joins up with the 40S-eIF1,eIF1A and eIF3 complex to create the 43 pre-initiation complex (Fig1.2).

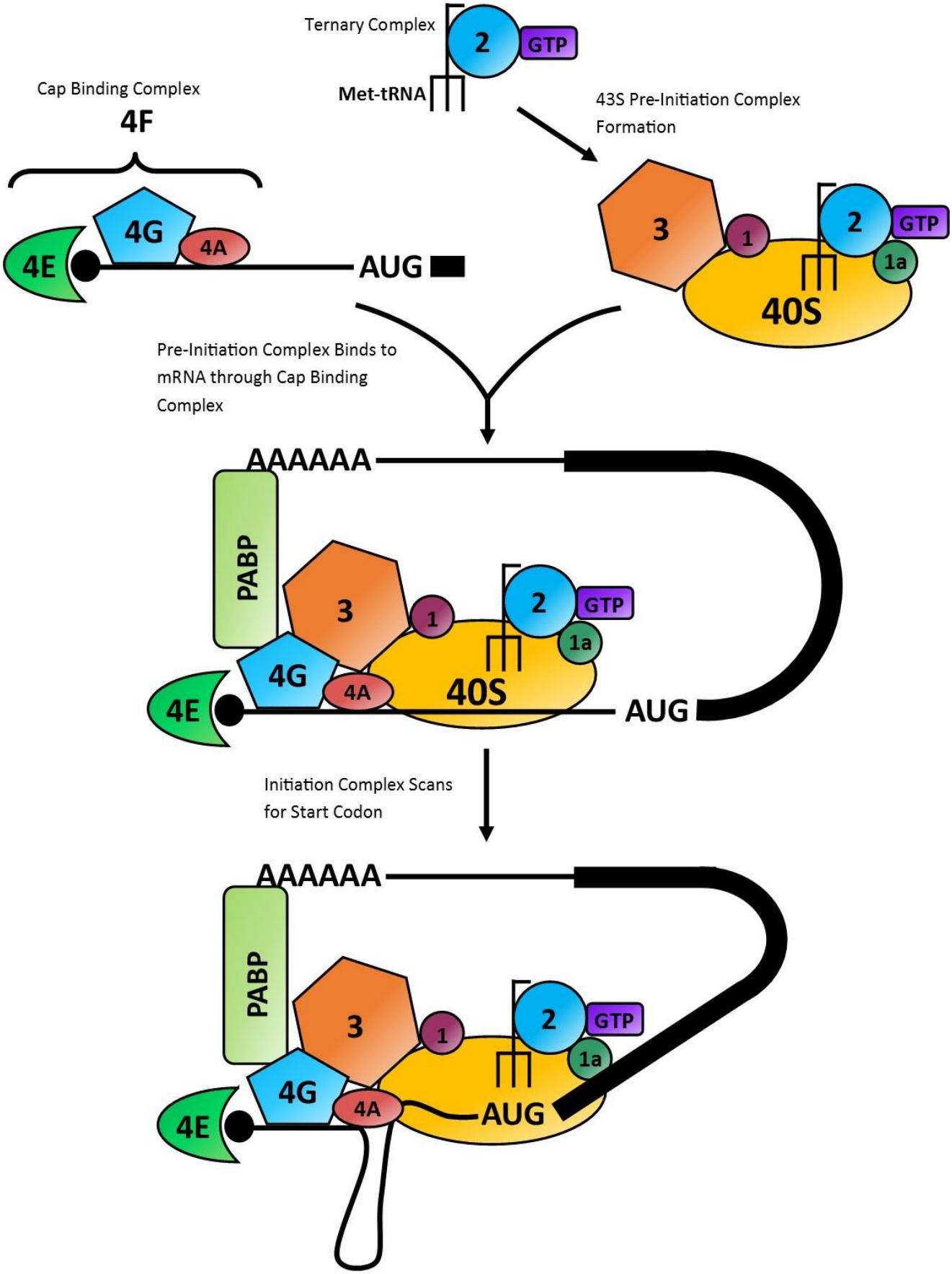

Figure 1.2. Cap-dependent Translation Initiation in Eukaryotes. The 43 S pre-initiation complex is formed by the binding of eIFs 1, 1A, 3 and the ternary complex. The cap-binding complex forms at the 5' cap of the mRNA through eIF4E binding. The 43S pre-initiation complex binds to the cap complex and begins scanning the mRNA for the start codon, where the initiator tRNA of the ternary complex binds, and translation can occur. eIFs are represented by number only.

The formation of the 43S pre-initiation complex is essentially governed by the local levels of the ternary complex, composed of the eukaryotic initiation factor eIF2, bound with GTP and the initiator Met-tRNA$_i$ as eIF1, eIF1A and eIF3 are already bound to the 40S ribosomal subunit following recycling. eIF3 stimulates eIF2 binding to the 40S subunit (Benne and Hershey 1978), making contacts with eIF3, eIF1 and eIF1A (Chaudhuri, Chowdhury, and Maitra 1999; Thomas et al. 1980). eIF5B is also thought to be recruited along with eIF2 and is important later in initiation, where it causes the dissociation of eIF1, eIF3 and eIF2-GDP from the 40S subunit to aid 60S binding (Thomas et al. 1980).

The 5' m7G cap provides the platform for the formation of the cap-binding complex required for cap-dependent translation initiation. The cap binding complex, often denoted as eIF4F, is composed of 3 initiation factors; eIF4A, eIF4G and eIF4E. There are three known isoforms of eIF4A, eIF4A1, II and III. Whilst 4AI and 4AII share ~90% sequence homology (Nielsen and Trachsel 1988), they are differentially expressed in tissues and are thought to have different cellular functions (Galicia-Vazquez et al. 2012). eIF4E binds to the cap to recruit the 43S complex to the mRNA (Sonenberg et al. 1978) (Fig 1.2). The 43S complex is intrinsically capable of attaching to unstructured 5' UTRs (Pestova and Kolupaeva 2002) but as almost all cellular mRNA feature secondary structures within their 5' UTRs, binding of eIF4F is generally essential for the 43S complex to bind to the mRNA. The eIF4A subunit unwinds the region close to the 5' cap, preparing it for the 43S complex (Ray et al. 1985). The mRNA binds to a cleft within the 40S subunit that closes through a non-covalent 'latch' formed by two of the helices of 18srRNA (Spahn et al. 2004).

After the 43S complex has bound to mRNA it proceeds to scan along the mRNA, downstream of the cap (Fig 2.3). Scanning requires unwinding of secondary structure to allow the passage of the ribosome. The helicase eIF4A is essential in this role, but eIF4G is also required for scanning even the weakest of secondary structures (Pestova and Kolupaeva 2002). eIF4G stabilises the closed, active conformation of eIF4A (Oberer, Marintchev, and Wagner 2005). The central role of eIF4A as the primary factor in the unwinding of secondary structure is highlighted by its requirement being directly proportional to the secondary structure present in the 5' UTR (Svitkin et al. 2001).

1.2.3 Codon Recognition, 48S Ribosome Formation & Subunit Joining

The 43S complex scans downstream until it reaches the first initiation codon (AUG) in a good context, consensus GCC(A/G)CCAUGG (Kozak 2001). The fidelity of initiation is maintained in part by eIF1, allowing the 43S complex to discriminate against non-AUG triplets and those that are within a poor context, as well as those within eight nucleotides of the 5' end of the mRNA (Pestova and Kolupaeva 2002). eIF1 can also dissociate ribosomal complexes that assemble at non-AUG triplets in its absence (Pestova, Borukhov, and Hellen 1998). eIF1A and eIF1 cooperate to promote an 'open' conformation of the 43S complex that allow mRNA to flow easily through the complex as it scans the mRNA (Passmore et al. 2007). Upon encountering an initiator codon, a 'closed' conformation is formed. This is achieved through the tightening of eIF1A-40S interaction and displacement of eIF1 from near the P-site (Maag, Algire, and Lorsch 2006; Lomakin et al. 2003). Codon-anticodon interactions form, giving rise to the 48S complex. After recognition, the ribosome commits to initiation at

that codon. This step also dissociates factors that occlude the surface that the 60S subunit binds to, namely eIF1, 1A, 2 and 3. This is mediated by eIF5, which binds to the β subunit of eIF2 and induces GTPase activity of the γ subunit when eIF2 is complexed with Met-tRNA$_i$ bound to the 40S subunit, acting as a classical GTPase activating protein (GAP) (Das and Maitra 2001). Consequently, the affinity of eIF2 for Met-tRNA$_i$ is reduced and causes the dissociation of eIF2-GDP and other eIFs from the 40S subunit facilitated by eIF5B and the 60S ribosomal subunit. eIF5B is a ribosome dependent GTPase that mediates ribosomal subunit joining, possibly by burying solvent-accessible surfaces on both subunits in a similar fashion to its prokaryotic homologue IF2 (Allen et al. 2005). Hydrolysis of eIF5B's GTP is not necessary for subunit joining but is required for release of eIF5B from the ribosome (Pestova et al. 2000).

1.2.4 Elongation, Termination and Recycling

Just two eukaryotic elongation factors (eEFs) assist in elongation, eEF1 and eEF2. eEF1 binds aminoacyl-tRNA in a GTP-dependent manner, directing the tRNA into the 'A' site of the ribosome where the next mRNA codon sits. The recognition of the codon by tRNA triggers hydrolysis of GTP, releasing eEF1 and allowing the tRNA into the A site. From here peptide bonds form between the residues. eEF2 aids in the translocation of the ribosome to the next codon (Dever and Green 2012) . Elongation continues until a stop codon (UAA, UGA or UAG) is encountered. Termination is catalysed by eukaryotic release factors (eRFs). eRF1 is responsible for recognition of the stop codon whilst eRF3 aids

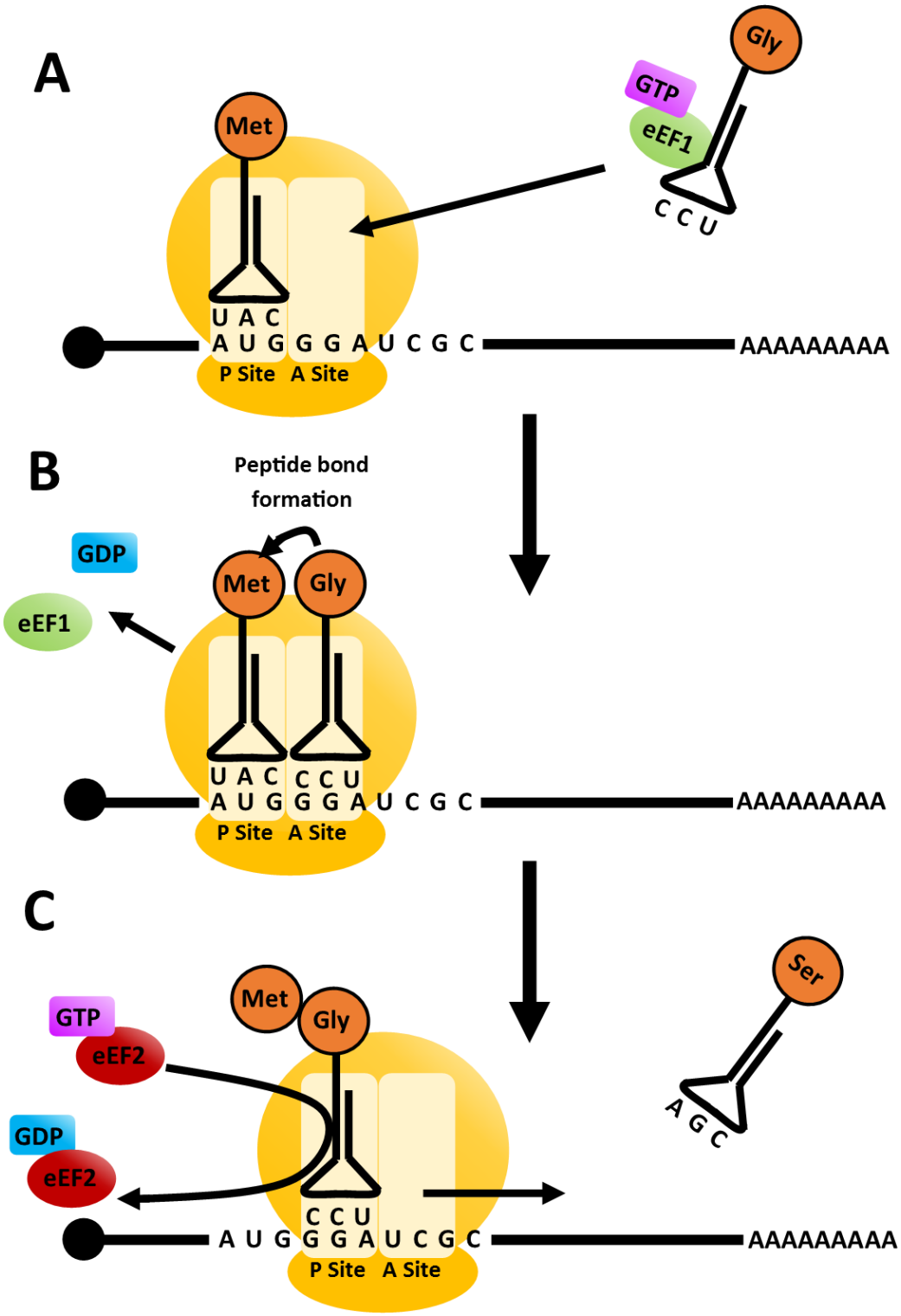

Figure 1.3 Translation Elongation in Eukaryotes. (A) eEF1 bound to tRNA and GTP directs the tRNA into the 'A 'site of the ribosome. **(B)** Recognition of the codon triggers GTP hydrolysis and release of eEF1. Peptide bonds form between the amino acids held in the 'P' and 'A' sites. **(C)** eEF2 aids in the translocation of the ribosome along the mRNA, clearing the 'A' site for the next tRNA

in peptide release. Ribosomes are recycled from previous rounds of translation through the dissociation of the subunits and ribosomal binding proteins. The 40S and 60S ribosomes are prevented from re-association by the reattachment of eIF3 to the 40S ribosome (Freienstein and Blobel 1975), along with eIF1 and eIF1a (Kolupaeva et al. 2005), occluding the 60S binding site. The 40S ribosome is then ready to bind another ternary complex and start another round of translation.

1.2.5 Translational Control

Gene expression is regulated at many levels; from chromatin remodelling in the nucleus to controlling the production of proteins at the translational level in the cytoplasm. Translational control is fundamental to a cell's ability to adapt to a changing environment in response to signalling molecules and stress conditions as it allows rapid increases in the cellular concentration of proteins. Control in translation is mostly exerted at the initiation stage, although regulation does occur at elongation through phosphorylation of eEF2, affecting the rate of protein synthesis (Yan et al. 2003). Control of initiation can occur through elements in the mRNA itself, or through controlling the activity of initiation factors.

1.2.5.1 Regulation of Initiation Factors

An important category of translational control involves the eIFs. Both eIF2 and eIF4E are regulated. When bound to GDP, phosphorylation of the alpha subunit of eIF2 causes it to act as an inhibitor of eIF2B, binding tightly and abrogating its guanine nucleotide exchange factor activity (Kimball 1999). This results in a

drop in eIF2-GTP-TC available for initiation, leading most mRNA translation to cease. Four mammalian kinases are known which phosphorylate eIF2α, EIF2AK1, PKR, PERK and GCN2. These kinases are activated under certain cellular stress in order to inhibit translation. PERK is activated under ER stress, GCN2 is active under amino acid starvation, whilst PKR is important in the anti-viral response, being activated by double stranded RNA of more than 40 bps. The cap binding eIF4E is subject to regulation by phosphorylation too, in response to certain stimuli. The MAP kinase-activated protein kinase (MNK1) binds to and phosphorylates eIF4G when eIF4G contacts eIF4E. Phosphorylated eIF4E has a greater affinity for the 5' cap, contributing to a more stable eIF4F complex. Regulation of this process comes from the eIF4E binding proteins (4E-BPs) which, when under-phosphorylated, bind to eIF4E, interfering with its ability to bind to eIF4G. Hyperphosphorylation of 4E-BPs occurs in response to growth factors or hormones.

1.2.5.2 Upstream Open Reading Frames

Upstream open reading frames (uORF) are open reading frames within the 5'UTR which can regulate expression by allowing ribosomes to begin scanning upstream of the primary ORF, downregulating expression. It is reported that around 50% of mammalian genes contain at least one short uORF, upstream of the main protein coding ORF (Calvo, Pagliarini, and Mootha 2009). A proportion of ribosomes scanning these mRNAs will begin translation at the uORF first before resuming translation at the ORF, reinitiating at these sites. Termination at these sites is thought to proceed as

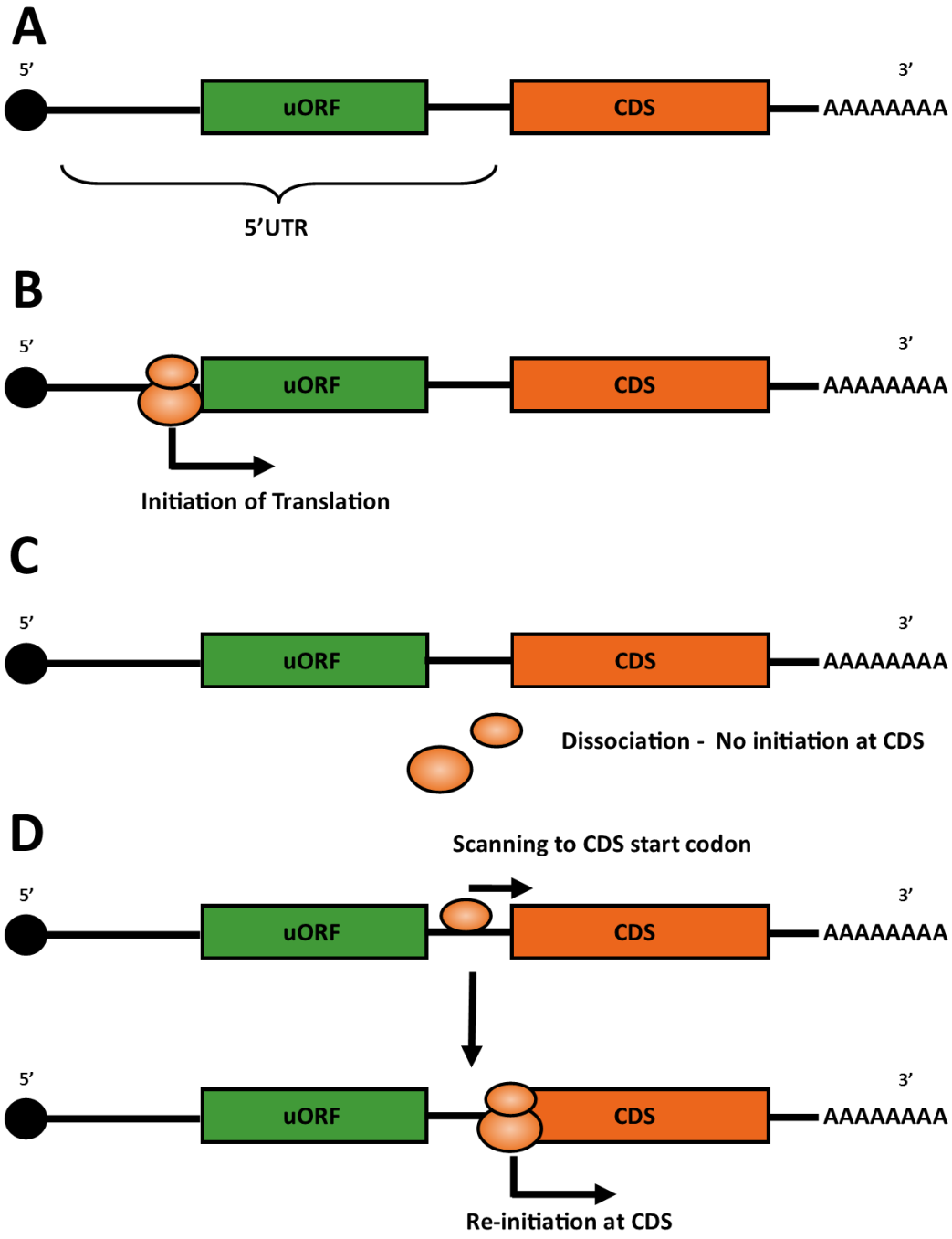

Figure 1.4. An Example of Upstream Open Reading Frames (uORF) in Eukaryotes. **(A)** Schematic of an mRNA containing an uORF. The uORF is situated within the 5'UTR. **(B)** The scanning ribosome initiates translation at the start codon of the uORF rather than the main coding region (CDS). **(C)** The ribosome may dissociate after the stop codon of the uORF and does not translate the protein from the CDS. **(D)** In some cases, the ribosome continues to scan after translating from the uORF and can reinitiate at the start codon of the CDS.

normal, with the 60S ribosomal subunit dissociating, but some 40S subunits remain attached to the mRNA and continue to scan (Hinnebusch 2005). The 40S subunit in this state is incapable of reinitiating, as it no longer has an eIF2-ternary complex (eIF2-TC) bound to it, but a new eIF2-TC may re-join during the scanning phase. Thus genes that contain uORFs can be regulated through the availability of eIF2-TC. The length rather than the sequence of uORFs appears to be the crucial factor in the efficiency of rescanning and reinitiation, with efficiency decreasing rapidly with increasing uORF length (Luukkonen, Tan, and Schwartz 1995). Secondary structure has a similar effect (Kozak 2001), suggesting it is the time the 40S subunit takes to reach the ORF that is important. This leads to the idea that the retention of some eIFs is necessary for rescanning, in particular eIF4G that binds to the mRNA as well as eIF3 to promote eIF2 binding.

1.2.5.3 RNA Binding Proteins

RNA-binding proteins (RBPs) allow sequence specific regulation of translation. Translation can be inhibited or enhanced through RBP binding to specific sequences. RBPs can bind to the 5’ UTR or 3’ UTR. 3’ UTR binding proteins are much more common than 5’ UTR RBPs, the only example of which are those that bind to an iron response element (IRE). IREs allow the regulation of genes in response to alterations in cellular iron concentration and are most commonly associated with ferritin mRNAs, although IREs have been found in other mRNAs. Under low iron concentration, iron response protein 1 (IRP1) and IRP2 bind to the IRE and this RNA-protein interaction prevents the 43S complex from loading on to the mRNA (Gray and Hentze 1994). The location of the IRE is

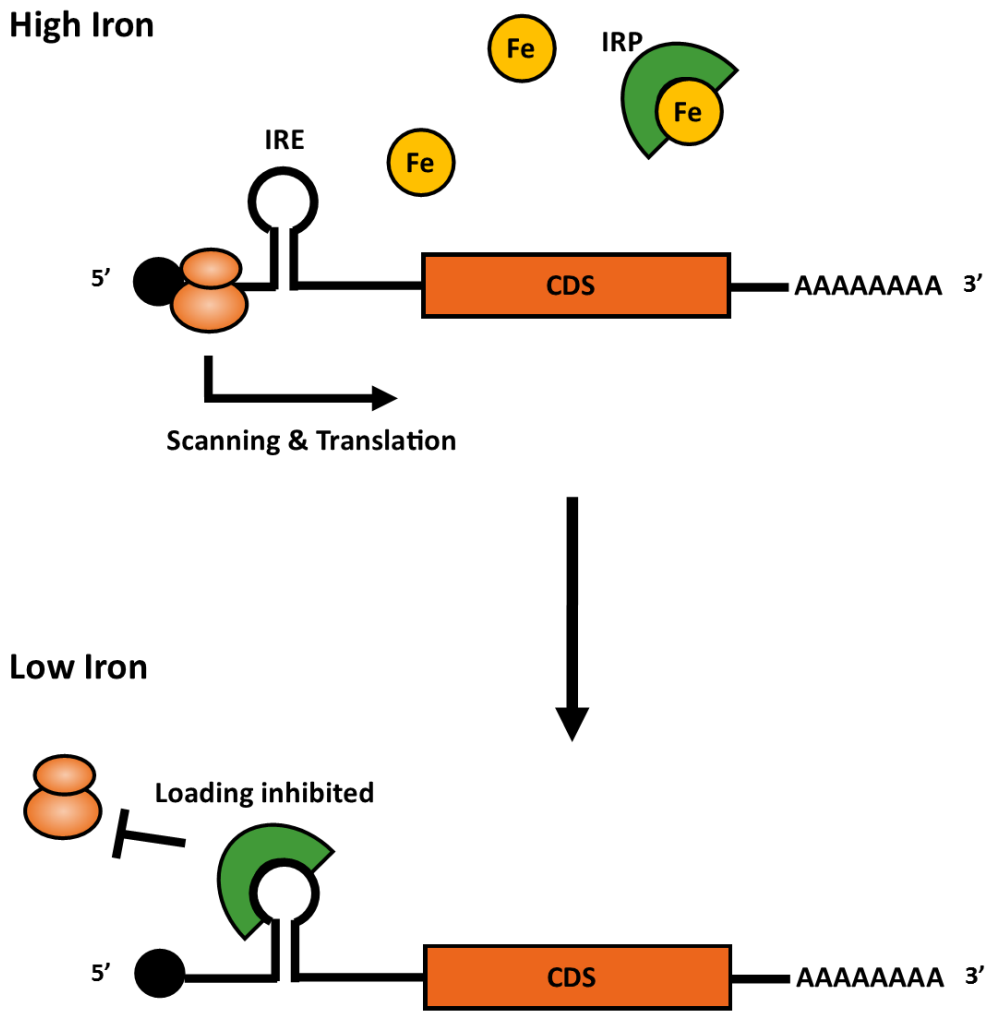

Figure 1.5. An Example of an Iron Response Element (IRE). Under high iron concentrations the iron response binding proteins (IRP) are inhibited by iron, allowing the ribosome to scan through to the start codon. Under low iron concentrations the IRPs bind to the IRE in the 5'UTR, occluding the region proximal to the 5' cap preventing the formation of the 43S pre-initiation complex and thus the mRNA is not translated.

important (in ferritin it is within 40 nucleotides of the cap), as inhibition is removed if the IRE is further away from the cap, suggesting that if loading is not inhibited, the 43S complex can displace the protein as it scans the mRNA (Goossen et al. 1990). At the 3' end, a majority of RNPs inhibit initiation through the development of a closed loop structure. The RBP binds to the 3' end but also makes contacts with an intermediate bridging protein. This bridging protein

binds to one of the cap binding proteins to cause the mRNA to loop in a structure unfavourable to initiation. An example of this is the cytoplasmic polyadenylation element binding protein (CPEB) which binds to its binding site in the 3'UTR. CPEB recruits Maskin that interacts with eIF4E, competing with eIF4G, inhibiting the formation of the cap binding complex and thus translation (Stebbins-Boaz et al. 1999).

1.2.5.4 microRNAs

MicroRNAs (miRs) are oligonucleotides, usually around 22 bp long which bind to specific mRNAs, targeting them for degradation or silencing them. It is estimated that that approximately half of the human genome is controlled by miRs. miRs are imperfectly complementary to regions of a particular mRNA and once bound, recruit an RNA-induced silencing complex (RISC). miRs are generated from double stranded (ds)RNA by a Dicer complex, which cleaves the miR from their precursor dsRNA. Argonaute proteins, a family of endonucleases, displace the miR from their complementary strand. The argonaute protein and RISC complex remain attached to the miR until it binds an mRNA, where the RISC complex directs the silencing of the target transcript. Silencing can occur through cleavage, de-capping or repression, by reducing mRNA stability through deadenylation (Guo et al. 2010). Curiously, it has been reported that miRs can also stimulate the activity of some mRNAs (Vasudevan, Tong, and Steitz 2007).

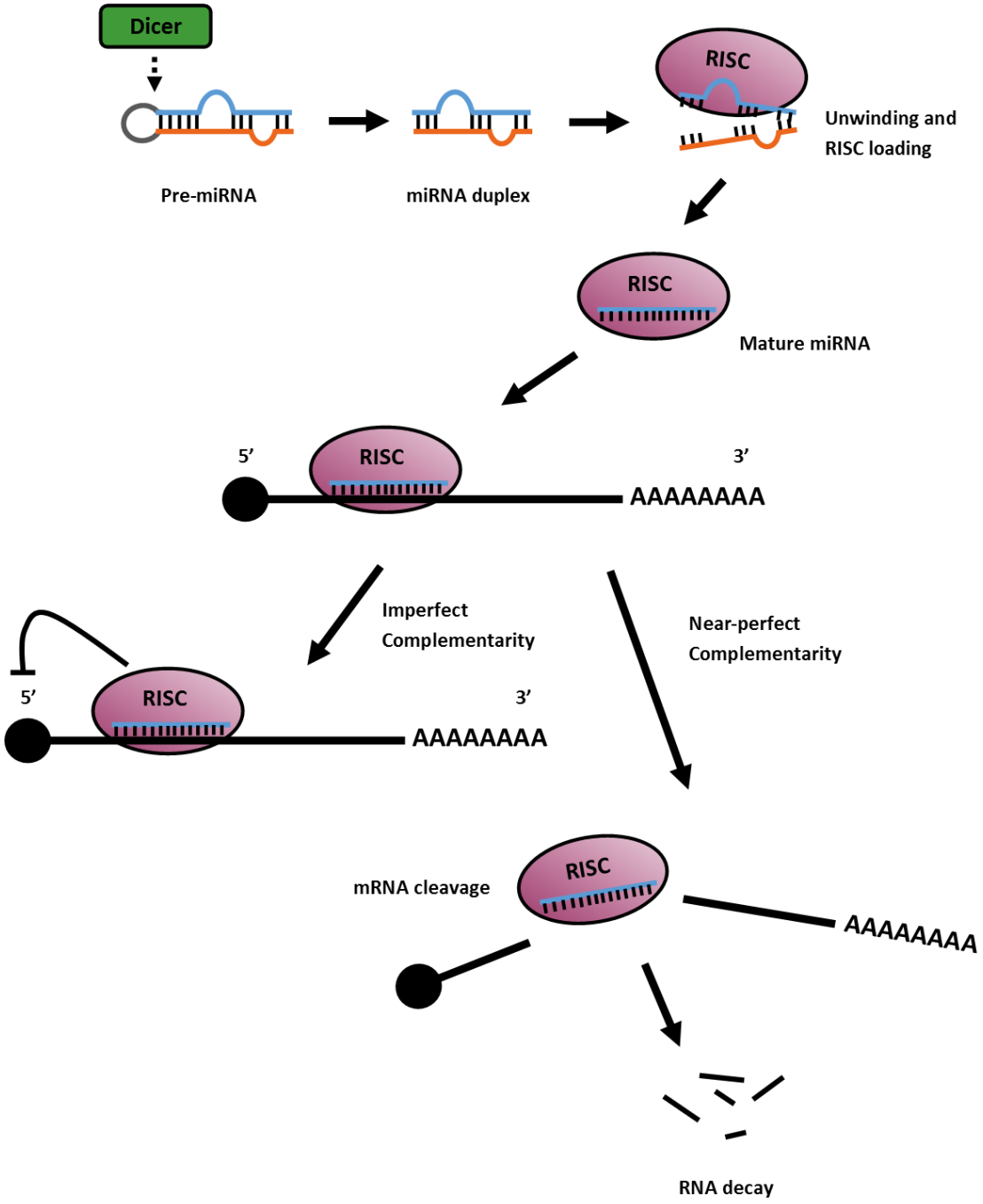

Figure 1.6. miRNA Biogenesis. Pre-miRNA, transported out of the nucleus are cleaved by Dicer into a miRNA duplex. The RISC complex displaces the two strands, binding to one of them to create mature miRNA. The miRNA binds to mRNAs with imperfect or near perfect complementarity, allowing the argonaute endonuclease to cleave the mRNA or, if the mRNA is imperfectly complementary, the RISC complexes directs the mRNA to be silenced.

1.3 Cap Independent Translation Initiation

Internal ribosome entry sites (IRESs) allow an alternative route for translation initiation that is independent of the cap, permitting formation of the 80S ribosome without the cap binding mechanism. First identified in viruses and subsequently found to be present in a number of cellular mRNAs, it is thought that translation via IRESs may have evolved before cap-dependent translation initiation, later becoming a secondary, regulatory form of translation in eukaryotes (Hernandez 2008). IRESs were first discovered in viral mRNAs. The presence of a 5' –terminal pU residue instead of a cap structure in poliovirus mRNA (Nomoto, Lee, and Wimmer 1976) generated the hypothesis that the poliovirus mRNA translation must occur in a cap-independent manner. The 5'UTRs of poliovirus and encephalomyocarditis virus (EMCV) were capable of allowing translation of the downstream cistron in a bicistronic mRNA construct, thus suggesting ribosomes are recruited directly to a region in the 5'UTR which allowed translation to occur (Pelletier and Sonenberg 1988; Jang et al. 1988). Viruses utilise IRESs in manipulation of the host's translational machinery. Cellular IRESs appear to be used as a form of translational control. There is some contention over the existence of cellular IRESs (Kozak 2005), but the consensus among researchers is that eukaryotic IRESs represent an important part in regulation of expression (Schneider et al. 2001; Hellen and Sarnow 2001). When cap-dependent translation is inhibited a subset of mRNAs continues to be translated through cap-independent mechanisms (Johannes et al. 1999). Many stresses increase the phosphorylation of eIF2α thus leading to a reduction in eIF2-GTP, reducing translation rates by inhibiting the formation of

the 43S pre-initiation complex. Low ternary complex levels directly increase the activity of a number of IRES containing mRNAs including vascular endothelial growth factor (VEGF), c-myc and cat-1 mRNAs (Fernandez, Bode, et al. 2002; Fernandez, Yaman, et al. 2002; Gerlitz, Jagus, and Elroy-Stein 2002). This seems paradoxical as ternary complex is required to recruit the initiator tRNA to the 40S ribosome in order to bind to the start codon before 80S ribosome formation. Some hypothesise that IRES-containing mRNAs can attract ternary complex more efficiently, thus remaining active under low concentrations, but a 2012 study suggests that eIF5B takes the role of eIF2 in recruiting and positioning the initiator tRNA at the start codon of the X-linked inhibitor of apoptosis protein (XIAP) IRES (Thakor and Holcik 2012), in a similar manner as seen in the classical swine fever virus (CSFV) and hepatitis C virus (HCV) IRESs (Pestova et al. 2008; Terenin et al. 2008). Yet this is not seen in other IRESs so is unlikely to be a universal mechanism (Thakor and Holcik 2012).

Many of the cellular IRESs reported are found in mRNAs coding for factors involved in growth, differentiation and apoptosis (Stoneley and Willis 2004). Translation through IRESs is important in these conditions, when global translation is inhibited some proteins are required to be produced to drive the cell's decision/fate in the particular scenario. For instance in apoptosis both the pro apoptotic proteins apoptotic protease-activating factor 1 (Apaf-1) and DAP5 and the antiapoptotic proteins XIAP, Bag-1 and B-cell lymphoma 2 (Bcl-2) are translated through IRESs (Henis-Korenblit et al. 2000; Sherrill et al. 2004). DAP5 is particularly interesting as it is an isoform of eIF4G, binding to the IRESs of Apaf-1, c-myc and XIAP, as well as its own IRES, stimulating

translation (Henis-Korenblit et al. 2000). It is thought that DAP5 acts as a scaffold, in a similar manner to its isoform, and promotes IRESs dependent translation through binding to eIF3 and eIF2β (Liberman et al. 2015).

The activity of an IRES can depend on a number of factors. Some IRESs require eIFs in order to operate, as well as other RNA-binding proteins. The secondary structure of an IRES can also play a role in an IRES' regulation. These characteristics are discussed below.

1.3.1 Requirement for Initiation Factors

Both viral and cellular IRESs usually have a requirement for some of the eIFs. Viruses utilise the cellular machinery to translate their mRNAs and for those viruses that contain IRESs in their mRNAs, they may disable some of the eIFs to gain an advantage over cellular mRNAs in the competition for ribosomes. For instance, in one of the first studies to analyse eIF requirements, it was found that the EMCV IRES does not require eIF4E but does require all other eIFs in order to recruit the 40S ribosome (Doudna and Sarnow 2007; Pestova, Hellen, and Shatsky 1996). Infection by EMCV causes the accumulation of eIF4E-BP, phosphorylating eIF4E inhibiting the binding of eIF4F (Gingras et al. 1996). Thus, EMCV mRNA is more readily translated over the host's mRNA. In poliovirus the viral protease 2A cleaves eIF4G, inhibiting it from binding to eIF4A and eIF3 and abolishing eIF4E binding, thus inhibiting cap-dependent translation (Marash and Kimchi 2005). The binding of the 40S ribosomal subunit to the HCV IRES does not require any initiation factors, although the ternary complex is required for its precise positioning at the start codon. eIF3,

normally required for 40S subunit association to mRNA, is not required for 40S binding in the HCV IRES, but is required for 60S ribosomal subunit binding (Pestova et al. 1998), and binds to domain III (Kieft et al. 2002).

The IRESs of the *myc* transcription factors are some of the best characterised cellular IRESs (Jopling et al. 2004; Spriggs et al. 2009; Stoneley et al. 1998). Although similar in function, c-*myc*, L-*myc* and N-*myc* have different requirements for translation initiation (Spriggs et al. 2009). Whilst the L-myc IRES requires PABP and eIF3 to be associated with eIF4G, c and N-*myc* only require the C-terminus of eIF4GI and eIF3 and not in a complex (Spriggs et al. 2009). All three myc IRESs require eIF4A for activation (Spriggs et al. 2009), suggesting that these IRESs must have their structure modified by eIF4A to allow ribosome passage/entry. Not much is known about the requirements of the epidermal growth factor receptor (EGFR) IRES, but, similar to the myc IRESs, requires eIF4A for function, suggesting that the EGFR IRES is highly structured (Webb et al. 2015).

IRES	Known Factor Requirements	References
EMCV	All except eIF4E	(Doudna and Sarnow 2007; Pestova, Hellen, and Shatsky 1996)
HCV	None, but eIF3 for 60S ribosome binding	(Pestova et al. 1998), (Kieft et al. 2002)
Poliovirus	Does not require eIF4A, 4G, eIF3, eIF4E	(Marash and Kimchi 2005)
c-myc	eIF4A, eIF4G, eIF3	(Spriggs et al. 2009)
l-myc	PABP, eIF3 and eIF4G (eIF4F), eIF4A	(Spriggs et al. 2009)
n-myc	eIF4A, eIF4G, eIF3	(Spriggs et al. 2009)
EGFR	eIF4A	(Webb et al. 2015)

Table 1.1. Eukaryotic Inititation Factor Requirements of Different IRESs.

1.3.2 IRES Structures

Whilst DNA exists mostly as a fully base paired double helix, the secondary structure of RNA is more complicated, containing both double stranded and single stranded regions. This leads to stem-loop formations and internal bulges, examples as shown in Fig 1.7. IRESs often have complex secondary structures, commonly stabilised by the high GC or AU content of the region, and are key to their function. The GC/AU rich areas cause the RNA strand to loop back upon itself, base pairing to create stem loops and bulges.

The *Picornaviridae* family is a large family of RNA viruses and is perhaps the most studied group of viruses which possess IRESs within their 5'UTRs. Detailed biochemical studies and structure prediction across the various members of the family show that picornavirus IRESs can be divided into two types based on their structure, Type 1 and Type 2 as shown in figure 1.8 (Jackson, Howell, and Kaminski 1990; Wimmer, Hellen, and Cao 1993). The IRES of hepatitis A virus (HAV) is distinctly different from these types and forms its own group, type 3. Type 1 IRESs are found in enterovirus and rhinovirus mRNA, whilst type 2 describe IRESs found in the mRNA of apthoviruses and cardioviruses. Each type has a distinct structural arrangement, despite variations in nucleotide sequence among the group; compensatory mutations restore Watson-Crick base pairings, retaining the structure. Type 1 consists of 6 distinct domains with an oligo-pyrimidine tract (Yn tract), 25

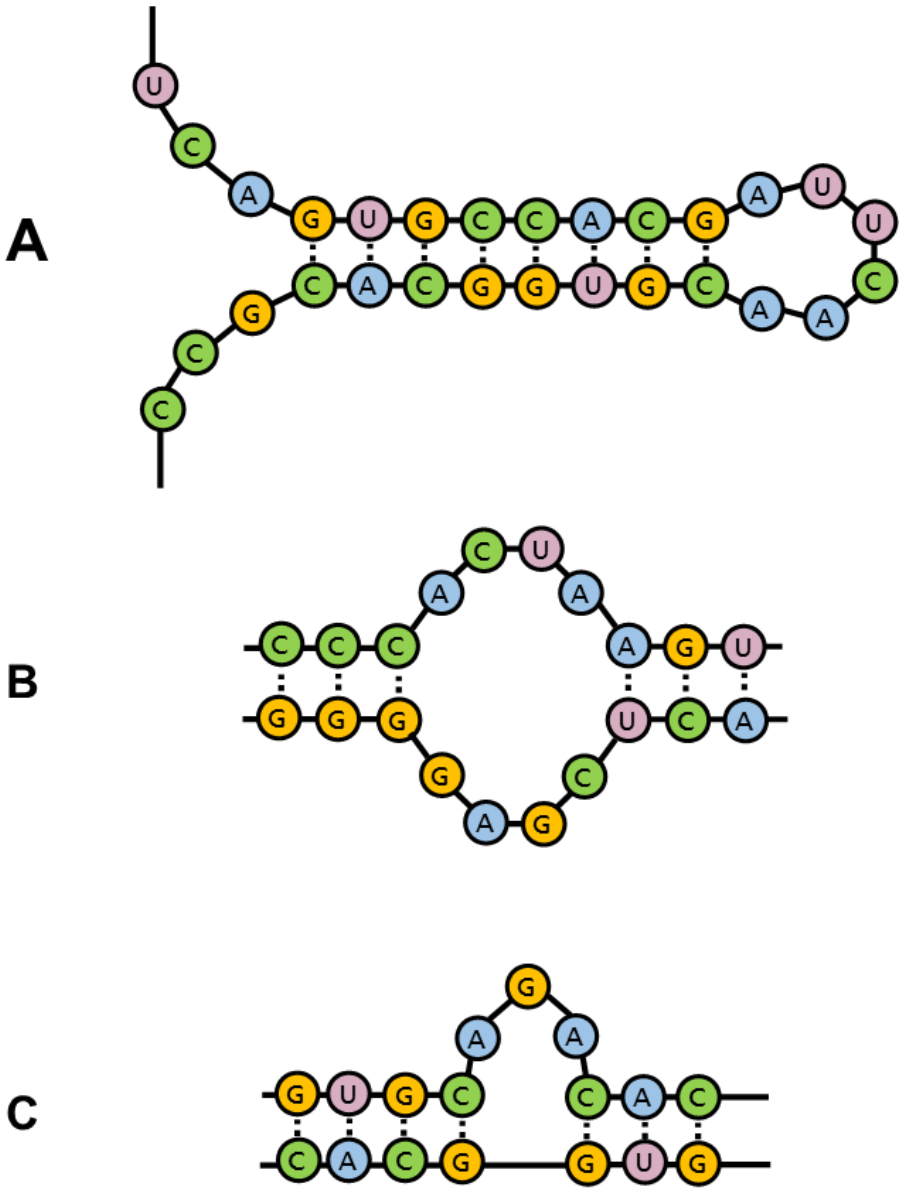

Figure 1.7 Examples of RNA Structures. Complementary bases can form double stranded regions, causing loops and bulges to appear. **(A)** An example of a stem loop structure. **(B)** An internal loop formed in the middle of a double stranded region. **(C)** A bulge, formed on one side of the double stand.

nucleotides upstream of an AUG codon, which is not the translation start codon. Type 2 IRESs also contain the Yn-AUG motif, but the AUG is the translation start codon and the 40S ribosomal subunit binds to this motif. The length of the tract and the distance to the AUG codon, in both types, is important for IRES function. Increasing the distance between the Yn tract and the AUG codon gradually decreases IRES activity (Kaminski, Belsham, and Jackson 1994), whilst decreasing the distance in poliovirus dramatically reduces activity (Pilipenko et al. 1992). This specificity also extends to structure, where point mutations or deletions are capable of disrupting the entire IRES suggesting that integrity of the IRES is an essential element for 80S ribosomal assembly (Stoneley and Willis 2004) For instance the GNRA motif found in all picornavirus IRESs in the 'A' loop of domain 4, does not tolerate point mutation at any of the four positions, whilst the sequence and structural organisation of the 3B loop are essential for IRES activity (Lopez de Quinto and Martinez-Salas 1997).

Structural regions are important for binding of both eIFs and IRES trans-acting factors (ITAFs). In type II picornaviral IRESs, eIF4G, 4A and 4B bind to the stem loops J/K/L of EMCV (Kolupaeva et al. 2003), causing conformational change to the structure, presumably to allow easier passage of the ribosome on the mRNA, as helicase activity was required for 48S preinitiation complex formation (Lomakin, Hellen, and Pestova 2000) . Mutations to these binding regions inhibit IRES activity (Clark et al. 2003). Analogous interactions were found in stem loop V of type I picornaviral IRESs (Ochs et al. 2003).

The IRES structure of the HCV flavivirus is distinct from those of the *picornaviridae* and is linked to the differences in initiation factor requirements between the two families. The HCV IRES only requires the bottom half of stem-loop III for binding of the 40S ribosomal subunit, yet it is not sufficient for IRES function, requiring domain II and the rest of domain III (Otto and Puglisi 2004), indicating that the formation of the 48S initiation complex on the mRNA is not the only requirement for IRES-dependent translation to occur. Cryo-electron microscopy revealed that domain II contacts the 40S subunit, causing it to tilt. Deletion of domain II does not affect the affinity of the 40S subunit, but does affect the conformational change, suggesting that the tilting of the 40S subunit guides the RNA into the mRNA binding cleft of the 40S subunit or opens up the binding cleft (Spahn et al. 2001).

The variation in structure and factor requirements between viral families aids in understanding the mechanisms of IRESs, however cellular IRESs are much more difficult to define. Whilst viral IRESs can be divided into types and share similar structures, no such patterns have emerged in cellular IRES studies. The L-myc and c-myc IRESs, despite being closely related, have wildly different structures (Le Quesne et al. 2001; Jopling et al. 2004). This has caused dispute over the importance of secondary structure in cellular IRESs. Yet there is substantial evidence that disruption of structures impacts IRES activity. Unlike viral IRESs, deletions within the IRES rarely disable the IRES. Rather, it is thought cellular IRESs are composed of a number of structural modules which act in concert to create an efficient IRES. This is true in the c-myc IRES (Stoneley et al. 1998; Le Quesne et al. 2001) but less so in the L-myc IRES;

although individual sequences contribute IRES activity, removal of sequences from the 5' or 3' end dramatically reduces IRES activity (Jopling et al. 2004). The N-myc IRES requires its entire sequence to function, with any deletions thought to inhibit the correct folding required for a functional IRES (Jopling and Willis 2001). The XIAP IRES features a 34nt Yn tract which is essential to its function, as deletion or base substitution disrupted IRES activity (Holcik et al. 1999). Unusually for cellular IRESs, this tract is similar to a double stranded region in the aquaporin 4 (AQP4) IRES, with similar consequences for activity upon deletion or base substation (Baird et al. 2007). However the structure of the XIAP IRES is not thought to be important for overall function, but that the Yn tract is crucial as it binds to the ITAF PTB, required for the IRES to function (Baird et al. 2007). There is then much variation among cellular IRES structures and only with more study can their function and importance be determined. Little is known about the structure of the EGFR IRES, although the high requirement for eIF4A for activity as mentioned above suggests a high degree of secondary structure is present and is likely to play a role in regulation of translation from the IRES (Webb et al, 2015).

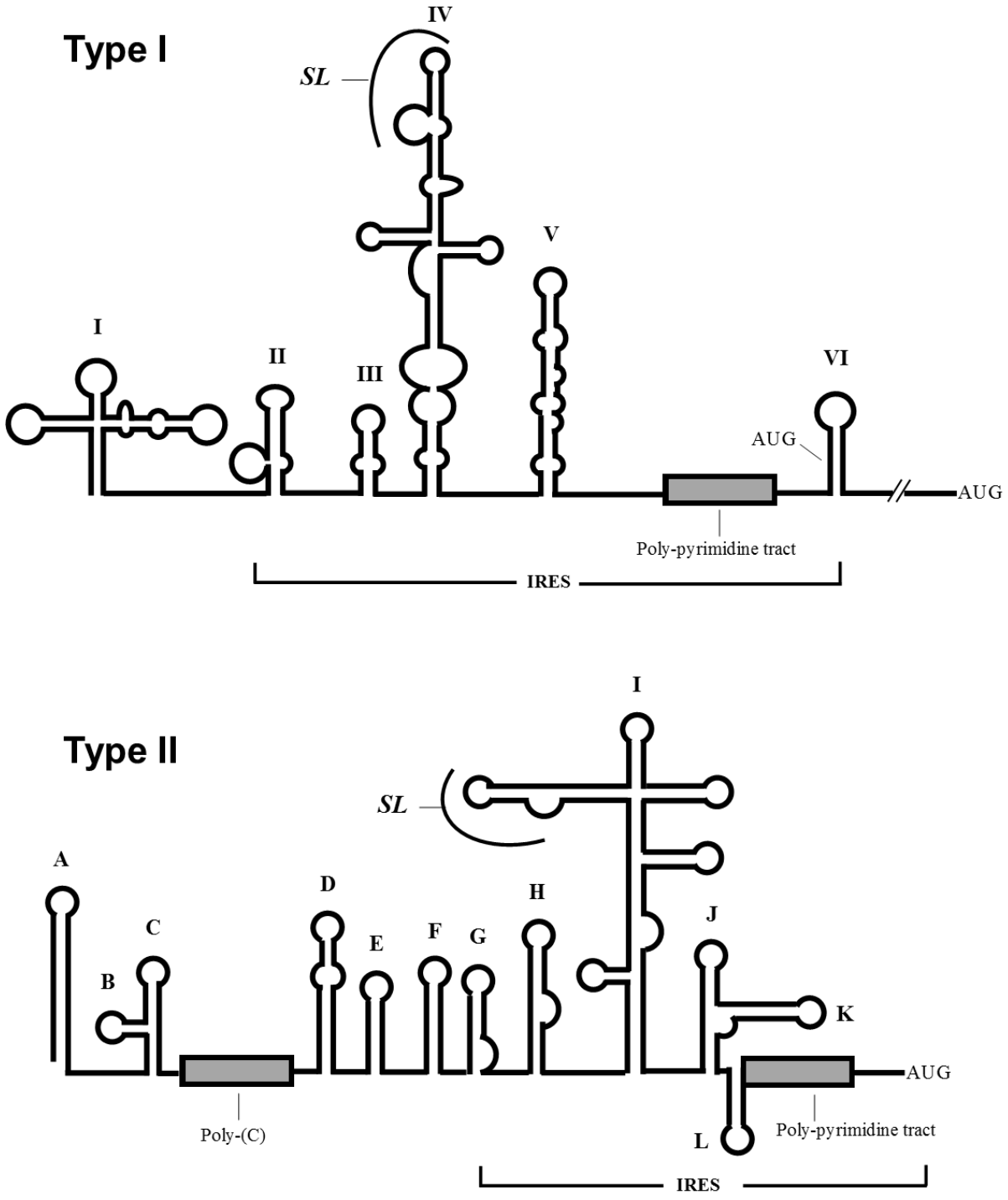

Figure 1.8 Types of Picornavirus IRES. Picornavirus IRESs form the first two groups of eukaryotic IRESs based on structure. Type I is defined by the 6 (I – VI) distinct domains, whilst Type II contains 12 notable stem loops. The region denoted as 'SL' is conserved between the two groups. Adapted from (Jang 2006).

1.3.3 IRES Trans-Acting Factors

The secondary structure of a 5' UTR is usually not enough to grant IRES activity. For maximal activity, IRES trans-acting factors (ITAFs) are required (Spriggs et al. 2005). The major role for ITAFs is in remodelling of and stabilising the structure of the IRES to allow the ribosome to bind. It is possible ITAFs may also act as a bridge between the RNA and translating ribosome. No ITAFs have been proposed as general regulators of IRES function, but the polypyrimidine tract-binding protein (PTB) appears to have the most widespread influence, interacting with at least the IRESs of Apaf-1, Bag-1, BiP and IGf1R (Mitchell et al. 2001; Pickering et al. 2003; Kim, Hahm, and Jang 2000). First identified as a protein that binds to Yn tracts in introns, PTB binds to viral IRESs through four loosely conserved RNA recognition motifs (Spriggs et al. 2005). The binding of PTB to IRESs through these domains is thought to make the ribosome landing site accessible to the ribosome. Other examples of structural rearrangement include the Apaf-1 and Bag-1 IRESs, which require the binding of their ITAFs to remodel the local structure to a single stranded region before ribosomes can bind (Mitchell et al. 2003; Pickering et al. 2004). The Apaf-1 IRES is only active in the presence of PTB. PTB also acts as an RNA chaperone for the EMCV IRES, stabilising its structure, required for its activity (Kafasla et al. 2009).

The ITAFs of the cat-1 IRES have been studied in detail. Under amino acid starvation the translation of a short uORF occurs in the cat-1 RNA. This causes the unwinding of the IRES element's secondary structure, without which the IRES remains in an inactive conformation (Fernandez, Bode, et al. 2002). This

process requires the phosphorylation of eiF2α. The remodelled IRES structure is then stabilized through interactions with the ITAFs hnRNP L and PTB (Majumder et al. 2009). Similarly, the SREBP-1 IRES has increased activity under endoplasmic reticulum stress governed by the subcellular relocation of hnRNP A1, which binds to the IRES (Damiano et al. 2013), yet hnRNP A1 can also be a negative regulator of IRES dependent translation initiation, inhibiting the XIAP IRES upon its subcellular relocation to the cytoplasm (Lewis et al. 2007). Indeed subcellular localisation of ITAFs appear to be crucial to their function as many reside in the nucleus. Many ITAFs have other functions inside the nucleus, such as RNA-binding motif protein 4 (RBM4) which has a regulatory role in pre-mRNA alternative splicing within the nucleus. RBM4 shuttles back and forth to the cytoplasm and, upon its phosphorylation, assists in the recruitment of eIF4A to IRESs, promoting translation (Lin, Hsu, and Tarn 2007). The phosphorylation of RBM4 depends upon the mitogen-activated protein kinase (MAPK) pathway, which is responsive to mitogens and extracellular stresses. Thus it is likely that under stresses where cap-dependent translation is inhibited, RBM4 is phosphorylated in order to promote IRES dependent translation.

1.3.4 IRESs in Disease

As discussed earlier, viral IRESs allow viral mRNAs to be preferentially translated over cellular mRNAs upon infection. Many of these viral IRESs have already been identified as potential therapeutic targets. For instance a small peptide, the lupus autoantigen La, can bind to the HCV IRES and block the binding of cellular trans-acting factors required for IRES activity (Dasgupta et

al. 2004), whilst prostaglandin A_1 forms a complex with the 40S ribosomal subunit, eIFs and HCV IRES, inhibiting initiation (Tsukimoto et al. 2015). Whilst the role of viral IRESs in disease may be obvious, cellular IRESs may play a role in a number of diseases. That cellular IRESs tend to be found in the 5'UTRs of factors involved in cell survival leads to a clear advantage for cancer cells to exploit them. An example of this has been found for the c-myc IRES in multiple myeloma (MM). A single point mutation in the genomic sequence of c-myc, a C to T transition (Paulin et al. 1996) was found in 42% of samples from MM patients, which increases c-myc expression through its IRES (Chappell et al. 2000). The mutation causes an additional stem loop structure to form (Chappell et al. 2000) and this increases the binding affinities of two ITAFs, PTB-1 and YB-1 to a proximal domain, domain 2 (Cobbold et al. 2010). Reducing the levels of these two ITAFs reduces c-myc expression levels in these cells. Mutations to the IRES sequence might represent only one method of increasing IRES-mediated translation in cancer. Work has also begun in the targeting of cellular IRESs in cancer. For instance the IRES of the tumour suppressor p53 IRES has two known ITAFs, translational control protein 80 (TCP80) and RNA helicase A (RHA) both of which upregulate p53 IRES activity (Halaby, Li, et al. 2015). Levels of TCP80 and RHA were found to be low in two cell lines and expression of both proteins were required for a significant increase in IRES activity (Halaby, Harris, et al. 2015). Thus medicines upregulating these proteins could aid in cessation of cancer progression.

As mentioned in section 1.1.3, translational control may be of importance in Alzheimer's disease, with both APP and 'tau' mRNAs containing IRESs. These IRESs rely upon the eIF4A helicase for their activity, suggesting that the structure present in these IRESs is important for the regulation of their expression (Bottley et al. 2010). Additionally, the APP 5'UTR contains an IRE stem loop, allowing increased expression under high iron levels, yet unlike the ferritin IRE mentioned above, only IRP1 not IRP2 binds to the APP IRE. Chelation of iron increases the binding of IRP1 to the APP IRE, decreasing expression (Cho et al. 2010). BACE1 contains three upstream ORFs which under oxidative stress and associated increase in phosphorylated eIF2α mediates the upregulation of translation (O'Connor et al. 2008). High levels of phosphorylated eIF2α in AD is well documented (Chang et al. 2002) and a prevailing hypothesis is that aberrant phosphorylation of eIF2α creates a feedforward loop in which the dysregulation of translation diminishes the functionality of the neuronal population. The eIF2α kinases, PKR and PERK are active in brain sections of AD mouse models (Page et al. 2006). Genetically removing PERK decreases elevated phosphorylation of eIF2α, reduced deficits in synaptic plasticity and memory (Ma et al. 2013). Thus, translational regulation of a subset of genes is likely to be of importance in AD and targeting these mechanisms may lead to novel therapies. It has been hypothesised that targeting the APP IRES could yield a possible treatment for Alzheimer's (Liu 2015), with recent reports demonstrating the dual action of memantine, an N-methyl-D-aspartate (NMDA) receptor antagonist which is already used as an Alzheimer's therapeutic, on the APP and tau IRESs as well as blocking the NMDA receptors (Wu and Chen 2009; Tasi et al. 2015). Other compounds, such

as NB34 derived from *Boussingaultia baselliodies*, are also under investigation for their ability to block the APP IRES (Tasi et al. 2015). Both the APP and the tau IRES require eIF4A for activity and blocking eIF4A with the small molecule inhibitor hippuristanol reduces the protein levels of APP, tau and amyloid β, as well as increasing the levels of proteins involved in oxidative stress defence (Bottley et al. 2010).

Targeting an IRES for upregulation of translation may also be a useful therapeutic technique. For instance, a switch exists for HIF1α under hypoxia from cap-dependent to cap-independent translation. However, this switch is inhibited upon the deletion of PTEN-induced putative kinase-1 (PINK1) (Lin et al. 2014), commonly found mutated in familial Parkinson's disease, and this leads to an increase in reactive oxygen species (ROS) thought to contribute to Parkinson's disease progression. Thus promoting HIF1α IRES activity may be effective at reducing ROS and slowing Parkinson's progression.

Aside from targeting the recognised contributors of AD, there is a case to be made for targeting the translational control of lesser known players. The epidermal growth factor receptor (EGFR) is perhaps better known for its role in cancer, but a substantial body of evidence suggests an involvement in AD. The most compelling evidence is that $A\beta_{42}$ oligomers bind to, and activate, the receptor, mediating the toxic effects of Aβ. Blocking the binding with allosteric inhibitors resulted in a reversal of memory loss in PS1/PS2 knockout mice, suggesting EGFR plays a major role in the loss of synaptic plasticity (Wang et al. 2012). The role of the EGFR IRES and translational control in AD remains uncertain, however it may allow for increased expression of the receptor under

conditions found in Alzheimer's disease. For instance, it is known that EGFR is upregulated under tumour hypoxia through the action of the alpha subunit of hypoxia inducible factor 2 (HIF2) (Franovic et al. 2007), although the mechanism by which this occurs is not known, the formation of complex involving HIF2α and a homologue of the cap-binding protein eIF4E, eIF4E2, may be involved (Uniacke et al. 2012). The EGFR IRES may play a part in this mechanism, as the IRES is active under hypoxic conditions (Webb et al. 2015). Hypoxia is thought to be present in AD, possibly as a result of cerebral ischemia or vascular diseases (Zhang and Le 2010; Franovic et al. 2007). That the APP, tau and EGFR IRESs share a high requirement for eIF4A may suggest that they have a common activation pathway (Bottley et al. 2010) (Webb et al. 2015). Further study of the translational control of EGFR and its IRES may reveal greater evidence of its involvement in Alzheimer's disease.

1.4 Epidermal Growth Factor Signalling

The epidermal growth factor receptor (EGFR) is a 1186 residue, 170kDa receptor tyrosine kinase, formed from the cleavage of the N-terminal signal sequence from the 1210 precursor protein (Ullrich et al. 1984). Over 20% of its mass is N-linked glycosylated, required for localisation to the membrane, where it is inserted, and plays a part in its function (Slieker and Lane 1986). EGFR consists of four extracellular domains, I-IV, a 23aa transmembrane domain, a juxtamembrane domain, a kinase domain and the carboxyl terminal (C-terminal) domain. Ligand binding occurs between domains I and III (Ogiso et al. 2002), as shown in figure 1.9

EGFR is a key modulator of a number of cellular processes such as, cell fate, proliferation, migration and apoptosis. EGFR binds extracellular ligands, translating their signal into a meaningful cellular response through activation of a wide array of signalling pathways. To create a downstream signal, EGFR binds its ligand and dimerises, either as a homodimer or a heterodimer with one of the three other members of the ErbB family; ErbB2, ErbB3 or ErbB4. The ability to form heterodimers creates ten possible combinations each activating a different set of signalling pathways, although the ErbB3-ErbB3 dimer is catalytically inert (Guy et al. 1994). Differences in the C-terminal domain alter which signalling molecules bind to the heterodimers. Heterodimerisation can also affect the internalisation and recycling of the receptor, which in turn affects the strength and duration of the signal. The traditional view of dimerisation is that ligand binding occurs first, followed by dimerisation (Tanner and Kyte 1999; Cochet 1988). However, dimers have

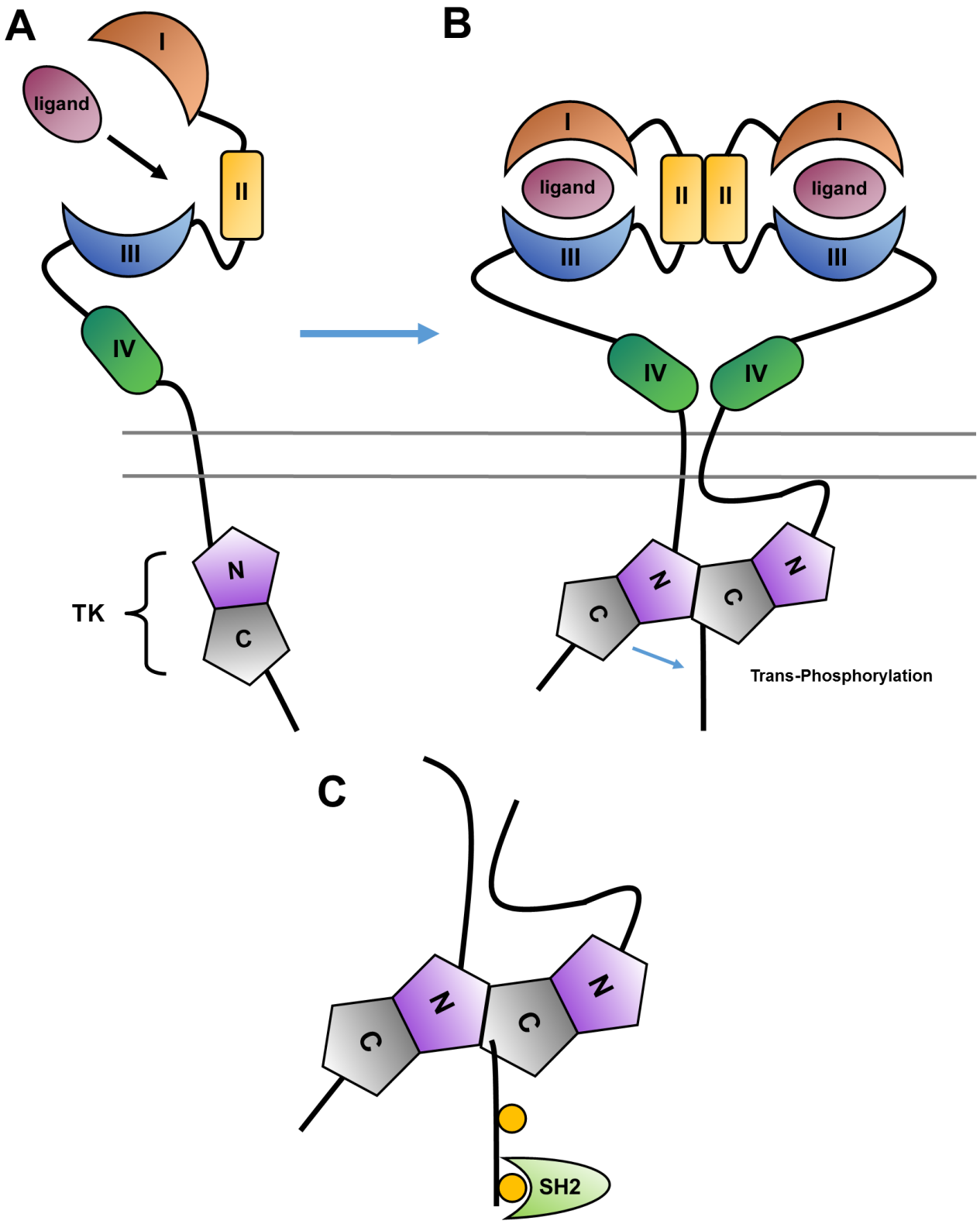

Figure 1.9. Ligand Binding and Activation of EGFR. Ligands bind to EGFR through the extracellular domains, I and III **(A)** Dimerisation occurs before or after ligand binding. Ligand binding repositions the intracellular domains, with the N-lobe of the tyrosine kinase domain (TK) of one dimer partner (the activator) binding to the C-lobe of the receiver **(B)**. The activator adopts an active conformation, allowing for trans-phosphorylation. Phosphorylated tyrosine residues allow for the binding of signalling proteins with SH2 or PTB domains **(C)**.

been observed at the surface without a ligand bound (Hofman et al. 2010) and it has been described that higher order oligomers, rather than dimers, are the predominant form of ligand-bound EGFR (Clayton et al. 2008). The other family members of EGFR vary in structure and thus in their ability to bind certain ligands and activate specific downstream pathways. Pathways activated by EGFR include MAPK, JNK and Akt. These pathways activate transcriptional programmes through transcription factors such as FOS, JUN and MYC, which lead to cell proliferation, differentiation, migration and adhesion (as reviewed in: (Yarden and Sliwkowski 2001))

1.4.1 Ligands and Activation of EGFR

The eponymous epidermal growth factor (EGF) is only one of seven ligands that bind to EGFR. Some ligands bind to multiple ErbB family members, such as epiregulin and NRG1β (Jones, Akita, and Sliwkowski 1999). Other ligands are very specific, with EGF and NRG4 only binding to EGFR and ErbB4 respectively. This overlap in specificity offers multiplicity and redundancy to the system, creating a robust signalling pathway. EGFR itself is the preferred receptor for seven of the 11 known ligands of the ErbB family, with only the neuregulins preferring ErbB4. Despite not binding any ligands (Klapper et al. 1999), the presence of ErbB2 in a heterodimer greatly enhances or prolongs its downstream signalling (Graus-Porta et al. 1997). Homodimers in general generate weaker signals than their heterodimer counterparts. Table 1 shows the ligands of the ErbB family and their preferred binding partner.

Ligand	Receptor			
	ErbB1 (EGFR)	ErbB2	ErbB3	ErbB4
EGF	+	-	-	-
TGF-α	+	-	-	-
HB-EGF	+	-	-	+
Amphiregulin	+	-	-	-
Betacellulin	+	-	-	+
Epigen	+	-	-	-
Epiregulin	+	-	-	+
Neuregulin 1	-	-	+	+
Neuregulin 2	-	-	+	+
Neuregulin 3	-	-	-	+
Neuregulin 4	-	-	-	+

Table 1.2 The Ligands of EGFR and the ErbB Family. (+) denote receptors which the ligand binds to, (-) receptors which cannot bind the ligand.

Ligand binding is required for receptors to become active. Ligand binding induces the predimerised EGFR to twist around a pivot point, repositioning the intracellular domains into an active kinase configuration (Moriki, Maruyama, and Maruyama 2001). The I, II and III domains play an active part in this reconfiguration, with a change in the conformation of the C-terminal end of domain II altering the angle between domains II and III, but conserving the interface between the two domain II's of the dimer. This alteration affects the

conformation of the intracellular domains, repositioning the kinase domains (Garrett et al. 2002; Ogiso et al. 2002). Removal of the entire ectodomain results in a constitutively active complex, suggesting the ectodomain prevents kinase activation (Chantry 1995). Interestingly, unlike many tyrosine kinases EGFR does not require phosphorylation of the activation loop within the kinase domain, despite a conserved tyrosine residue (Tyr845) (Hubbard, Mohammadi, and Schlessinger 1998; Zhang et al. 2006). Mutation of this tyrosine to phenylalanine does not disable activation of the kinase or its function (Tice et al. 1999). Crystal structures reveal that EGFR is activated allosterically by ligand binding, by forming an asymmetrical dimer. One kinase domain is the 'activator' the other, the 'receiver'. The C-lobe of the activator contacts the N-lobe of the receiver, inducing conformational changes disrupting *cis*-autoinhibitory interactions. The receiver kinase adopts an active conformation without phosphorylation of the activation loop (Zhang et al. 2006). A simplified diagram of this is shown in figure 1.9 This mechanism is exploited in some small cell lung cancers through mutations to the *cis*-autoinhibitory interactions, allowing activation of the kinase without ligand binding (Sharma et al. 2007).

1.4.2 Signalling Pathways

Once in the active conformation, the kinase domains of EGFR perform transautophosphorylation, phosphorylating a number of tyrosine residies at the c-terminal end of the protein. The exact tyrosine residues that will be phosphorylated is determined by the ligand which is bound to the receptor and the dimer partner (Olayioye et al. 1998). Phosphorylation can also be carried out by other kinases such as SRC and JAK-2 (Tice et al. 1999; Yamauchi et al.

1997). Phosphorylation of the tyrosine residues in the kinase domains allows the binding of signalling molecules with either Src homology 2 (SH2) or phosphor—tyrosine binding domains (PtB). Other proteins such as CBL, PI3K-C2b and STAT5B associate with EGFR in an indirect manner (Fukazawa et al. 1996; Wheeler and Domin 2001; Kloth et al. 2003). The sequence divergence between the different members of the ErbB family in their C-terminal domains allows for higher affinity for certain signalling molecules to bind, increasing the multiplicity of signals from the EGFR family. This is demonstrated well by the differences between EGFR and ErbB3. Phosphoinositide 3-kinase (PI3K) has multiple binding sites on ErbB3 through its SH2 domains (Hellyer, Cheng, and Koland 1998), and binds extremely efficiently, whilst EGFR binds PI3K much less efficiently (Fedi et al. 1994). Yet the ubiquitin ligase c-CBL, phospholipase Cγ and GAP binds to EGFR but not ErbB3 (Fedi et al. 1994). Despite these differences a number of signalling pathways are shared between the different heterodimers. The RAS and MAPK pathways are invariably activated, and PI3K is activated by most active dimers, but the potency of the signal differs among receptors (Soltoff and Cantley 1996).

In short, these pathways utilise a series of serine and threonine kinases to carry the signal to nuclear transcription factors which upregulate the transcription of genes involved in growth, differentiation and cell survival. A simplified diagram of these pathways can be seen in figure 1.10 As an example, the MAPK pathway begins with the adaptor protein Grb2. Grb2 is constitutively bound to SOS, an exchange factor for RAS. This complex is usually localised to the cytoplasm. Grb2 can bind to tyrosines Y^{1068} or Y^{1086} (Batzer et al. 1994) but can also bind indirectly to EGFR through phosphorylated SHC, itself binding to EGFR

through its PtB domain (Sasaoka et al. 1994). The relocalisation of the Grb2-SOS complex to the plasma membrane allows it to interact with RAS, which is associated with the membrane. SOS, as mentioned, is a GTP exchange factor for RAS, and it proceeds to exchange GDP for GTP, activating RAS. RAS is a GTPase which acts as a molecular switch, activating a large number of proteins. In the MAPK pathway it binds to RAF-1, switching on its serine/threonine kinase activity. RAF-1, through a series of other kinases leads to the nuclear translocation of ERK-1 and ERK-2 which catalyse the phosphorylation of nuclear transcription factors. Other targets of RAS include PI3K and AKT leading to activation of mTOR and inducing cell growth.

1.4.3 EGFR in Cancer

Of the diseases that EGFR is involved in the most well-known is cancer. The *EGFR* gene is a commonly amplified in a number of cancers. Persistent activation of EGFR allows for uncontrolled proliferation. Overexpression of EGFR can occur through amplification of the *EGFR* gene, receptor activating mutations or removal of negative regulators. The variant III mutation of EGFR involves an in-frame deletion of 801 bp spanning exons 2-7, resulting in the absence of 267 aa from the extracellular domain. This results in the receptor being incapable of binding any ligands yet displays low level constitutive signalling, accompanied by reduced internalization and downregulation (Gan et al, 2013).

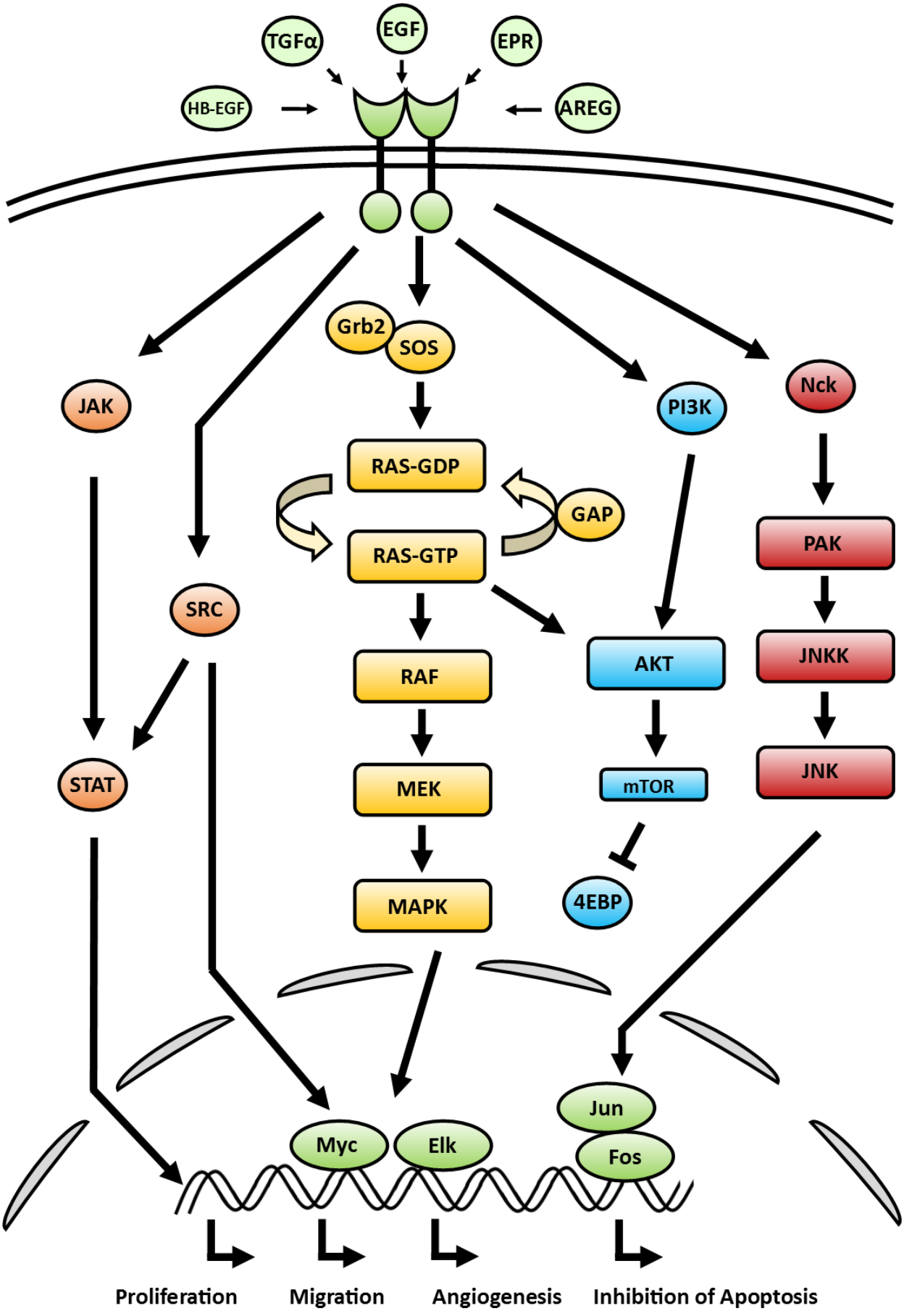

Figure 1.10 Signalling Pathways Activated Through EGFR. Upon ligand binding, EGFR phosphorylates a number of signalling molecules which transmit the signal through their cascades. Transcription factors are activated and upregulate expression of genes involved in cell growth and proliferation.

The EGFRvIII mutation is expressed in 25-64% of cases of glioblastoma multiforme (Saikali et al. 2007) and 20-36% in breast cancer (Ge, Gong, and Tang 2002).

Other common mutations include the short-in frame deletions of exon 19 and a point mutation in exon 21. These two mutants account for 90% of EGFR mutations found in non-small-cell lung cancer (NSCLC) (Li et al. 2008). In glioblastoma and NSCLC, *EGFR* gene amplifications or mutations are found in 20-40% of cases. However incidence of gene amplification or mutations in other cancers is rare (Blehm et al. 2006; Spindler et al. 2006). This finding is important as those cancers bearing no EGFR mutations are less sensitive to gefitinib, an inhibitor of EGFR (Mok et al. 2009). *EGFR* amplification correlates poorly with protein levels in invasive breast carcinoma, with 75% of cases with overexpression of EGFR lacking gene amplifications (Kersting et al. 2004). A loss of translational control may explain other incidences of overexpression. Low levels of the miR133b, which targets the 3'UTR of EGFR and inhibits downstream signalling, is decreased in some lung cancers, and treatment with miR133b improves the effectiveness of gefitinib (Liu et al. 2012). Similarly, EGFR is translationally upregulated by tumour hypoxia through a mechanism controlled by HIF2, as mentioned in section 1.3.4 (Franovic et al. 2007). The IRES in EGFR has been shown to be upregulated by hypoxia, suggesting that it could be a potential mediator of this hypoxic pathway (Webb et al. 2015), however other reports indicate a complex formed in the 3'UTR by HIF2α as the source of this phenomenon (Uniacke et al. 2012).

1.4.4 EGFR in Neurodegeneration

There is substantial evidence that implicates EGFR in Alzheimer's disease, but its role in the disease is uncertain. In rat brains, expression of EGFR reduces with age (Hiramatsu et al. 1988). EGFR is present within the neuritic plaques of AD brains (Birecree et al. 1988) and is found in a number of tissues from AD brains including, vascular endothelial cells, entorhinal cortex, middle temporal and superior frontal gyrus and the primary visual cortex (Liang et al. 2007), as well as having greater expression in astrocytes (Ferrer et al. 1996). EGFR is also associated with a number of conditions found in AD. EGFR is activated by metal ion activity (Wu et al. 2004) and as discussed previously, AD is commonly associated with high levels of iron, zinc and copper, leading to neurotoxicity and aggregation of Aβ (Atwood et al. 1998; Atwood et al. 2000; Bush et al. 1994). Carriers of the ApoE4 allele have been shown to have higher levels of EGFR when compared to ApoE3 carriers (Conejero-Goldberg et al. 2011). EGFR's ligand, EGF is raised in the plasma of AD brains (Marksteiner et al. 2011). EGFR is activated under inflammatory conditions and is involved in the innate immune response (Sorensen et al. 2006; Pastore et al. 2008). EGFR signalling pathways upregulate expression of a number of cytokines, including interleukins 1, 5 and 8 and chemokine ligand 2 (CCL-2) (Huang et al. 2014; Brook et al. 2000; Winzen et al. 1999; Clark et al. 2009). Inhibition of EGFR also reduces astrocyte activation and cytokine secretion in reactive astrocytes (Li et al. 2014). As stated above, hypoxia increases EGFR expression and hypoxia is thought to occur in AD, attributed to cerebral ischemia or vascular diseases (Zhang and Le 2010; Franovic et al. 2007).

Most of this evidence could be classed as circumstantial, yet there is also evidence that EGFR is directly involved in the regulation of some of the main protagonists of AD. For instance, stimulation by EGF results in rapid production of APP (Slack et al. 1997; Tang, Guan, et al. 2010) and EGFR can induce APP cleavage in SH-SY5Y cells (Minopoli et al. 2007). AICD, the product of γ-secretase cleavage of APP, binds to the EGFR promoter and represses transcription, but in PS1/2 knockout mice, EGFR levels are increased (Zhang et al. 2007).

Inhibition of EGFR signalling may be an effective treatment in AD. Upregulation of Ras activity has been shown to cause neuronal cell death and degeneration (Botella et al. 2003). $A\beta_{42}$ oligomers bind to EGFR, activating the tyrosine kinase and this was found to mediate the toxicity of Aβ. Inhibition of EGFR signalling with allosteric inhibitors, gefitinib and erlotinib, reversed memory loss associated with PS1/2 knockout in mice and *Drosophila* (Wang et al. 2012)

It has previously been shown that the EGFR 5'UTR contains an IRES (Webb et al. 2015). This IRES may be an important site of translational regulation in Alzheimer's disease. As stated above, the IRES is active during hypoxic conditions, when cap-dependent translation is globally inhibited and has a high requirement for eIF4A (Webb et al. 2015). The hypoxic conditions observed in Alzheimer's disease (Zhang and Le 2010; Franovic et al. 2007) may also drive the IRES-mediated translation of EGFR. Investigating the effects of other conditions that occur in AD on the IRES will aid in understanding how the IRES is activated and its potential as a therapeutic target.

1.5 Aims of this Project

EGFR is an important mediator in a number of processes and diseases, yet the translational control of EGFR remains largely unexplored. The IRES within the 5'UTR of EGFR has not been fully characterised, and furthering the knowledge of its activation could lead to potential therapies against overexpression of the protein, mediated by the IRES.

EGFR has been identified as a potential mediator of disease progression in Alzheimer's disease, yet the effects of EGFR activation through ligand binding on the translatome has not been examined. Translational control has already been shown to be important in regulating the expression of APP, BACE1 and MAPT, suggesting alterations to the translational profile plays a part in the disease.

The aim of this project was to further characterise the IRES of EGFR and determine its potential as a therapeutic target. This will be achieved through observing the conditions in which the IRES is active using bicistronic luciferase plasmids and dual luciferase reporter assays. The structure and functional regions of the IRES will be examined through RNA structure mapping using selective 2'-hydroxyl acylation and primer extension and deletion analysis. The capability of antisense oligonucleotides to block cap-independent translation via the EGFR IRES will be examined and a 3d cell culture model will be developed for future use in assessing drug delivery systems. Finally the translational profile of EGFR activation by EGF stimulation will be studied using polysome profiling and RNA-seq techniques.

2. Materials & Methods

2.1 Tissue Culture

2.1.1 Solutions and Reagents

Phosphate buffered saline (PBS): 4.3mM Na_2HPO_4, 1.5mM KH_2PO_4, 137mM NaCl, 2.7mM KCl, pH 7.4.

High Glucose Dulbecco's Modified Eagles Medium (DMEM) (Sigma?)

Heat-inactivated foetal bovine serum (FBS) (Gibco)

Heat-inactivated horse serum (HS) (Gibco)

Fugene 6 Transfection Reagent (Promega)

*Trans*IT-Oligo Transfection Reagent (Mirus)

MTT Solution: 4mg/ml 2-(3,5-diphenyltetrazol-2-ium-2-yl)-4,5,-dimethyl-1,3-thiazole bromide (Alfa Aesar), dissolved in PBS.

2.1.2 Cell Lines and Maintenance

Four human cell lines were used during the course of this project, HeLa (cervical epithelial carcinoma), U87-MG (glioblastoma), MCF7 (breast cancer) and SH-SY5Y (neuroblastoma). All cells were grown in tissue culture treated plasticware (TPP) flasks with a growth area of $75cm^2$ (T75). The Growth medium used was DMEM supplemented with 10% FBS and 2mM L-glutamine, with the exception of the SH-SY5Y cells that were maintained in high glucose DMEM supplemented with 10% FBS, 2mM L-glutamine and 1% horse serum (HS). All cells were maintained at 37°C and under a humidified atmosphere containing 5% CO_2. Cells were grown to near confluence and then subcultured

by removing the media, washing with PBS and dissociating the cells from the flask with 1 x trypsin-0.5 mM EDTA solution. Cells were then diluted in fresh media and seeded at a density of $2.1x10^6$ cells/T-75.

2.1.3 Generation & Maintenance of 3D Spheroids

Cells were plated into 96 well microplates coated with an Ultra-Low Attachment surface (Sigma-Aldrich) at a range of densities, from $1x10^2$-$1x10^5$. Cells were grown in DMEM supplemented with 10% FBS and 2mM L-glutamine. To encourage cells to form spheroids, plates were centrifuged lightly at 100rpm for 2 minutes immediately after seeding. Cells were allowed to grow for up to 7 days to achieve spheroids of the desired size. Media was replaced every 48 h.

2.1.4. Transient Transfection

Cells were prepared for transfection of DNA plasmids using the above dissociation procedure, followed by seeding into 24 well plates, at a density of $5x10^4$ per well. Fugene 6 reagent was used for the transfection, using the manufacturer's instructions. For each well, 300 ng of DNA plasmid and 1µl Fugene 6 was used. Firstly, 50 µl serum free media was combined with the Fugene 6 and incubated at room temperature for 5 minutes before the plasmid DNA was added, and left to incubate at room temperature to allow the reagent-DNA complex to form. The solution was then added to the wells and incubated at 37°C, 5% CO_2 in a humidified incubator for 24 hours before treatment or being assayed for luciferase activity.

2.1.5 Transfection of Modified Oligonucleotides

2'OMe RNA oligonucleotides were used to block translation of reporter mRNAs by binding to specific regions of the RNA. These anti-sense oligomers do not cause degradation of the RNA, rather providing a steric block.

2.1.5.1 Modified oligonucleotide sequences

2'OMe RNA Oligonucleotide Name	Sequence (5'-3')
Upstream Control	GGCGCUCACACCGUGCGG
Positive Control	GGCAUCUUCCAUGGUGGCUU
Scrambled 20mer	ACGAGGCGGAGUAAUCGUAG
Scrambled 17mer	GCGGAUCGAACGAAUGU
5'UTR_191-207	AUACUGGACGGAGUCAG
5'UTR_208-223	CCGGCUCUCCCGAUCA
3'UTR_662-676	CAGUAAGUACCGUGGGGACA

Table 2.1. Modified 2'O Methyl Oligonucleotide Sequences

2.1.5.2 Transient transfection of 2'OMe oligonucleotides

24 hours after transient transfection of plasmid DNA, cells were transfected with 2'OMe RNA oligonucleotides. *Trans*It-Oligo Reagent (Mirus) was used for the transfection and manufacturer's guidelines were followed. Per well, 3ul *Trans*IT-Oligo Reagent was added to 50µl serum free media and mixed. Oligonucleotide was added to the serum:*Trans*IT-Oligo Reagent, to reach a final concentration of 2µM per well and incubated for 20 minutes at 25°C. The mix was then added dropwise to the wells, briefly rocked and incubated at 37°C for 24 hours before lysis.

2.1.6. Generation of Stable Cell Lines

Cells were seeded in a 6 well plate at a density of $2x10^5$ / well. Transfection of plasmids containing a neomycin phosphotransferase gene was achieved with Fugene 6, in a similar manner to above, except the amounts of transfection reagent and plasmid were increased to 6µl and 1.8µg respectively. Cells were incubated for 24h before selection medium was applied. Selection medium consisted of High Glucose DMEM, 10% FBS, 2mM L-glutamine and 150ng/µl of G418. Media was changed daily, and cells were incubated until non-expressing cells had died and high confluency of expressing cells achieved. Cells were subsequently dissociated from the wells and transferred to T75 flasks. Cells were passaged for a number of generations before use, to ensure gene stability.

2.1.7 MTT Assay

Cells were seeded into 96 well plates at a density of $5x10^3$ cells/well. Plates were incubated at 37°C, 5% CO_2 for 24 hours before being treated. After treatment, cells were incubated for another 24 hours at 37°C, 5% CO_2 before addition of 50µl MTT Solution to each well. Plates were shaken for 5 minutes and plates incubated for 3 hours at 37°C, 5% CO_2. Media was aspirated and the formazan product resuspended by addition of 15µl DMSO to each well. Plates were shaken for 5 minutes again before being read in a plate reader. Readings were taken at 560nm, with background subtracted from readings at 670nm.

2.1.8 Microscopy

For 2d cultures, an EVOS FL (ThermoFisher) microscope was used, with RFP and GFP light cubes. These had excitations wavelengths of 531/40 nm and 470/22 nm respectively, with emission wavelengths of 593/40 nm and 510/42 nm respectively. An exposure time of 500 ms was used for all image captures. Images obtained were analysed in ImageJ. For 3D cell imaging cell masses were analysed by fluorescence confocal microscopy, using a Zeiss LSM 510. Excitation wavelengths of 488 nm and 543 nm were used, whilst emission wavelengths of 509-520 nm and >550 nm were used for GFP and DsRed fluorescence capture respectively. Z-level slices were taken 19µm apart and the images obtained analysed using the Zeiss LSM image browser.

2.2 Molecular Biology Techniques

Reagents and Solutions

TE: 10mM Tris-HCl, pH7.5, 1mM EDTA

1xTAE: 40mM Tris, 40mM acetic acid, 1mM EDTA, pH 8.0.

1xTBE: 89mM Tris base, 89mM Boric acid, 3mM EDTA, pH 8.0

TBF1: 30mM Potassium acetate, 10mM $CaCl_2$, 50mM $MnCl_2$, 100mM RbCl, 15% glycerol

TBF2: 10mM MOPS pH6.5, 75mm $CaCl_2$, 10mM RbCl, 15% glycerol

Primer Sequences (Sigma-Aldrich)

Primer Name	Sequence (5'-3')
EGFR SpeI F	GATTACAACTAGTCCCCGGCGCAGCGCGGCCGC
EGFR NcoI R	GATTACACCATGGCGCTGCTCCCCGAAGAGCTCG
pRF_EGFR_A_R	GCCGCCTCCCATGGGTCGGGCGCTC
pRF_EGFR_B_F	GTGTGAGCGACTAGTGCGGCCGAGGC
pRF_EGFR_B_R	GTCGTCCGGCCATGGCGGCGGCGGC
pRF_EGFR_C_F	CCCGGCGGCCGACTAGTCCCAGACCG
pRF_EGFR_C_R	CTGGACGGAGTCCATGGGCCGTGCG
pRF_EGFR_D_F	ACCACCGCGCACTAGTCCCCTGACTC
pRF_EGFR_D_R	CCCCGAAGAGCCATGGCCGGCTCTCC
pRF_EGFR_E_F	GATCGGGAGACTAGTGAGCGAGCTCT
EYFP Upstream F	GATTACAATTAATAGTAATCAATTACG
EYFP Up F	CAACTCCGCCCCATTGACGC
EYFP Down R	GACAAACCACAACTAGAATGC
EGFR AgeI F	GATTACAACCGGTCCCCGGCGCAGCGCG
EGFR AgeI R	GATTACAACCGGTCGCTGCTCCCCGAAGAGC

Table 2.2 PCR Primer Sequences

2.2.3. Luciferase Assays

Media was removed and cells washed with PBS before addition of 50µl 1 x Passive Lysis Buffer (Promega) for each well of a 24 well plate. Cells were dissociated from the well bottom by scraping and 5µl of this suspension was added to individual well in a black, round bottomed 96 well plate. Luciferase activity was determined using a dual-luciferase kit (Promega), and a GloMax-96 microplate luminometer (Promega). Following the kit's protocol, 25µl of each reagent (LarII, followed by Stop&Glo) was added to each well and luminescence measured over a 10 second integration time after addition of each reagent.

2.2.4 Polymerase Chain Reaction

For downstream applications, such as cloning, DNA was amplified from vectors or cDNA templates using polymerase chain reaction (PCR). Typically, 50-100ng of vector was used per reaction, along with 1 unit of either Phusion DNA polymerase (NEB) or Taq DNA polymerase (NEB). These were added to a reaction mix containing either 1 x Phusion GC buffer or 1x Taq DNA polymerase buffer, 200µM dNTPs, 0.5µM of each primer and 5% DMSO. Reactions were performed in a Techne TC-512 gradient PCR machine. DNA was denatured at 98°C (Phusion) or 94°C (Taq) for 2 minutes before entering a cycle of denaturation at 98/94°C for 30 seconds, annealing at 50-65°C for 30 seconds and extension at 72°C (Phusion) or 68°C (Taq) for 1 minute. 35 cycles were completed before entering a final extension period at 72/68°C for 5 minutes. DNA products were visualised by agarose gel electrophoresis.

2.2.5 Agarose Gel Electrophoresis

DNA was separated according to its molecular weight by electrophoresis in agarose gels. Typically, 1% (w/v) agarose gels were used, although for samples less than 50 base pairs in length, gels up to 2% (w/v) were used. Agarose was melted in 1x TAE and cast in to plastic trays after addition of 2µl 10mg/ml ethidium bromide or 1x SYBR Safe DNA gel stain (Thermo Fisher Scientific). DNA was mixed with 6x loading dye and loaded into the gel. The gel was submerged in 1x TAE and a voltage of 100v was applied for 1 hour to separate the DNA. DNA bands were visualised using a UV transilluminator or a Gel Doc XR+ System (BioRad).

2.2.6 Purification of DNA

2.2.6.1 Crude preparations for colony screens

Single *E.coli* colonies were inoculated into700µl LB medium containing antibiotic. Cultures were grown overnight in a shaking incubator at 37°C. Cultures were then centrifuged at 13000rpm for 5 minutes and the pellet resuspended in 100µl TE. Cells were lysed by addition of 200µl solution II (1% SDS, 0.2M NaOH), mixed and incubated at 25°C for 2 minutes. 150µl 7.5M ammonium acetate was added to precipate proteins, and the mixture centrifuged for 10 minutes at 13000rpm. The resulting supernatant was mixed in a new Eppendorf tube with 900µl 100% ethanol and centrifuged for 30 minutes at 13000rpm. The supernatant was then removed and the pellet allowed to dry before being resuspended in nuclease free water.

2.2.6.2 Using Machery Nagel Plasmid Miniprep Kit

Picked colonies were grown in 5ml cultures of LB containing ampicillin or kanamycin, depending on the plasmid transformed. Cultures were grown overnight in a 37°C shaking incubator.

2.2.6.3 Purification of DNA from agarose gel

DNA was excised from gels using a scalpel and purified using Nucleospin Gel and PCR Clean-Up kit (Macherey Nagel), following the manufacturer's instructions.

2.2.7 Determination of Nucleic Acid Concentrations

DNA and RNA concentrations were determined using a Nanodrop 100 spectrophotometer (Thermo Scientific) by measuring the optical absorbance at 260nm.

2.2.8 Restriction Digests

DNA was digested using restriction digestion enzymes and their associated buffer (NEB). The enzymes used were SpeI HF, NcoI HF and FseI. The CutSmart buffer (NEB) was used in reactions for all three enzymes, at a temperature of 37°C. Reaction volumes were typically 20µl and digests were incubated at recommended temperature for 1-2 hours.

2.2.9 Alkaline Phosphatase Treatment

Single digests of vectors were treated with alkaline phosphatase were dephosphorylated in order to stop re-ligation of the vector during ligation. Linearised plasmid DNA was treated with 1U Antarctic Phosphatase (NEB).

Reactions were incubated at 37°C for 5 minutes. DNA was then separated by agarose gel electrophoresis.

2.2.10 Ligations

DNA fragments were ligated into DNA plasmids using T4 DNA ligase (promega). Typical reaction volumes were 10µl and vector:insert molar ratio of 1:3 was used. Two types of buffer were used, a 10X buffer and a quick ligation 2X buffer which contained polyethylene glycol (PEG).

2.2.10.1 Using 10X T4 Ligase buffer

10X T4 ligase buffer (NEB) was added to the vector:insert mixture before addition of 400U T4 ligase (NEB). Reactions were made up to 10µl with nuclease free H_2O. Reactions were incubated overnight at 4°C. Reactions were then heat inactivated at 65°C for 10 minutes, chilled on ice for 5 minutes and then transformed into 50µl competent DH5α *E.coli* cells.

2.2.10.2 Using 2X Quick Ligation Buffer

The 2X quick ligation buffer (NEB) was added to 5µl of vector:insert mix. 400U T4 DNA ligase (NEB) was added and the reaction incubated at 25°C for 15 minutes before being placed on ice. The reaction was not heat inactivated, but transformed directly into 50µl competent DH5α *E.coli* cells.

2.2.11 Phenol: Chloroform Extraction

To remove contaminants from DNA samples, phenol:chloroform extraction was performed. An equal volume of phenol and chloroform:Isoamyl alcohol was added to the DNA sample and vortexed. The sample was then centrifuged at

13400rpm for 1 minute. The aqueous layer was then transferred to a new tube and the DNA precipitated.

2.2.11.1 DNA Precipitation

To the DNA, 0.1% (v/v) 3M sodium acetate, pH 5.2 and 250% (v/v) 100% ethanol was added and mixed. The mix was centrifuged for 30 minutes at 13400rpm. The resulting supernatant was discarded and the pellet washed in 70% ethanol. The sample was centrifuged for 10 minutes at 13400rpm and the supernatant discarded once more. The pellet was allowed to air dry for 5 minutes before being resuspended in nuclease free H_2O.

2.2.11.2 RNA extraction by phenol:chloroform

For RNA, the procedure is the same as in 2.2.11, except that acidic phenol, pH4.5, was used instead.

2.2.12 Polysome Profiling

2.2.12.1 Preparation of sucrose gradients

Sucrose solutions containing between 60-10% sucrose and 1x gradient buffer (3M NaCl, 150mM $MgCl_2$, 150 mM Tris-HCl, pH 7.5, 1mg/ml cylcohexamide, 10mg/ml heparin) were layered in Sorvall PA 12ml tubes. 1.6ml of each sucrose solution, starting from the highest density, was added to the tube and frozen at -80°C before addition of the next layer. The 7 concentrations of sucrose were 10%, 18%, 26%, 34%, 42%, 50% and 60%. Once all layers were added, gradients were stored at -80°C until use, where they were slowly defrosted overnight at 4°C.

2.2.12.2 Preparing cell lysates

Cells were seeded in 15cm^2 plates at a density of 5x10^6 per plate. Cells were incubated at 37°C, 5% CO_2 for 24 hours before being treated. Treatments will be described in chapter 5. 24 hours after treatment cells were treated with 100ng/ml cycloheximide for 2 minutes at 37°C, 5% CO_2 before being placed on ice. Medium was removed and cells washed with 5ml PBS containing 100ng/ml cycloheximide. Cells were then harvested by scraping in 5ml PBS containing 100ng/ml cycloheximide followed by centrifugation at 1600rpm in a chilled, 4°C centrifuge for 4 minutes. The supernatant was then removed and 0.5ml ice cold lysis buffer (1X gradient buffer, 1% TritonX100) added to the cell pellet. The pellet was resuspended and centrifuged at 13400rpm in a chilled 4°C centrifuge for 1 minute. The resulting supernatant was then added carefully to the top of the sucrose gradient.

2.2.12.3 Separation of mRNA.

mRNAs were separated according to polysomal association by centrifugation of the lysate through the gradients at 38000rpm (182106 x g) for 2 hours at 4°C in a Sorvall Discovery 100SE centrifuge using the Sorvall TH-641 rotor and associated buckets, which were chilled at 4°C before use.

2.2.12.4 Fractionation of mRNA

Gradients were passed through a 'gradient machine' in order to separate the mRNA into fractions. The machine consisted of a UV/vis detector (UA-6 teledyne, ISCO), a motorised pump (KD Scientific), a mechanical trace and an automatic fraction collector. The machine was cleaned through with ddH_2O, 70% ethanol and ddH_2O. The machine was then primed with 65% blue sucrose

(1x gradient buffer, 65% sucrose, 0.25% Bromophenol Blue) and then pumped into the bottom of the gradient at a flow rate of 1ml/min, pushing the sample through the uv/vis detector, with the lowest density fraction going through first. The OD was read at 254nm and recorded onto a trace. 1ml fractions were collected and 3ml 7.7M Guanidine HCl and 4ml 100% ethanol added. Samples were mixed and stored at -20°C overnight. mRNA fractions were pooled into subpolysomal and polysomal fractions as determined by the trace. 2.5M $LiCl_2$ was added and the pooled samples incubated at -20°C overnight. Samples were centrifuged at 13000rpm in a chilled 4°C centrifuge for 30 minutes and the supernatant discarded. The pellet was resuspended in 300µl nuclease free H_2O followed by addition of 68mM NaOAc, pH 5.2, and 75% ethanol. Samples were incubated at -20°C for 30 minutes followed by centrifugation at 13000rpm for 30 minutes in a chilled, 4°C centrifuge. The supernatant was again removed and the RNA pellet washed in 75% ethanol, mixed for 10 minutes and centrifuged for 5 minutes at 13000rpm in a chilled 4°C centrifuge. The pellet was then resuspended in 50µl nuclease free H_2O and the concentration measured using a Nanodrop Spectrophotometer 1000 (Thermo Scientific).

2.2.13 RNA-seq Analysis

Library preparation for RNA-seq was performed using TruSeq Stranded Total RNA Sample kit (Illumina), per manufacturer's instructions. Briefly, ribosomal RNA is removed from the sample through ribo-depletion. RNA is then fragmented and reverse transcribed into cDNA. Adapter sequences are ligated to the cDNA strands and are enriched through PCR, generating 30 million reads for each library. Adapters used in this project were TruSeq LT adapters

(Illumina). Sequencing was conducted using the NextSeq500 system (Illumina), generating 75bp paired end reads.

2.3 Bacterial Techniques

2.3.1 Preparation of Competent *E.coli*

E.coli cells can be made chemically competent through a series of salt washes, allowing them to take up plasmid DNA during a brief heat-shock treatment at 42°C. It is important that the cells and all reagents used are kept at 4°C, as transformation efficiency decreases when cells are allowed to warm up to room temperature.

A 5ml LB starter culture was grown overnight from a single *E.coli* colony. This starter culture was then added to 500ml of LB supplemented with 20mM $MgSO_4$. The culture was grown until the OD, measured at A600, was between 0.4 and 0.6. The cells were pelleted at 4000rpm in a chilled 4°C centrifuge. Cells were resuspended in 100ml ice cold TBF1 and incubated on ice for 5 minutes. The cells were again pelted, before being resuspended in 10ml ice cold TBF2 and incubated on ice for 1 hour. Following this, the cells were aliquoted and snap frozen in liquid nitrogen. The cells were stored in -80°C for future use.

2.3.2 Transformation

Ligation reactions were added to 50µl competent DH5α *E.coli* and the mixture were incubated on ice for 10 minutes, before being heat-shocked at 42°C for 1 minute. The mixtures were incubated on ice for 2 minutes before 1ml of LB was added. Mixtures were incubated in a shaking incubator for 1 hour at 37°C. Cells were then pelleted by centrifuging at 13000rpm for 5 minutes. Cells were

resuspended in 50µl LB and spread onto an LB-agar plate which contained either kanamycin (30µg/ml) or ampicillin (100µg/ml) depending on the plasmid's resistance gene. Plates were incubated at 37°C overnight. Colonies were then picked for growth in liquid LB cultures for DNA purification or used directly in a colony PCR.

2.4 Radiation Techniques

2.4.1 5' End Labelling of Oligonucleotides with ^{32}PγATP

Oligonucleotides were radiolabelled with ^{32}P by polynucleotide kinase (PNK) in the following reaction:

60µM Oligonucleotide

2µl γ^{32}P ATP

2µl 10X T4 PNK buffer (NEB)

1µl PNK (NEB)

H_2O up to a final reaction volume of 20µl

The reaction mix was incubated at 37°C for 30 minutes followed by inactivation at 65°C for 20 minutes. Unincorporated radiolabels were removed from the mix by filtration through a G-50 Sephadex column

2.5 Selective 2'Hydroxyl Acetylation & Primer Extension (SHAPE)

2.5.1 Reagents

10x N-methylisatoic acid: 130mM, dissolved in DMSO

3.3x Folding Mix: 333mM HEPES, pH 8.0, 20mM $MgCl_2$, 333mM NaCl

SHAPE Enzyme Mix: 250mM KCl, 167mM Tris HCl, pH 8.3, 1.67mM each dNTP (dATP, dCTP, dGTP, dTTP), 17mM DTT and 10mM $MgCl_2$.

Acid Stop Mix: 4:25 (v/v) mixture of 1M unbuffered Tris-HCl, and stop dye (85% formamide, 0.5x TBE, 50mM EDTA, pH 8.0, containing bromophenol blue and xylene cyanol dyes)

2.5.2 SHAPE Primers

Primer Name	Sequence (5'-3')
SHAPE REVTRANS	GAACCGGACCGAAGCCCG
SHAPE_R with linker	GAACCGGACCGAAGCCCGATTTGGATCCGGCGAACCGGATCGACGGTGCTCCCCGAAGAGC
FIRST 80 F	TAATACGACTCACTATAGGGGGCCAACGGGCCAACCCCGGCGCAGCGC
FIRST 80 R	GAACCGGACCGAAGCCCGATTTGGATCCGGCGAACCGGATCGAGTTGGCGGCGAGGCGGGGA
MID 80 F	TAATACGACTCACTATAGGGGGCCAACGGGCCAAGCTAGCCCCGGCGGC
MID 80 R	GAACCGGACCGAAGCCCGATTTGGATCCGGCGAACCGGATCGAGTTGGCGGCGAGGCGGGGA
SHAPE EGFR 80 F	TAATACGACTCACTATAGGGGGCCTTCGGGCCAAGCCACAACCACCGCG

2.5.3 In Vitro Transcription

DNA was amplified by PCR using a forward primer containing at its 5' end a T7 RNA polymerase promotor. The linear DNA was then transcribed using the RiboMax Large Scale RNA Production System (T7). Usually, 30µl reactions were conducted. Reactions were assembled at room temperature and consisted of 6µl 5X T7 transcription buffer, 7.5mM rNTP mix, 1-3µg linear DNA and 10µl T7 Enzyme Mix. The reaction was incubated at 37°C for 3 hours before addition of 1U RQ1 DNase per µg DNA added to the reaction and incubation at 37°C for 15 minutes. The resulting RNA was purified by phenol/chloroform extraction, as detailed in 2.2.11.2

2.5.4 Modification of RNA with N-methylisatoic Acid

2 pmol of RNA was diluted in 12µl 0.5x TE and heated to 95°C for 2 minutes before being placed on ice for 2 minutes. 6µl 3.3xFolding Mix was added and the mixture was incubated at 37°C for 20 before being split equally between two tubes, labelled '+' and '-'. 1µl 10xNMIA was added to the '+' sample, and 1µl DMSO added to the '-'sample. The samples were incubated for a further 45 minutes at 37°C. The samples were then ethanol precipitated by addition of 90µl H_2O, 4µl 5M NaCl, 1µl 20mh/ml glycogen, 2µl 100mM EDTA pH8, and 350µl ethanol (100%), and incubating at -80°C for 30 minutes followed by centrifugation at 13000rpm for 30 minutes in a chilled (4°C) centrifuge. The pellets were then resuspended in 10µl 0.5xTE.

2.5.5 Primer Extension

3µl of radiolabelled primer was added to the '+' and '-' samples, and annealed to the RNA by heating to 65°C for 5 minutes, cooling to 35°C for another 5 minutes and placing on ice for 1 minute. 6µl SHAPE Enzyme Mix was added and tubes heated to 52°C for 1 minute before addition of 200U Superscript III. Samples were incubated at 55°C for 15 minutes before the RNA was degraded by addition of 1µl 4M NaOH and heating to 95°C for 5 minutes. 29µl Acid Stop Mix was added and again incubated at 95°C for 5 minutes.

2.5.6 Sequencing Ladder Generation

3µl of radiolabelled primer was added to four separate samples of untreated RNA and annealed to the RNA by heating to 65°C for 5 minutes, cooling to 35°C for another 5 minutes and placing on ice for 1 minute. To each tube 10mM of either ddATP, ddCTP, ddGTP or ddTTP was added, along with 100µM dNTP mix and tubes heated to 52°C for 1 minute before addition of 200U Superscript III. Samples were incubated at 55°C for 15 minutes before the RNA was degraded by addition of 1µl 4M NaOH and heating to 95°C for 5 minutes. 29µl Acid Stop Mix was added and again incubated at 95°C for 5 minutes.

2.5.7 Denaturing acrylamide gel electrophoresis of DNA

To separate single stranded, radiolabelled DNA fragments, denaturing polyacrylamide gels were used, which utilised acrylamide solutions at a ratio of 19:1, acrylamide:bis-acrylamide. Gels of 8% were made by combining 14g urea, 4ml 10X TBE, 8ml 40% acrylamide (19:1 acylamide:bis-acrylamide, Accugel, National Diagnostics) and 28ml H_2O to make a final volume of 40ml. The

mixture was polymerised by addition of 75µl TEMED and 75µl APS. Gels were cast between two glass plates, which had been cleaned with ethanol. Gels were pre-run at 800V in 1xTBE for 30mins.Typically, 2µl of sample was loaded onto the gel and run for 1.5-2h at 1000V, until the lower dye had reached the end of the gel. Gels were transferred onto blotting paper, covered in cling film and dried in a vacuum gel drier for 1 h at 80°C. Dried gels were exposed to phosphor screens (GE Healthcare) overnight in a light-sealed exposure cassette (GE Healthcare).

2.5.8 Imaging of Phosphor Screens

Imaged using a Storm 860 molecular imager (Amersham) and its associated software, Imagequant software (Amersham).

2.5.9 SHAPE Reactivity Calculations

Relative reactivities were calculated using the boxplot method (Hajdin *et al*, 2013). The interquartile distance, *d*, was determined from the subtraction of the upper and lower quartiles (Q_u and Q_L) after the raw reactivities of each nucleotide position, R_i were ordered from highest to lowest. Outliers were removed, after determination by: $R_i > Q_U + 1.5 * d$. No more than 5% of the dataset were removed as outliers. R_{max}, the mean reactivity of the 10% most reactive nucleotides, was determined and the reactivity of each nucleotide divided by R_{max} to normalise the data.

3. Translational Control of EGFR through its 5'UTR

IRESs allow expression of mRNAs when cap dependent translation is inhibited. This inhibition can come from a number of physiological conditions such as amino acid deprivation and hypoxia. However, not all IRESs respond to all types of cell stress. The intricate nature of these pathways suggests that IRESs are part of heavily regulated systems that respond to particular stresses. Understanding when and how an IRES is activated is important in developing treatments for certain diseases.

An IRES within the EGFR 5'UTR has been previously discovered and maintains EGFR expression under hypoxic conditions, whilst having a high requirement for the eIF4A helicase, suggesting the structure of the IRES is important in its function and regulation (Webb et al. 2015). Identifying the structure could aid in the development of therapeutics which block binding of trans-acting factors, or modify the structure to inhibit the IRES. As translational control of EGFR has been shown to be an important factor in some cancers, along with potentially having a role in neurodegeneration it is important to characterise its translational regulation (Wang et al. 2012; Franovic et al. 2007)

The aim of this section was to further characterise the EGFR IRES by analysing the conditions in which the IRES is active and maintain EGFR expression,

characterise the structure of the IRES and discover important regions of the IRES which contribute to its function through deletion analysis.

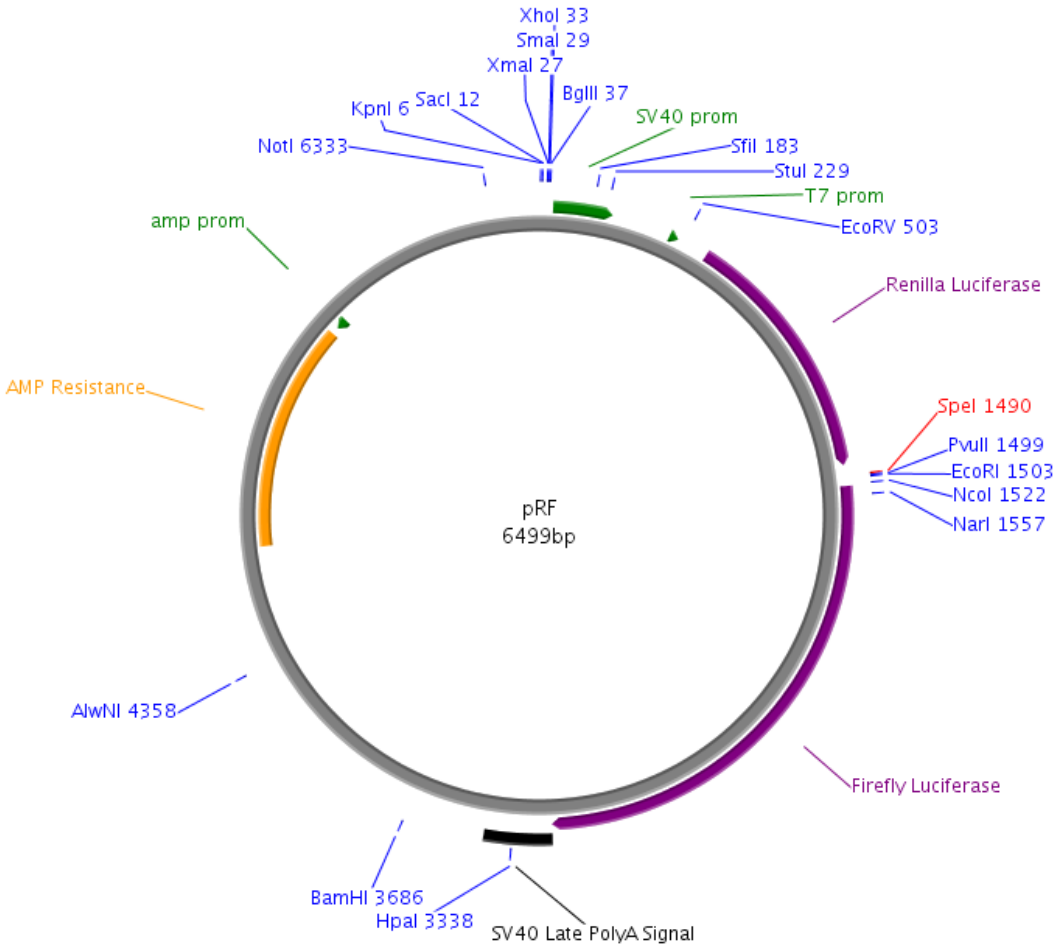

Figure 3.1 pRF Vector Map

3.1 Plasmids and Cloning

A common method of investigating IRES activity is through the use of bicistronic vectors; vectors that allow the expression of two or more gene products from a single promotor. Insertion of the IRES element between the two gene sequences allows for independent expression of the two reporter gene sequences, where the latter gene can only be expressed through internal initiation of translation by the IRES element. We used the pRF vector which allows the co-expression of the *Renilla reniformis* luciferase and the firefly (*Photinus pyralis*) luciferase. These luciferases are evolutionarily distinct; both their structures and substrates are different, allowing their reactions to be differentiated as detailed in section 2.2.3. The pRF vector map can be seen in figure 3.1.

In order to analyse IRES activity the 5'UTRs of EGFR (NM_005228.3) and beta-tubulin (NM_001293212.1) were inserted into the pRF vector (Fig.3.1) between the *Renilla* and firefly luciferase ORFs. The 5'UTR was amplified using primers EGFR *Spe*I and EGFR *Nco*I, as shown in section 2.2, via PCR and both vector and PCR product were digested with *Spe*I and *Nco*I restriction enzymes before being ligated together. These plasmids are referred to as pREF and pRTubF respectively.

The p15 vector (Fig. 3.2) contains a single firefly luciferase ORF and was co-transfected with the pSV-β-Galactosidase plasmid, containing a lacZ ORF, as a normalisation control (Fig 3.3). Two plasmids were previously created with the

p15 vector. The first, P15E contained the 5'UTR of EGFR, which was inserted upstream of the firefly luciferase ORF at the *Hind*III site, having first been amplified using the EGFR *Hind*III F and EGRF *Hind*III R primers via PCR and digested with *Hind*III. The second plasmid, p15E3UTR contained both the 5'UTR of EGFR, as before, and the 3'UTR of EGFR (as shown in section 3.7). The 3'UTR was amplified using primers 3UTR F and 3UTR R, digested with *Fse*I and inserted at the *Fse*I site downstream of the firefly ORF.

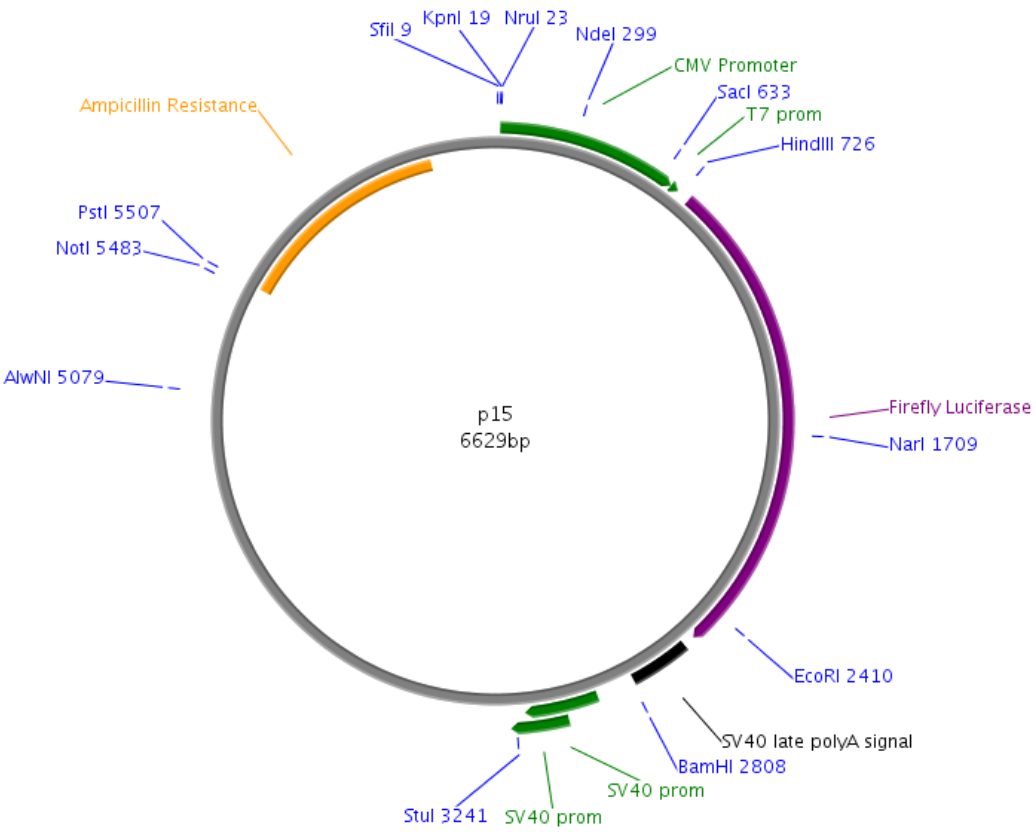

Figure 3.2 p15 Vector Map

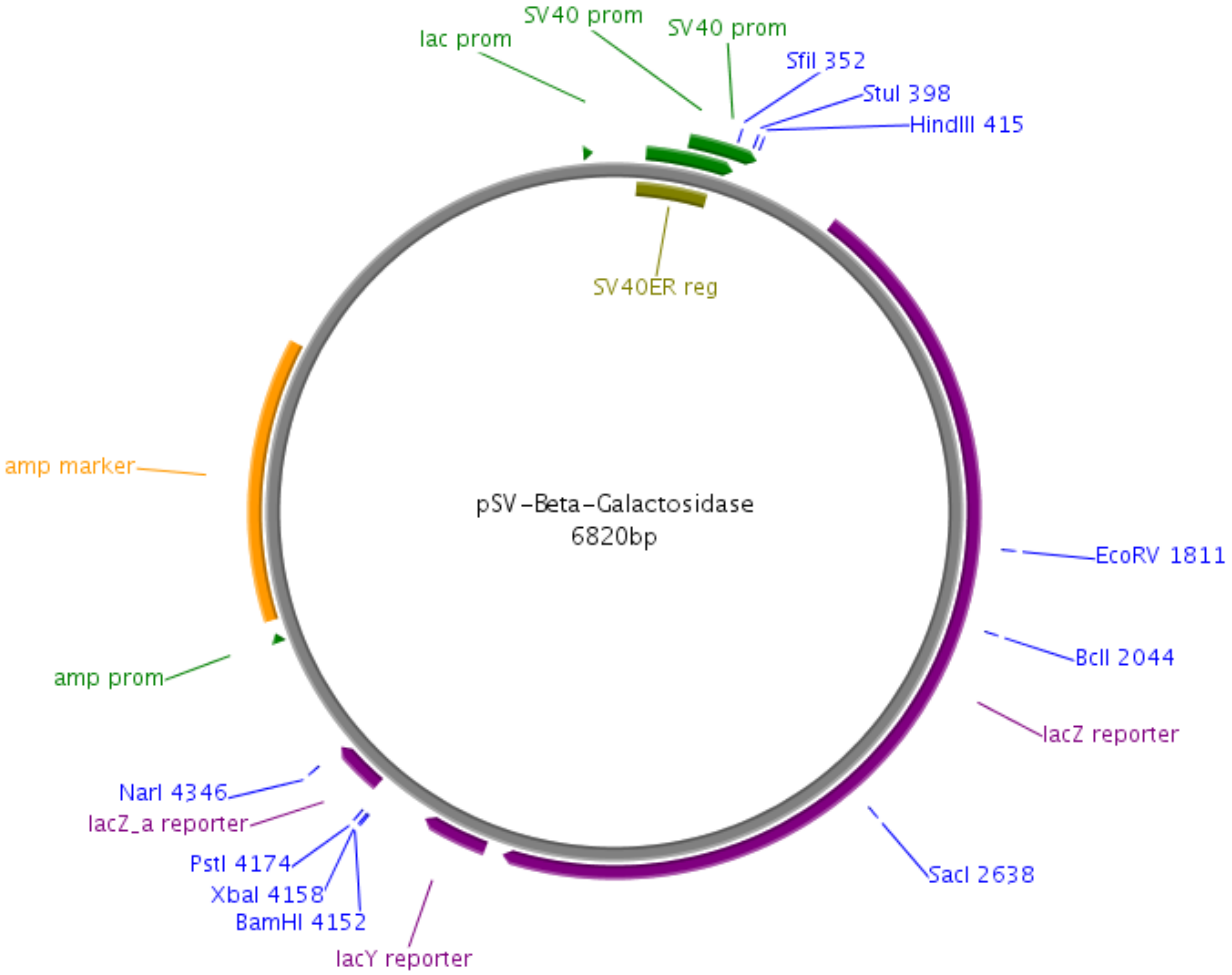

Figure 3.3 pSV-β-Galactosidase Vector Map

3.2 Endoplasmic Reticulum Stress

Endoplasmic reticulum stress occurs through accumulation of misfolded or unfolded proteins. The unfolded protein response (UPR) is activated upon a high level of unfolded proteins and serves to arrest the cell cycle as well as attenuating translation through the protein kinase RNA-like endoplasmic reticulum kinase (PERK) receptor, which phosphorylates eIF2α. Further steps involve upregulating expression of proteins involved in malfolded protein chaperoning.

ER stress has long been connected with Alzheimer's disease, causing an increase in β-amyloid (Sato et al. 2001) and inducing the pathology of the tau protein (Ho et al. 2012). ER stress causes EGFR activation through a signalling mechanism involving angiotensin II and tumour necrosis factor-α-converting enzyme (TACE) (Takayanagi et al. 2015). Thus ER stress and EGFR may be linked in the progression of Alzheimer's disease. We wished to analyse whether ER stress could increase EGFR production through translational control.

To induce ER stress we used the chemicals thapsigargin and tunicamycin. Tunicamycin blocks glycoprotein biosynthesis in the ER, leading to stress, whilst thapsigargin lowers the calcium levels within the ER through inhibition of the sarcoplasmic/endoplasmic reticulum Ca^{2+} ATPase (SERCA). This causes chaperones within the ER to lose their chaperone activity, causing accumulation of unfolded proteins.

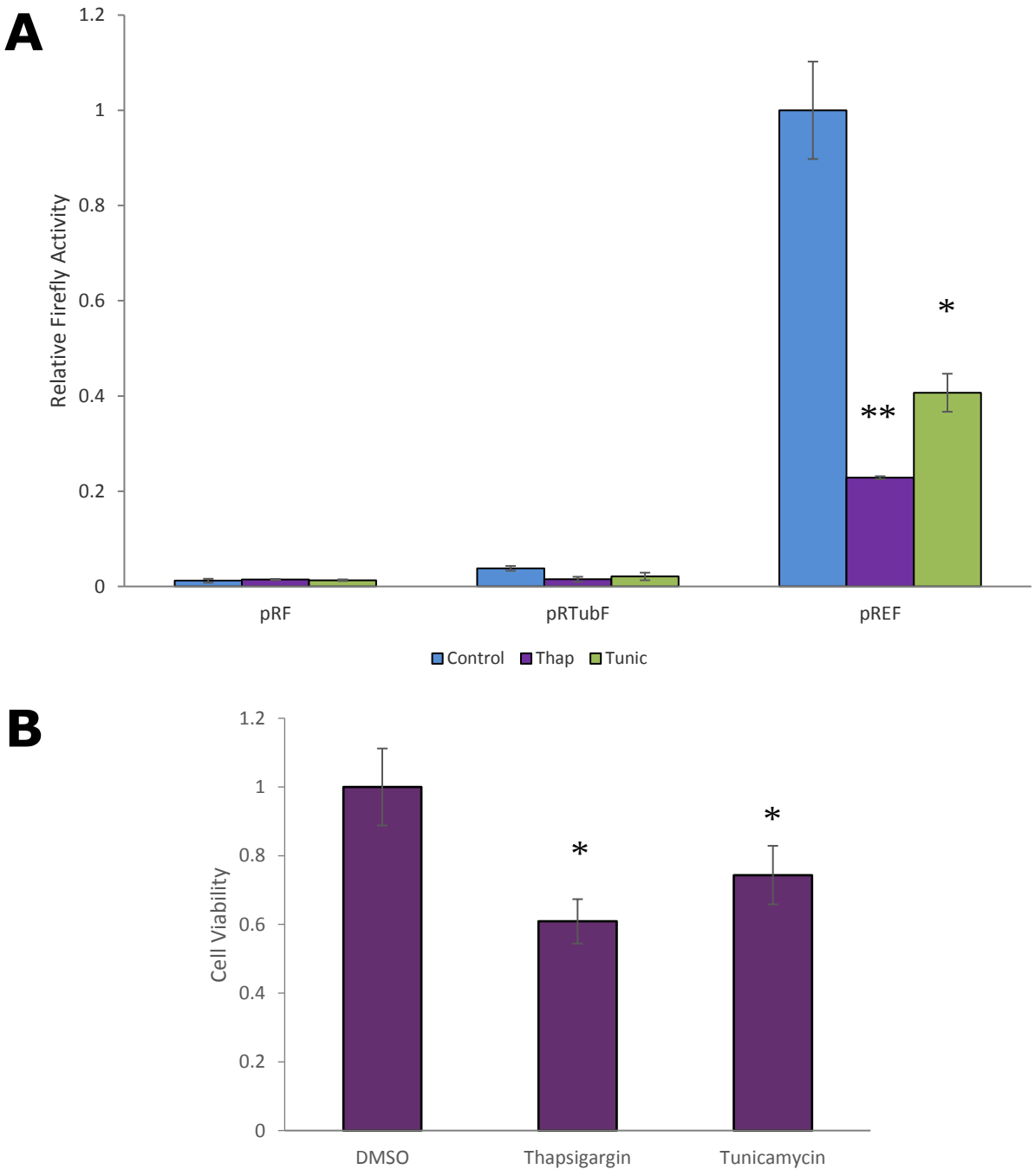

Figure 3.4 The Effect of Endoplasmic Reticulum Stress Inducers on EGFR IRES Activity in U87-MG cells. (A) pRF plasmids were transfected into U87-MG cells in a 24 well plate. 24 hours after treatment with either 1 µM thapsigargin or 4 mg/ml tunicamycin, cells were lysed and assayed for luciferase activity. Relative firefly activity is firefly luciferase activity divided by *Renilla* luciferase activity. Values are normalised to pREF control. n =3, error bars represent standard deviation of three biological replicates. **(B)** Cell viability as measured by MTT assay after treatment with 1 µM thapsigargin, 10 mM tunicamycin or DMSO. n = 3, error bars represent standard deviation of three biological replicates. "*" indicates $p < 0.05$, "**" indicates $p < 0.01$. Significance tested by t-test.

24 hours after treatment, both thapsigargin and tunicamycin result in a lower relative expression of firefly luciferase in pREF, thapsigargin treatment reducing IRES activity by 77.16% ($p < 0.01$ by t-test), whilst tunicamycin reduced activity by 59% ($p < 0.05$ by t-test). This indicates IRES activity is reduced during ER stress. As expected there is little firefly activity in the empty pRF vector as well as from the 5'UTR of the 'housekeeping gene' beta-tubulin (pRtubF), acting as a negative control.

To determine whether the treatments given affected the viability of cells, we performed an MTT assay on cells after treatment (Fig 3.4b). We found that treating cells with 10 μM thapsigargin reduced cell viability by 39% and by 26% when treated with 4 mg/ml tunicamycin ($p < 0.05$ by t-test). This is expected given that ER stress leads to cell cycle arrest, thus cell metabolism will be lowered. In MCF7 cells, both thapsigargin and tunicamycin result in lesser reductions in EGFR IRES activity compared to U87-MG cells at 33% and 23% respectively (Fig 3.5a), however these were both found to be statistically insignificant ($p > 0.05$, by t-test), but displayed similar viability to U87-MG cells (Fig 3.5b). This difference between cell lines could indicate that the mechanism which reduces IRES activity in U87 cells is not present in MCF7 cells. This could be a missing ITAF, a genetic abnormality within either of the cell lines, or differences in how the IRES is folded. This would be in a similar vein to discoveries in the HIV-1 IRES which is thought to fold differently in cells where it is active, dependent on the availability of certain ITAFs (Plank, Whitehurst, and Kieft 2013). Further analysis could determine the cause of such divergent results, and whether this feature exists is relevant *in vivo*.

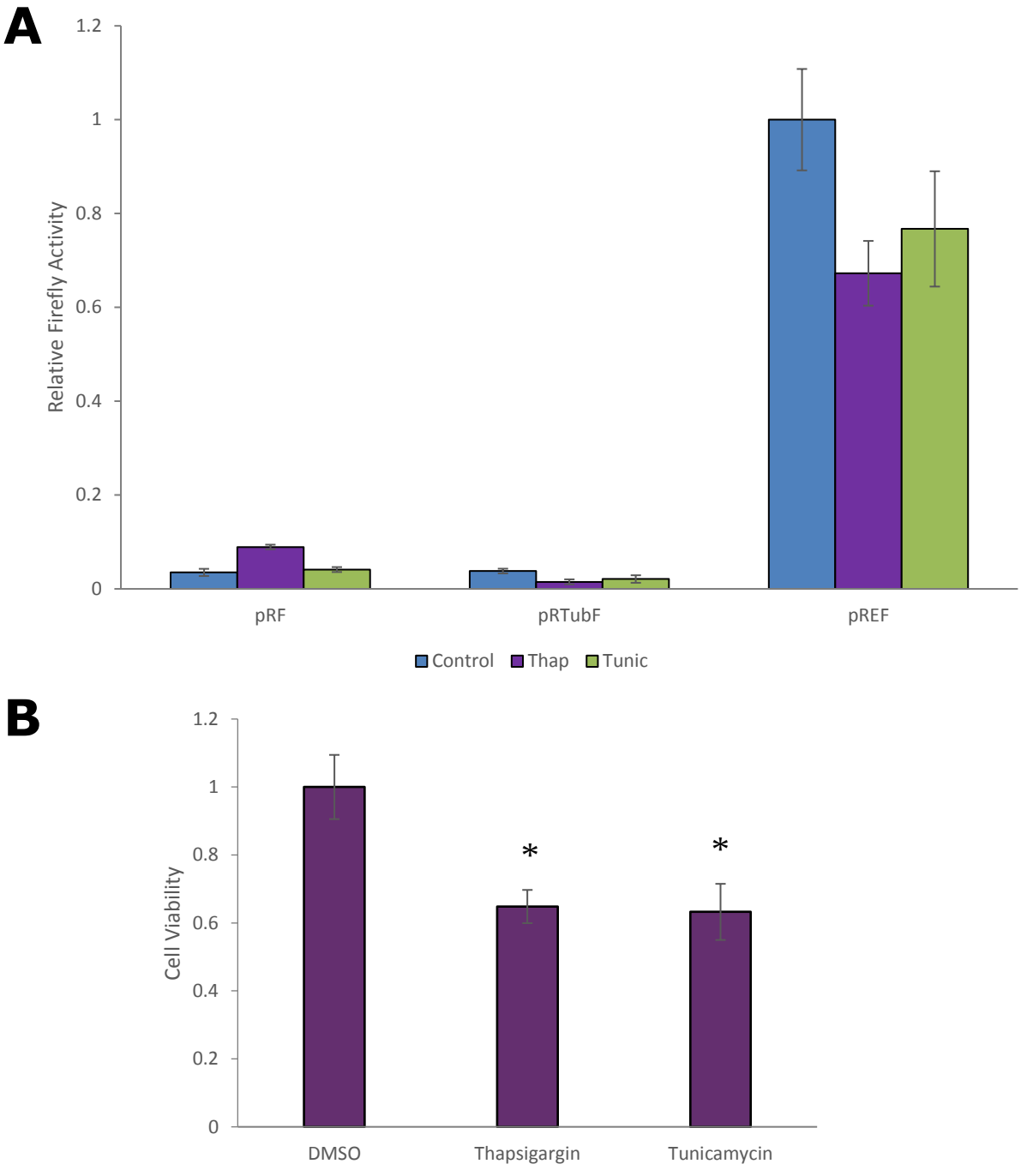

Figure 3.5 The Effect of Endoplasmic Reticulum Stress Inducers on EGFR IRES Activity in MCF7 cells. (A) pRF plasmids were transfected into MCF7 cells in a 24 well plate. 24 hours after treatment with either 1 μM thapsigargin or 4 mg/ml tunicamycin, cells were lysed and assayed for luciferase activity. Relative firefly activity is firefly luciferase activity divided by *Renilla* luciferase activity. Values are normalised to pREF control. n = 3, error bars represent standard deviation of three biological replicates. **(B)** Cell viability as measured by MTT assay after treatment with 1 μM thapsigargin, 10 mM tunicamycin or DMSO. n = 3, error bars represent standard deviation of three biological replicates. . "*" indicates $p < 0.05$. Significance tested by t-test.

3.3 Effect of Serum Starvation

Serum starvation mimics a nutritional deprivation of cells, most notably, a lack of amino acids and growth factors. Under such conditions, protein production is inhibited. In Alzheimer's disease both tau and BACE-1 have increased protein expression under serum starvation (Mohamed et al. 2014; Faghihi et al. 2008), and suggests that low nutrient availability could be a factor in an increased production in β-amyloid. A number of other IRESs have been shown to be active under serum starvation such as the sterol-regulatory-element-binding protein 1 (SREBP-1) (Damiano et al. 2010), XIAP (Holcik et al. 1999) and p27 IRESs (Miskimins et al. 2001). We thus assessed the activity of the EGFR IRES under serum starvation.

U87-MG and MCF7 cells were transfected with either pRF, pREF or pRtubF plasmids and subjected to 24 hours of serum starvation (0.5% FBS). In U87-MG cells, serum starvation caused relative firefly activity to increase for pREF by 2.7 fold, ($p < 0.05$) with *Renilla* luciferase activity dropping by 60% whilst firefly activity is retained (Fig 3.6a). In the empty vector and pRtubF, *Renilla* activity dropped by 55%, whilst pRtubF remained similar. This indicates EGFR translation in U87-MG cells is maintained during nutrient deprivation through IRES activity. Cell viability dropped by 20% following serum starvation (Fig 3.6b).

In contrast, serum starvation in MCF7 cells results in a reduction in both *Renilla* and firefly luciferase activity for pREF, resulting in no change in

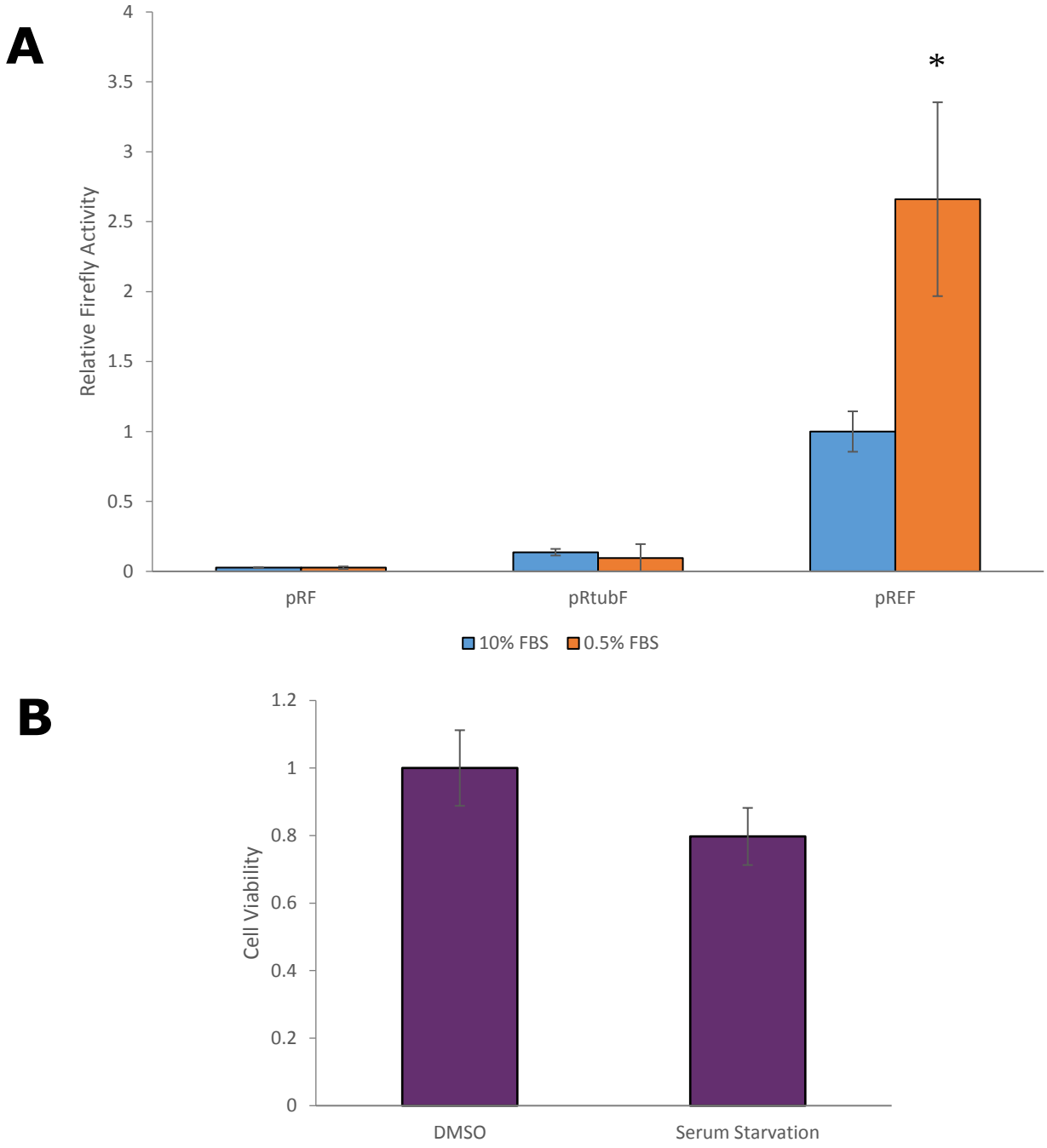

Figure 3.6 The Effect of Serum Starvation on EGFR IRES Activity in U87-MG cells. (A) pRF plasmids were transfected into U87-MG cells in a 24 well plate. 24 hours after serum starvation treatment, cells were lysed and assayed for luciferase activity. Relative firefly activity is firefly luciferase activity divided by *Renilla* luciferase activity. Values are normalised to pREF control. n =3, error bars represent standard deviation of three biological replicates. **(B)** Cell viability as measured by MTT assay after serum starvation treatment or DMSO. n = 3, error bars represent standard deviation of three biological replicates.. "*" indicates $p < 0.05$. Significance tested by t-test.

relative firefly activity ($p > 0.05$), as shown in figure 3.7a. This again may indicate there is cell specificity to the IRES' activity. Curiously, no reduction in cell viability was observed in MCF7 cells (Fig.3.7b), which may indicate the cell line is better able to withstand serum starvation. However, the presence of phenol red within the culture medium may explain this observation. Phenol red acts as a weak estrogen in MCF7 cells, activating the estrogen receptor and increasing proliferation (Berthois et al, 1986). Thus, in these circumstances cap-dependent translation initiation may not be inactivated in MCF7 cells, as signals for proliferation are received despite the low serum environment.

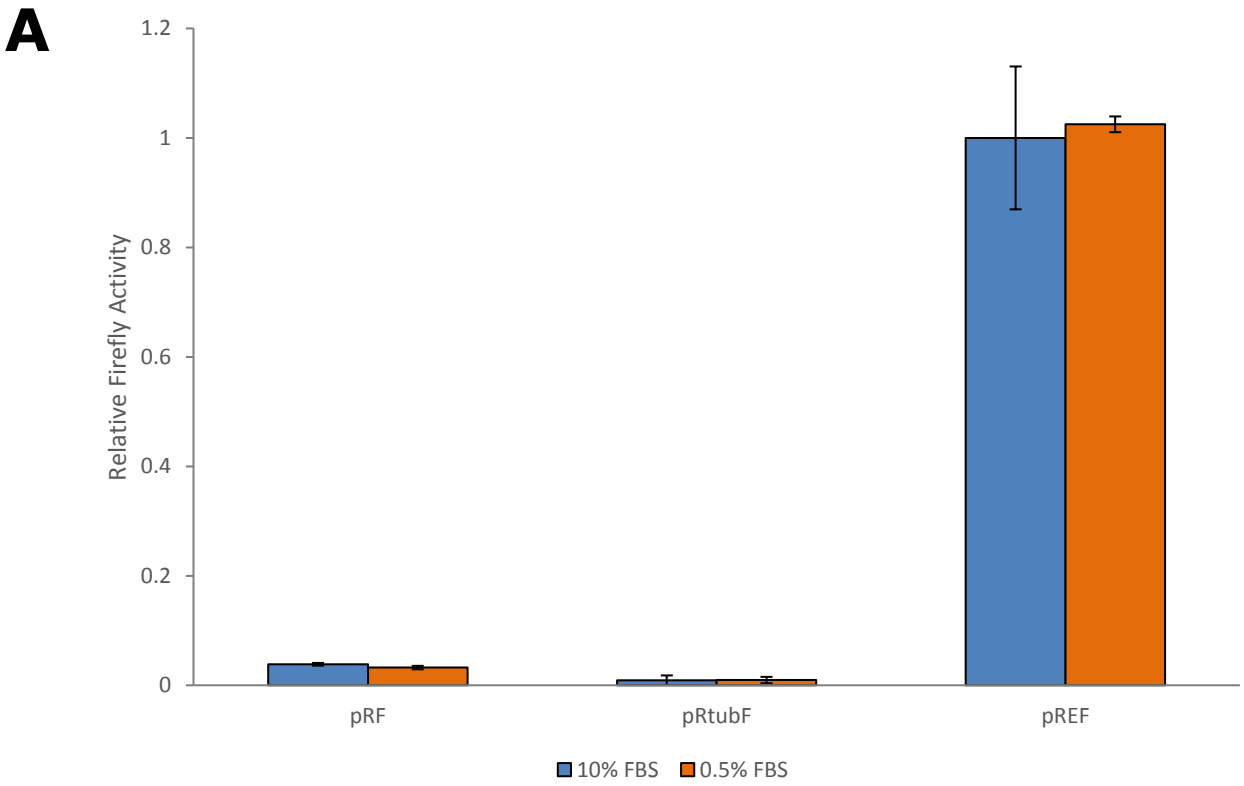

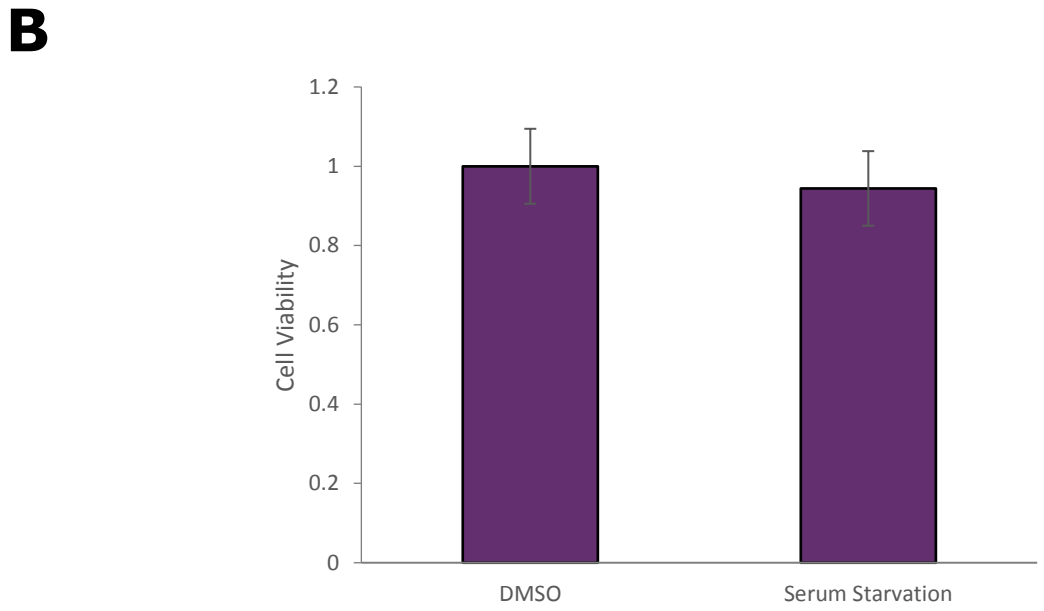

Figure 3.7 The Effect of Serum Starvation on EGFR IRES Activity in MCF7 cells. **(A)** pRF plasmids were transfected into MCF7 cells in a 24 well plate. 24 hours after serum starvation treatment, cells were lysed and assayed for luciferase activity. Relative firefly activity is firefly luciferase activity divided by *Renilla* luciferase activity. Values are normalised to pREF control. n = 3, error bars represent standard deviation of three biological replicates. **(B)** Cell viability as measured by MTT assay after serum starvation treatment or DMSO. n = 3, errors bars represent standard deviation of three biological replicates. Significance tested by t-test.

3.4 Effect of EGF Stimulation

EGF is one of several ligands of EGFR that results in downstream signalling and upregulation of genes involved in cell proliferation and growth. In Alzheimer's, low EGF plasma levels have been used as a biomarker to predict cognitive decline (Chen-Plotkin et al. 2011), although a number of studies found the opposite to be true (Bjorkqvist et al. 2012; Marksteiner et al. 2011). Along with this, EGF stimulates the production of two APP isoforms (Robakis et al. 1991). U87-MG cells were treated with increasing concentrations of EGF to determine the effects on IRES activity, compared with serum starved cells.

Treating cells with EGF resulted in a general increase in *Renilla* luciferase activity for pRF and pREF (Fig 3.8). The empty vector showed a 2.3 fold increase in *Renilla* for 50 ng/µl and 3.5 fold increase in 150 ng/µl and 200 ng/µl EGF, whilst for pREF this was 2.2, 2.3 and 2.7 fold respectively. These are significantly different from the control ($p < 0.05$, by ANOVA), but not statistically different from each other ($p > 0.05$, ANOVA) This indicates that general translation within the cells was increased. An increase was also found in firefly luciferase activity in pREF, but *Renilla* luciferase activity increased by a greater amount as reflected by the relative firefly activities shown in Fig.3.9. Relative firefly activity drops by 36%, 31% and 42% in pREF for 50 ng/µl (EGF+), 100 ng/µl (EGF++) and 200 ng/µl (EGF+++) EGF respectively ($p < 0.05$ against control, by ANOVA). This shows that, as would be expected, EGF causes an increase in overall translation, but that cap-dependent translation is the major source of this increase. The IRES is not favoured suggesting that the

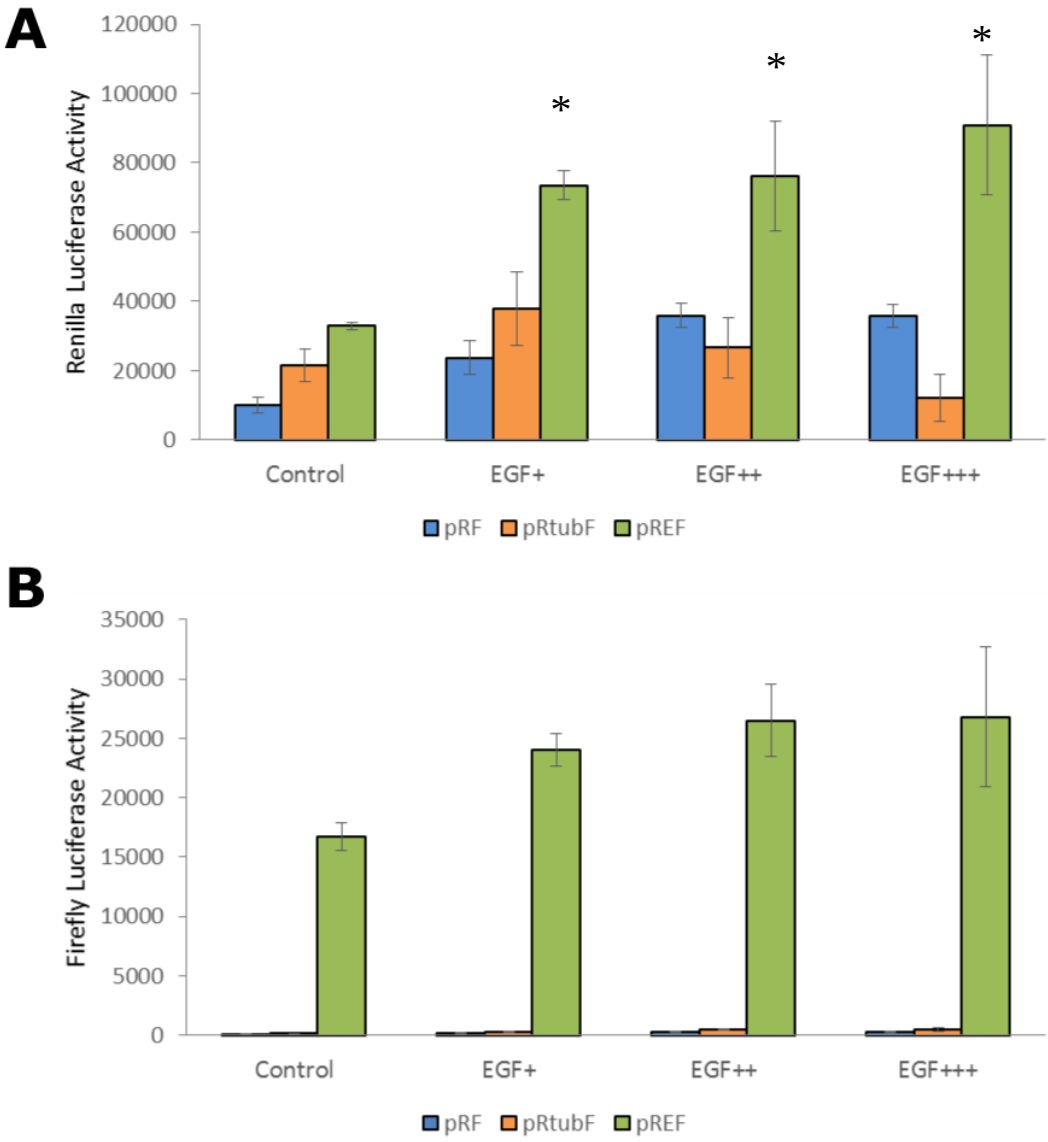

Figure 3.8 The Effect of EGF Stimulation on *Renilla* and Firefly luciferase Activity of pRF plasmids in U87-MG cells. pRF plasmids were transfected into U87-MG cells in a 24 well plate. 24 hours after serum starvation treatment, cells were treated with varying concentrations of EGF for 1 hour before being lysed and assayed for luciferase activity. n = 3, error bars represent standard deviation of three biological replicates. **(A)** *Renilla* luciferase activity **(B)** Firefly luciferase activity. EGF + = 50 ng/µl, EGF++ = 100 ng/µl, EGF+++ = 200 ng/µl.. "*" indicates $p < 0.05$. Significance tested by ANOVA.

cap is better at recruiting ribosomes. It could be the case that factors that aid in ribosome binding to the IRES are downregulated in response to growth factors.

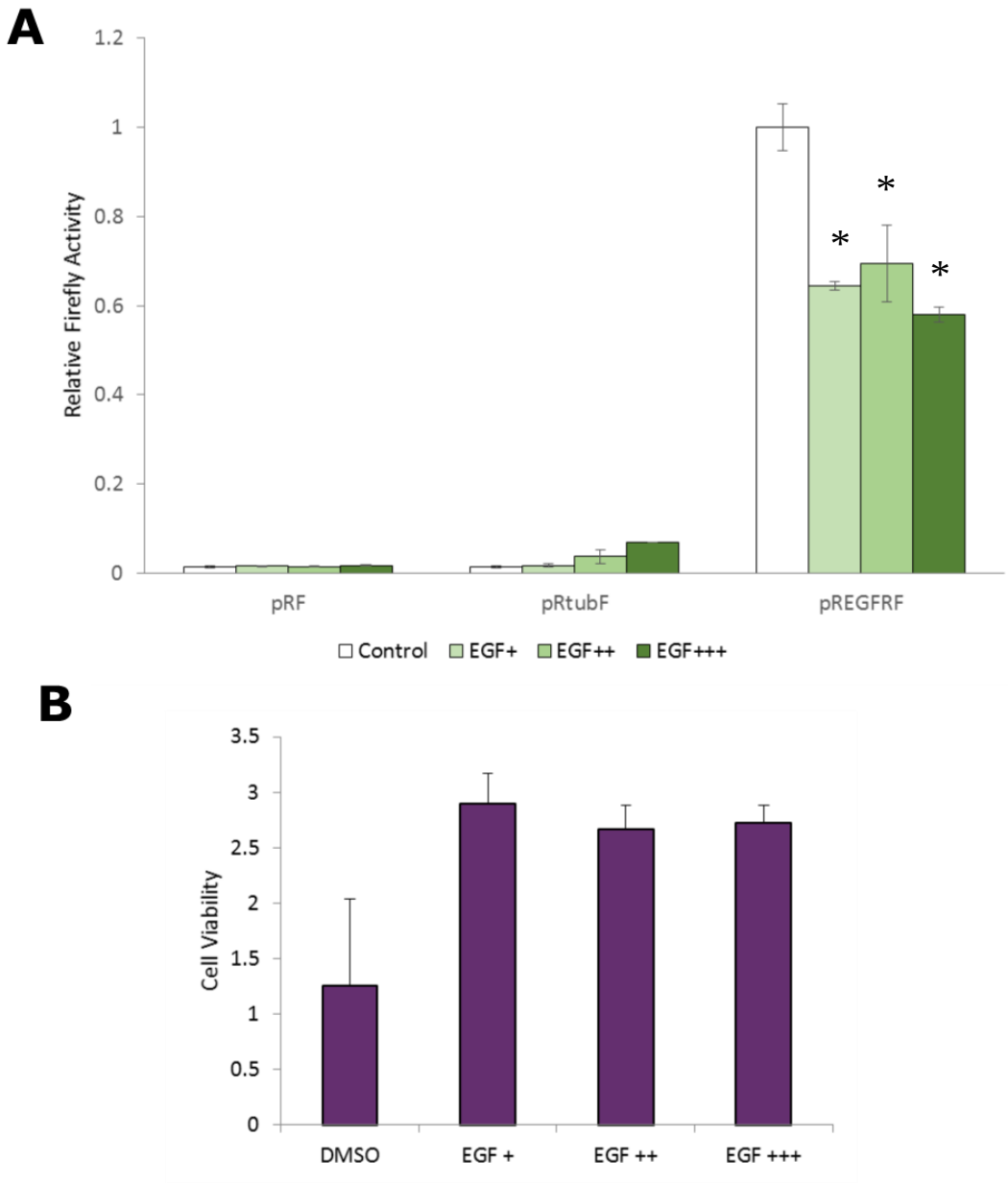

Figure 3.9 The Effect of EGF Stimulation on EGFR IRES Activity in U87-MG cells. (A) pRF plasmids were transfected into U87-MG cells in a 24 well plate. 24 hours after serum starvation treatment, cells were treated with varying concentrations of EGF for 1 hour before being lysed and assayed for luciferase activity. Relative firefly activity is firefly luciferase activity divided by *Renilla* luciferase activity. Values are normalised to pREF control. n = 3 error bars represent standard deviation of three biological replicates. **(B)** Cell viability as measured by MTT assay after serum starvation treatment or DMSO. n = 2, error bars represent standard deviation of three biological replicates. EGF + = 50ng/µl, EGF++ = 100ng/µl, EGF+++ = 200ng/µl. "*" indicates $p < 0.05$. Significance tested by ANOVA.

3.5 Deletion Analysis

A striking difference between many viral and cellular IRESs is their degree of modularity. Viral IRESs are extremely sensitive to deletions and point mutations, often disabling the IRES. This is particularly true at the 3'- boundary, close to the start codon, where deletion of just 11nts from the EMCV IRES completely abolishes activity (Kaminski, Belsham, and Jackson 1994). However the IGR IRES of *Dicistroviridae* contains two distinct domains which can function independently (Jang and Jan 2010). Many cellular IRESs are less sensitive to deletions and indeed smaller segments of the IRES are capable of initiating translation, but with a much lower activity (Stoneley and Willis 2004). It is thought that some cellular IRESs are modular, with each segment increasing the overall activity of the IRES. This can be through favourable binding sites for the ribosome, stabilising structures or binding sites for ITAFs. A segment could, for instance, hold binding sites for ITAFs that are only expressed under certain conditions, and hold the key to upregulating IRES-driven translation for that stress. Deletion analysis provides key information for how the IRES functions and which parts are key to activation. The c-myc IRES, one of the best characterised IRESs, has been analysed by deletion analysis which revealed that removal of individual predicted structures did not disable the IRES, but in concert had a much higher inactivation (Le Quesne et al. 2001). Alternatively, it has been shown that a short 50nt element is responsible for mediating translation (Cencig et al. 2004), similar to the *Gtx* IRES (Chappell, Edelman, and Mauro 2000). This element itself could be divided into two 14nt modules which act independently of each other

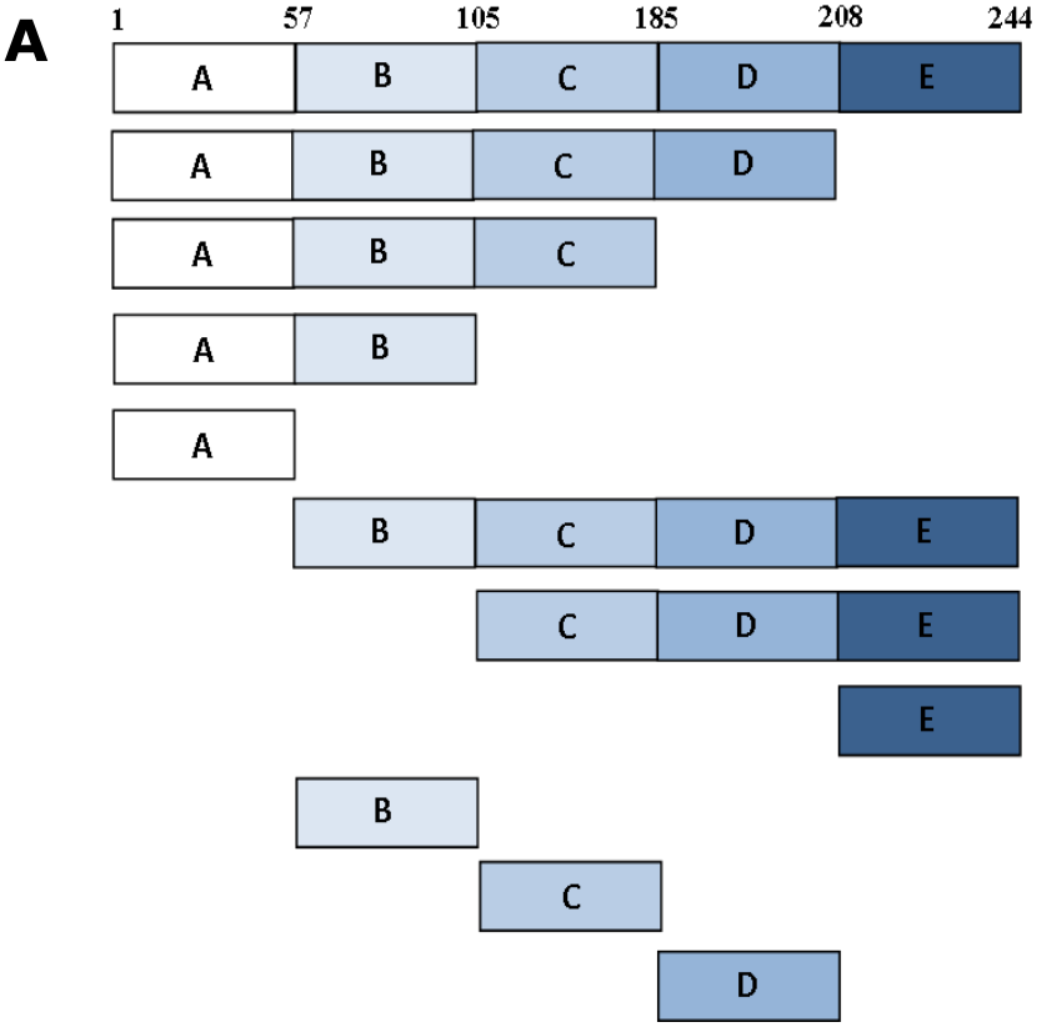

B

CCCCGGCGCAGCGCGGCCGCAGCAGCCTCCGCCCCCCG-
CACGGTGTGAGCGCCCGACGCGGCCGAGGCGGCCGGAGTC
CCGAGCTAGCCCCGGCGGCCGCCGCCGCCCAGACCGGACG
ACAGGCCACCGTCGGCGTCCGCCCGAGTCCCCGCCTCGCC
GCCAACGCCACAACCACCGCGCACGGCCCCCTGACTCCGT
CCAGTATTGATCGGGAGAGCCGGAGCGAGCTCTTCGGGGA
GCAGCG

Figure 3.10 Representation of the fragments of the EGFR 5'UTR. **(A)** The top construction is the full length, 244nt long 5'UTR. The numbers at the top show the boundaries between fragments. Fragments were inserted into the pRF vector at the SpeI and NcoI sites. **(B)** The EGFR 5'UTR sequence coloured coded for each fragment.

(Cencig et al. 2004), although there have been concerns that such short sequences may be splice sites or cryptic promotors (Lemp et al. 2012; Jackson 2013). In comparison, and despite their homologous activity, the L-myc IRES is more sensitive to deletion, with removal of less than 50nt from either the 5' or 3' end reducing IRES activity considerably (Jopling et al. 2004).

To assess the requirement of sections of the EGFR IRES for activity, sections of the IRES were amplified from pREF via PCR, using the corresponding primers as detailed in section 2.2.2, to generate a range of fragments. The lengths and sequences of these fragments are shown in figure 3.10. These fragments were then inserted into the pRF plasmid between the *Renilla* and firefly luciferase genes using the SpeI and Nco1 restriction sites. Fragment plasmids were then

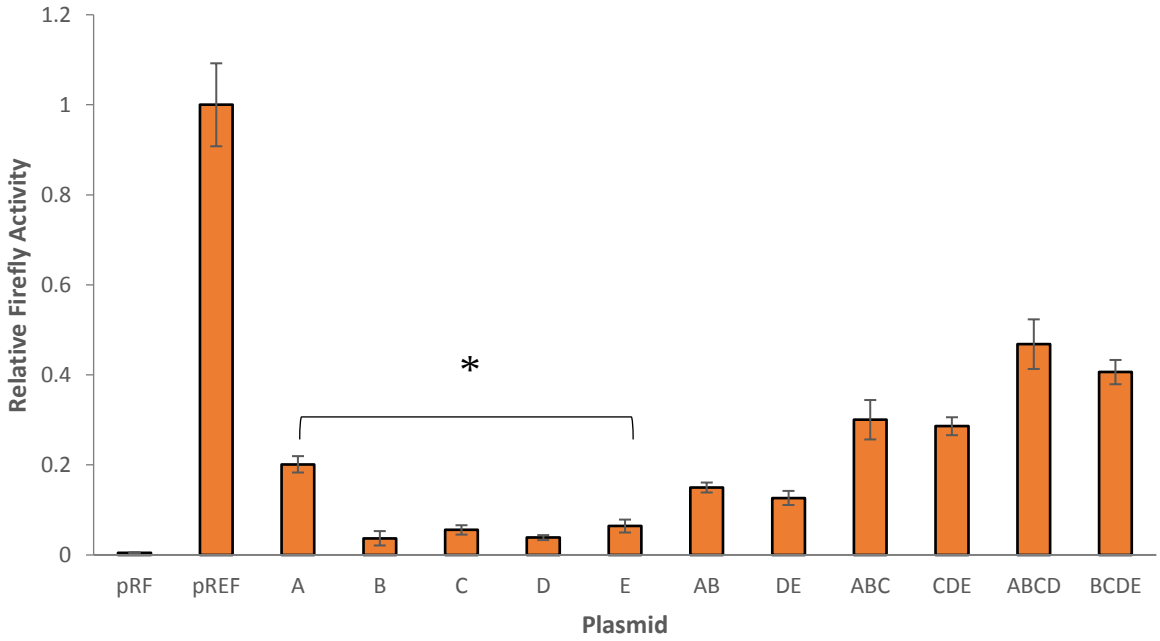

Figure 3.11 Deletion Analysis of the EGFR 5'UTR in U87-MG Cells. Truncated versions of the EGFR 5'UTR were transfected into cells in a 24 well plate. Cells were lysed and assayed for luciferase activity after 24 hours. Relative firefly activity is firefly luciferase activity divided by *Renilla* luciferase activity. Values are normalised to pREF control. n =3, error bars represent standard deviation of three biological replicates. "*" indicates $p < 0.05$. Significance tested by ANOVA.

transfected into U87-MG and MCF7 cells and after 24 hours the cells were lysed and the lysate assayed for luciferase activity.

In U87-MG cells it was observed that the fragments, B, C, D and E resulted in little firefly activity, each conferring less than 10% of the full length activity (figure 3.11). The first half of the sequence, ABC, and the second half, CDE, both showed a large reduction in relative firefly activity, at 30% and 29% that of the full length sequence. Removing the first 57nts from the sequence (fragment BCDE) results in a reduction of relative firefly activity by 61%. Interestingly, the first 57nts alone (fragment A) can confer 20% of the activity of the full length sequence, significantly more than fragments B, C, D or E ($p < 0.05$ by ANOVA) and has similar activity to fragments AB (15%), suggesting

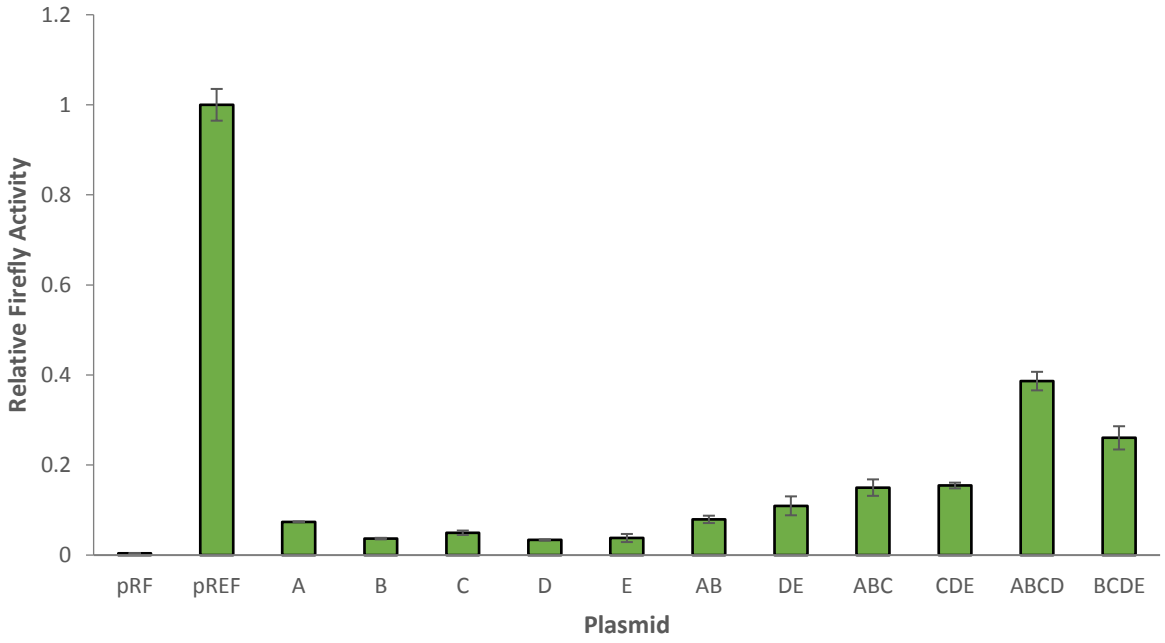

Figure 3.12 Deletion Analysis of the EGFR 5'UTR in MCF7 Cells. Truncated versions of the EGFR 5'UTR were transfected into cells in a 24 well plate. Cells were lysed and assayed for luciferase activity after 24 hours. Relative firefly activity is firefly luciferase activity divided by *Renilla* luciferase activity. Values are normalised to pREF control. n = 3, error bars represent standard deviation of three biological replicates. Significance tested by ANOVA.

that the first 57nts plays an important role in IRES function. Removal of just the final 36nts (fragment ABCD) reduces activity by 63%, despite fragment E itself generating under 10% activity of the full length, suggesting that the IRES is not modular and that the IRES relies on the entire sequence for full functionality.

Similarly, in MCF7 cells (figure 3.12) fragments B, C, D and E show little relative firefly activity, all under 5% that of the full length sequence, whilst AB and DE have a vastly reduced activity, at 8% and 11% respectively that of the full length. Again, ABC and CDE show slightly higher activity, although significantly lower than that of U87-MG cells both at 15% ($p < 0.05$ for both fragments, by ANOVA) that of the full length. Curiously, fragment A confers only 7% relative activity in MCF7 cells, a statistically significant reduction from the 20% found in U87-MG cells ($p = <0.05$, by ANOVA) however its absence reduces activity by 74%, as seen in fragment BCDE.

These data suggest that the activity of the EGFR IRES can be influenced by cell type. Both U87-MG cells and MCF-7 cells are known to express low levels of EGFR (Piao et al. 2009; Kuruppu 2016), however it is thought that EGFR amplification is a fundamental process in glioblastoma formation (Halatsch et al. 2006) and in a 3D format U87-MG cells produce a significantly higher amount of EGFR (Franovic et al. 2007). The differences in relative firefly activity for the truncated, 'A' IRES suggests a difference in the RNA binding proteins or ITAFs expressed between the two cell lines, which could either assist or inhibit IRES activity.

To assess whether parts of the IRES were responsible for mediating a response to stress conditions transfected cells were treated with the fragment plasmids with serum starvation and thapsigargin. In U87-MG cells, no effect was seen in B, C or D, activity remains zero in these. In A, no significant effect was observed ($p > 0.05$, by ANOVA). Serum starvation, as seen before, increased firefly activity in the full length 5'UTR by 24%. In the shorter sequences, serum starvation had a greater effect on CDE and BCDE than on the full length, increasing their relative firefly activities by 57% and 39% respectively ($p < 0.05$, by ANOVA) (figure 3.13). In AB, serum starvation raised relative firefly

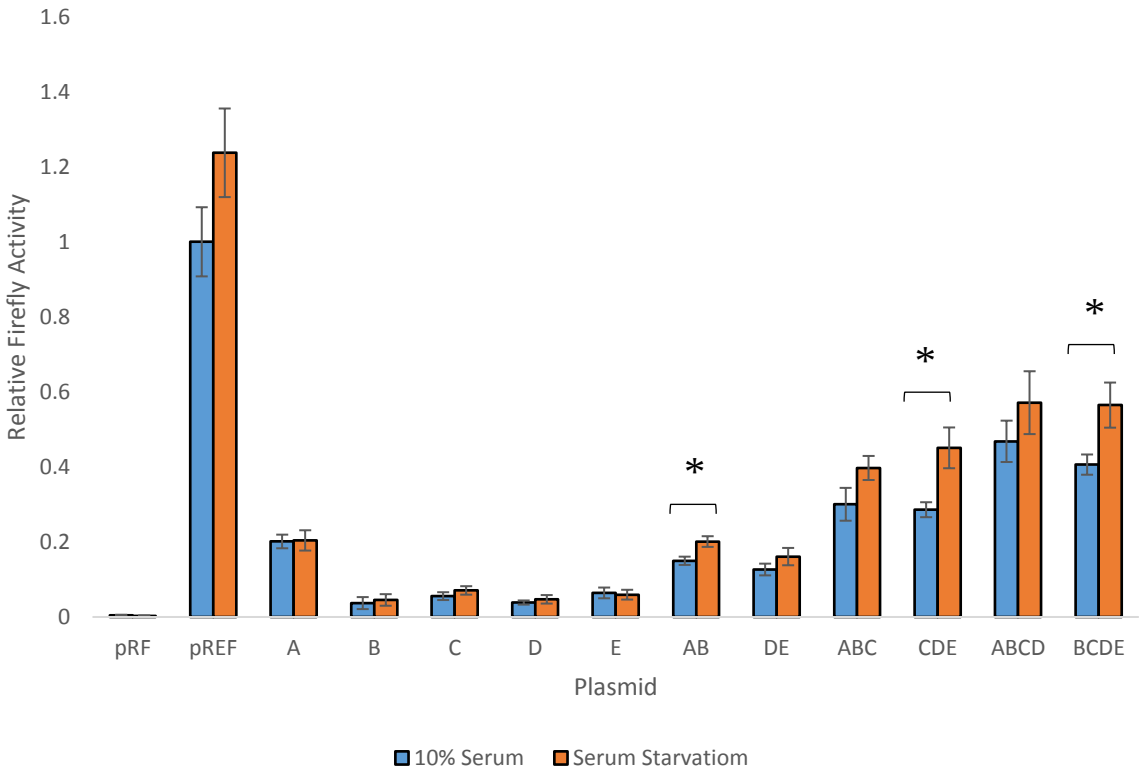

Figure 3.13 Deletion Analysis of the EGFR 5'UTR in U87-MG Cells after Serum Starvation. Truncated versions of the EGFR 5'UTR were transfected into cells in a 24 well plate. Cells were treated with media containing 0.5% FBS and lysed and assayed for luciferase activity after 24 hours of treatment. Relative firefly activity is firefly luciferase activity divided by *Renilla* luciferase activity. Values are normalised to pREF control. n = 3, error bars represent standard deviation of three biological replicates. "*" indicates $p < 0.05$. Significance tested by ANOVA.

activity by ~34%, ($p < 0.05$ by ANOVA), however serum starvation did not increase relative firefly activity significantly in A.

It was shown previously that thapsigargin dramatically reduced relative firefly activity in U87-MG cells (figure 3.4). The effect of thapsigargin treatment was tested on the truncated versions of the EGFR 5'UTR (figure 3.14). It was found that for the shortest fragments, B, C and D, no effect was seen, although this is not surprising due to the absence of firefly activity in the control. The A fragment displayed a 44% decrease in relative firefly activity. For the longer fragments, thapsigargin reduced relative firefly activity although the effect was

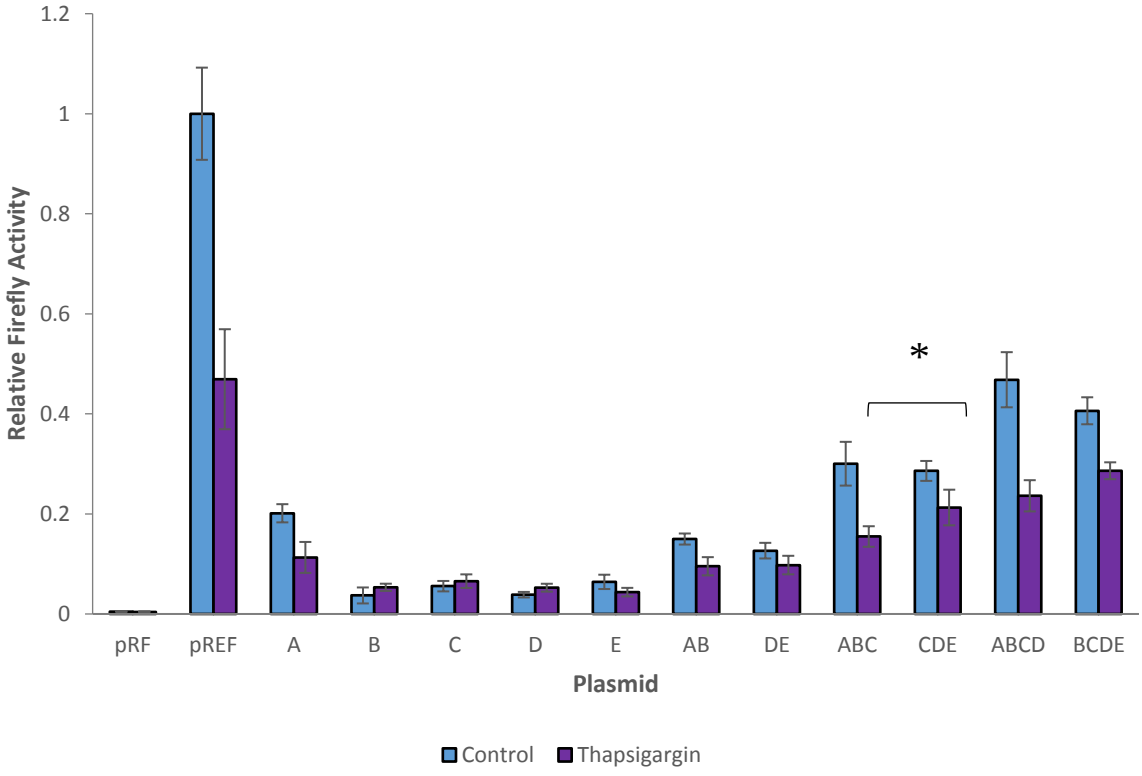

Figure 3.14 Deletion Analysis of the EGFR 5'UTR in U87-MG Cells after Treatment with Thapsigargin. Truncated versions of the EGFR 5'UTR were transfected into cells in a 24 well plate. Cells were treated with 1μM thapsigargin and lysed and assayed for luciferase activity after 24 hours of treatment. Relative firefly activity is firefly luciferase activity divided by *Renilla* luciferase activity. Values are normalised to pREF control. n =3, error bars represent standard deviation of three biological replicates. "*" indicates $p < 0.05$. Significance tested by ANOVA.

more limited than in control. The smallest effect was seen in DE with a reduction of 23%, followed by CDE at a 26% reduction, whilst AB, ABC and BCDE showed decreases by 36%, 48%, and 30%. This may indicate that the method by which thapsigargin inhibits the IRES is dependent on the 5' side of the UTR; the difference between the relative firefly activities of ABC and CDE is highly significant ($p < 0.05$ by ANOVA).

Previously it was discovered that the ribosome binds to the IRES was between bases 183 and 219, a location found within the DE fragment (Webb et al. 2015). However the data shown here indicate that the IRES remains active when this location is removed, as shown by the activity generated in the A, AB and ABC fragments. It is likely that the discovered landing site is where the majority of the ribosomes are recruited to the IRES but that a smaller proportion can bind further upstream. The reason for this is unknown, however there are IRESs which direct the expression of two different proteins from two different sites, but no alternative splice sites have been identified in the EGFR mRNA. It is possible that the recruitment further upstream is carried out by a specific factor, whose conditions to activating the IRES remain unknown, although the lowered activity observed in fragments A and AB and in MCF7 cells suggests it may not be expressed or is inhibited in these cells. The identification of this factor, or other ITAFs which bind to the IRES, may yield therapeutic targets against upregulation of EGFR.

3.6 Use of Hypoxic Mimics

The EGFR IRES has been shown to remain active under hypoxic conditions (Webb et al. 2015), but whether common hypoxic mimetics could be used as a substitute for a hypoxic chamber has not been recorded. Hypoxic mimics would represent an easier method to study the hypoxic activation of the EGFR IRES, but studying their effect on the IRES could also uncover the mechanism of hypoxic activation.

There are a number of compounds that have been identified as mimicking hypoxia. The three used here, Cobalt chloride ($CoCl_2$), deforoxamine (DFX) and Nickel Chloride ($NiCl_2$) all affect HIF1α. $CoCl_2$ stabilises HIF1α through binding to the VHL-binding domain (Yuan et al. 2003) and also appears to upregulate translation of HIF1α through the PI3K pathway (Chachami et al. 2004). DFX induces HIF1α activity through chelating iron (Wang and Semenza 1993). Nickel chloride induces HIF1α through an unknown mechanism (Goldberg, Dunning, and Bunn 1988; Salnikow et al. 2000). Three cell lines, SH-SY5Y, HeLa and MCF7, were transfected with pRF, pREF and pRtubF plasmids and treated with hypoxic mimics for 24 hours before being assayed for luciferase activity (Fig 3.15).

In all three cell lines both $CoCl_2$ and $NiCl_2$ had minimal effect on relative firefly activity, reducing activity by no more than 10%. DFX had a significant impact on relative firefly activity. In SH-SY5Y, DFX reduced activity by 32%, in HeLa

by 42% and in MCF7 by 36% ($p = 0.012$, 0.003 and 0.016 respectively, by t-test).

These effects are in contrast to that observed in hypoxia (Fig 3.16), where *Renilla* luciferase activity is reduced due to cap-dependent translation initiation inhibition, but firefly activity is retained, increasing the relative firefly activity by 62% in MCF7 cells and by 52% in U87-MG cells ($p < 0.05$). These data may indicate that use of hypoxic mimics does not produce an effect analogous to true hypoxia. Indeed, a number of studies display the differences between mimic and hypoxia. Reactive oxygen species (ROS) play a key part in hypoxic signalling yet DFX does not increase ROS levels (Bartolome et al. 2009). Meanwhile, the action of $CoCl_2$ appears to be dependent on ROS production in order to induce HIF1α (Triantafyllou et al. 2006). A large scale gene expression study on DFX treatment found that it altered the expression of around 1000 probe sets of which only 23% were also altered by hypoxia (Vengellur et al. 2005). Interestingly, hypoxic mimic activity is usually attributed to activation of HIF1α, not HIF2α. Although related, HIF1α and HIF2α are structurally different. Both are embryonically lethal when knocked out, yet act through different mechanisms (Kotch et al. 1999; Compernolle et al. 2002). Although $CoCl_2$ has been shown to activate both HIF1α and HIF2α in Huh7 cells it only activated HIF1α in liver cancer cells (Befani et al. 2013), suggesting cell specificity. HIF1α induces the glycolytic pathway (Wang et al. 2005) whilst HIF2α regulates genes important for tumour growth and cell cycle progression, for instance c-myc (Gordan et al. 2007). This leaves the intriguing question as to whether hypoxic activation of the EGFR IRES is directed through a HIF2α mechanism. It has already been

reported that HIF2α is recruited to the 3'UTR of EGFR during hypoxia, and is thought to contact the cap and upregulate cap-dependent expression (Uniacke et al. 2012).

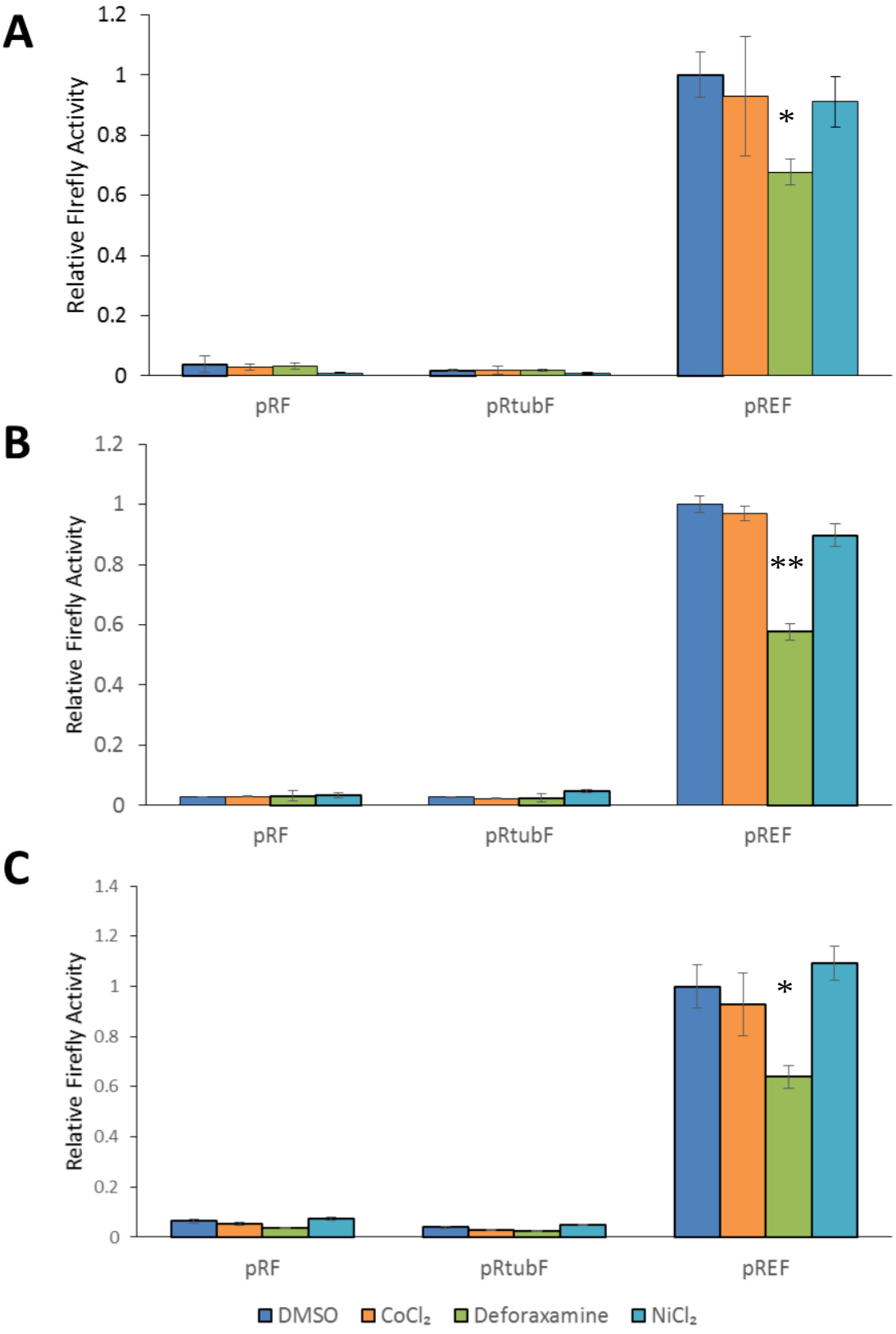

Figure 3.15. Effect of Hypoxic Mimics on the EGFR IRES in Three Cell Lines. pRF plasmids were transfected into SH-SY5Y (**A**), HeLa (**B**) and MCF7 (**C**) cells and were treated with either 75 µM $CoCl_2$, 0.65 mM DFX ,5 µM $NiCl_2$ or DMSO. 24 hours later cells were lysed and assayed for luciferase activity. Relative firefly activity is firefly luciferase activity divided by *Renilla* luciferase activity. Values are normalised to pREF DMSO control. n = 3, error bars represent standard deviation of three biological replicates. "*" represent $p < 0.05$, "**" represent $p < 0.01$. Significance tested by t-test.

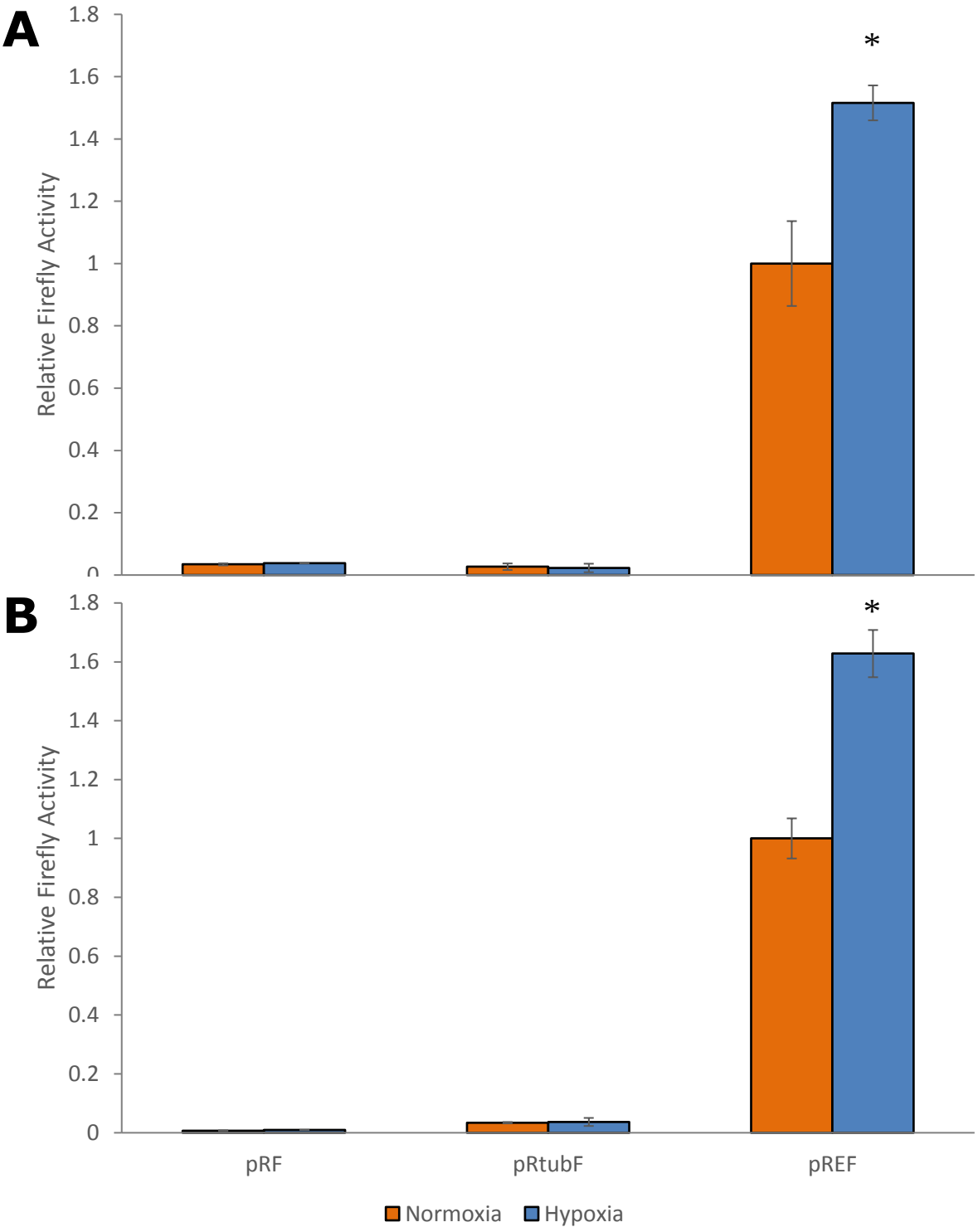

Figure 3.16. Effect of Hypoxic on the EGFR IRES in two Cell Lines. pRF plasmids were transfected into MCF7 (**A**) and U87-MG (**B**) cells and were exposed to 0.5% O_2 for 24 hours, before they were lysed and assayed for luciferase activity. Relative firefly activity is firefly luciferase activity divided by *Renilla* luciferase activity. Values are normalised to pREF normoxic control. n = 3, error bars represent standard deviation of three biological replicates. "*" represent p <0.05. Significance tested by t-test.

3.7 The 3'UTR in hypoxia

As mentioned in the previous section, it has been reported that an oxygen-regulated complex binds to a region within the EGFR 3'UTR and proceeds to contact the 5' cap to activate translation (Uniacke et al. 2012). Yet this report suggested that the 5'UTR alone does not confer hypoxic translation, in contrast to our previously reported data (Webb et al. 2015). The 3'UTR contacting the cap through binding proteins has been observed in both viruses and eukaryotes. Rotavirus mRNA is capped but not polyadenylated. The binding protein NSP3 binds to the 3'UTR and contacts the cap to circularise it to allow efficient translation (Vende et al. 2000), whilst in EMCV a polyA tail binding protein contacts the IRES in the 5'UTR (Bergamini, Preiss, and Hentze 2000). In eukaryotes, an interaction between the 5'UTR and 3'UTR of p53 is critical for its translation (Chen and Kastan 2010).

The effects of the 3'UTR on IRES activity was analysed in the p15 luciferase plasmid. The 3'UTR was inserted into the p15 vector downstream of the firefly luciferase ORF and either with or without the 5'UTR inserted upstream. These plasmids were then co-transfected with the lacZ plasmid for normalisation.

The introduction of the 3'UTR into the p15_EGFR plasmid resulted in a reduction in relative firefly activity in both normoxic and hypoxic conditions (69% and 68% respectively). However, the increase in relative firefly ratio between normoxia and hypoxia remained the same in each plasmid; in p15_E5'UTR relative firefly activity increases by 43%, in p15_E5'UTR+3'UTR the increase is 45% ($p < 0.05$). This indicates that the IRES is still capable of upregulating internal translation initiation but that the 3'UTR inhibits translation for both cap-dependent and cap-independent initiation.

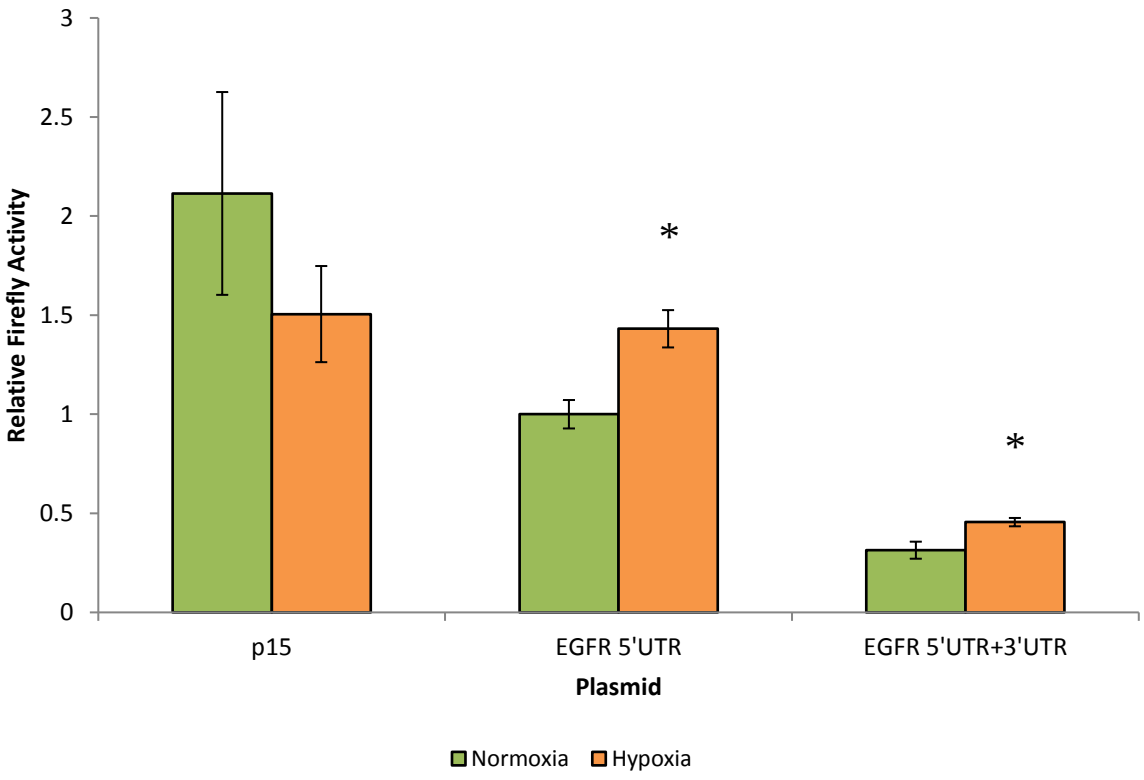

Figure 3.17 Effects of the 3'UTR of EGFR on IRES activity. The p15 vector, containing the 5'UTR with and without the 3'UTR of EGFR was co-transfected with the lacZ plasmid into U87-MG cells. Cells were exposed to either 0.5% O_2 or normoxic conditions for 24 hours before being lysed and assayed. Relative firefly activity is firefly luciferase activity divided by beta-galactosidase activity. Values normalised to EGFR 5'UTR normoxic firefly activity. n = 3, error bars represent standard deviation of three biological replicates. "*" represent $p < 0.05$. Significance tested by t-test.

Further investigation is needed to clarify these differing results. It is possible that the exact conditions used by Uniacke et al (2012)were different to ours, although the same cell type and conditions were used. Why the 5'UTR in their experiments shows no signs of IRES activity is unclear.

3.8 Blocking the IRES with Modified Oligonucleotides

Antisense oligonucleotides are short nucleotide sequences of RNA which bind to specific, complementary 'sense' mRNA, disrupting translation in a number of ways. The most common is through degradation by RNase H, a property found in morpholino type oligonucleotides. 2'-O-methyl (2'OMe) oligonucleotides do not have this property and are resistant to degradation by RNase H (Yoo et al. 2004). Duplexes formed from 2'OMe oligos have increased stability and binding affinity (Shen et al. 2003). 2'OMe oligonucleotides can block the binding of ribosomes at the initiation site when targeted to the 5' end of an mRNA, causing a reduction in protein expression (Summerton 1999). Anti-sense oligonucleotide therapies have been showing promise for a wide array of diseases including cancer and HIV (Dias and Stein 2002b; Jakobsen et al. 2007). Studies on blocking viral IRESs have been conducted, in particular on the hepatitis C virus IRES, with some success (Tallet-Lopez et al. 2003). Antisense oligonucleotides have also been studied for their potential in increasing translation from downstream primary ORFs by blocking uORFs (Liang et al. 2016). It is thought that oligonucleotides can be unwound by the ribosomal machinery as it is scanning, but targeting start codons and regions proximal to the cap impede translation (Dias and Stein 2002a). Here, the

effectiveness of 2'OMe oligonucleotides in blocking ribosomal entry at the IRES, and thus the inhibition of cap-independent translation initiation whilst leaving cap-dependent translation unaffected was investigated.

The 2'OMe oligonucleotide sequences can be seen in table 3.1. Two oligonucleotides were designed which were complementary to the region within the IRES previously identified as the ribosome binding site. Three control oligonucleotides were used. These were the upstream control, which is complementary to a region in the 5'UTR of EGFR 5' to the region previously identified as the ribosome binding site. The positive control oligo is complementary to the start codon of the firefly luciferase ORF. The Scrambled

Oligo Name	Sequence (5'-3')	Description
IRES1	AUACUGGACGGAGUCAG	Binds to 5'UTR between nts 191-207
IRES2	CCGGCUCUCCCGAUCA	Binds to 5'UTR between nts 208-223
Upstream Control	GGCGCUCACACCGUGCGG	Binds upstream of ribosome landing site, at nts 36-44
Scrambled 17	GCGGAUCGAACGAAUGU	Scrambled version of IRES1
Positive Control	GGCAUCUUCCAUGGUGGCUU	Binds at the luciferase start codon

Table 3.1 Modified Oligonucleotide Sequences. Sequences are complementary to the regions the oligonucleotides bind to in the mRNA, as stated in the description. Each nucleotide within the oligonucleotide has the 2'O-methyl modification.

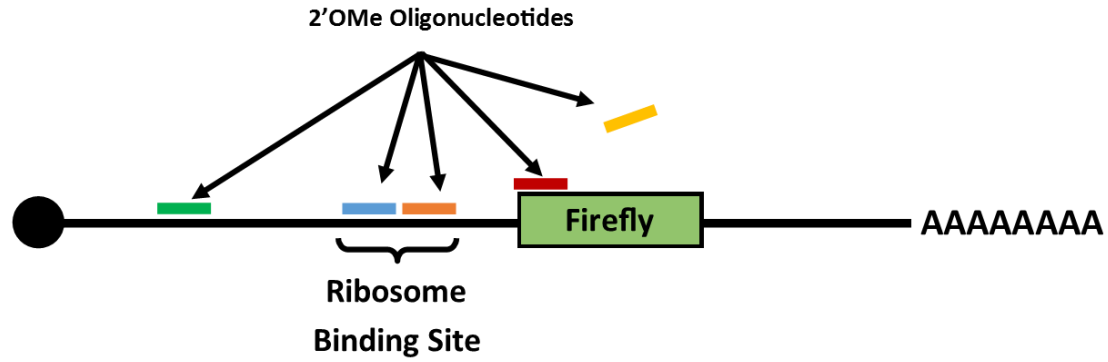

CCCCGGCGCAGCGCGGCCGCAGCAGCCTCCGCCCCCCGCACGGTGTGAGCGCCCGACGCG
GCCGAGGCGGCCGGAGTCCCGAGCTAGCCCCGGCGGCCGCCGCCGCCCAGACCGGACGAC
AGGCCACCGTCGGCGTCCGCCCGAGTCCCCGCCTCGCCGCCAACGCCACAACCACCGCGC
ACGGCCCCCTGACTCCGTCCAGTATTGATCGGGAGAGCCGGAGCGAGCTCTTCGGGGAGC
AGCG

Figure 3.18 Schematic of Modified Oligonucleotide Attack on the EGFR 5'UTR. Two oligonucleotides were designed that bound to the ribosome binding region, IRES1 (blue bar) and IRES2 (orange bar). A positive control (red bar) binds the start codon of the firefly ORF, whilst an upstream control (green bar) binds upstream of the ribosome binding site. A scrambled sequence version of IRES1 (yellow bar) was used as a negative control.

17 oligo is not complementary to any region, a scrambled version of the IRES1 oligo, it is designed to reveal any inherent toxic effect of the oligonucleotides on translation. The oligonucleotide binding sites can be seen in figure 3.18 Oligonucleotides were transfected into U87-MG cells that were previously transfected with the p15 or p15E plasmids along with the LacZ plasmids as a control, as described in section 2.1.5.

The effectiveness of the oligonucleotides is demonstrated in Figure 3.19. Firstly, the effectiveness of 2'OMe oligos to block translation is demonstrated by the positive control, reducing relative firefly activity in all constructs and conditions, significantly reducing activity by 73% and 74% in p15 and p15E in

normoxia respectively and 71% and 72% in p15 and p15E in hypoxia, when compared to non-transfected cells (p = <0.005 in all cases).

In p15, all other oligos perform as expected and have no significant effect on relative luciferase activity in either normoxia or hypoxia, having no binding sites on the plasmid. The effect of the oligos in p15E however require more in depth analysis. Firstly, the IRES1 and IRES2 oligos have differing effects on luciferase activity. IRES2 appears to have no impact on IRES mediated translation, with a non-significant reduction in normoxia of 12% and hypoxia of 3.5% when

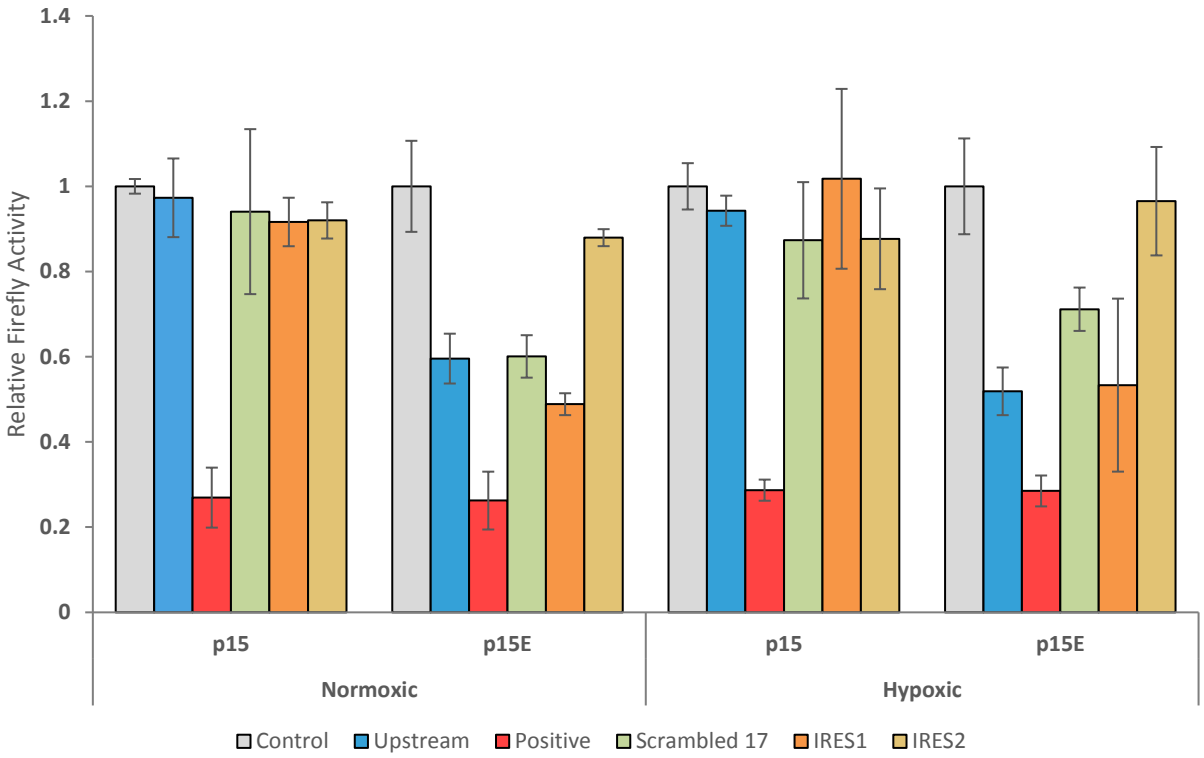

Figure 3.19 Oligonucleotide Attack of the EGFR IRES. U87-MG cells were transfected with p15 or p15E, along with lacZ. Oligonucleotides were then transfected into the cells and cells exposed to hypoxic or normoxic conditions for 24 hours before lysis and assaying for luciferase activity. Values normalised to DMSO control (grey bars). Relative firefly activity is firefly activity divided by beta-galactosidase activity. n = 2, error bars represent standard deviation of three biological replicates. Significance tested by t-test.

compared to the untransfected control. This is in contrast to IRES1, which significantly reduces relative luciferase activity by 51% in normoxia and 47% in hypoxia ($p = <0.005$ and 0.006 respectively), with no effect on p15. This may suggest that ribosomes bind the 5'UTR before nt 208, reducing the current ribosome landing area by 13 nucleotides. However, the oligonucleotide may fail to bind to the mRNA. Oligonucleotides must compete for binding with secondary structures and binding proteins (Dagle and Weeks 2001). Further experimentation with oligonucleotides binding to different regions and of different lengths could validate whether ribosomes bind to the region.

The upstream oligo appears to unexpectedly exert some effect on translation. Whilst no effect is seen on p15 transfected cells, in p15E transfected cells a reduction of 40% and 48% is seen in normoxia and hypoxia respectively. This reduction is significant ($p = <0.005$). The proximity of the oligo to the cap (position 36 in the 5'UTR) may interfere with cap-dependent ribosomal binding. It is thought that the helicase activity of the translation initiation complex can remove short RNA oligonucleotides from mRNA (Dagle and Weeks 2001), but it may be that the oligonucleotide is too long for the helicase to effectively unwind or too close to the cap. However, if the helicase could not remove the oligonucleotide it should be the case that both the IRES1 and IRES2 oligo would be capable of blocking both cap and cap-independent translation, which should reduce firefly activity to a level similar to that of the positive control oligo. A length of 20 nucleotides is long enough to prevent leaky scanning (Kozak 1991), therefore the 36 nucleotides before the upstream oligonucleotide binding site should be enough for the formation of the pre-initiation complex. Thus it is likely

that the reduction observed is indeed related to IRES mediated initiation. There are two possibilities of how the upstream oligo can affect IRES-mediated initiation. The first is that more ribosomes enter the 5'UTR further upstream than previously thought. There is a significant difference between the upstream and IRES1 luciferase activities ($p = 0.036$), with IRES1 reducing activity 11% more than upstream, thus it is possible that more ribosomes are impeded at the primary entry point between nucleotides 191-208, and a smaller percentage blocked further upstream. The second possibility is that the binding of the antisense oligonucleotides to the 5'UTR compromises the structure of the IRES. Antisense oligonucleotides have been shown to disrupt RNA secondary structure in HIV (Vickers et al. 1991) and in rabbit reticulocytes (Walker, Elela, and Nazar 1990), inhibiting protein synthesis (Crooke 1992). Thus it may not be necessary to block the ribosome entry site to reduce IRES activity, rather the disruption of the structure may be just as effective.

The scrambled 17 control oligo also displays unexpected results, significantly reducing luciferase activity by 40% and 29% in p15E in normoxic and hypoxic conditions respectively ($p = <0.005$ in both cases). Toxicity caused by oligonucleotide transfection is often a concern, although Crooke *et al* argue that these concerns from early experiments were caused by poor oligonucleotide preparation, resulting in impurities entering the cells with the oligonucleotides (Crooke and Mirabelli 1992). Further, no reductions in luciferase activity was observed in the p15 transfected cells, suggesting that the oligonucleotide specifically affects the sequence in the p15E vector. The likely cause is that the oligo binds the 5'UTR despite the scrambled sequence. A four nucleotide

stretch, *CGGA*, is the only commonly shared sequence between the IRES1 and scrambled oligo, however the first seven nucleotides of the scrambled oligo is complementary to nts 136-142 within the 5'UTR which was not detected before synthesis. It will be important to test new scrambled oligos on the 5'UTR before further experiments are conducted.

3.9 Characterising the Structure of the 5'UTR with SHAPE

The importance of structural motifs in cellular IRESs is debated. Viral IRESs have been found to possess structures that can recruit ribosomal subunits (Wilson et al. 2000) and initiation factors (Kolupaeva et al. 1998; Lopez de Quinto and Martinez-Salas 2000). A number of viral IRESs have also been shown to share structural similarities without sequence similarity, such as the HCV IRES and CSFV IRES (Brown et al. 1992) and EMCV with other cardiopicornaviruses (Pilipenko et al. 1989). However, such similarities have not been found in cellular IRESs. The closely related transcription factors L-myc and c-myc both contain IRESs but with very different structures (Le Quesne et al. 2001; Jopling et al. 2004). This may reflect greater diversity in the conditions under which cellular IRESs are active. Whereas viral IRESs can be viewed as a tool used by viruses to hijack translational machinery during global translation inhibition, cellular IRESs are more likely to be involved in promoting expression of a particular mRNA in response to a plethora of conditions. For example, the apoptosis pathway features a number of important proteins promoted through IRES-mediated translation initiation (Spriggs et al. 2005).

It has been reported that cellular IRESs with weaker secondary structure, as defined by Gibbs free energy, have higher activity (Xia and Holcik 2009), suggesting that structure can play a part in regulating IRES activity. Indeed, the Apaf-1 and Bag-1 IRESs require the binding of their ITAFs which remodel the

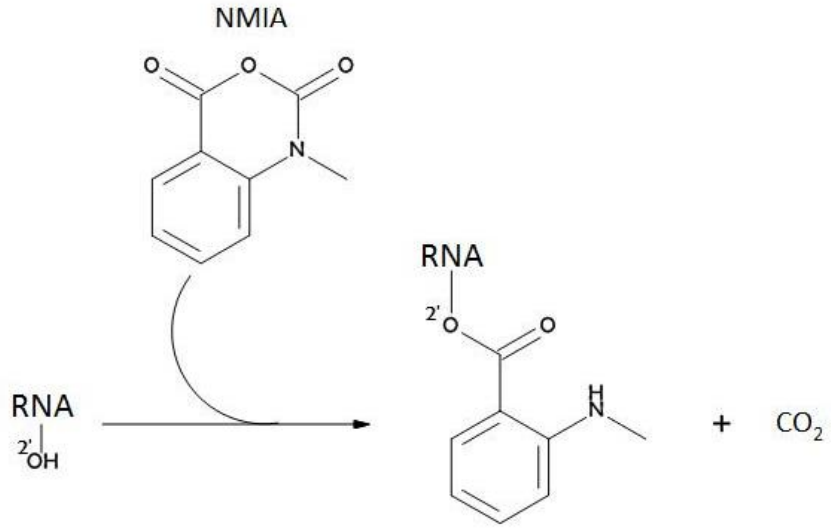

Figure 3.20. Reaction of N-methylisotoic anhydride (NMIA) with RNA. When RNA is in a flexible conformation, NMIA forms the ester at the 2' position on the nucleotide's ribose.

local structure to a single stranded region to allow ribosomes to bind (Mitchell et al. 2003; Pickering et al. 2004) and PTB acts as an RNA chaperone for the EMCV IRES, stabilising its structure, required for its activity (Kafasla et al. 2009).

Thus, resolving an IRES' structure is important for determining the overall function and regulation of the IRES and this knowledge can then be exploited to create new therapeutics. Mapping of RNA secondary structures can be done in a number of ways. Traditional methods use enzymes, such as RNase A, V1 and T1 or chemical reagents (e.g. Dimethyl sulphate (DMS), kethoxal (KE)), to cleave bonds between nucleotides in the backbone of the RNA, thus generating fragments of RNA that can be analysed on polyacrylamide gels after primer extension (as reviewed in (Stern, Moazed, and Noller 1988)). The c-myc and L-myc IRESs have been characterised in this way (Le Quesne et al. 2001; Jopling

et al. 2004). However to generate a full picture of the RNA structure multiple enzymes must be used in concert, increasing experimental complexity – it is difficult to combine the individual enzymic reactivities into a clear structure (Merino et al. 2005).

Selective 2'-Hydroxyl Acylation and Primer Extension (SHAPE) was developed in the early 2000's and exploits the dependence of the reactivity of the 2'-ribose position in the RNA on the position of 3' phosphodiester anion (Chamberlin, Merino, and Weeks 2002). SHAPE allows for a single reagent to score every nucleotide in an RNA sequence on its ability to react with the reagent. The 2' hydroxyl group of RNA is readily accessible to reagents when single stranded, however when involved in a structure, whether secondary or tertiary, reactivity is reduced. These 2'O adducts block the passage of reverse transcriptase, such that cDNA sequences can be generated from treated RNA to create a library of cDNA fragments of varying lengths (Merino et al. 2005). Combined with a radiolabelled primer, the cDNA can be analysed by polyacrylamide electrophoresis and SHAPE reactivities assigned to single nucleotide resolution. The reagent N-methylisotoic anhydride (NMIA) has been shown to be a particularly effective reagent for SHAPE, forming a 2-methylaminobenzoic acid nucleotide 2' ester, as shown in figure 3.20.

Fragment 1
CCCCGGCGCAGCGCGGCCGCAGCAGCCTCCGCCCCCCGCACGGTGTGAGCGCCCGACGCG
GCCGAGGCGGCCGGAGTCCCGA

Fragment 2
GCTAGCCCCGGCGGCCGCCGCCGCCCAGACCGGACGACAGGCCACCGTCGGCGTCCGCCC
GAGTCCCCGCCTCGCCGCCAAC

Fragment 3
GCCACAACCACCGCGCACGGCCCCCTGACTCCGTCCAGTATTGATCGGGAGAGCCGGAGC
GAGCTCTTCGGGGAGCAGCG

5' Linker
GGCCUUCGGGCCAA

3' Linker
UCGAUCCGGUUCGCCGGAUCCAAAU

RT Binding Site
CGGGCUUCGGUCCGGUUC

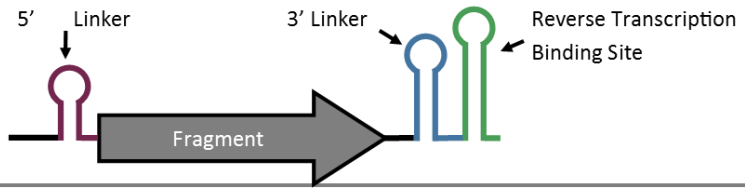

Figure 3.21. Fragmented Sequences of the EGFR 5'UTR used in SHAPE. The two flanking linkers and the reverse transcriptase binding region. The lower diagram shows the position and folding of the flanking regions in the mRNA.

A schematic of the protocol for SHAPE can be seen in figure 3.22, and is described in detail in section 2.5. To study structural motifs within the EGFR IRES we performed SHAPE analysis on three segments of the 5'UTR, each ~80 nucleotides in length. These segments are fragment 1, spanning nucleotides 1-82, fragment 2 spanning nucleotides 83-163 and fragment 3 spanning nucleotides 164-244. The sequences of the fragments can be seen in figure 3.21.

The resulting sequencing gel images can be seen in figure 3.23. Intensities of bands were measured using ImageJ. The band relating to the full-length

extension product (as seen in figure 3.23) was used to normalise each band in the corresponding lane, to account for differences in total cDNA between lanes. In order to discount structure induced pausing of the reverse transcriptase, absolute NMIA activities were calculated by subtracting the intensities from the (-) lane from the intensities from the (+) lane at each position. Absolute reactivities were normalised according to the boxplot method (Hajdin et al. 2013) to place reactivity on a scale from 0 to 2, as described in section 2.5.9. The SHAPE reactivities of fragments 1, 2 and 3 can be seen in figures 3.24, 3.25 and 3.26 respectively.

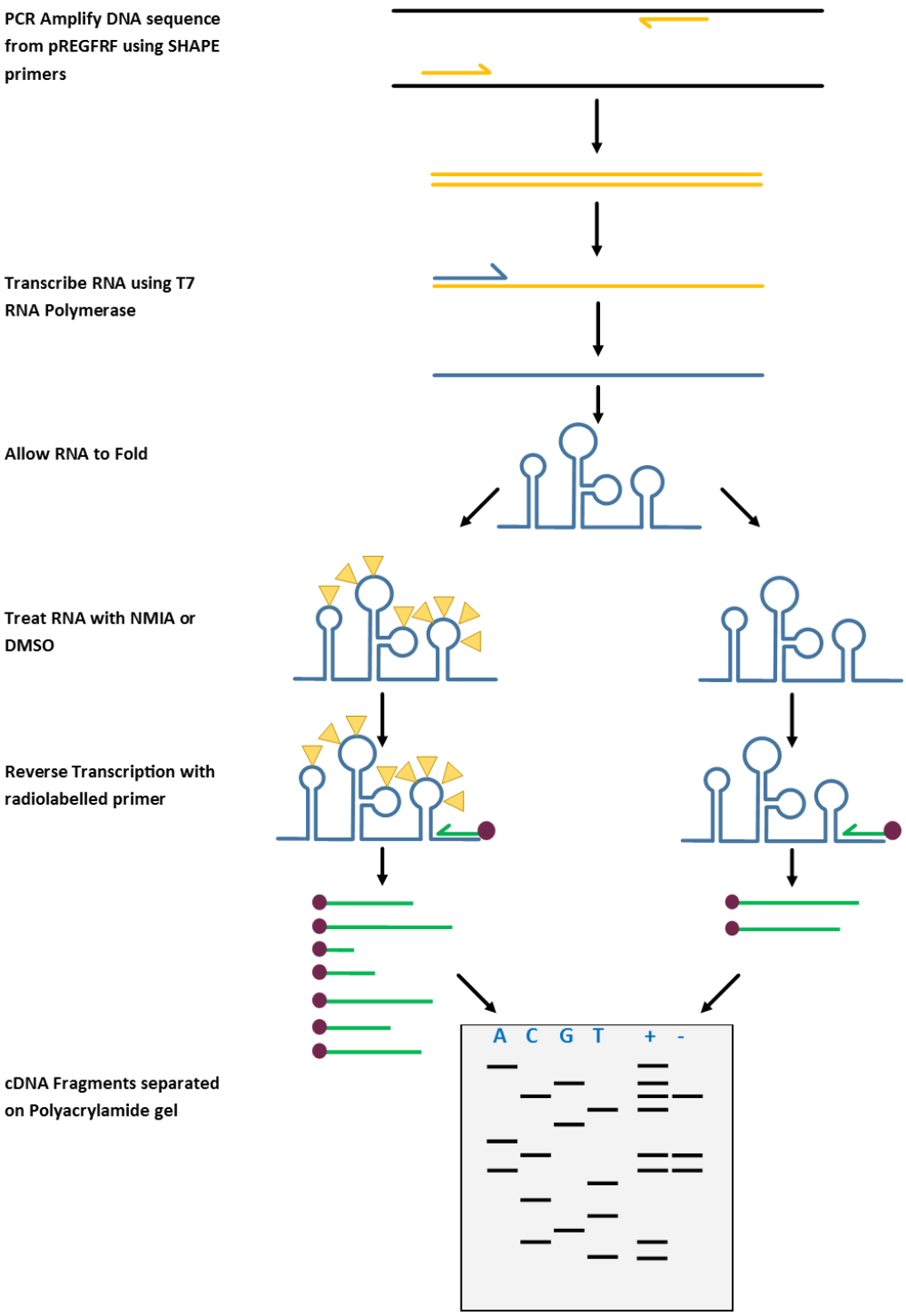

Figure 3.22. Schematic Diagram of SHAPE Protocol. Black lines = Plasmid DNA, yellow lines = PCR amplified DNA, blue lines = RNA, green lines = cDNA. Yellow triangles represent NMIA, whilst mauve dots represent ^{32}P radiolabels.

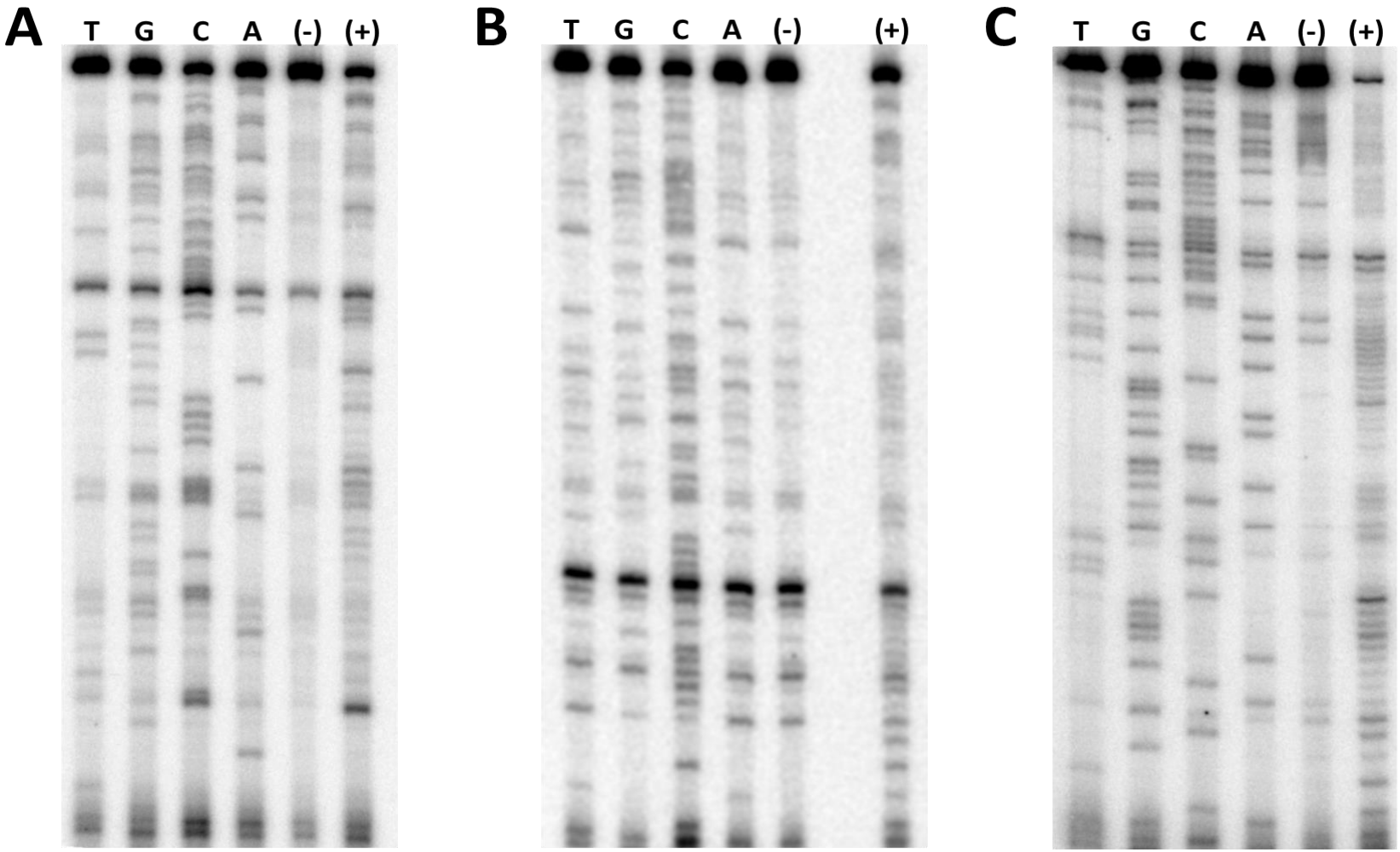

Figure 3.23. SHAPE Analysis of the EGFR 5'UTR. The three 5'UTR fragments were transcribed into RNA, treated with NMIA and reverse transcribed into cDNA using a radiolabelled primer. Resulting fragments were then run on an 8% polyacrylamide gel for 1.5-2hrs at 1000v and then exposed to phosphorimaging plates overnight. Representative gels of fragments 1, 2, and 3 are shown in **A, B** and **C** respectively. (-) represents DMSO treated RNA, (+) represents RNA treated with 10mM NMIA.

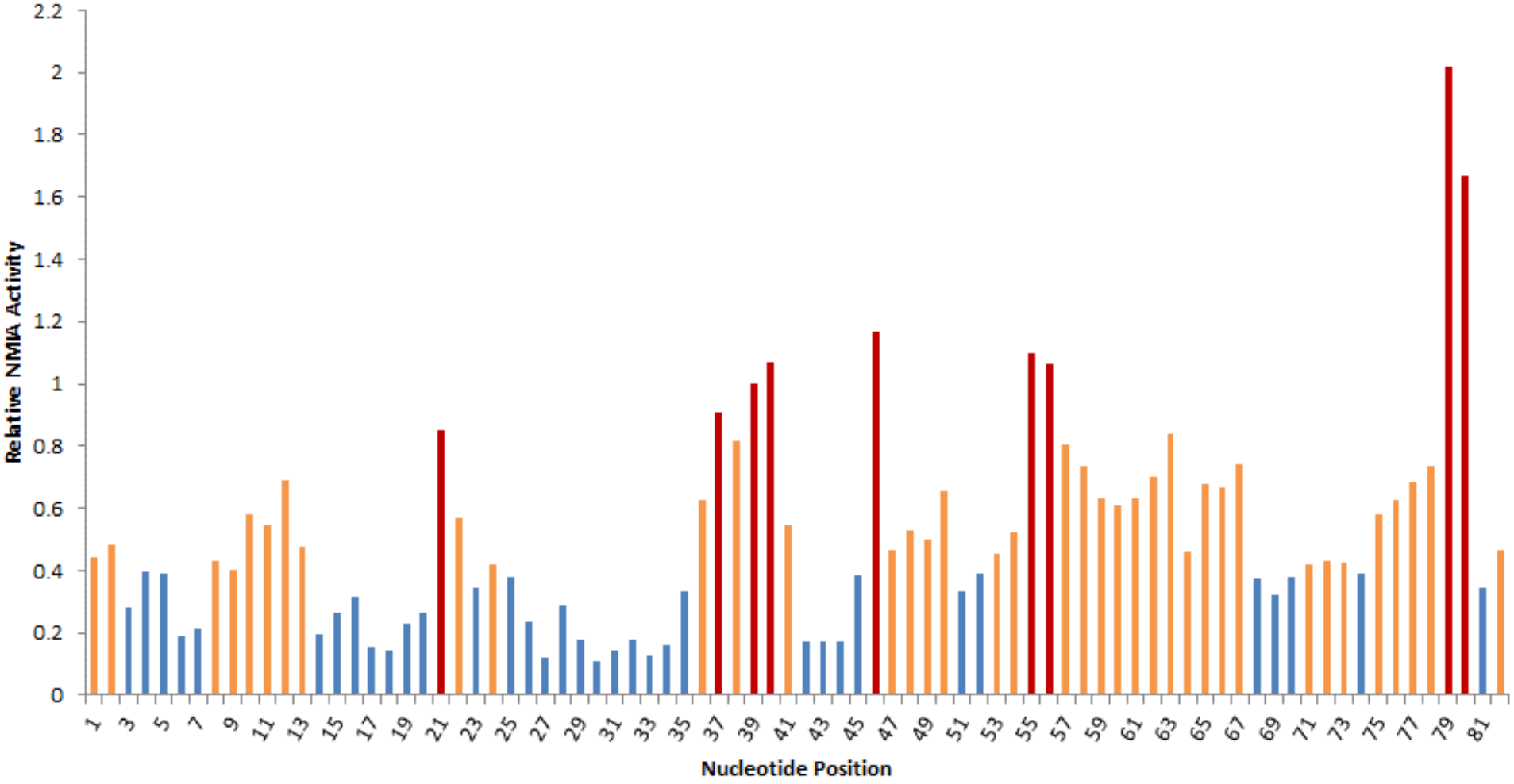

Figure 3.24. SHAPE analysis of Fragment 1. Relative NMIA reactivity is derived from the 10% most reactive nucleotides. Red bars represent nucleotides with relative reactivity > 0.85, orange bars represent relative reactivity between 0.84 – 0.4, whilst blue bars represent nucleotides with < 0.4 relative reactivity. n = 3, values are the average of three separate repeats.

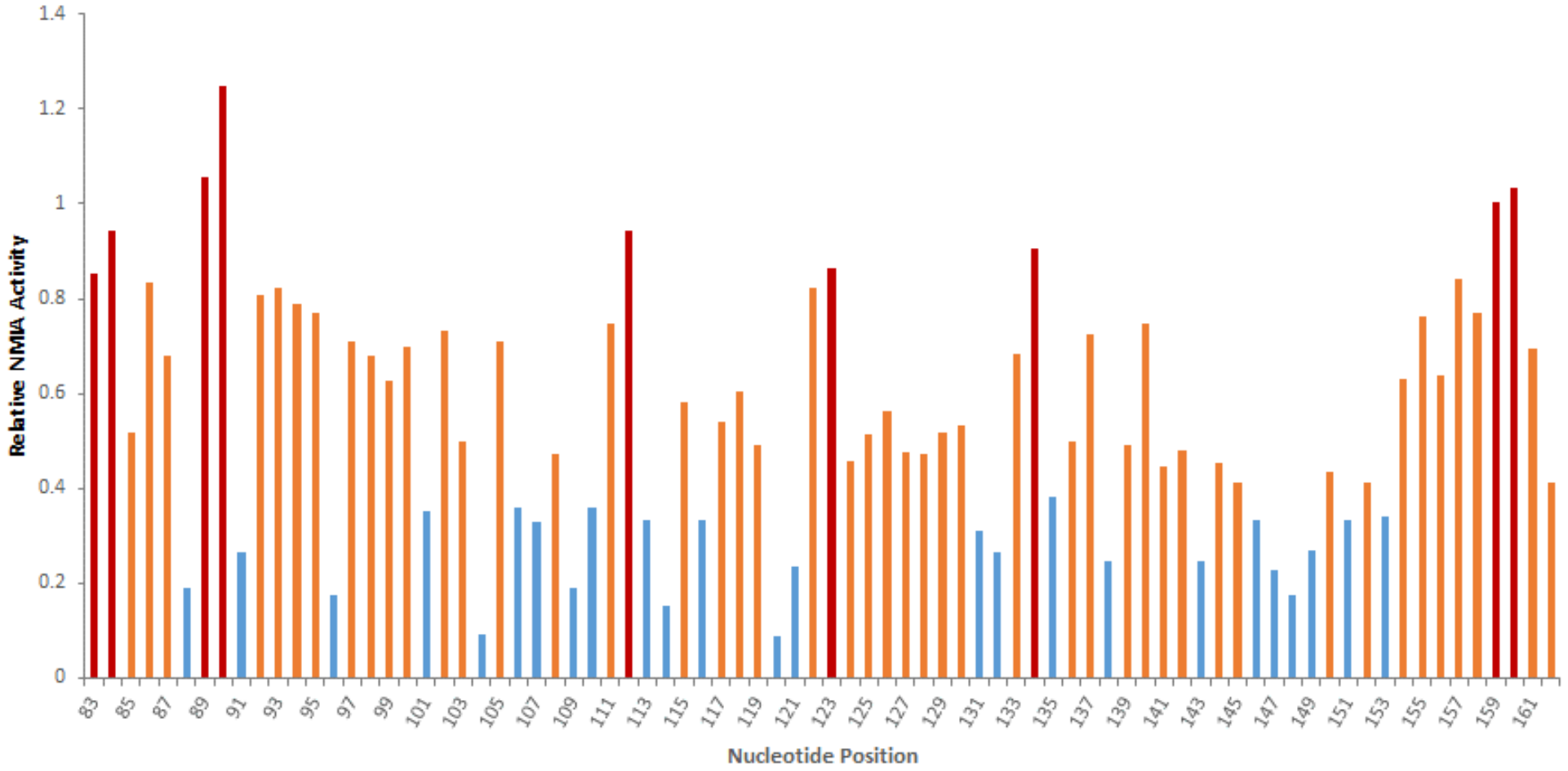

Figure 3.25. SHAPE analysis of Fragment 2. Relative NMIA reactivity is derived from the 10% most reactive nucleotides. Red bars represent nucleotides with relative reactivity > 0.85, orange bars represent relative reactivity between 0.84 – 0.4, whilst blue bars represent nucleotides with < 0.4 relative reactivity. n = 3, values are the average of three separate repeats.

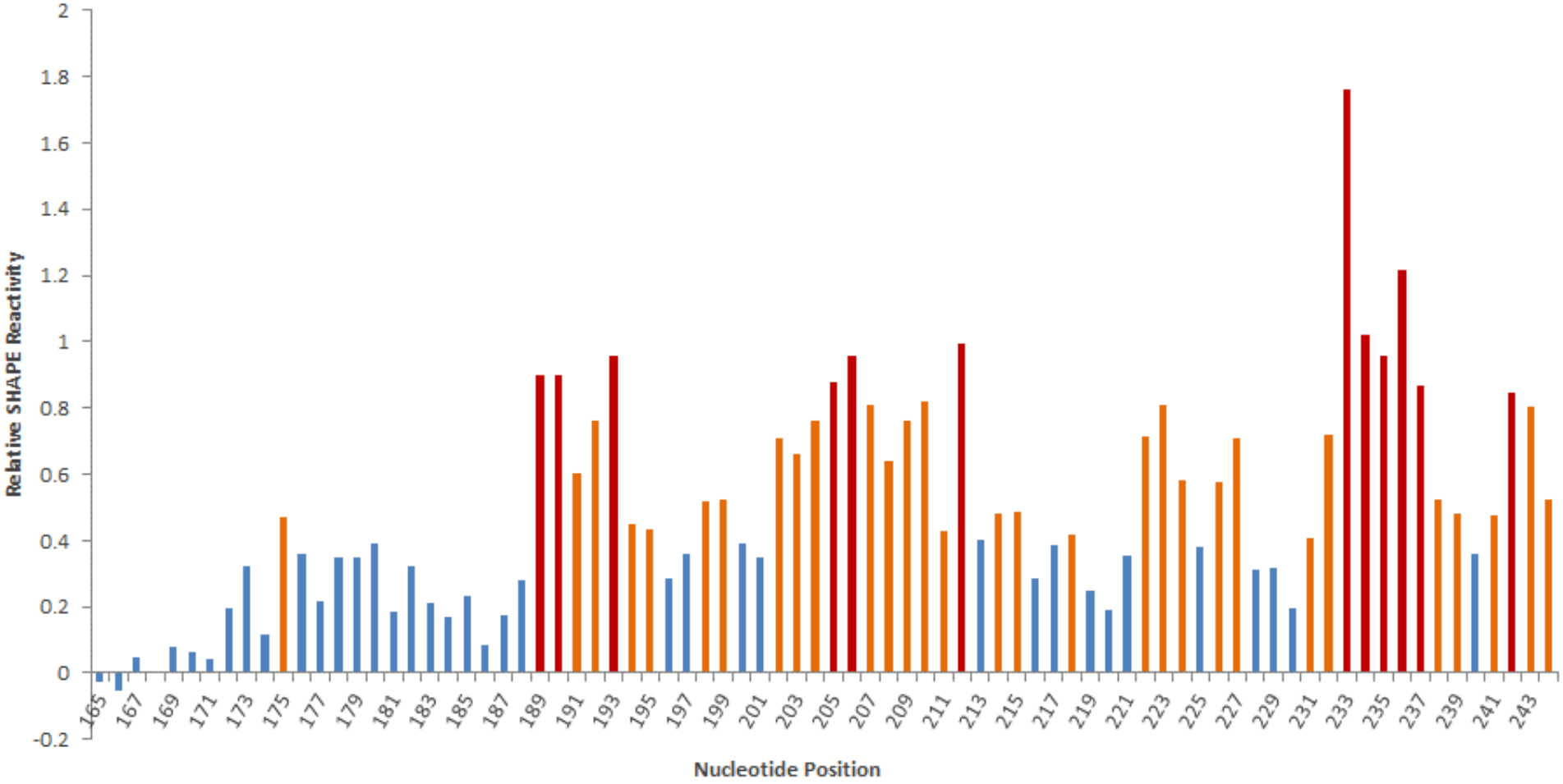

Figure 3.26. SHAPE analysis of Fragment 3. Relative NMIA reactivity is derived from the 10% most reactive nucleotides. Red bars represent nucleotides with relative reactivity > 0.85, orange bars represent relative reactivity between 0.84 – 0.4, whilst blue bars represent nucleotides with < 0.4 relative reactivity. n = 3, values are the average of three separate repeats.

High SHAPE reactivity is usually defined as between a value of >0.85, with values between 0.84 and 0.4 considered 'intermediate' and <0.4 as unreactive, when the boxplot method is used (Hajdin et al. 2013). From figures 3.24-3.26, regions where NMIA has bound and forced the reverse transcriptase to pause and are therefore unlikely to be involved in RNA-RNA interactions are shown, with red bars indicating a normalised reactivity of >0.85, orange bars indicating intermediate reactivity, between 0.84 and 0.4, and blue bars indicating unreactive nucleotides of <0.4. In fragment 1, 9 nucleotides have high SHAPE reactivity, 38 have intermediate and 35 are unreactive, indicating a number of loops connected by double stranded regions. By contrast, fragment 2 is decidedly unstructured; 9 nucleotides are highly reactive and 46 have intermediate reactivity with only 25 unreactive nucleotides, pointing towards a highly unorganised structure. Fragment 3 displays 12 highly reactive nucleotides, 30 intermediate and 39 unreactive nucleotides, with three distinct regions of high reactivity possibly indicating loops, surrounded by double stranded, structured regions. Curiously, the first 10 nucleotides of the fragment have very low activity compared to the corresponding sections, where usually the beginnings of the sequence is often seen as single stranded. However it is likely that this low activity is caused by the high intensity of bands in the (-) lane seen in figure 3.23. It is likely this is due to experimental error, as bands in the (+) lane should be equal or greater than those in the (-) lane, when adjusted for the amounts of cDNA loaded in each lane. However, we were unable to obtain results in subsequent repeats that did not contain this anomaly.

Adjusting predicted structures using SHAPE data

The SHAPE data produced can be used to improve the accuracy of structure prediction software by constraining nucleotides to be single stranded, forcing the program to predict a structure based around these nucleotides. There are a number of RNA prediction programs available, with differing methods of prediction. There are almost as many different algorithms as there are prediction programs. Perhaps the most commonly used is the Zuker algorithm (Mathews et al. 1999), which uses free energy minimisation to rank structures by their free energies. However, the structure with the lowest free energy is not always the true functional structure. Folding kinetics, such as those often seen in protein folding, could lead to an RNA structure with a higher energy, with an intermediate phase which can help to direct the RNA towards the functional structure (Zarrinkar and Williamson 1994). Most prediction software utilise a number of algorithms, with other commonly used ones including Wuchty (Wuchty et al. 1999) which computes all possible secondary structures within a narrow free energy range, generating structures that may be missed by the Zuker algorithm, and the McCaskill algorithm, which uses a partition function calculation to assess the probabilities of bases pairing (McCaskill 1990).

The program that was chosen to calculate the secondary structure of the 5'UTR of EGFR was RNAstructure, which uses the latest thermodynamic parameters from the Turner lab within the Zuker algorithm, in combination with the MaxExpect algorithm (Lu, Gloor, and Mathews 2009) and a pseudoknot program. A benefit to using RNAstructure is the ability to directly input SHAPE data which causes the algorithm to discount structures that do not conform with

the inputted data (Mathews et al. 2004). The program grades the strength of the SHAPE reactivity, usually not incorporating weak modification, The most important aspect of the algorithm is that it does not just assign the reactive bases as single stranded, rather it can assign SHAPE reactivities to bases close to hairpins (Deigan et al. 2009). Using the algorithm in this way is a lot more powerful than manually constraining nucleotides in programs such as mFold where the user must specify whether the base is single or double-stranded, rather than allow the program access to the complete raw data, letting the program fit the reactivities to its models. This also removes bias and error when manually constraining bases.

Predicted structures and structures after application of our SHAPE data were generated for each fragment and the differences compared. Figures 3.27-3.29 show the structures for each fragment. A circle comparison diagram of base pairing between the predicted and empirically derived structures was generated for each fragment, as shown in figures 3.30-3.32.

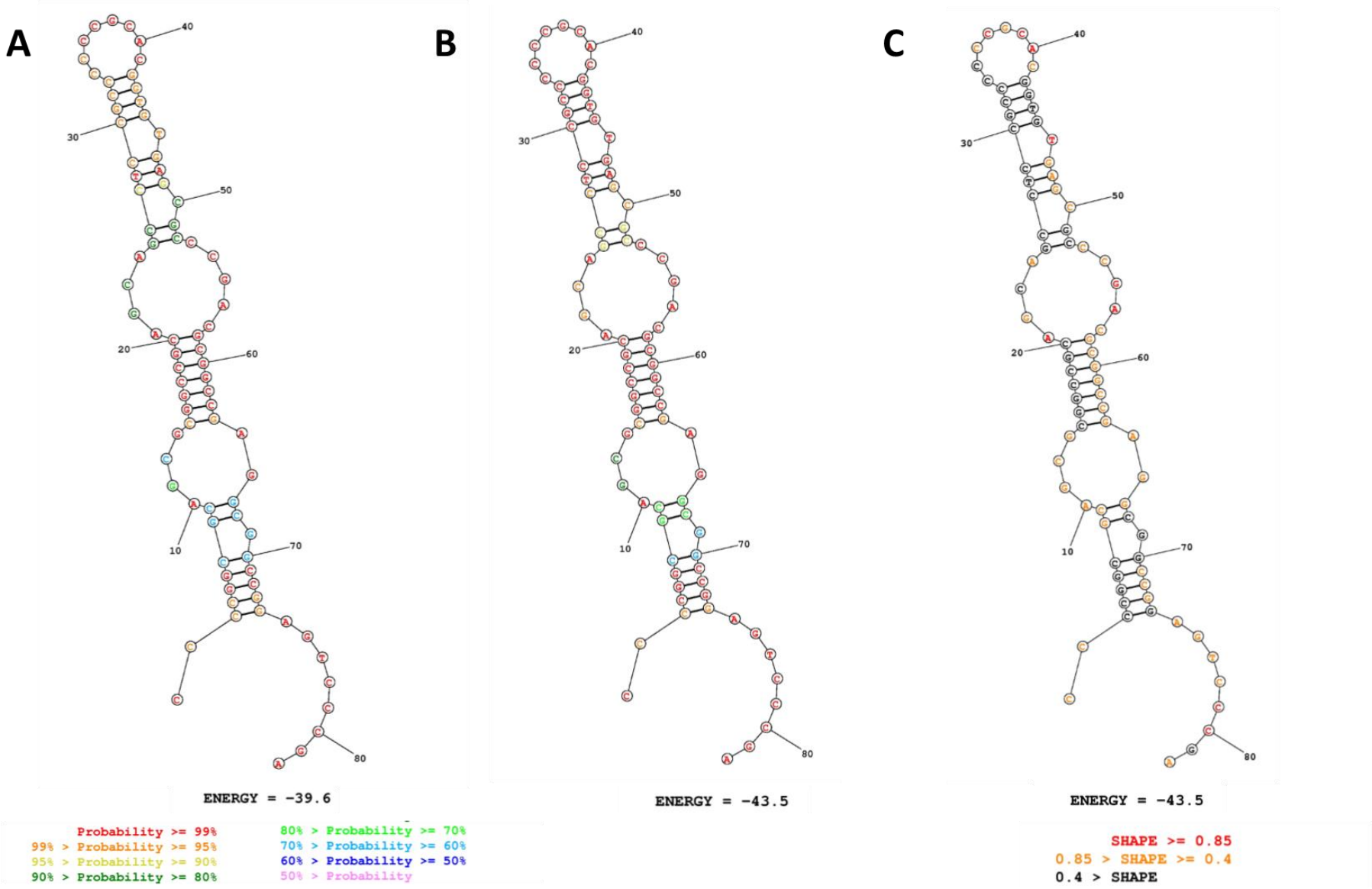

Figure 3.27 Predicted and Empirically Derived Structures of Fragment 1. A) The predicted structure of fragment 1 before SHAPE data is applied, colours denote probability of the nucleotide being in the correct state. **B)** The predicted structure after application of SHAPE data. **C)** SHAPE reactivity of each nucleotide, colours denote reactivity.

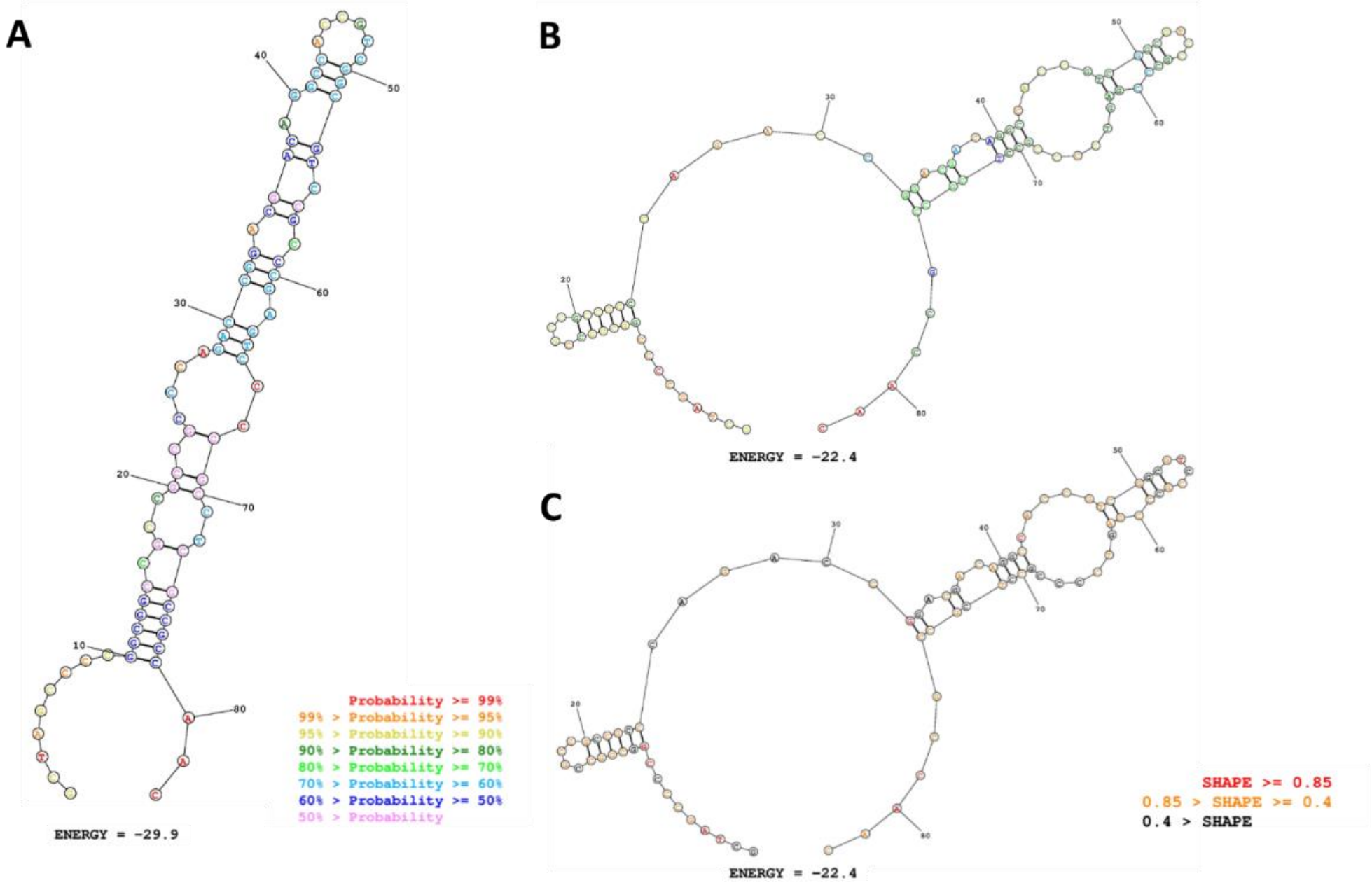

Figure 3.28 Predicted and Empirically Derived Structures of Fragment 2. A) The predicted structure of fragment 2 before SHAPE data is applied, colours denote probability of the nucleotide being in the correct state. **B)** The predicted structure after application of SHAPE data. **C)** SHAPE reactivity of each nucleotide, colours denote reactivity.

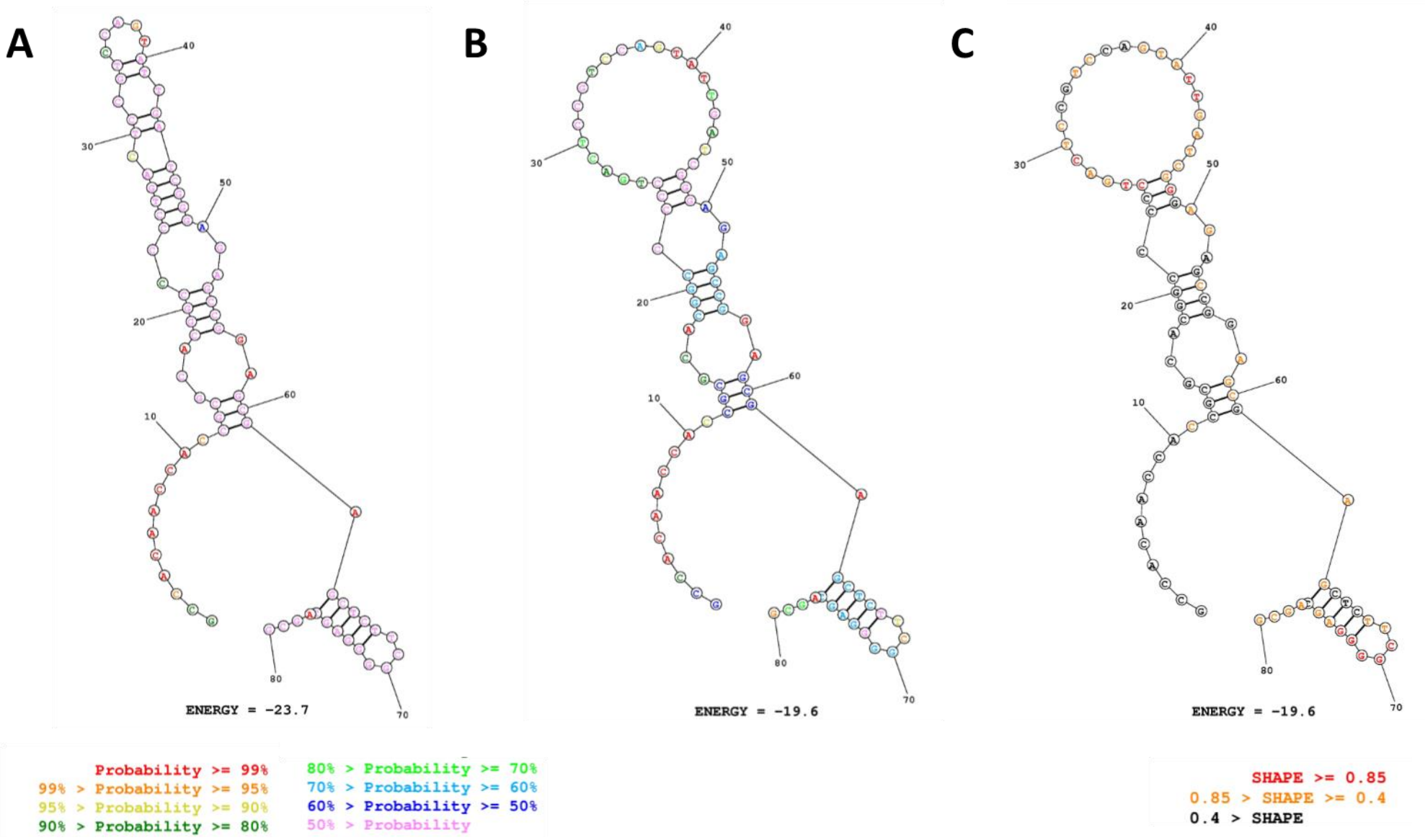

Figure 3.29 Predicted and Empirically Derived Structures of Fragment 3. A) The predicted structure of fragment 3 before SHAPE data is applied, colours denote probability of the nucleotide being in the correct state. **B)** The predicted structure after application of SHAPE data. **C)** SHAPE reactivity of each nucleotide, colours denote reactivity.

For fragment 1, RNAstructure generates only one possible structure, featuring 2 interior loops, 3 bulges, and a single stem loop (figure 3.27). Inputting our SHAPE data increases the confidence in this structure, with nucleotides within the double stranded region of the stem loop between nucleotides 30 and 46 all showing an increase to >=99% probability. The single stranded region of the loop itself features 3 nucleotides with high SHAPE activity. The bulge at nt46 shows a distinctively higher reactivity (1.17) to the adjacent nucleotides, 45 and 47 (0.38 and 0.46 respectively). Interestingly, the intermediately reactive nucleotides 58-64 sit within a stem with contrasting reactivity; nucleotides 58-64 show an average reactivity of 0.66 whereas nucleotides 14-20 on the opposite side of the stem have an average reactivity of 0.22. Whilst nucleotides with intermediate reactivity may fall within double stranded regions, particularly proximal to loops, these two strands share an almost identical space. One possible reason for this phenomenon is a structural switch, where two stable structures are present in the mixture (Kenyon et al. 2011). Thus in the alternate structure the nucleotides with higher reactivity are single stranded and the low reactivity nucleotides are paired differently. Confirmation of the presence of this switch and whether it has biological function would require further study. The comparison of base pairings between predicted and empirically-derived structures for fragment 1 shows no differences (figure 3.27).

Figure 3.28 shows the structures for fragment 2. Unlike fragment 1, there is a stark contrast between the predicted structure and the SHAPE adjusted structure. A major feature missing from the predicted structure is a long stretch

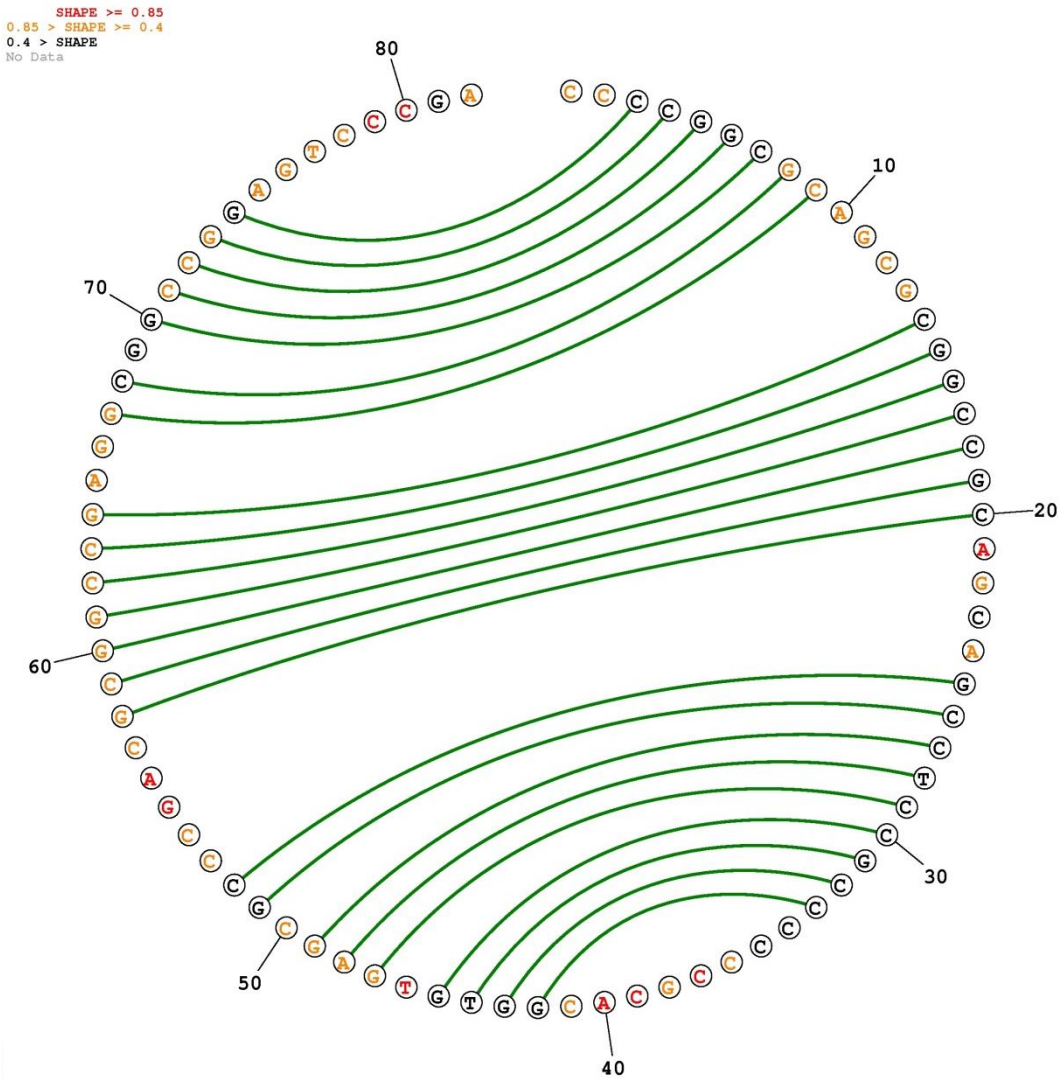

Figure 3.30. Base Pair Comparison Between Predicted and Adjusted Structures for Fragment 1. Green lines indicate base pairs that occur in both structures, red lines are those that are only found in the predicted structure and black lines are those found only in the adjusted structure. The SHAPE reactivity of each nucleotide is shown.

of single stranded nucleotides at the end of the sequence (nt66-82). Our SHAPE data, as seen in figure 3.28c reveals a potentially unstable structure – many of the nucleotides within the double stranded region between nucleotides 112 and 156 have intermediate to high SHAPE reactivity, although this could be due to the proximity of the 3 bulges and the interior loop to one another. The

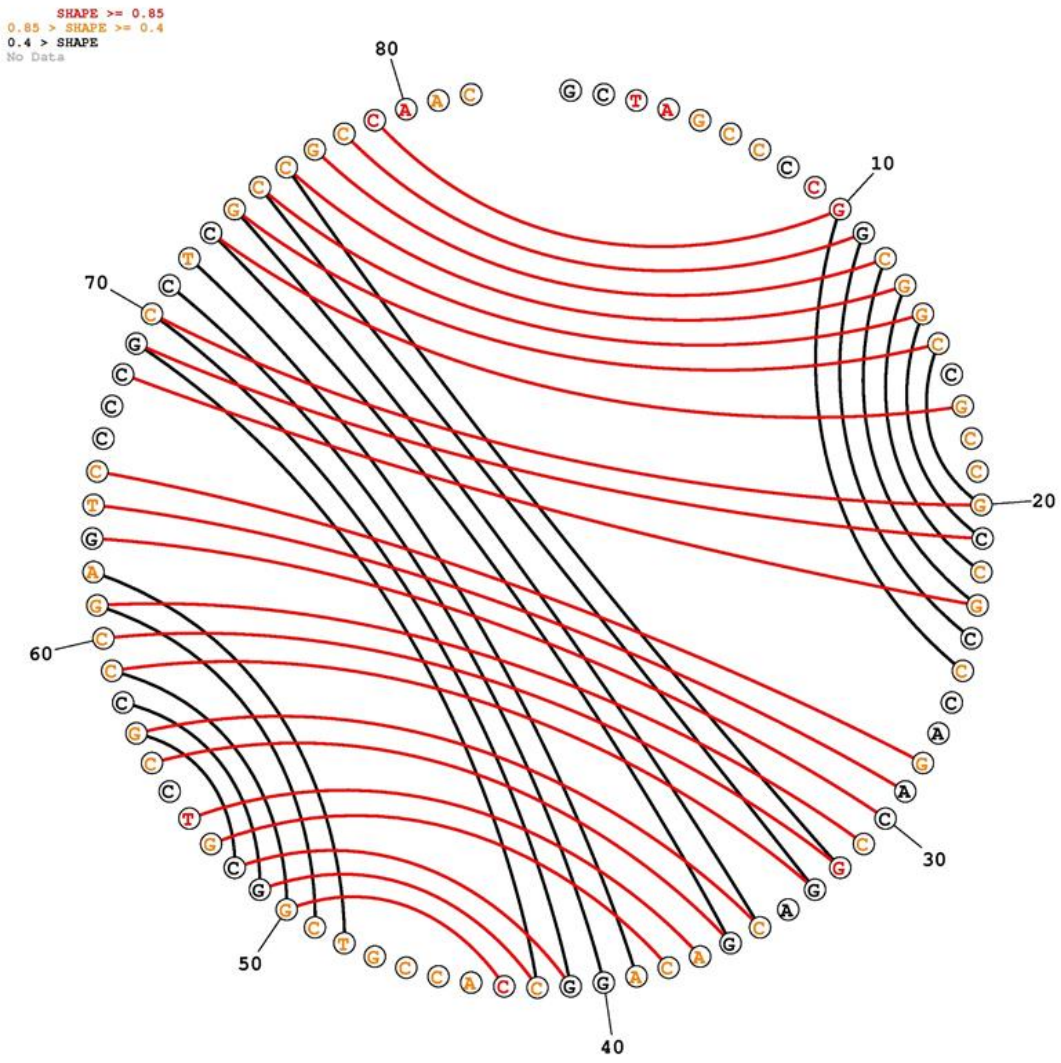

Figure 3.31 Base Pair Comparison Between Predicted and Adjusted Structures For Fragment 2. Green lines indicate base pairs that occur in both structures, red lines are those that are only found in the predicted structure and black lines are those found only in the adjusted structure. The SHAPE reactivity of each nucleotide is shown.

base pair comparison (figure 3.31) shows that none of the 23 predicted pairs are present in the final structure.

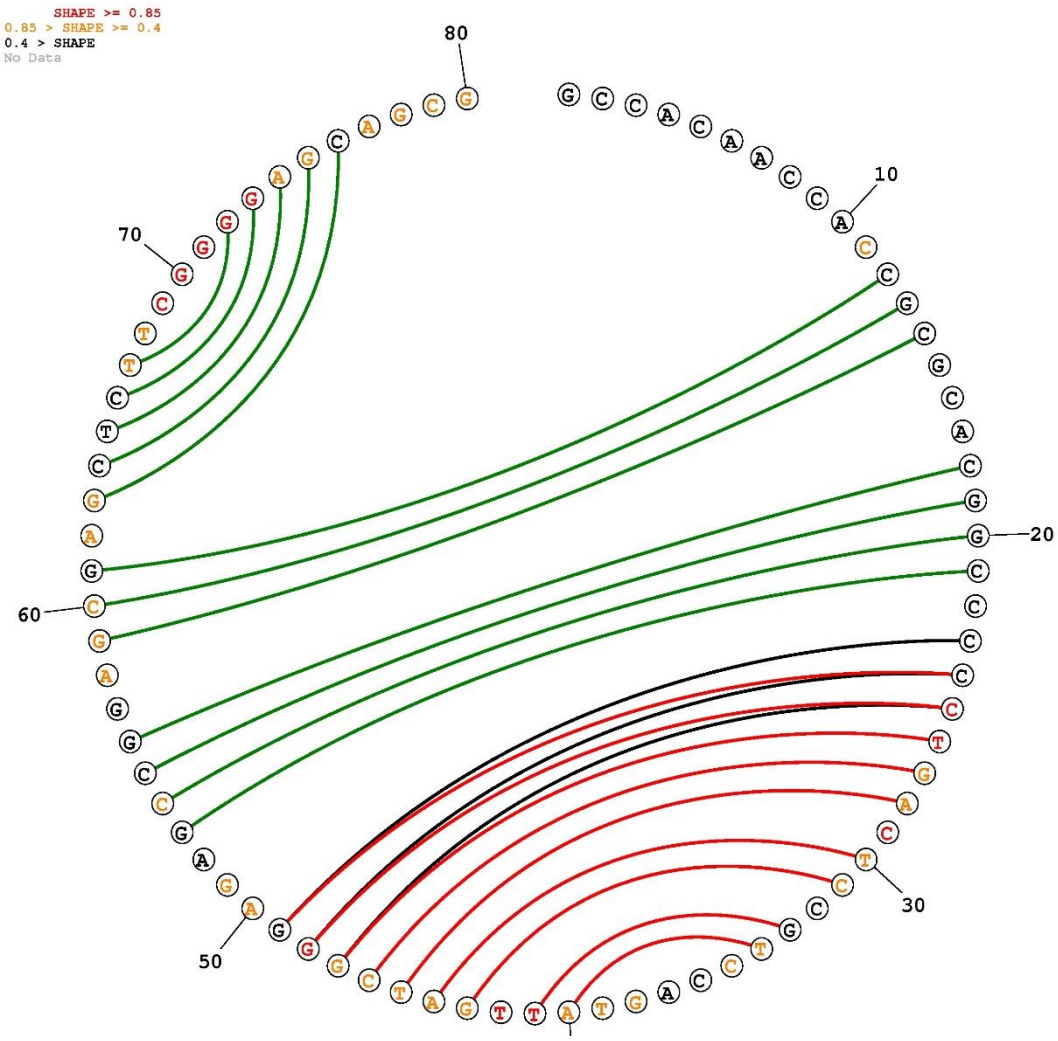

Figure 3.32 Base Pair Comparison Between Predicted and Adjusted Structures For Fragment 3. Green lines indicate base pairs that occur in both structures, red lines are those that are only found in the predicted structure and black lines are those found only in the adjusted structure. The SHAPE reactivity of each nucleotide is shown.

The adjusted structure for fragment 3 (figure 3.29) contains 2 interior loops and 2 stem loops. The large stem loop between nucleotides 190 and 211 is missing in the predicted structure, and features 5 highly reactive and 14 intermediately reactive nucleotides. Interestingly, the smaller stem loop between nucleotides 226 and 240 is conserved between the predicted and adjusted structures, and

features some of the most reactive nucleotides in the structure within the loop (nt 233 = 1.76, 234 = 1.02 and 236 = 1.21). The high reactivity of these nucleotides at the tip of the loop, in comparison to the larger loops overall intermediate reactivity (0.64) along with the loop's location at the end of the 5'UTR and thus proximal to the start codon, may indicate an important function for this loop. When base pairs between the predicted and adjusted structure are compared (figure 3.32) 12 pairs are found in both structures, particularly those associated with the stem loop at the end of the sequence and within the larger central stem (18-21 nt and 53-56 nt). Bases 47-49 shift there partner by one base (22-24 nt to 23-25 nt), caused by the introduction of the large loop.

3.10 Discussion

The results presented in this chapter demonstrate the conditions under which the EGFR IRES is either favoured or unfavoured route of translation initiation. Whilst it was found that the IRES was favoured in serum starvation and not favoured in ER stress in the U87-MG cell line, this was untrue in MCF7 cells where the activity of the IRES was not increased under serum starvation or reduced in activity under ER stress. However, as stated in section 3.3, the presence of phenol red in the culture medium may generate proliferation signals through the estrogen receptor and in turn allow cap-dependent translation initiation to occur despite the stress environment (Berthois et al, 1986). Differences in the cellular environment between the cell lines could have an impact on IRES activity, as was found for the HIV-1 IRES (Plank, Whitehurst, and Kieft 2013), where it is postulated that the IRES adopts different conformations which can be stabilised through ITAFs. The availability of particular ITAFs within the cell could have a dramatic impact on the IRES' stress response. Identification of ITAFs which bind to the EGFR IRES in future experiments could unveil how the EGFR IRES is modulated by binding proteins and how differing expression levels of ITAFs influence IRES behaviour in different tissues and how this impacts on disease.

The EGFR IRES is not a modular IRES. Deletion analysis revealed that deletion of just the first 57 nts or the last 36 nts from the 5'UTR sequence dramatically reduced IRES activity, although there was differential activity between MCF7 and U87-MG cells when only the first 57 nts are present, suggesting that there

is a difference in the binding proteins expressed between these cell types. Identification of proteins which bind the IRES will provide more detail into the mechanism of EGFR IRES activation.

A structural model of the EGFR 5'UTR was determined through the use of SHAPE. The data was compared to predicted models and was used to improve the models. A loop close at the end of the 5'UTR was discovered whose proximity to the start codon may indicate an important regulatory function. Along with this, a potential structural switch was located, which, *in vivo*, may be regulated by binding proteins. However, whether these structures are relevant *in vivo* will require further experiments. In general, performing *in vitro* structure analysis does not take into account binding proteins which modify the RNA structure. These interactions could be transient and used to control the activity of the structure or they could be more fundamental to the folding of the RNA as it is translated. Thus further study is required in order to determine the importance of SHAPE-derived structures through deletion of structural regions or through base substitution to disrupt the structure. One of the latest developments in RNA structure determination is an *in vivo* SHAPE method, *in vivo* click selective 2'-hydroxyl acylation and profiling experiment (icSHAPE) which utilises a cell permeable SHAPE reagent, coupled with a biotin moiety allowing for purification with streptavidin-conjugated beads (Spitale et al. 2015). This method could be used to derive structures under different conditions and reveal the importance in structural changes for IRES activation. Although one of the virtues of the SHAPE method is that it can provide structural information for every base in a sequence, it may be wise to validate this data

with more traditional techniques. One reason for this is the presence of "intermediate reactivity", reactivity which is not defined as unreactive (typically <0.3) but also not reactive with SHAPE reagents (>0.7). Although some of these nucleotides are at the base of loops, many fall into double stranded areas, leaving their status open to interpretation.

Finally, the effectiveness of antisense oligonucleotides to disrupt translation initiation by the EGFR IRES was investigated. Our data suggests the EGFR IRES is highly susceptible to antisense oligonucleotides binding within the 5'UTR. Initially it was believed that binding at the ribosome binding site would be necessary to block incoming ribosomes, but an oligonucleotide upstream of this region was determined to have inhibited IRES-dependent initiation. This may be due to disruption of important regulatory structures or binding proteins. Further experiments with oligonucleotides binding to different regions may reveal how oligonucleotides disrupt the IRES and investigating the toxicity of oligonucleotide therapy will be necessary to determine whether blocking the IRES is a feasible strategy for tackling overexpression of EGFR by its IRES.

4. Creating a 3d model to study translational control in tumour masses

In conventional 2D cell culture many features are lost that are found *in vivo*. These include extracellular matrices and cell to matrix interactions important for proliferation and differentiation, cell to cell contacts as well as gradients of nutrients, signalling molecules, metabolites and oxygen (Pampaloni, Reynaud, and Stelzer 2007; Mazzoleni, Di Lorenzo, and Steimberg 2009). The lack of these in 2D cell culture can lead to problems in transferability of therapeutics from cell culture to live animal models as a significant effect in a 2D monolayer may be a negligible effect in a tissue. That 3D cultures exhibit a different gene expression profile compared to 2D cultures highlights the problem of relying on conventional cell culture for drug discovery (Bissell, Hall, and Parry 1982) Whilst living animal and tissue models remain the most effective method for therapeutic development, the use of *ex vivo*, 3D models can reduce the gap between 2D and animal models. 3D cell cultures exhibit features that are more relevant to *in vivo* conditions and findings made in 3d cell culture are more likely to translate to animal models (Vinci et al. 2012). The subsequent increase in predictability of drug efficacy from 3D-based drug and toxicity screens could also reduce the number of animals used for drug testing (Marx 2006).

The evaluation of drug delivery systems in 2D culture can also prove problematic. For instance, the lack of extracellular barriers in 2D culture can suggest a delivery system is more effective than it truly is (Goodman, Ng, and

Pun 2008). Likewise the homogenous nature of 2D culture fails to account for phenotypic differences among cells and gradients in pH and nutrients. Thus a 3D model for delivery system evaluation provides more information on how delivery particles will interact with cells *in vivo*.

3D cultures can take a number of forms, from tissue explants supported on metal grids (Toda et al. 2002), to artificial skin models where primary fibroblasts cultures are seeded onto biodegradable fibre mesh. Cellular spheroids are perhaps the simplest system to implement and take advantage of the tendency of many cell types to aggregate (Pampaloni, Reynaud, and Stelzer 2007) and are a good choice for studying therapeutic effectiveness and for high-throughput screens (Ivascu and Kubbies 2006). A number of techniques exist for creating 3D spheroids, such as the hanging drop method, where cells are suspended in droplets of media on the lids of culture dishes (Del Duca, Werbowetski, and Del Maestro 2004), spinner flasks (Wartenberg et al. 2001) and rotary cell culture systems (Unsworth and Lelkes 1998). These methods come with advantages and disadvantages. For instance the hanging drop method is time consuming and makes media exchange difficult, but can be inexpensive and creates homogenous spheroids suitable for high-throughput experiments (Breslin and O'Driscoll 2013; Kim, Stein, and O'Hare 2004), whereas rotary systems require specialised equipment, but spheroids are much more simple to culture (Breslin and O'Driscoll 2013).

Ultra-low attachment (ULA) plates allow the creation of self-forming 3D spheroids by blocking the cells from attaching to the surface of the plate using a hydrophilic coating forcing the cells to grow in suspension and form contacts

with each other, whilst the 'U' shape of the well promotes a single, centrally located spheroid. These plates have been shown to be successful in creating spheroids in a range of cell lines from many tumor types, including U87-MG (Vinci et al. 2012). However, some cell lines required the addition of Matrigel, a protein mixture containing laminin, entactin and collagen, in order to form spheroids (Vinci et al. 2012). Culturing using ULA plates is simple and reproducible and so were chosen for this project.

In recent years there has been interest in creating 3D-based models of Alzheimer's disease, although the complexity of neuroanatomy and the lack of true understanding of key pathogenic steps makes development challenging (Lee et al. 2016). Some success can be found in the creation of a 3D-differentiated model, exhibiting both neuronal and glial cell types, where Aβ aggregation occurs (Choi et al. 2014). The use of this type of model however is outside the scope of this project.

The aim of this study was to create a cost-effective, easily repeatable and reproducible 3D model for studying translational control and to assess its potential as a model for testing delivery systems for therapeutics targeting IRESs.

4.1 Plasmids and Cloning

To observe differences in the environment within the spheroid the fluorescent protein expressing plasmids, pEYFP-C1 and pDsRed-C1, which express GFP and DsRed respectively were used. The vector maps can be seen in figure 4.1. The 5'UTR of EGFR was amplified by PCR using the EGFR-AgeI F and EGFR-AgeI R primers, digested with AgeI and ligated into the pEGFP-C1 plasmid at the AgeI site, 5' to the GFP coding region, allowing GFP to be expressed through cap-independent translation initiation driven by the IRES within the 5'UTR. In the following experiments DsRed was used as a control to normalise changes in GFP expression.

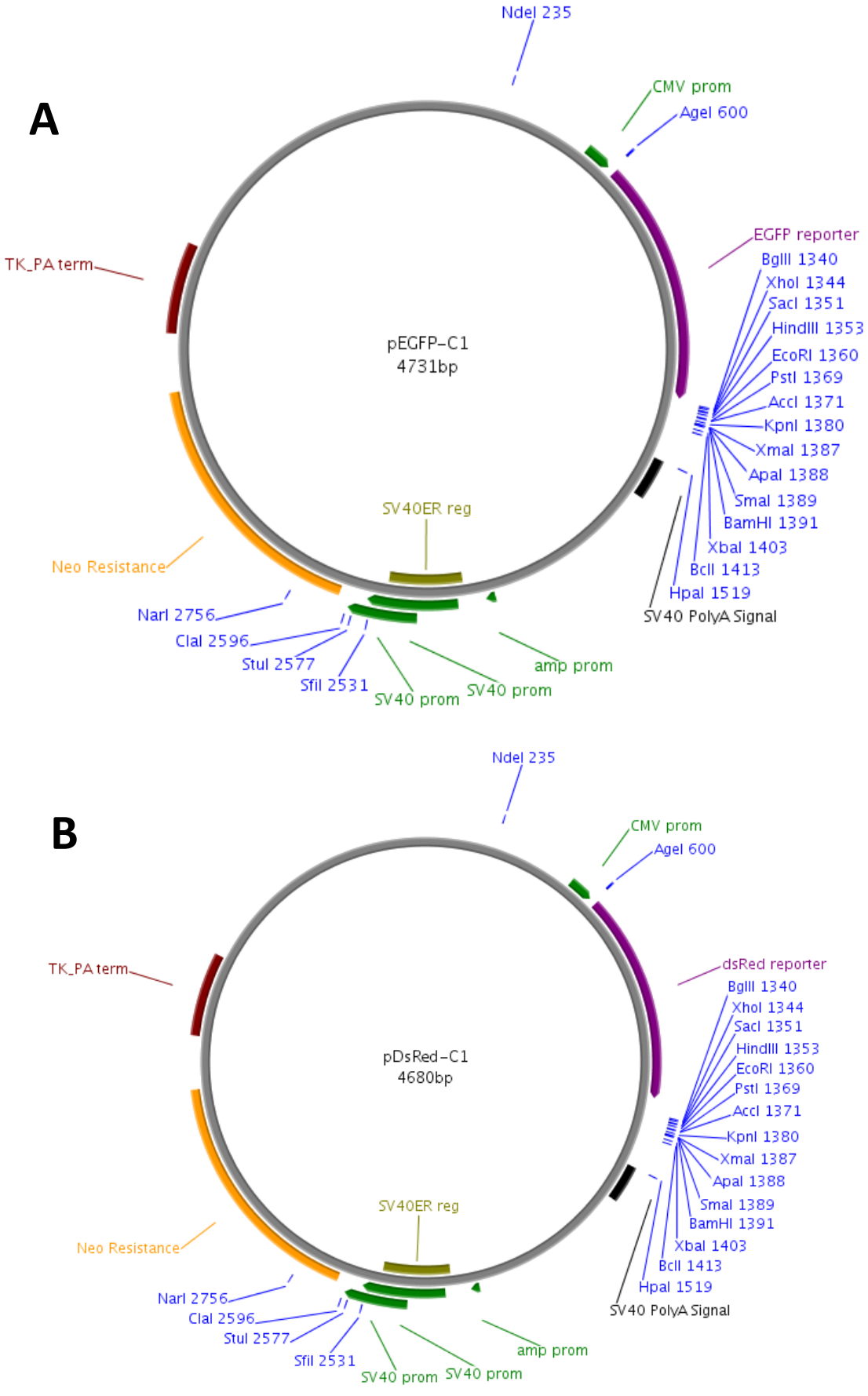

Figure 4.1 Vector Maps of pEGFP-C1 (A) and pDsRed-1 (B)

4.2 Generation of Stable Cell Lines

Culturing cells in 3D presents difficulties for transient transfection. Cells were therefore transfected before spheroid formation and selection media applied to create a cell line which stably expresses the fluorescent protein. Stable cell line generation requires the use of an antibiotic effective on eukaryotic cells. Geneticin (G418), inhibits the elongation step of translation in both prokaryotes and eukaryotes. Resistance to G418 is conferred by the Neomycin resistance gene *neo*, found in both GFP and DsRed plasmids.

In order to determine the concentration of G418 antibiotic necessary to only kill non-transfected cells, a dose-response experiment was performed on U87-MG cells. This allows identification of the optimal dose of G418, the concentration in which all cells are dead after 7 days of selection. U87 cells were plated at $1x10^6$ cells/ml into 6 well plates. After 24 hours cells were treated with varying concentrations of G418 (as shown in fig.4.2). Cells were observed every day for 14 days, and the day in which all cells in each well had died was recorded. As shown in figure 4.3, concentrations above 700ng/µl killed all the cells within 24 hours and concentrations below 100ng/µl did not kill cells until after 11 days. The optimal dose was determined to be 120ng/µl, thus this concentration was used in the creation of the stable cell lines.

Two stable cell lines were created, one transfected with the DsRed plasmid and one with the GFP-5-UTR plasmid. Cells were transfected using Fugene 6 following the protocol as detailed in section 2.1.6. Cells were treated with

120ng/µl G418 for 2 weeks, with cell death occurring to non-transfected cells. Cells were then allowed to grow until confluency and expanded into T150 flasks. After expansion, the polyclonal cell line was frozen in liquid nitrogen for further use.

Attempts were made to create monoclonal cell lines to improve the consistency of downstream experiments, but were not successful; single cells plated into 96 well plates failed to expand and mostly died, under optimal, low and untreated G418 concentrations, as well as in higher serum conditions. It is possible that the U87-MG cell line requires a higher degree of growth factors or cell-cell contact in order to grow and divide. Due to these difficulties it was decided to continue our investigations with a polyclonal cell line.

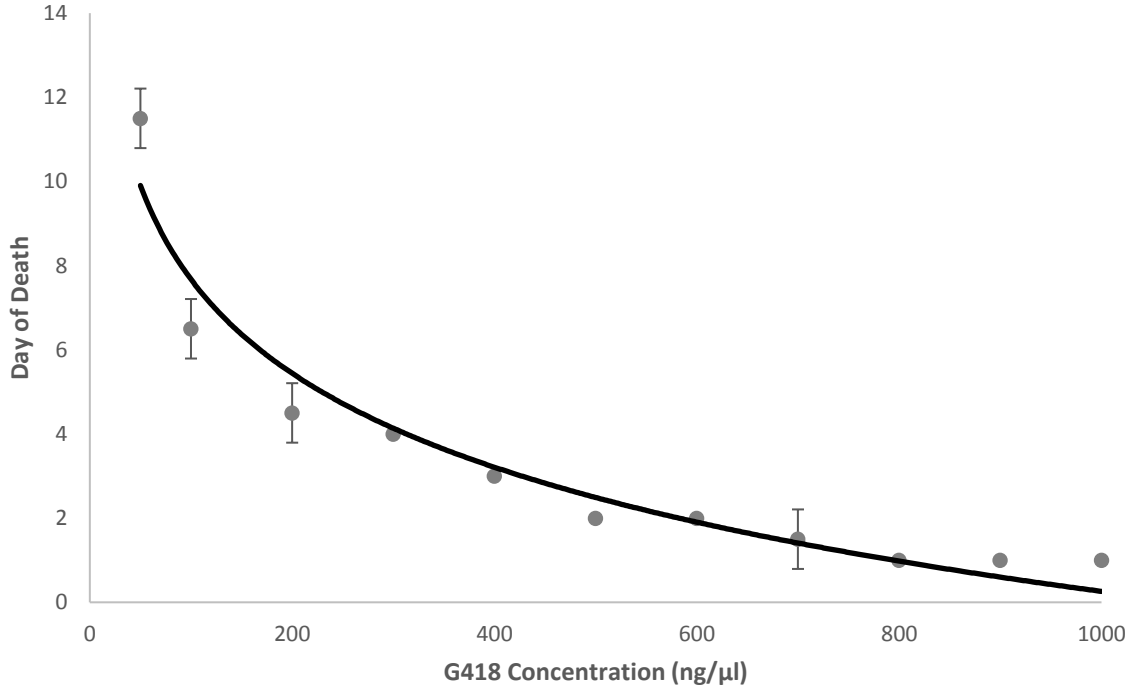

Figure 4.2. G418 Kill Curve for U87-MG cells. Cells were plated at a density of $1x10^6$ in a 6 well plate before addition of G418. Day of death indicates the day in which no living cells remain in the wells. Average of three repeats, error bars indicate standard deviation.

4.3 Stable Cell Lines in 2D Culture

The stable cell lines were tested for their response to normoxic, hypoxic and serum starvation conditions in standard 2D cultures, under which the IRES in the 5'UTR of EGFR is found to be active in luciferase reporter plasmids. Cells were subjected to treatment for 24 hours before imaging under an EVOS FL microscope, as seen in figure 4.3. The average fluorescence of GFP was calculated and normalised against the average DsRed fluorescence in each treatment. Exposure times were standardised throughout. The relative fluorescence for each treatment can be seen in figure 4.4.

Similar to the expression seen in pRF, GFP-5'UTR has increased relative expression under hypoxia and serum starvation with significant increases of 2-fold ($p = 0.0023$ by t-test) and 1.8-fold ($p = 0.036$ by t-test) in relative expression recorded respectively. This is compared to the 1.5-fold and 2.7-fold increase recorded from the luciferase reporters, as shown in sections 3.3 and 3.6. These results indicate that the EGFR IRES is capable of directing translation of the fluorescent protein from these vectors. However, as can be seen in the bright field images in figure 4.3, a large proportion of cells are not expressing GFP or DsRed. This is most likely caused by the use of a polyclonal cell line, where there will be cells that either express the protein at extremely low levels or are resistant to the antibiotic. Whilst it is clear that GFP-5'UTR responds to treatments in a similar manner to the luciferase plasmids, the presence of these non-expressing cells is a concern for later experiments as they may possess a growth advantage over the expressing cells and thus may out compete them.

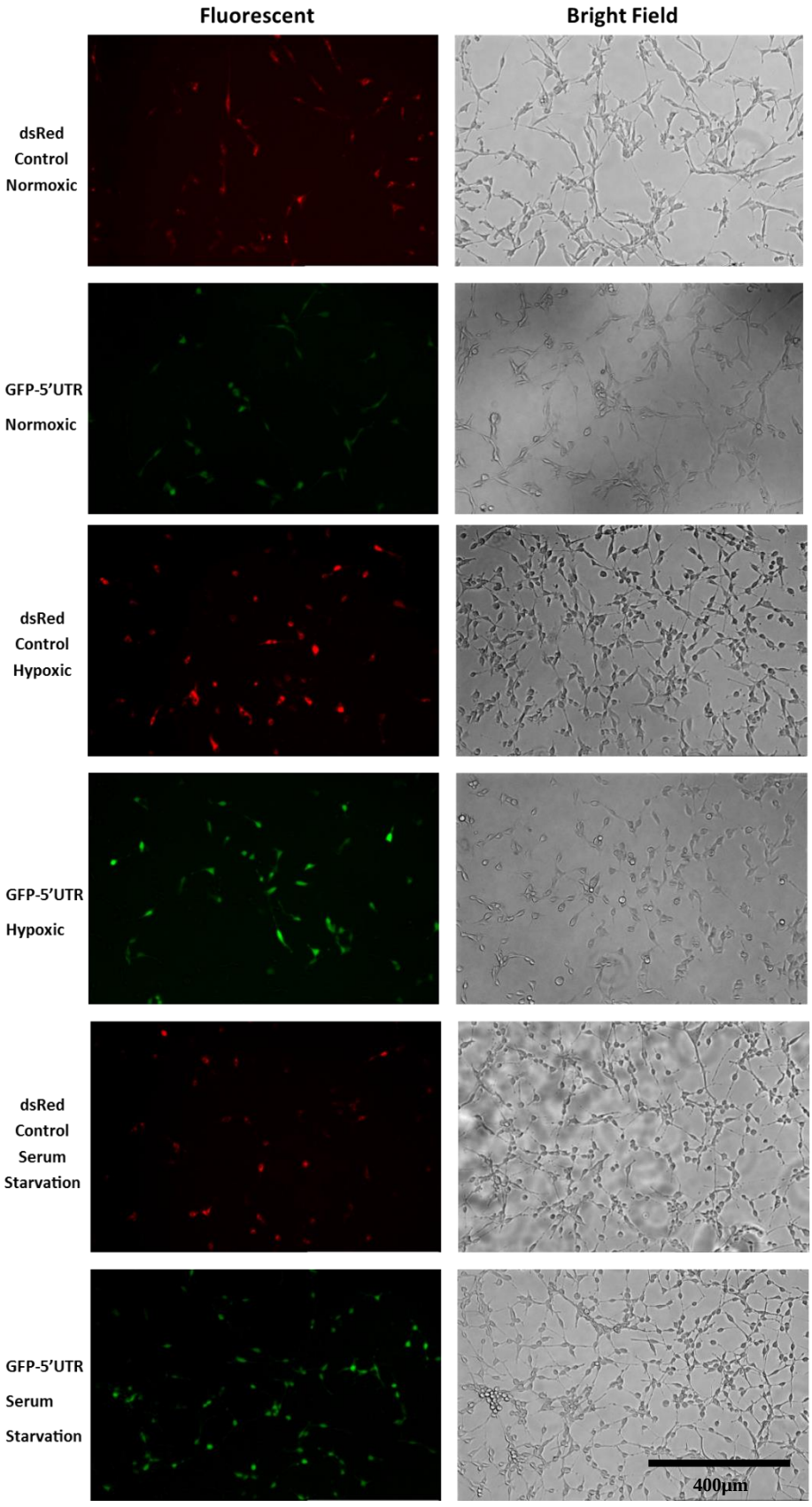

Figure 4.3. Expression of Fluorescent Reporters Under Stress Conditions. Cells stably expressing GFP or DsRed were plated into 6 well plates at a density of 150,000 cells/ well. Cells were incubated at 5% CO_2, 37°C for 24 hours either at 1% O_2, 0.5% serum or normoxic conditions, before analysis under an EVOS FL microscope. Excitation and emission wavelengths used for capture are detailed in section 2.1.8. Images displayed are representatives of three repeats.

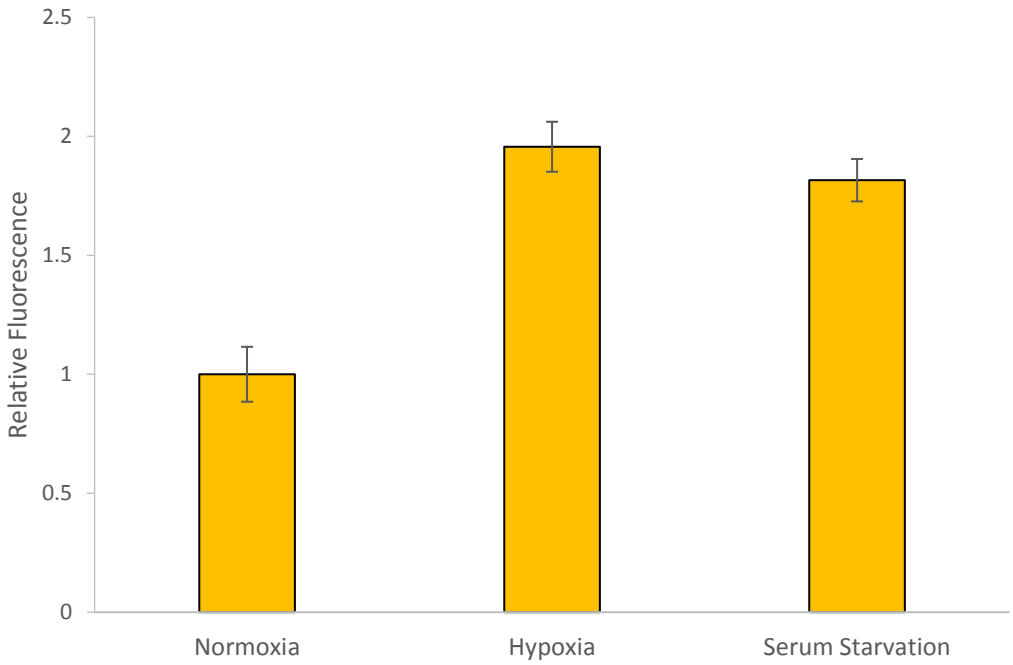

Figure 4.4. Relative Fluorescence of GFP-5UTR in U87MG cells Under Stress Conditions. Average fluorescence of cells imaged were calculated in ImageJ. n = 3, error bars represent standard deviation of three biological replicates.

4.4 Determining the Size of 3D Spheroids

The size of a spheroid has a major effect on the cells at the centre of the culture. Necrotic cores can occur in cellular structures over 500 μm in diameter, whilst gradients in O_2 concentrations can occur in spheroids of at least 400 μm in diameter, although some cell types develop gradients with a diameter as low as 200 μm (Sutherland et al. 1986). More recent studies suggest that a zone of quiescent cells exists within even small spheroids of 100 μm in diameter, which may become necrotic with time (Langan et al. 2016). Size can also effect the diffusion of nutrients and oxygen into the structure. Langan et al suggests that spheroids with a diameter of ~100 μm have a hypoxic core of only 8μm, (Langan

et al. 2016) with larger spheroids gaining an exponentially greater area of hypoxic cells in proportion to their total area. Spheroids incubated for longer periods than a week also had a larger area of hypoxic cells, with necrosis occurring (Langan et al. 2016).

The aim of this study was to create spheroids that possessed necrotic, hypoxic and normoxic regions to simulate an environment which could be more relevant for Alzheimer's disease. Cells were seeded into ULA plates at a range of densities, grown for 1 week and the spheroid size was assessed under an LSM510 confocal microscope .As shown in figure 4.5, all seeding densities led to a minimum diameter of 400 μm, but at the lowest density, 1000 cells (A), the spheroids were unstable, forming loose, non-spherical accumulations. To ensure spheroids would not disperse and to have substantial hypoxic regions, the minimum seeding density was set at 5,000 cells (C). Larger seeding densities (F and G) produced spheroids over 800 μm in diameter. These may contain large regions of necrosis (Sutherland et al. 1986), thus the maximum seeding density was limited to 25,000 cells.

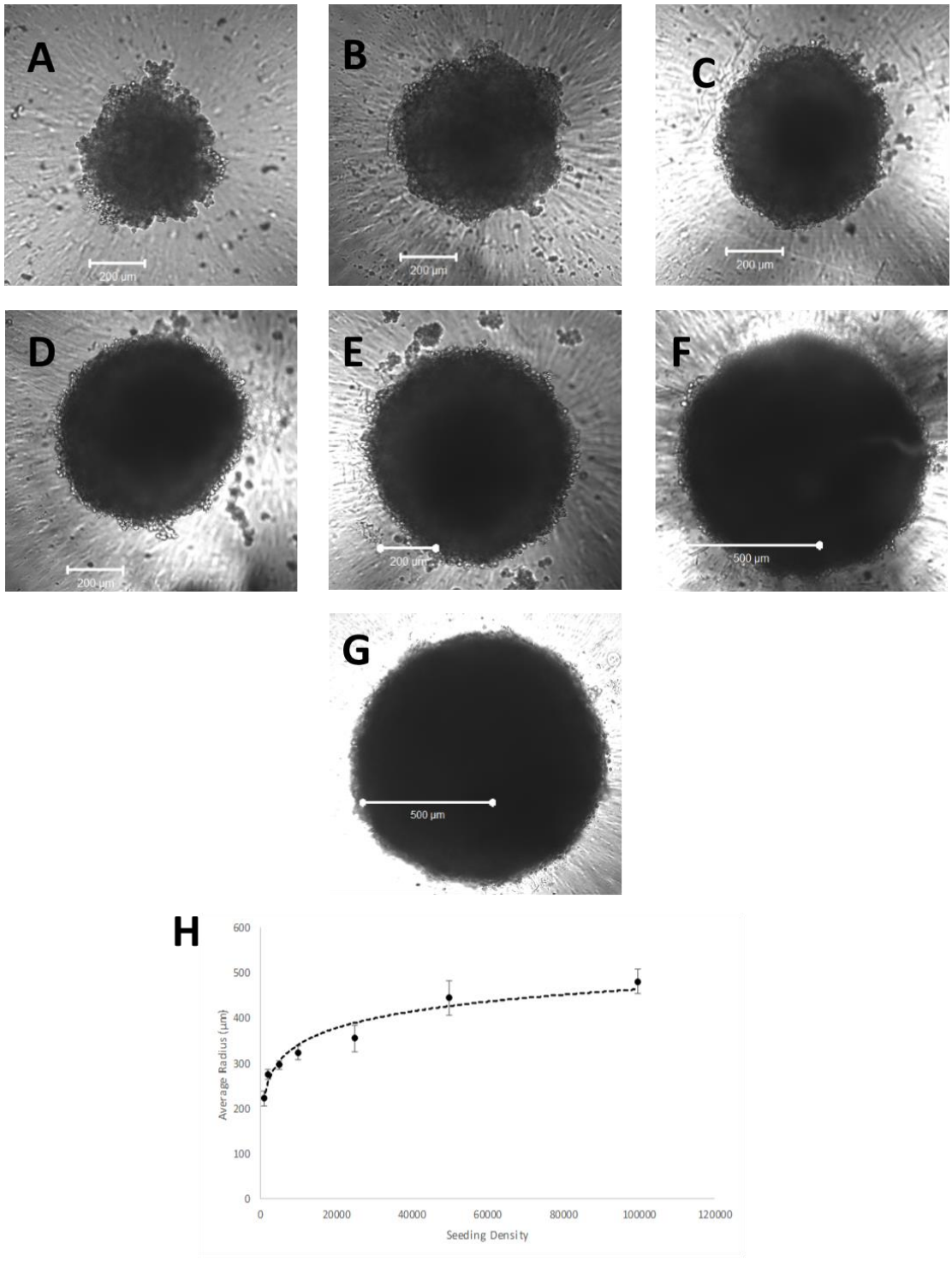

Figure 4.5 Sizes of Spheroids at Different Seeding Densities. A-G - Seeding densities of 1000, 2000, 5000, 10,000, 25,000, 50,000 and 100,000 cells/well respectively. H – The average radius of spheroids after incubation for each seeding density.

4.5 pH Measurements of 3D Cultures

A spheroid of a large enough size should create an inner core of cells with limited access to nutrients and oxygen. In order to test the spheroids for hypoxia, the intracellular pH was measured. A number of studies have shown that prolonged exposure to hypoxic conditions increases intracellular pH in cancer cells. In non-cancer cells pH tends to decrease due to cessation of oxidative phosphorylation and activation of glycolysis (Lipton 1999). In cancer cells, alkalinisation by Na^+/H^+ exchange pumps (NHE) and through carbonic acid uptake is key to survival (Ivanov et al. 2001). Exposure to chronic hypoxa causes pulmonary arterial smooth muscle cells to shift their intracellular pH above 6.8, towards a pH of 7.4 (Rios et al. 2005). This is through activation of NHE pumps in the plasma membrane which move H^+ ions into the extracellular region, utilising the Na^+ gradient, thus increasing internal pH (Madden et al. 2001). In glial cells, NHE pumps play an important role in preventing cell death when cells returning to normoxia from hypoxic conditions (Bondarenko, Svichar, and Chesler 2005), so it is likely that NHE pumps will be active during hypoxia in our cell line and cause an increase in intracellular pH.

The seminaphthorhodafluor (SNARF)-4F 5-(and-6)-carboxylic acid, acetoxymethyl ester, acetate is a cell permeable dye which exhibits a significant pH-dependent emission shift, from yellow-orange to deep red under acidic and basic conditions. As such the SNARF-4F dye can be used to quantitatively measure a shift in intracellular pH through the ratio of the two emission wavelengths across the 3D culture. In order to determine the pH, SNARF-4F

must be calibrated in a series of pH adjusted buffers. Figure 4.6 shows the calibration curve, based on the work by Hunter & Beveridge (Hunter and Beveridge 2005). This curve can then be used to assign the ratios observed to the pH.

3D cultures were incubated with SNARF-4F at a concentration of 20 μM in PBS for 1 hour in the plates. Cells were then analysed using an LSM510 confocal microscope, with an excitation of 488 nm and emissions at wavelengths of 543 nm and 650 nm were recorded. The ratio of 543/650 nm was calculated and the pH assigned based on the calibration curve. Figure 4.7 shows 3D cells of plating density 300 stained with SNARF-4F. The image was taken at the mid z-level

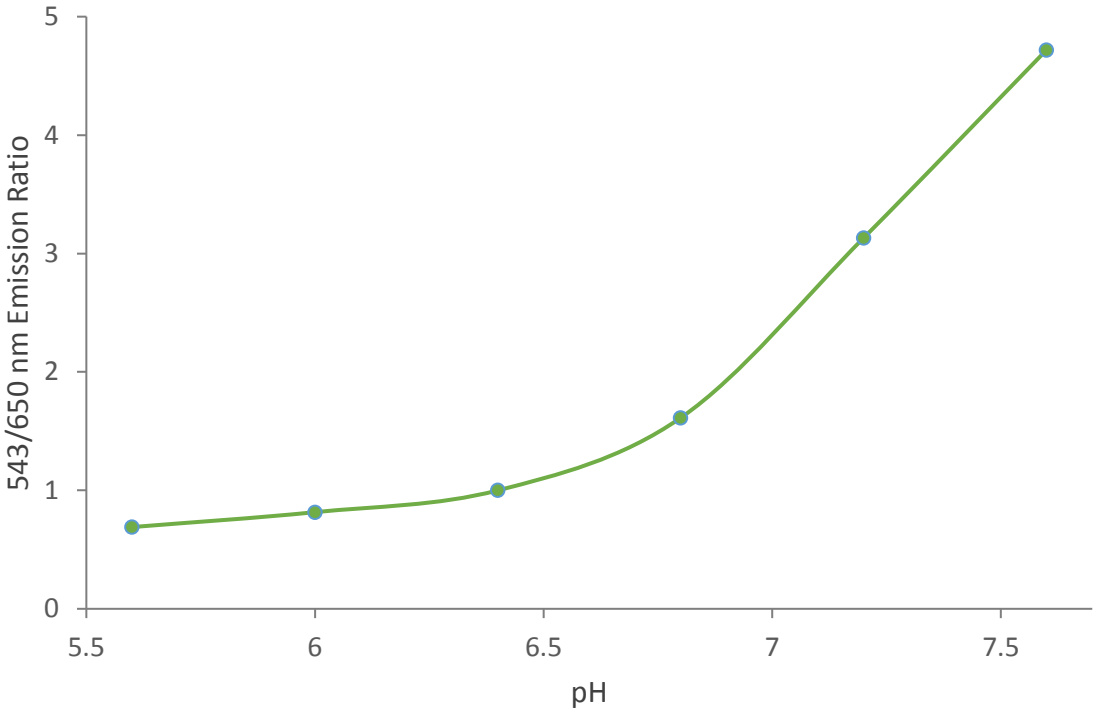

Figure 4.6 SNARF-4F pH Calibration Curve. Derived from the works by Hunter and Beveridge, 2005. 1mM SNARF-4F was added to pH-adjusted 50mM HEPES. Emission spectra were recorded in a spectrofluorometer, excitation 488 nm, emission 543 nm and 650 nm. The ratio of these two emission wavelengths was then calculated for each pH buffer.

point, i.e. a cross-section of the spheroid. Curiously, the centre of the spheroid showed no emission at either 543 nm or 650 nm. The permeability of SNARF-4F is high, so it is believed it will penetrate the spheroid. An increase in dosage to 100 μg and a longer incubation time did not improve the emissions from the centre of the spheroid. Measuring the cells that had taken up the dye, it was found that there was a significant increase in pH from outer cells (>300 μm from centre), with an average pH of 6.7, to the cells closer to the centre of the 3D culture (<200 μm), with an average pH of 7.3 ($p = <0.0005$ by t-test), suggesting that cells on the surface of the spheroid experience a very different environment to cells adjacent to them within the structure. The unstained central region is approximately 300 μm in diameter. It was hypothesised that this region could be necrotic, and this will be discussed in later sections.

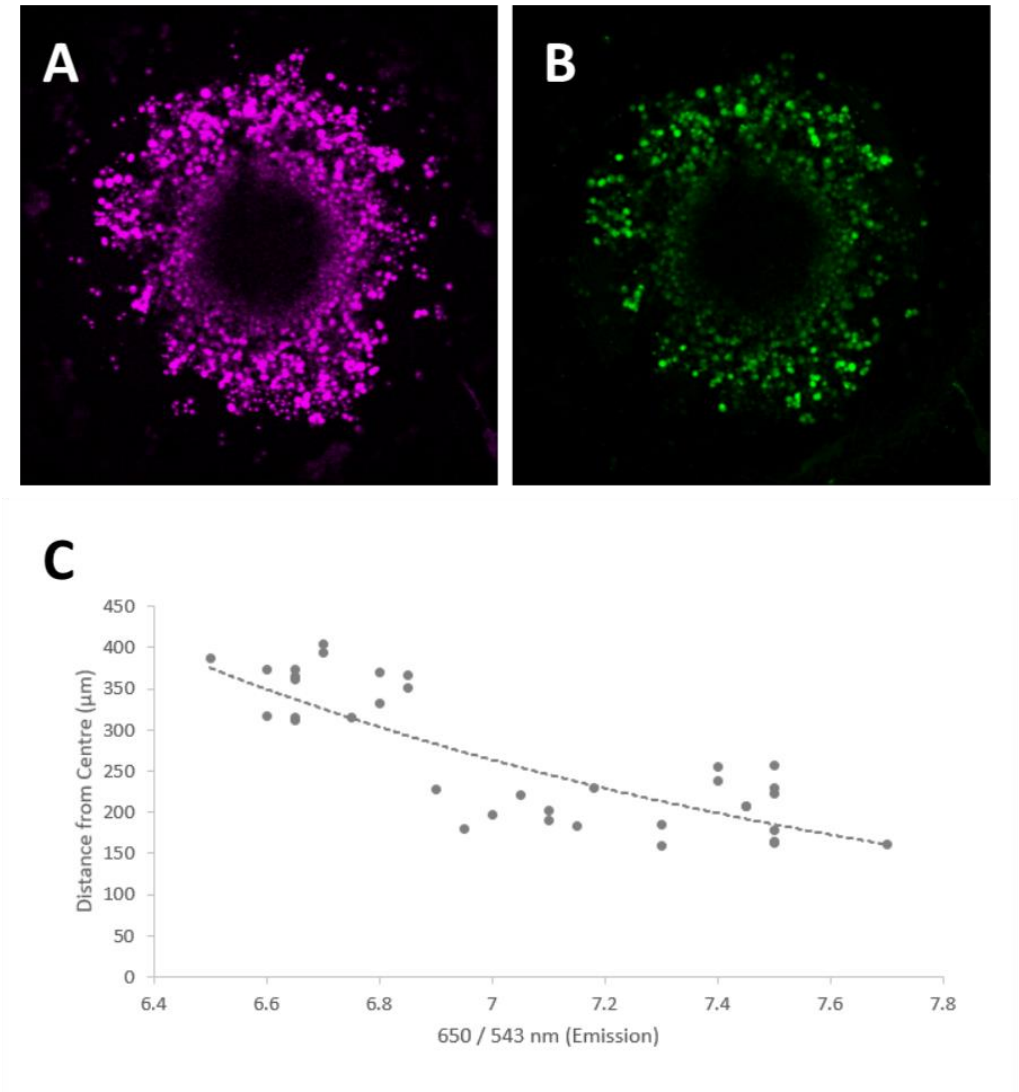

Figure 4.7 The Intracellular pH is Higher in Cells Closer to the Core of the Spheroid. 3D cultures were incubated with 20 µM SNARF-4F for 1 hour before being analysed for uptake using an LSM510 confocal microscope, at excitation wavelength of 488 nm and emissions at 650 nm (**A**) and 543 nm (**B**). The ratio of 650:543 was used to assign pH to cells. The change in pH in relation to the distance from the centre of the spheroid was calculated (**C**)

4.6 Fluorescence and Shape of 3D Cultures

In order to determine how the 3D environment affects the activity of the EGFR IRES the GFP-5UTR and DsRed stable cell lines were seeded into ULA plates. Equal amounts of the GFP-5'UTR and DsRed stable cell lines were mixed and seeded into each well and incubated for 1 week. Five seeding densities were used: 25000, 20000, 15000, 10000 and 5000 cells/well, denoted as S5, S4, S3, S2 and S1. Spheroids were then analysed under an LSM510 confocal microscope with excitation wavelengths of 488 nm and 543 nm and emissions of 509-520 nm and >550 nm for GFP and DsRed respectively. Images were captured through a series of 'z-level' slices, which were spaced 19μm apart. Figure 4.8 shows an example of the fluorescence detected from both GFP and DsRed from the S5 spheroid, at the bottom, mid-point and top of the 3d culture. Two observations can be made from these images. Firstly, cells form a ring at the highest point in the structure, 152 μm from the bottom. There is no top to the spheroid. Secondly, there are no fluorescing cells within the centre of the culture, except for the very bottom of the structure. The structure of the 3d culture was investigated by reconstructing the shape from the z-levels using the ImageJ 3d viewer plugin (Schmid et al. 2010). Screen captures of the S5 model are shown in figure 4.9. The structure formed indicates that the cells may not have formed a spheroid; rather a 'bowl' shape can be seen. It is likely that the SNARF-4F staining seen in figure 4.7 is not due to low permeability into the core of the cell mass, but rather that there is no core. There are a number of possibilities to why this shape occurs. The most obvious is that the cells are incapable of forming a spheroid structure, that cell to cell contacts cannot be made. This seems unlikely

however as observations in our lab of 2d cultured U87 cells suggest that at high confluency cells grow on top of each other readily, whilst U87-MG cells have been used previously in both ULA plates (Vinci et al. 2012) and in hanging drop methods (Howes et al. 2007). However, aggregates of U87-MG cells do disperse

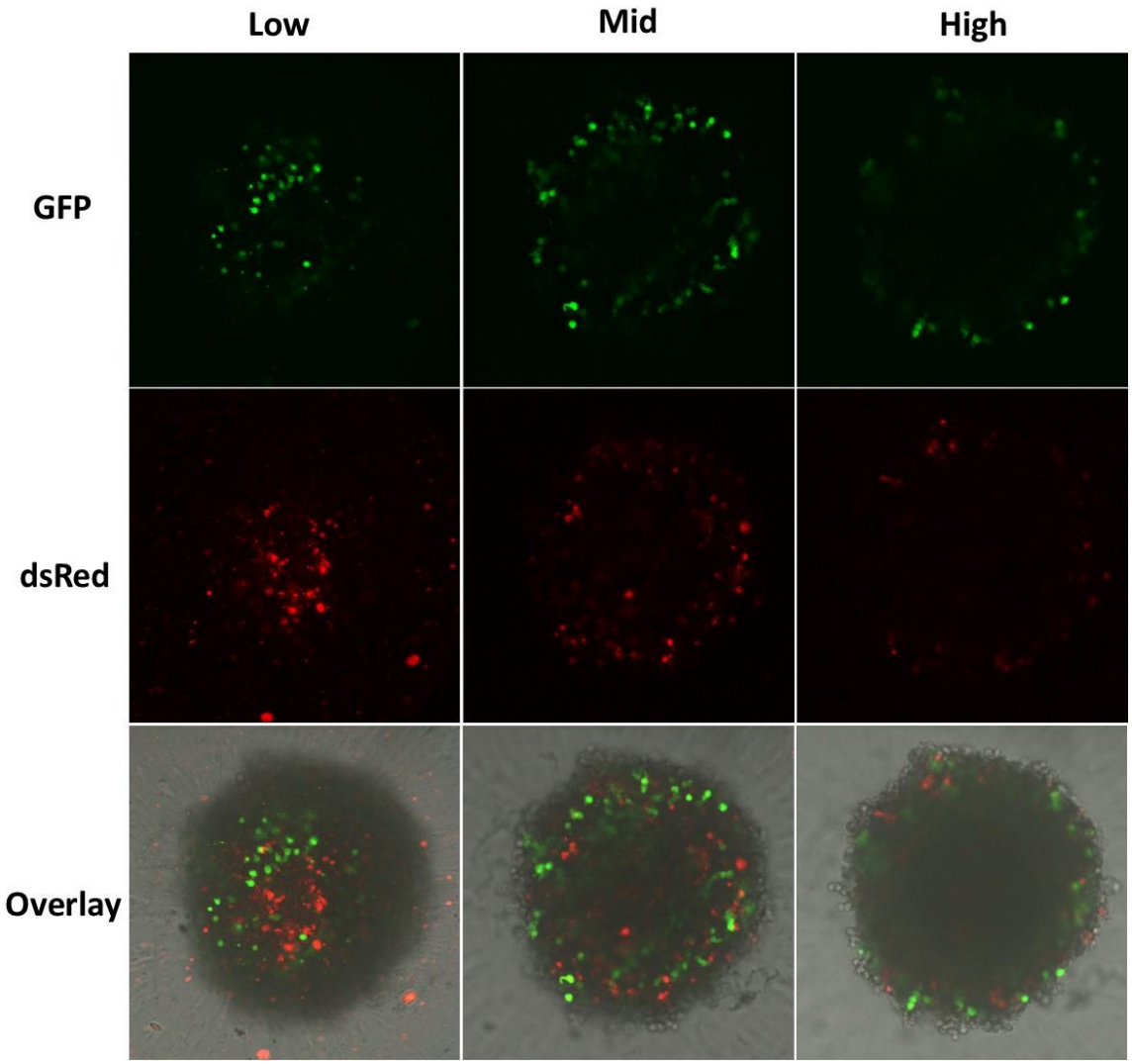

Figure 4.8 Fluorescence Detected Through Z-levels of the S5 Spheroid. GFP-5UTR and DsRed stable cell lines were seeded together into ULA plates at equal seeding densities. The 'S5' spheroid had a seeding density of 25000 cells After 1 week cells were analysed in an LSM510 confocal microscope with excitation wavelengths of 488nm and 543nm and emissions of 509-520 nm and >550 nm for GFP and DsRed respectively. Images were captured through Z slices 19 µm apart to image the entire spheroid.

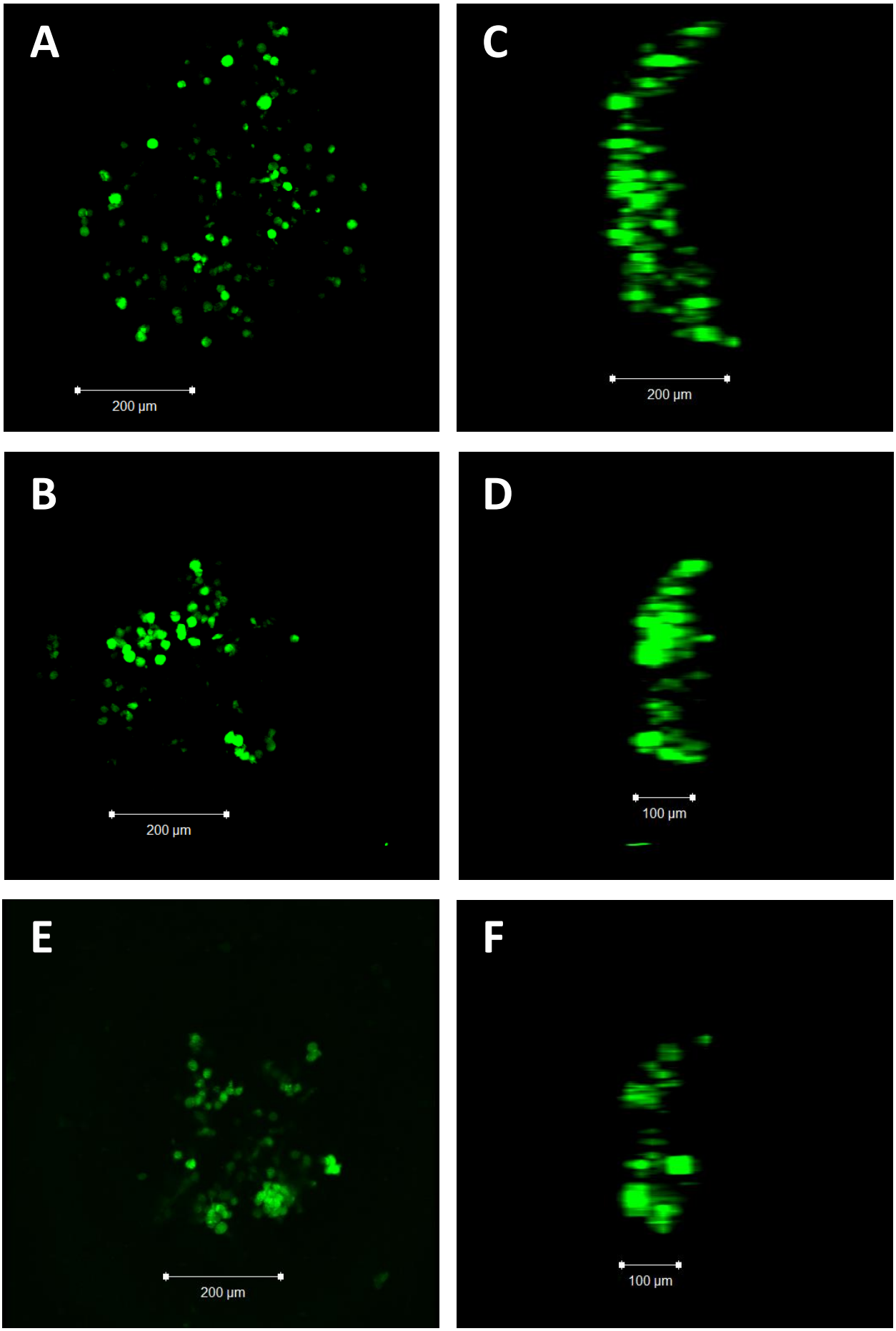

Figure 4.9 Shape of 3d Cultures. Image slices captured by LSM510 confocal microscope were analysed by 3D viewer plugin for ImageJ. **(A+C)** Top and side view of S3 culture, **(B+D)** Top and side view of S5 culture, **(E+F)** Top and side view of S1 culture.

quickly to form monolayers (Sabari et al. 2011) and disperse at a much higher velocity than other glioblastoma lines, suggesting that cell-cell cohesion may be low in this cell line. It is also possible that the surface of the well is not in fact inhibitory to cell growth and the cells are simply growing along the curvature of the well, however cells remained tightly packed and not dispersing widely as seen in 2d culture. This method of spheroid formation itself may not be adequate for some cell types. In the hanging drop method, cells float freely, making no contact with the plate. This means that the seeded cells will become the centre of the spheroid. Conversely, in the ULA method the seeded cells form the bottom of the spheroid. Making contact with the well bottom reduces the growth potential of the seeded cells and may reduce access to nutrients at the beginning of the growth period. If cells with fewer contacts are more likely to proliferate this may mean faster proliferation at the sides over the centre. This would not be a problem for the hanging drop method as the seeded cells will always form a core. Whilst the cells are not directly attaching to the plate they may be resting on the curved surface, ultimately resulting in a bowl structure with weak cohesion. It might be possible to improve spheroid formation by addition of Matrigel to wells before seeding, providing an extracellular matrix (ECM) analogue for cells to bind to. Matrigel based culture could be considered closer to *in vivo* conditions, but may differ significantly in composition to neuronal ECM.

Despite the shape, GFP and DsRed fluorescence readings were taken from cells at the bottom of the well and from the sides through the z-levels and determined the GFP/DsRed ratio at each z-level. As shown in figure 4.10 and 4.11, in the

largest structure, S5, relative GFP fluorescence gradually decreases with distance from the bottom of the well. At 150 μm from the bottom relative GFP fluorescence is significantly reduced by 30% ($p = 0.042$ by t-test). The same is true for the S4 and S2 cultures, with reductions of 23% ($p = 0.006$ by t-test) at 114 μm and 30% ($p = 0.05$ by t-test) at 76μm respectively, although the highest z-level in these structures show reductions that are not significant. A non-significant reduction is seen in the S3 structure, with a reduction of 24% at 100 μm. The smallest structure, S1, did not show a reduction, with relative GFP fluorescence remaining fairly constant throughout. This suggests a gradient exists within the culture medium, in which the bottom of the well experiences a stressed environment lacking in nutrients or oxygen in which the IRES is favoured over cap-dependent translation and the development of this environment may be dependent on the size of the structure. Whether this is through hypoxia, lowered nutrient concentration or other stress conditions was not verified.

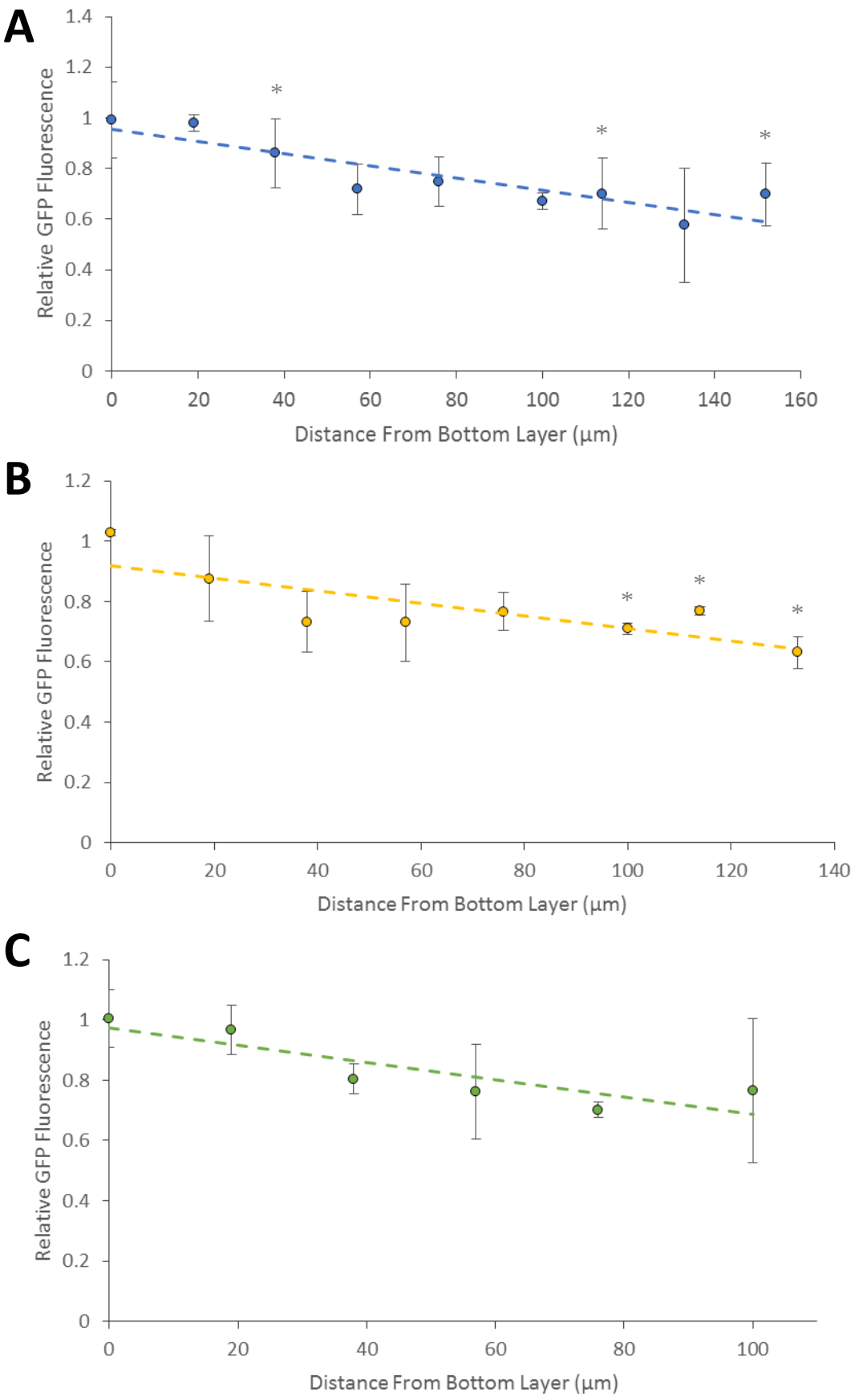

Figure 4.10 Relative GFP Fluorescence Across the S5, S4 and S3 3D Cultures. GFP and DsRed fluorescence intensities were measured using ImageJ. The ratio of GFP to DsRed intensity was measured for each Z-slice (average of 10 readings). Error bars are standard deviation. '*' represent $p < 0.05$ against the bottom layer value.

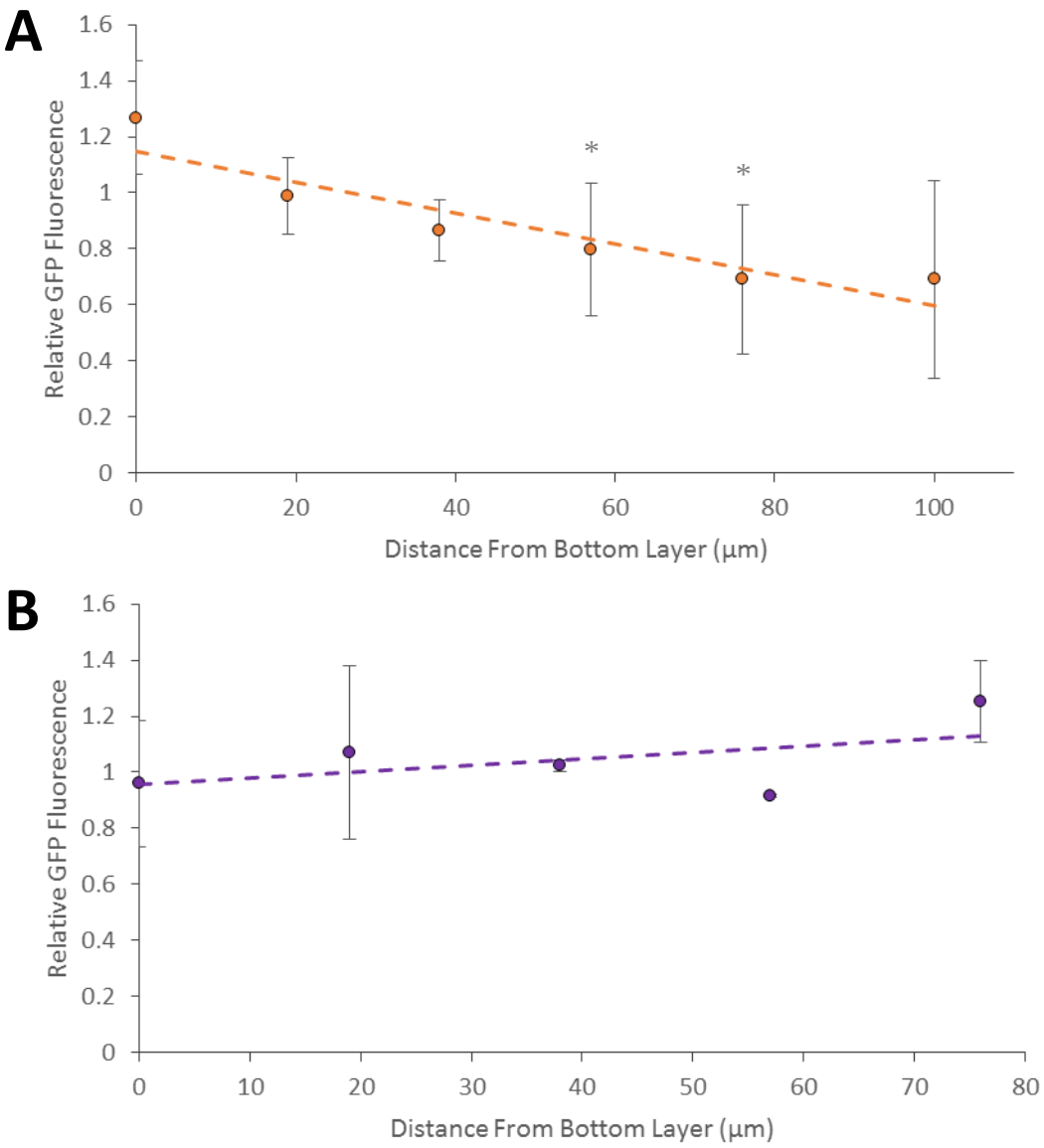

Figure 4.11 Relative GFP Fluorescence Across the S2 and S1 3D Cultures. GFP and DsRed fluorescence intensities were measured using ImageJ. The ratio of GFP to DsRed intensity was measured for each Z-slice (average of 10 readings). Error bars are standard deviation. '*' represent $p < 0.05$ against the bottom layer value.

4.7 Discussion

The results presented here demonstrate that the 5'UTR of EGFR exhibits IRES activity in hypoxic and serum starved conditions. Fluorescent plasmids were successfully transfected into U87-MG cells to create stably expressing cell lines, although attempts to create monoclonal cell lines failed. Seeding individual cells by limiting dilution proved difficult and cells that were successfully plated either did not grow or died shortly after. Fluorescence-activated cell sorting (FACS) could aid in seeding more fluorescing clones and increasing the likelihood of generating a growing monoclonal culture. If a minimum number of neighbouring cells are required for growth in U87MG cells, FACS could be used to select high GFP expressing clones and seed them into the same well, creating a polyclonal line with a greater number of highly expressing cells.

Although initial experiments appeared to show colonies grew and resembled spherical structures in ultra-low attachment plates, analysis of these structures using confocal microscopy revealed a "bowl" shaped culture. Previous studies have used ultra-low attachment plates to create 3d spheroids of U87-MG cells (Vinci et al. 2012) but attempts to do so in this project failed. The structures created appeared to consist largely of monolayers. This suggests that the cells fail to form extensive cell-cell contacts, preferring to lie along the surface of the well. It has been shown that U87-MG cells disperse from aggregates quickly (Sabari et al. 2011) and high invasiveness may be a characteristic of the cell line. Future experiments could utilise Matrigel to create an ECM similar to that found *in vivo* which may aid in cell cohesion.

A significant difference in relative GFP fluorescence between the bottom and the top of the 3D structures was demonstrated in structures generated from a seeding density over 10000 cells/well. The smallest structure showed no difference in relative GFP fluorescence. This indicates that a size-dependent gradient may exist in the culture medium, starving the cells at the bottom of the structure of nutrients or oxygen, activating the IRES activity in the 5'UTR of EGFR. Thus whilst the model is perhaps not representative of tumour masses, it does display cells experiencing different environments within close proximity of each other and could still be used in testing gradients of stress.

5. Translational Profile of EGF Stimulation

Stimulation by EGF causes the activation of number of signalling cascades resulting in an increase in transcription of genes involved in proliferation, differentiation and cell survival. Perturbations in the transcriptional control of expression of these genes is well known to be important in cancer but over the last several years the importance of translational control in cancer has come to light (Truitt and Ruggero 2016). The role of EGFR in Alzheimer's disease has already been discussed, and it is therefore no surprise that its ligand, EGF, may affects genes and proteins involved in AD. It has been reported that EGF stimulation causes a rapid release of APP, which is thought to be through activation of protein kinase C (PKC) (Slack et al. 1997; Tang, Guan, et al. 2010). Additionally, elevated plasma EGF have been reported in AD (Marksteiner et al. 2011), although this is disputed by studies which show the opposite to be true (Chen-Plotkin et al. 2011; Bjorkqvist et al. 2012). Whilst the transcriptional effects of EGF stimulation has received wide attention, data regarding the effects on the translatome are lacking. Whilst certain biochemical changes are known to occur, such as a rapid increase in intracellular calcium concentration (Cheyette and Gross 1991), how these changes are mediated is not known. Knowledge of EGF's effect on the translation of specific mRNAs will aid in our understanding of its role in disease and identifying new therapeutic targets. A study on the translational and transcriptional effects of EGF stimulation in HeLa cells suggests a disconnect between the transcriptome and translatome, with 90% of the variation in expression found to be through translational control only;

just 5% of genes were both transcriptionally and translationally upregulated (Tebaldi et al. 2012). Thus it would be erroneous to presume an increase in transcription would correlate with an increase in protein expression and thus a direct role in Alzheimer's disease.

There is little information on the effects of EGF stimulation on translational efficiency. Of the reports that do exist, these usually regard expression of a single protein, such as the translational upregulation of Aurora-A by the activation of the PI3K/Akt/mTOR and MEK/ERK pathways (Lai et al. 2010). The advent of next generation sequencing coupled with polysome profiling offers us an opportunity to study the pathways and groups of genes which are translationally upregulated or downregulated by EGF signalling and may aid our understanding of its role in disease.

Our aim in this study was to reveal the translatome of EGF stimulation, by assessing those mRNAs which are have a greater translational efficiency following treatment.

5.1 Polysome Profiling EGF Stimulated Cells

The number of ribosomes associated with an mRNA can be used as a measure of translational efficiency. A higher number of attached ribosomes indicates that an mRNA has a higher level of protein synthesis. Thus under a given condition those mRNAs which have more bound ribosomes than in control can be regarded as being translationally upregulated in response to the stimulus.

In order to separate mRNAs based on the number of ribosomes attached, a sucrose density gradient is used. Cell lysates are applied to the column and, under high speed centrifugation, will sediment into different layers of the gradient depending on their density, such that 'heavier', highly translated mRNAs with more ribosomes will move to the lower fractions, whilst 'lighter', less translationally active mRNAs with few associated mRNAs won't migrate as far, appearing in higher fractions. This principle is shown in Figure 5.1.

Cell preparation for fractionation is described in section 2.2.12. Briefly, U87-MG cells were serum starved for 24 hours before being stimulated with 200ng/ml of EGF for 1 hour before lysis. Lysates were loaded onto sucrose gradients and centrifuged for 2 hours at 38000rpm (182106 x g), 4°C.

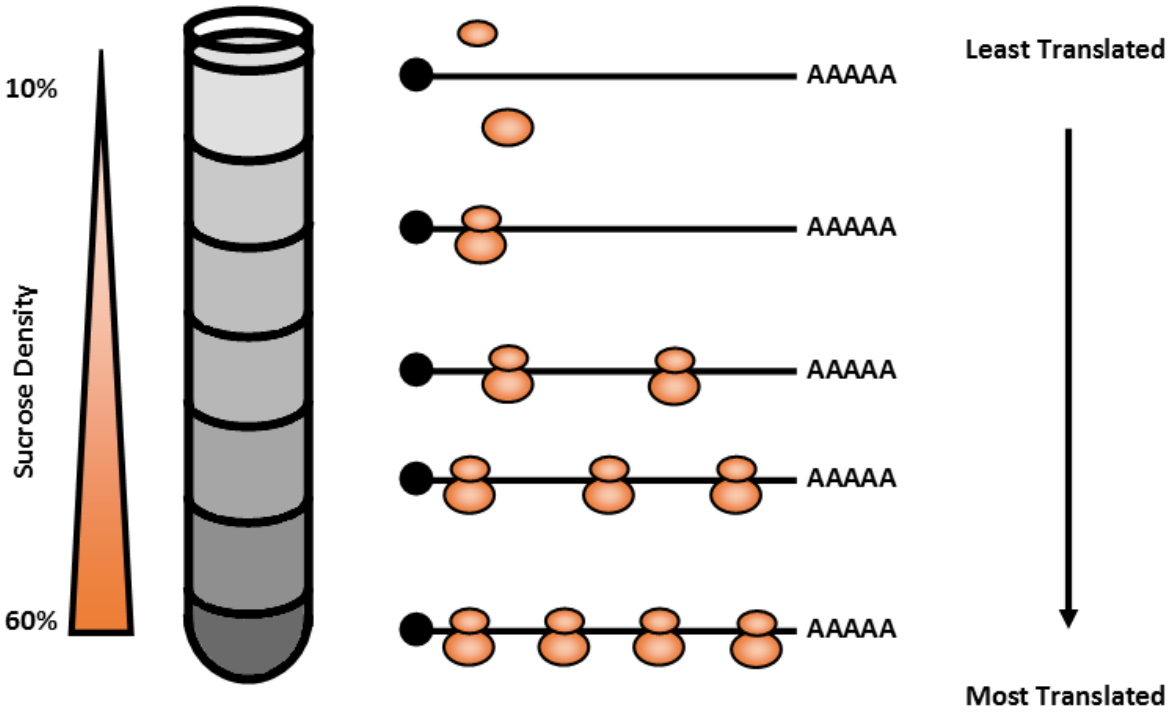

Figure 5.1 Measurement of Translational Efficiency by Sucrose Density Gradient Centrifugation. Highly translated transcripts are associated with more ribosomes, making these transcripts 'heavier'. 'Heavier' transcripts can be separated from 'lighter' transcripts by centrifugation in a sucrose density gradient.

By measuring the absorbance of the fractions at 260 nm a polysome profile is created; a plot showing the distribution of ribosomal subunits throughout the gradient. This plot can then be used to guide the division of the 1 ml fractions into subpolysomal and polysome pools. As shown in figure 5.2, the profile follows a typical pattern of three large peaks, representing the binding of 40S, 60S and 80S ribosomes, followed by a series of smaller peaks which represent increasing numbers of ribosomes. Thus those mRNAs that fall in fractions 1-5 have at most 1 whole ribosome bound, and are 'sub polysomal', whilst those from 6-12 have >1 ribosome, and are thus polysomal. The RNA samples are then purified, with $LiCl_2$ washes, to remove contaminating heparin, and ethanol

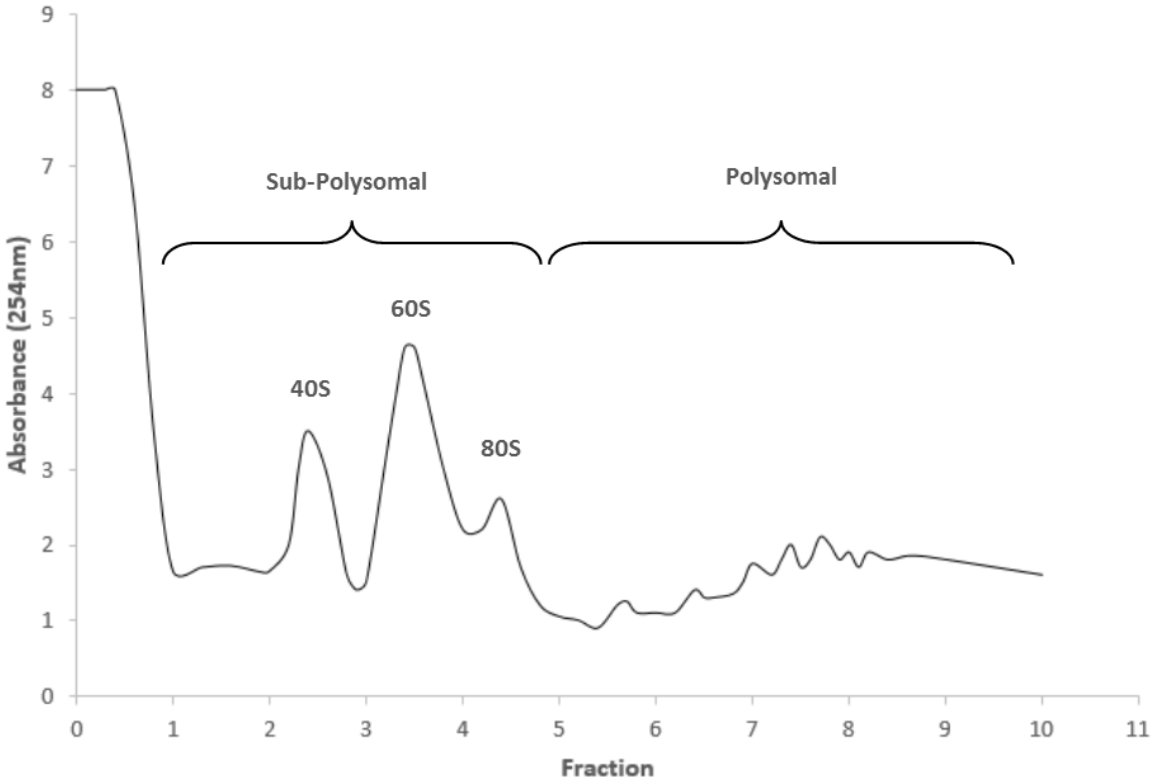

washes as described in section 2.2.13.

Figure 5.2 Polysome Profiling of EGF Stimulated Cells. RNA was fractionated using sucrose density gradients and the ribosomal content was quantified by reading the optical density of each fraction at 254nm. Fractions were pooled into subpolysomal (1-5) and polysomal (6-10) samples.

5.2 RNA Sequencing

High-throughput mRNA sequencing, RNA-seq, allows for the quantification of the entire transcriptome. Unlike microarray methods, the sequencing approach directly determines cDNA sequence, allowing the generation of a much larger data set and removes the inherent bias of probe selection. However RNA-seq is not free from bias (Finotello et al. 2014). Such bias include fragment bias, read mapping uncertainty and base composition. The Cufflinks program used in this project includes solutions to some of these biases (Roberts et al. 2011).

RNA-seq was performed on the pooled fractions by the University of Nottingham's DeepSeq facility using the NextSeq500 system (Illumina) and TruSeq LT adapters, generating 30 million reads for each library. Briefly, the fractions were submitted to ribosome depletion, removing ribosomal RNA (rRNA) to make optimal use of sequencing capacity. RNA was then fragmented and transcribed into cDNA with addition of adapters. Reads of 75bp paired ends were generated.

The sequencing reads were analysed for quality using the FastQC program (Andrews 2010). FastQC checks the per-base sequence quality of reads, per-sequence GC content and shows any over-represented sequences. The quality of reads in all samples was found to be of good quality and did not further processing. Adapter sequences, however, were removed from reads using the Trimmomatic program (Bolger, Lohse, and Usadel 2014).

The sequencing reads were then aligned to the reference genome. The reference genome and annotation used in this project was the most recently updated human genome from USCS, hg38 (Rosenbloom et al. 2015). The Bowtie program is regarded as one of the most efficient alignment programs, using an FM (full text minute space) index to store the reference genome sequence and allow for rapid searches (Langmead et al. 2009). Alignment with this FM index allows reads to be aligned at a rate of tens of millions per CPU hour. However, Bowtie in isolation cannot map reads with large gaps, thus it cannot align reads that span introns. The TopHat program was created to get past this limitation and uses Bowtie as an alignment engine (Trapnell, Pachter, and Salzberg 2009). First, TopHat uses Bowtie to map all reads to the reference genome. TopHat allows Bowtie to report more than one alignment for each read, up to 10. Any reads that align more than this are regarded as low complexity reads and are excluded. TopHat can find splice junctions without a reference annotation by mapping reads to the genome and identifying potential exons. TopHat then builds a database of possible junctions from this initial mapping information and maps the reads to the splice junctions to confirm them.

The Cufflinks suite of programs takes the aligned reads generated from TopHat and quantifies them (Trapnell et al. 2010). Cufflinks filters out background and artificial transfrags using a rigorous statistical model of RNA-seq. Expression levels are calculated from reads based on reads counts are directly proportional to the. As part of library construction to optimise output, cDNA fragments are generally size-selected, meaning that a transcript that is twice as long as another will produce twice as many reads despite a similar abundance. Cufflinks

normalises the read count to the length of transcript they are mapped to (Roberts et al. 2011). Counts are also normalised to the total yield to allow comparison between runs where different volumes of sequencing reads may occur. Incorporating these two normalisation steps gives the unit 'fragments per kilobase of transcript per million mapped fragments', or FPKM.

In order to assess the samples for differential expression in the Cuffdiff program (Trapnell et al. 2013), they must be merged together into a single, larger index. This was executed using the Cuffmerge program. The subpolysomal and polysomal transcripts for each condition were merged together, creating an EGF and a DMSO master transcriptome. The transcriptomes were also merged with the reference annotation from UCSC. Genes were then assessed for differential expression through the Cuffdiff program. Differential expression was calculated first between the two transcript lists, subpolysomal and polysomal. The change in this subpolysomal-polysomal ratio for each gene was then calculated between DMSO and EGF conditions to generate a value which represented the fold change in polysomal shift after treatment with EGF.

As only 1 biological replicate for each condition and sub/polysomal fraction was used, we sought to reduce false positives in the differential expression. To achieve this, firstly only genes with a log_2 fold change of +/- 1 were included in the upregulated and downregulated transcript lists. Secondly, transcripts with low abundance were removed. To set this limit the abundances, which were determined from the combined FPKM values of all samples for each gene, were analysed in a histogram. As seen in figure 5.3, most genes fall within the boundaries of the -2 and 1 bins, with a long tail of genes of higher abundancies from the 4 to 11 bins. Relatively fewer genes are found in the -3 to -6 bins. Thus

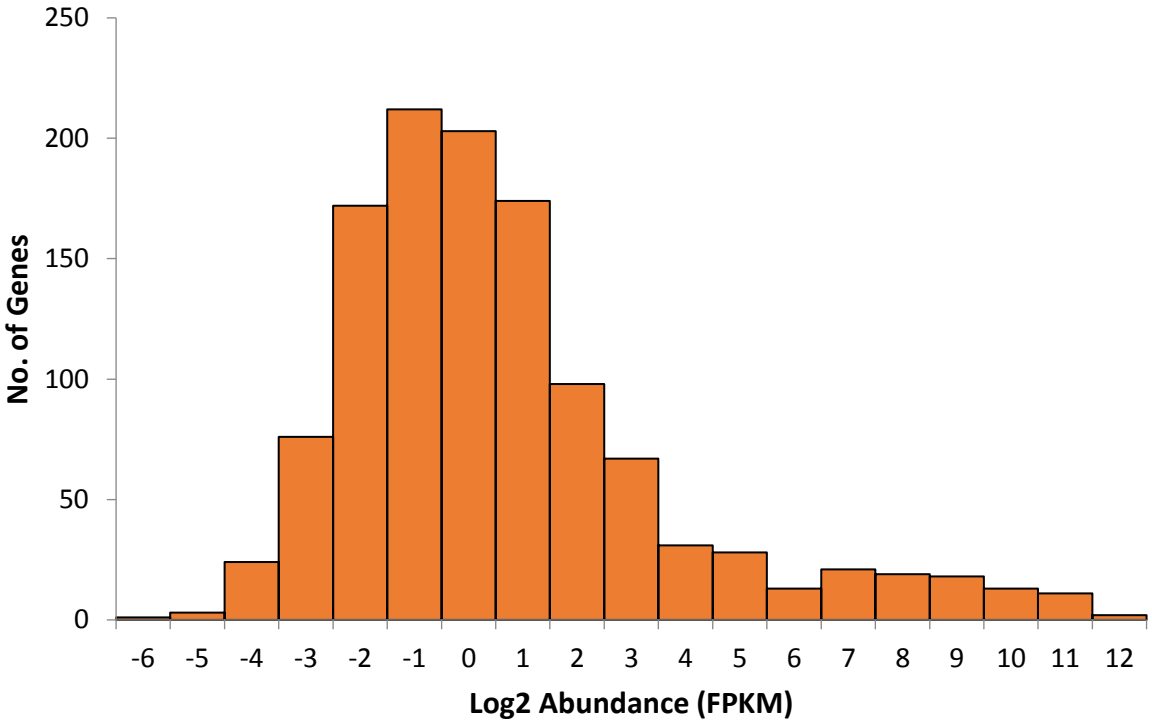

Figure 5.3. Distribution of Abundancies of Upregulated and Downregulated Genes. The abundance of each gene was calculated from the sum of the subpolysomal and polysomal FPKM values of both treatments (DMSO and EGF). The Log_2 of this value was then used to place the data into bins with intervals of 1.

a lower boundary for inclusion in the gene lists at -3 $\log_2$ FPKM. This produced a list of 557 upregulated mRNAs and 639 downregulated mRNAs.

5.3 Analysis of Enriched Genes in Relation to Alzheimer's Disease

Analysis of the gene lists was completed through the Database for Annotation, Visualisation and Integrated Discovery (DAVID), a web-based program which clusters genes into various categories including, but not limited to, function, pathway and tissue expression, according to the Gene-Ontology (GO) annotations attributed to them (Dennis et al, 2003).

Caution must be used when assessing RNAseq data for evidence of disease involvement. Validation of expression by quantitative PCR is necessary in order to draw firm conclusions. However, analysis of the pathways and function lists can aid in formation of hypotheses and influence the direction of further research. The major functional groups and pathways which correlate with the gene lists of discussed below.

5.3.1 Alzheimer's Disease

With the GAD_DISEASE annotation, it can be seen that among the genes in the upregulated list, 27 of them are associated with Alzheimer's disease, whilst 2 Alzheimer's related genes are found in the downregulated list. These genes are shown in table 5.1.

A number of the genes found on the list have been shown to be regulated by EGF in other studies. These include 5-lipoxygenase activating protein (ALOX5AP), matrix metallopeptidase 9 (MMP9), apolipoprotein E (ApoE) and cystatin C (CST3). ALOX5AP is necessary for the activation of ALOX5, a non-heme iron dioxygenase which plays a key role in the synthesis of leukotrienes and in mounting inflammatory responses. The increase in ALOX5AP by EGF correlates well with the observation of EGFR-mediated transcriptional upregulation of ALOX5 (Lee et al. 2010) and with EGF activation of calcium channels through ALOX5-mediated leukotriene production (Peppelenbosch et al. 1992). Polymorphisms of both the ALOX5 and ALOX5AP genes have also been suggested as being involved in AD (Qu, Manev, and Manev 2001) (Manev and Manev 2006). ALOX5 is found to be elevated in post-mortem brains of AD patients (Ikonomovic et al. 2008), and has been proposed to be involved in the production of Aβ (Firuzi et al. 2008). MMP9 is a matrixin, involved in the degradation of the extracellular matrix and operating during angiogenesis and wound repair. In Alzheimer's, MMP9 levels are increased in the plasma of AD patients (Lorenzl et al. 2003) and inhibition of MMP9 in mice improves cognitive impairment caused by Aβ (Mizoguchi et al. 2009). Tau is a substrate of MMP9 and is cleaved in a manner that facilitates aggregation (Nubling et al. 2012). The EGF signalling pathway has been implicated in upregulation of MMP9 in NSCLC (Cox, Jones, and O'Byrne 2000), increasing MMP9 mRNA levels and protein expression through the JAK/STAT pathway, primarily JAK3 (Kim et al. 2009).

Gene	Accession No.	DMSO Poly/Sub	EGF Poly/Sub	EGF/DMSO Ratio	Log2 Fold Change
CACNB2	783	0.025	1.534	62.478	5.965
CTNNA3	29119	0.082	1.249	15.138	3.920
SERPINC1	462	0.161	1.249	7.769	2.958
OGDHL	55753	0.231	1.202	5.199	2.378
LRP5	4041	0.151	0.727	4.809	2.266
PTPN6	5777	0.126	0.544	4.313	2.109
DRD4	1815	0.323	1.219	3.775	1.917
CALHM1	255022	0.114	0.426	3.719	1.895
ALOX5AP	241	0.507	1.769	3.488	1.802
UCP3	7352	0.046	0.144	3.172	1.665
CETP	1071	0.962	2.917	3.032	1.600
CALML3	810	0.221	0.638	2.888	1.530
ACTN3	89	0.736	2.115	2.876	1.524
JAKMIP3	282973	0.306	0.877	2.866	1.519
MMP9	4318	0.283	0.754	2.665	1.414
KCNJ11	3767	0.155	0.411	2.647	1.404
LTB4R	1241	0.611	1.612	2.638	1.400
MRC1	4360	0.207	0.541	2.620	1.389
SAA2	6289	1.292	3.363	2.603	1.380
EIF3A	8661	0.511	1.208	2.362	1.240
SLK	9748	0.664	1.553	2.338	1.225
PITX3	5309	1.460	3.290	2.253	1.172
EGR2	1959	0.657	1.446	2.202	1.139
IL18	3606	0.344	0.706	2.055	1.039
DYDC1	143241	0.140	0.285	2.030	1.021
ANK3	288	0.642	1.301	2.026	1.018
APOE	348	3.140	1.459	0.465	-1.106
CST3	1471	3.118	1.381	0.443	-1.175

Table 5.1. Enriched Genes Associated With Alzheimer's Disease. Ontological clustering performed by DAVID web-tool. Poly/Sub = FPKM of polysomal fraction divided by FPKM of subpolysomal fraction. Log_2 fold change of Polysomal:Subpolysomal ratio between EGF treatment and DMSO treatment.

LRP5 is of interest as there are conflicting reports of its role in AD. LRP5 is one of several low density lipoprotein receptor related proteins (LRPs) which are involved in the Wnt pathway. LRP5 is a transmembrane receptor and acts as a co-receptor with LRP6 to the Frizzled receptor, which transduce canonical WNT signals. Early reports suggested LRP expression is reduced in the brains of AD patients (Kang et al. 2000) and is neuroprotective through the binding of soluble and cell surface APP (Kounnas et al. 1995; Knauer, Orlando, and Glabe 1996) as well as binding and internalising ligands which form complexes with Aβ such as ApoE (Yang et al. 1999), lactoferrin and α2-macroglobulin (α2M) (Qiu et al. 1999). Thus LRP seems to modulate Aβ deposition by increasing its clearance. Yet LRP, which is only expressed in neurons in normal brains, is found to be upregulated in reactive astrocytes, associated with mature amyloid plaques, in AD (Rebeck et al. 1993). It has also been found that restoring LRP function to LRP-deficient cells increases Aβ synthesis and that blocking LRP with the LRP antagonist receptor-associated protein (RAP) significantly lowers Aβ production (Ulery et al. 2000).

Interestingly, just two genes associated with Alzheimer's disease appear on the downregulated list; ApoE and CST3. Both ApoE and CST3 have allelic risk factors, and both are regarded as possible therapeutic targets and are found to be low in AD. The ApoE4 isoform is known to be the major genetic risk factor for AD, whilst it is generally regarded that increasing the expression of any of the ApoE isoforms improves Aβ clearance, although some dispute this. Two studies have shown that removing one copy of either ApoE3 or E4 isoforms actually reduces Aβ levels (Kim et al. 2011; Bien-Ly et al. 2012). Yet the majority of

published literature suggests ApoE aids in clearance either through proteolytic degradation (Jiang et al. 2008) or more recently by indirect means through receptor binding (Zlokovic et al. 2010; Verghese et al. 2013). Thus these results might indicate a pathway by which Aβ clearance becomes impaired through a reduction in available ApoE proteins, caused by an increase in EGF signalling. However a 1997 study suggests the opposite, that EGF increases ApoE secretion and treatment with EGF could ameliorate ApoE deficiencies (Baskin et al. 1997). EGF treatment in this study lasted for 48 hours, as opposed to the 1 hour treatment, so it is possible effects seen in that study are caused by alterations in transcriptional control and a sustained exposure to high levels of EGF in serum.

CST3 is a cysteine protease inhibitor and is often used as a biomarker of kidney function. The data herein suggests EGF reduces CST3 expression, and other studies support this, with activation of EGFR reducing CST3 levels in nasopharyngeal carcinoma cells (Tang, Guan, et al. 2010). There are conflicting reports for the role of CST3 in AD, with primary reports showing CST3 colocalising with plaques, suggesting a role in plaque growth (Steinhoff et al. 2001). However, subsequent reports disagree with this view. Reduced levels of CST3 in the serum of elderly men was associated with development of AD (Sundelof et al. 2008) and CST3 inhibits Aβ oligomerisation *in vitro* (Tizon et al. 2010). CST3 binds the Aβ region of APP, increasing the levels of secreted APP but not the levels of secreted Aβ (Pawlik et al. 2004). This association inhibits Aβ fibril formation (Sastre et al. 2004). Along with this, a polymorphism of *CST3* (commonly referred to as *CST3 B*) is a risk factor for AD and causes a reduction in CST3 levels (Benussi et al. 2003). This polymorphism has also been

linked to a greater risk of AD when combined with the APOE4 allele (Beyer et al. 2001; Cathcart et al. 2005).

Aside from genes that are regarded as being directly or indirectly involved in Alzheimer's disease pathology, there are number of conditions associated with the disease.

5.3.2 Inflammation

Eighteen genes related to inflammation are found in the upregulated list, and are listed in table 5.2. Inflammation has been long associated with Alzheimer's disease, yet whether it is involved in the cause of the disease is still uncertain. More recent evidence points to a contributing role (Heppner, Ransohoff, and Becher 2015). The neuroinflammation which occurs in AD pathology differs to that of neuroinflammatory diseases such as encephalitides in that it is driven by innate immune cells rather than adaptive immune cells (Prinz et al. 2011). Thus glial cells, such as astrocytes and microglial cells contribute highly to this response. EGF and its receptor EGFR are known to be involved in eliciting the inflammatory response. EGFR drives the expression of a number of proteins involved in the innate immune response to skin injury (Sorensen et al. 2006). The action of the EGF signalling pathway has also been found to be involved in the development of the inflammatory microenvironment in hepatocellular carcinoma (Berasain et al. 2009) and it is likely that this is through the ERK signalling pathway, stimulating interleukin-8 (Huang et al. 2014). In neuronal inflammation, inhibition of EGFR signalling reduces the inflammatory response of microglial cells and reduces the secondary damage associated with

inflammation in spinal cord injury (Qu et al. 2012). Inhibition of EGFR also reduces astrocyte activation and pro-inflammatory cytokine secretion in reactive astrocytes (Li et al. 2014). Indirectly, EGFR can be attributed to neuroinflammation through the MAPK/ERK pathway, with MAPK regulating pro-inflammatory cytokines in a post-transcriptional manner (Clark et al. 2009). The p38 MAPK class of MAPKs is also responsible for IL-1, IL-5 and IL-8 production, and chemokine ligand 2 (CCL2) (Brook et al. 2000; Winzen et al. 1999), which may be involved in AD (Kiyota et al. 2013; Sheng et al. 2001).

6 of the 16 genes on the inflammatory list are also found on the Alzheimer's disease list, highlighting their association. One of these 6, interleukin 18 (IL-18) has been shown to be upregulated in the frontal lobe of AD patients (Ojala et al. 2009) and increases the production of Aβ through the induction of BACE-1 and increased APP processing in neuronal cells (Sutinen et al. 2012). SERPINC1 and F1 are also found on both lists. The SERPIN superfamily is a large group of extracellular and intracellular protease inhibitors, and are involved in a wide array of processes, one of which is inflammation. SERPINF1 is unusual as it is a non-inhibitory SERPIN, is a regulator of angiogenesis and thought to be neurotrophic (Irving et al. 2000), thus SERPINF1 may mediate the proliferative signal induced by EGF stimulation (Yamada, Ikeuchi, and Hatanaka 1997). In inflammation, SERPINF1 appears to be anti-inflammatory, reducing both tumour necrosis factor alpha (TNF) as

Gene	Accession No.	DMSO Poly/Sub	EGF Poly/Sub	EGF/DMSO Ratio	Log2Fold Change
ALOX5AP	241	0.507	1.769	3.488	1.802
CCL3L1	6349	0.398	2.076	5.215	2.383
CYP4F11	57834	0.478	1.534	3.212	1.683
IL18	3606	0.344	0.706	2.055	1.039
ITGB6	3694	0.284	0.675	2.374	1.248
LTB4R	1241	0.611	1.612	2.638	1.400
LTB4R2	56413	0.611	1.612	2.638	1.400
MMP25	64386	0.090	0.286	3.168	1.663
NLRC4	58484	0.484	1.468	3.032	1.600
PGLYRP1	8993	0.482	0.986	2.047	1.033
PTGDR	5729	0.312	0.696	2.232	1.159
PTGIS	5740	0.197	0.581	2.951	1.561
SAA2	6289	1.292	3.363	2.603	1.380
SAA2-SAA4	100528017	1.292	3.363	2.603	1.380
SAA4	6291	1.292	3.363	2.603	1.380
SERPINC1	462	0.161	1.249	7.769	2.958
SERPINF1	5176	0.383	1.169	3.051	1.609
THBS1	7057	0.261	0.673	2.575	1.365

Table 5.2. Enriched Genes Associated With Inflammation. Ontological clustering performed by DAVID web-tool. Poly/Sub = FPKM of polysomal fraction divided by FPKM of subpolysomal fraction. Log_2 fold change of Polysomal:Subpolysomal ratio between EGF treatment and DMSO treatment.

well as IL-18 in mouse models (Zhou et al. 2009), and SERPINF1 -/- mice produce a proinflammatory phenotype (Shin, Sorenson, and Sheibani 2014). However, SERPINF1 is also known to interact with proteins involved in APP processing (De Jager et al. 2014). SERPINC1, also known as antithrombin is a small protein involved in the inhibition of coagulation enzymes. Curiously, one of its targets, thrombin, is thought to be elevated in AD brains (Akiyama et al. 1992; Yin et al. 2010) and has been suggested to act as a mediator of inflammation and ROS production (Tripathy et al. 2013). For these reasons, thrombin has been identified as a possible target for treatments (Rami 2012; Tripathy et al. 2013). Yet SERPINC1 itself has been found in amyloid deposits, neurofibrillary tangles and hippocampus in AD brains, and in some cases within astrocytes, along with an increased level of mRNA within astrocytes (Kalaria et al. 1993).

5.3.3 Calcium Ion Transport and Homeostasis

Twelve genes involved in calcium ion transport are translationally upregulated in response to EGF stimulation, as shown in table 5.3. EGF is known to activate calcium signalling, and cause an increase intracellular Ca2+ concentration (Bryant et al. 2004). Increases in intracellular calcium concentration have been well documented in AD. The calcium hypothesis of AD suggests that sustained disruption to calcium homeostasis is causative of neurodegeneration (Khachaturian 1987), but how calcium levels cause the development of lesions and plaques is unknown. However, a key prerequisite of the calcium hypothesis is the early dysregulation of calcium homeostasis. This has been seen in a number of mouse models (Larson et al. 1999; Leissring et al. 2000) as well as

samples from high risk humans, where calcium signalling is altered months before extracellular Aβ is detected (Etcheberrigaray et al. 1998). Of the genes involved in calcium ion transport or homeostasis, a few have been directly linked to Alzheimer's disease. For instance, S100A1, a calcium sensor, is elevated in a number of neurological disorders (Zimmer et al. 2005), binding to ryanodine receptors (RYR) in AD brains (Afanador et al. 2014). Alterations to RYR binding and function may be important in the early stages of AD (Kelliher et al. 1999). Inhibition of S100A1 has been postulated as a potential strategy for reducing abhorrent Ca^{2+} signalling in AD (Afanador et al. 2014). The cysteine protease, calpain 3 (CAPN3) also has links to AD, with calcium-dependent activation implicated in the cleavage of APP (Liu et al. 2005). Activated calpain is also thought to increase tau protein aggregation (Yang and Ksiezak-Reding 1995; Jin et al. 2015). EGF signalling is required for calpain activation, (Glading et al. 2000) and is thought to occur through the ERK pathway even in the absence of increased cellular calcium (Glading et al. 2004). Calpain is also known to cleave and inactivate the sodium-calcium exchanger, preventing calcium efflux from the cell (Atherton et al. 2014).

Twenty three downregulated genes are associated with calcium homeostasis, including ApoE. The ApoE4 isoform has been shown to be associated with a higher intracellular calcium concentration following brain injury than other isoforms (Jiang et al. 2015), but the mechanism by which this occurs is unknown. In the same study, cells that lack ApoE entirely have even higher levels of intracellular calcium than those treated with ApoE4, suggesting that it

Gene	Accession No.	DMSO Poly/Sub	EGF Poly/ Sub	EGF/DMSO Ratio	Log2 Fold Change
CACNB2	783	0.025	1.534	62.478	5.965
P2RX3	5024	0.325	2.925	8.991	3.169
STIM1	6786	0.178	1.467	8.263	3.047
PTPN6	5777	0.126	0.544	4.313	2.109
DRD4	1815	0.323	1.219	3.775	1.917
CALHM1	255022	0.114	0.426	3.719	1.895
CACNG8	59283	0.243	0.736	3.031	1.600
CAPN3	825	0.154	0.447	2.912	1.542
GCG	2641	0.345	0.906	2.628	1.394
CATSPER2	117155	0.454	1.193	2.626	1.393
JPH2	57158	0.614	1.599	2.605	1.381
TEX101	83639	0.135	0.309	2.294	1.198
S100A1	6271	0.327	0.740	2.263	1.178
ATP2A3	489	1.285	2.903	2.259	1.176
TRPV3	162514	0.358	0.773	2.161	1.111
CHRFAM7A	89832	0.381	0.773	2.028	1.020

Table 5.3. Enriched Genes Associated With Calcium Ion Transport. Ontological clustering performed by DAVID web-tool. Poly/Sub = FPKM of polysomal fraction divided by FPKM of subpolysomal fraction. Log_2 fold change of Polysomal:Subpolysomal ratio between EGF treatment and DMSO treatment.

could be a loss of function, not gain, that causes E4 carriers to have higher intracellular calcium levels. With this in mind, a reduction in ApoE in general would result in an increase in intracellular calcium concentration. Thus our data suggest that EGF stimulation could mediate dysregulation of calcium regulation through reducing the expression of proteins important for calcium ion homeostasis and by upregulating proteins which cause an increase in intracellular calcium concentration.

In conclusion, although an upregulation in translation of a single protein identified as being involved in Alzheimer's disease may not be justification for attributing EGF stimulation as a protagonist in AD progression, the combination of genes affected and their associated functions constructs a scenario which have many characteristics found in Alzheimer's disease. Validation of the upregulation and downregulation of these genes should be completed before further investigations into EGF's role in Alzheimer's disease, but these preliminary data suggests that EGF signalling could represent an important area of research for therapeutics.

Gene	Accession No.	DMSO Poly/Sub	EGF Poly/Sub	EGF/DMSO Ratio	Log2 Fold Change
GALR2	8811	5.630	0.599	0.106	-3.233
PYGM	5837	0.470	0.052	0.111	-3.166
CSRP3	8048	7.148	0.976	0.136	-2.873
HTR1D	3352	1.509	0.214	0.142	-2.816
JSRP1	126306	1.864	0.287	0.154	-2.699
NPFF	8620	0.204	0.044	0.215	-2.220
JPH3	57338	1.809	0.425	0.235	-2.088
GPR35	2859	0.547	0.160	0.292	-1.774
ELANE	1991	0.493	0.151	0.307	-1.704
S1PR4	8698	1.942	0.602	0.310	-1.690
HCRTR1	3061	0.846	0.302	0.357	-1.485
AGT	183	3.428	1.347	0.393	-1.348
TNNI3	7137	0.678	0.287	0.422	-1.243
CIB2	10518	0.589	0.263	0.446	-1.166
EDN2	1907	1.303	0.592	0.455	-1.137
GNAT2	2780	3.061	1.398	0.457	-1.130
PRKACA	5566	2.140	0.991	0.463	-1.111
APOE	348	3.140	1.459	0.465	-1.106
CD40	958	2.041	0.949	0.465	-1.105
PTGER1	5731	1.433	0.685	0.478	-1.065
CORO1A	11151	1.595	0.790	0.496	-1.013
FPR1	2357	3.307	1.643	0.497	-1.009
CYBA	1535	3.238	1.610	0.497	-1.008

Table 5.4. Enriched Genes Associated With Calcium Homeostasis. Ontological clustering performed by DAVID web-tool. Poly/Sub = FPKM of polysomal fraction divided by FPKM of subpolysomal fraction. Log_2 fold change of Polysomal:Subpolysomal ratio between EGF treatment and DMSO treatment.

5.3.4 Diabetes

Diabetes is generally accepted to be a risk factor for development of Alzheimer's disease. Some studies show that type II diabetes can increase the risk of dementia by 50-150% (Li, Song, and Leng 2015). The mechanisms involved in this association are unknown, but several have been proposed including insulin resistance and deficiency, vascular inflammation and metabolic syndromes.

Both AD and type II diabetes have been shown to have insulin signalling abnormalities (de la Monte and Wands 2005). Defective insulin signalling increases Aβ production and its aggregation (Wang et al. 2010; Yamamoto et al. 2012). Similarly, high levels of cholesterol have been seen in AD and is known to increase Aβ synthesis through APP processing by modulating gamma secretase activity. (Cole et al. 2005). Hyperglycaemia can damage the brain through oxidative stress (Biessels et al. 2002).

One of the most prominent links between diabetes and AD is ApoE. In diabetes, ApoE is poorly lipidated as the cholesterol transporter ABCA1 is reduced (Tang, Kanter, et al. 2010). ABCA1 deficiency is associated with impaired ApoE secretion in the brain (Hirsch-Reinshagen et al. 2004) and exacerbates Aβ deposition in ApoE4 carries, suggesting that poor lipidation of ApoE reduces clearance of Aβ (Fitz et al. 2012). ApoE4 is also risk factor for diabetes (El-Lebedy, Raslan, and Mohammed 2016), associated with poor clearance of cholesterol (Knouff et al. 1999). Insulin resistance is associated with inflammation. Expression of interleukins are particularly noted to be

Gene	Accession No.	DMSO Poly/Sub	EGF Poly/Sub	EGF/DMSO Ratio	Log2 Fold Change
CTNNA3	29119	0.082	1.249	15.138	3.92
CD37	951	0.242	2.945	12.143	3.602
MC4R	4160	0.202	2.114	10.451	3.386
CPAMD8	27151	0.725	6.951	9.587	3.261
IL2RB	3560	0.338	2.889	8.559	3.098
SERPINC1	462	0.161	1.249	7.769	2.958
RIC3	79608	0.643	4.736	7.361	2.88
MYH7B	57644	0.31	1.968	6.344	2.665
ICAM4	3386	0.143	0.851	5.954	2.574
VAV1	7409	0.611	3.37	5.517	2.464
LRP5	4041	0.151	0.727	4.809	2.266
SLC25A21	89874	0.188	0.893	4.751	2.248
IRAK3	11213	0.116	0.541	4.642	2.215
SOCS2	8835	0.351	1.63	4.644	2.215
CXCL16	58191	0.374	1.606	4.294	2.102
ERBB4	2066	1.842	7.794	4.232	2.081
DRD4	1815	0.323	1.219	3.775	1.917
KSR2	283455	0.585	2.14	3.658	1.871
HPX	3263	0.246	0.882	3.585	1.842
ACVRL1	94	0.564	2.015	3.572	1.837
OCA2	4948	0.188	0.66	3.513	1.813
MASP2	10747	0.454	1.535	3.383	1.758
CYP4F2	8529	1.948	6.409	3.289	1.718
UCP3	7352	0.046	0.144	3.172	1.665
MMP25	64386	0.09	0.286	3.168	1.663
PKP1	5317	0.555	1.744	3.139	1.65
SERPINF1	5176	0.383	1.169	3.051	1.609
COL3A1	1281	0.33	1.004	3.046	1.607
CETP	1071	0.962	2.917	3.032	1.6
PTGIS	5740	0.197	0.581	2.951	1.561
ACTN3	89	0.736	2.115	2.876	1.524
PTK6	5753	0.203	0.58	2.861	1.517
MMP9	4318	0.283	0.754	2.665	1.414
KCNJ11	3767	0.155	0.411	2.647	1.404
GCG	2641	0.345	0.906	2.628	1.394
SAA2	6289	1.292	3.363	2.603	1.38
SAA4	6291	1.292	3.363	2.603	1.38
THBS1	7057	0.261	0.673	2.575	1.365
ITGB6	3694	0.284	0.675	2.374	1.248
PTGDR	5729	0.312	0.696	2.232	1.159
CD22	933	0.537	1.107	2.06	1.043
IL18	3606	0.344	0.706	2.055	1.039
PGLYRP1	8993	0.482	0.986	2.047	1.033

Table 5.5. Selected Upregulated Transcripts Associated With Diabetes. Ontological clustering performed by DAVID web-tool. Poly/Sub = FPKM of polysomal fraction divided by FPKM of subpolysomal fraction. Log_2 fold change of Polysomal:Subpolysomal ratio between EGF treatment and DMSO treatment.

common between AD and diabetes, with elevated IL-18 associated with greater risk of development of type II diabetes (Thorand et al. 2005).

The role of EGF in diabetes is not fully understood. There are contradictory reports of EGF levels in diabetes. Early reports found low levels of EGF in the plasma of genetically diabetic mice (Kasayama, Ohba, and Oka 1989), whilst treatment with EGF "cures" chronic diabetes in mice by regeneration of beta cells in the pancreas (Baeyens et al. 2014). However, inhibition of EGFR signalling attenuates kidney enlargement in experimental diabetes (Wassef, Kelly, and Gilbert 2004), and deletion of EGFR in podocytes attenuates diabetic nephropathy (Chen, Chen, and Harris 2015). It could be the case that EGF's role in diabetes is tissue specific.

59 genes associated with diabetes are translationally upregulated following EGF stimulation, however 74 genes associated with diabetes are downregulated. Selected enriched genes can be seen in table 5.5 and 5.6. Of the upregulated genes, 35% are also found on either the inflammation or Alzheimer's disease lists. The downregulated lists contains a diverse range of genes. Some of these have been shown to be downregulated in diabetes, such as the apolipoproteins APOE and APOA5, involved in triglyceride storage and whose reduction is linked to obesity, (Zheng, Zhao, and Yan 2013) and also genes related to insulin, including Acyl-CoA dehydrogenease (ACADS) (Hornbak et al. 2011), oncostatin M, whose deficiency results in obesity, adipose inflammation and insulin resistance (Komori et al. 2014) and cathespin H, which regulates β-cell function with deficiency causing low insulin levels (Floyel et al. 2014). But many of the downregulated genes are thought to be important in diabetes

progression, such as MMP10, which contributes to the inflammatory response in type I diabetes (Toni et al. 2013) and found elevated in corneal epithelium of diabetic patients (Matsumura et al. 2015; Saghizadeh et al. 2001), and pleckstrin (PLEK), another protein involved in inflammation, which has been shown to be commonly phosphorylated in diabetes, increasing cytokine secretion (Ding et al. 2007). That some inflammatory genes are upregulated but others are downregulated suggests that either EGF stimulation operates a specific inflammatory pathway, not just an inflammatory response, or possibly that the effect is tissue specific. Thus this data suggests that EGF's main role in diabetes is through promoting pro-inflammatory signalling, with potential for causing insulin resistance.

Gene	Accession No.	DMSO Poly/Sub	EGF Poly/ Sub	EGF/DMSO Ratio	Log2 Fold Change
IL12RB2	3595	4.033	0.22	0.054	-4.199
FAM151A	338094	1.957	0.197	0.101	-3.309
ARHGAP8	23779	1.638	0.178	0.109	-3.201
PRR5-ARHGAP8	553158	1.638	0.178	0.109	-3.201
CSRP3	8048	7.148	0.976	0.136	-2.873
LGALS2	3957	8.493	1.278	0.15	-2.733
HRASLS2	54979	0.873	0.16	0.183	-2.452
SERPINA6	866	5.335	1.035	0.194	-2.365
ADORA3	140	1.276	0.252	0.197	-2.342
PRKCZ	5590	1.849	0.376	0.203	-2.299
PPP1R1B	84152	2.109	0.457	0.216	-2.208
PLEK	5341	2.042	0.45	0.22	-2.183
MIP	4284	1.029	0.229	0.223	-2.167
CELF2	10659	1.768	0.445	0.252	-1.989
TNFSF18	8995	4.222	1.064	0.252	-1.988
ACSM3	6296	1.623	0.424	0.261	-1.938
CYP1A1	1543	0.402	0.106	0.263	-1.928
MGP	4256	6.128	1.617	0.264	-1.922
SOAT2	8435	0.684	0.181	0.264	-1.92
ICOSLG	23308	2.905	0.78	0.268	-1.897
IL12RB1	3594	1.927	0.54	0.28	-1.836
CLCNKA	1187	1.597	0.454	0.284	-1.814
MYRF	745	1.413	0.403	0.285	-1.811
OSM	5008	1.054	0.312	0.296	-1.759
CTSH	1512	0.401	0.119	0.298	-1.748
KCNE2	9992	1.233	0.368	0.299	-1.744
GP1BA	2811	2.381	0.712	0.299	-1.742
MDGA2	161357	1.701	0.511	0.3	-1.736
CFAP43	80217	0.829	0.252	0.304	-1.72
CLCNKB	1188	0.303	0.102	0.336	-1.575
SELL	6402	2.525	0.853	0.338	-1.566
PYY	5697	0.839	0.295	0.351	-1.51
MMP10	4319	6.619	2.615	0.395	-1.34
APOH	350	2.302	0.974	0.423	-1.241
APOA5	116519	0.438	0.192	0.439	-1.187
SERPINB2	5055	3.006	1.365	0.454	-1.139
APOE	348	3.14	1.459	0.465	-1.106
CD40	958	2.041	0.949	0.465	-1.105
MMP15	4324	4.316	2.058	0.477	-1.068
ACADS	35	2.911	1.44	0.495	-1.015

Table 5.6. Selected Downregulated Transcripts Associated With Diabetes. Ontological clustering performed by DAVID web-tool. Poly/Sub = FPKM of polysomal fraction divided by FPKM of subpolysomal fraction. Log_2 fold change of Polysomal:Subpolysomal ratio between EGF treatment and DMSO treatment.

5.4 Analysis of Sequence

The 5'UTR, 3'UTR, coding region and full mRNA sequence of each gene in the upregulated and downregulated lists was assessed in Biomart (Durinck et al. 2005) and the length and nucleotide composition of each transcript was quantified using a linux based program. The nucleotide composition of the 5'UTR of a transcript can reveal the likelihood of structures being presented based on the GC content. Figure 5.4 displays the sequence composition among the 5'UTRs, 3'UTRs, coding regions and full length sequences of the genes in the upregulated and downregulated lists. As can be seen, there is no significant difference in nucleotide content between the upregulated (UP) and downregulated (DOWN) genes in any of the groups ($p = 0.95$, by chi squared test). To further test the presence of structures within the 5'UTRs, the 5'UTR sequences were submitted to the ViennaRNA program to determine the minimum free energy structure for each 5'UTR (Lorenz et al. 2011). Genes which have lower free energies can be considered to be more structured. Figure 5.5 shows a boxplot of the minimum free energies of genes in the UP or DOWN lists. UP genes have a median of -56.6 kcal/mol, whilst DOWN genes have a median of -54.2 kcal/mol. An overlap in the 95% confidence intervals of the two medians suggesting that there is no significant difference in minimum free energy between the upregulated and downregulated sets. This correlates well with the similar GC content between the UP and DOWN genes, as shown in figure 5.4 and suggests that structural regions within the 5'UTR do not play a key role in the translational control of transcripts following EGF stimulation.

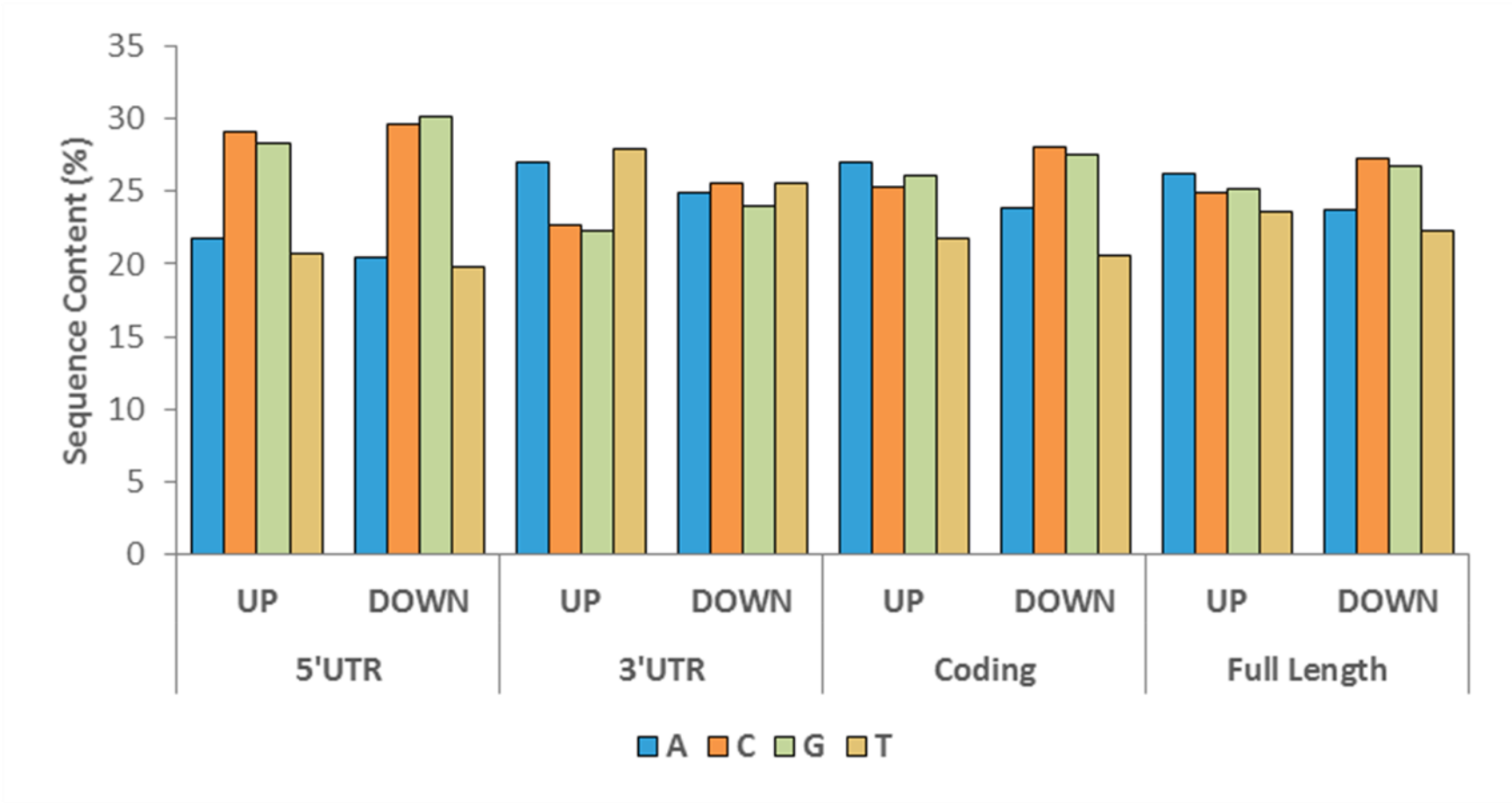

Figure 5.4 Sequence Composition of Differentially Translated Transcripts. Average nucleotide composition of 5'UTRs, 3'UTRs, coding regions and full length transcripts of upregulated (UP) and downregulated (DOWN) genes in response to EGF stimulation.

Lastly, the sequence lengths of the mRNAs were measured. Figures 5.6 and 5.7 display the Log10 sequence length of the 5'UTRs, 3'UTRs, coding regions and full length transcript for genes on the upregulated and downregulated lists, against their Log2 fold change. This data is also shown in figures 5.8 and 5.9 in boxplot format for easier analysis. For the 5'UTR, as shown in figure 5.8, the upregulated genes have a higher median sequence length (188 vs. 160) and third qurartile (326 vs. 282.5) than the list of downregulated genes although the interquartile distance (IQR) for the UP genes is larger (220 vs 201), indicating a larger spread of 5'UTR lengths among the upregulated genes. The 95% confidence intervals of the median values do not overlap (177 vs 167), suggesting there is a significant difference in the distribution of lengths between the datasets. The length of the 3'UTR does not appear to differ between the two datasets. As seen in figures 5.6b and 5.8b, the upregulated genes exhibit a higher third quartile than the downregulated genes, yet the medians are identical, with the lengths of the upregulated genes having a greater spread, as shown through the IQR. The downregulated genes meanwhile, contain a much greater number of outliers (3 x IQR + third quartile). The 95% confidence intervals of the median overlap considerably, and thus it is unlikely to be a significant difference between the two datasets. No significant difference is found for the coding region, as shown in figures 5.7a and 5.9a, whilst the length of the cDNA in upregulated genes (figure 5.7b and 5.9b) shows a right skew but no significant difference from the median of the downregulated genes. Taken together, this data suggests that the length of the 5'UTR is an important factor in those genes upregulated under EGF stimulation.

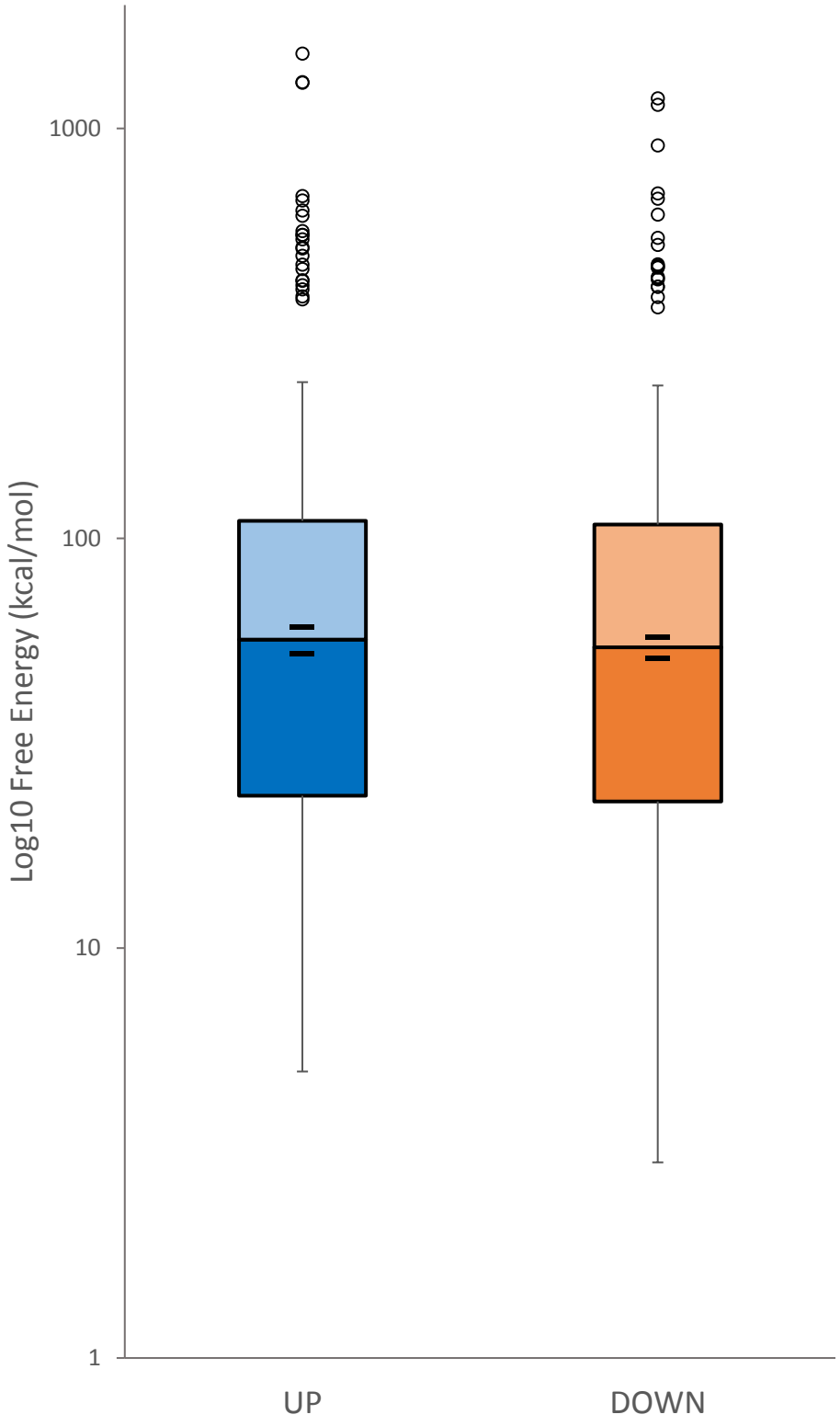

Figure 5.5. Average Minimum Free Energies of 5'UTR Sequences of Genes Upregulated and Downregulated by EGF Stimulation. Minimum free energy was calculated by the ViennaRNA program. Error bars represent 95% confidence intervals.

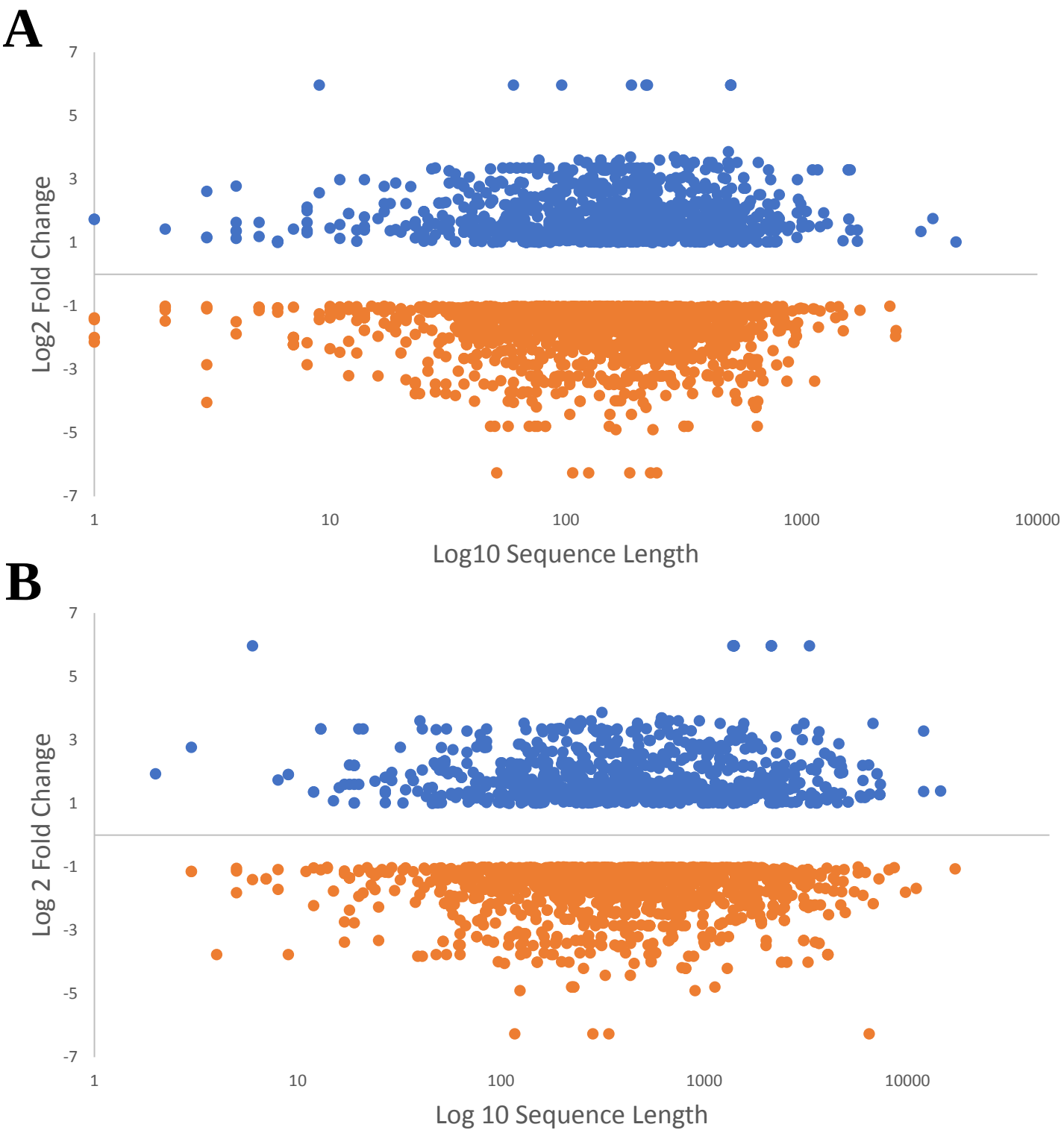

Figure 5.6. UTR Sequence Length of Genes Upregulated and Down Regulated by EGF Stimulation. Blue dots represent genes upregulated by EGF, orange dots those that are downregulated. (A) 5'UTR length, (B) 3'UTR length.

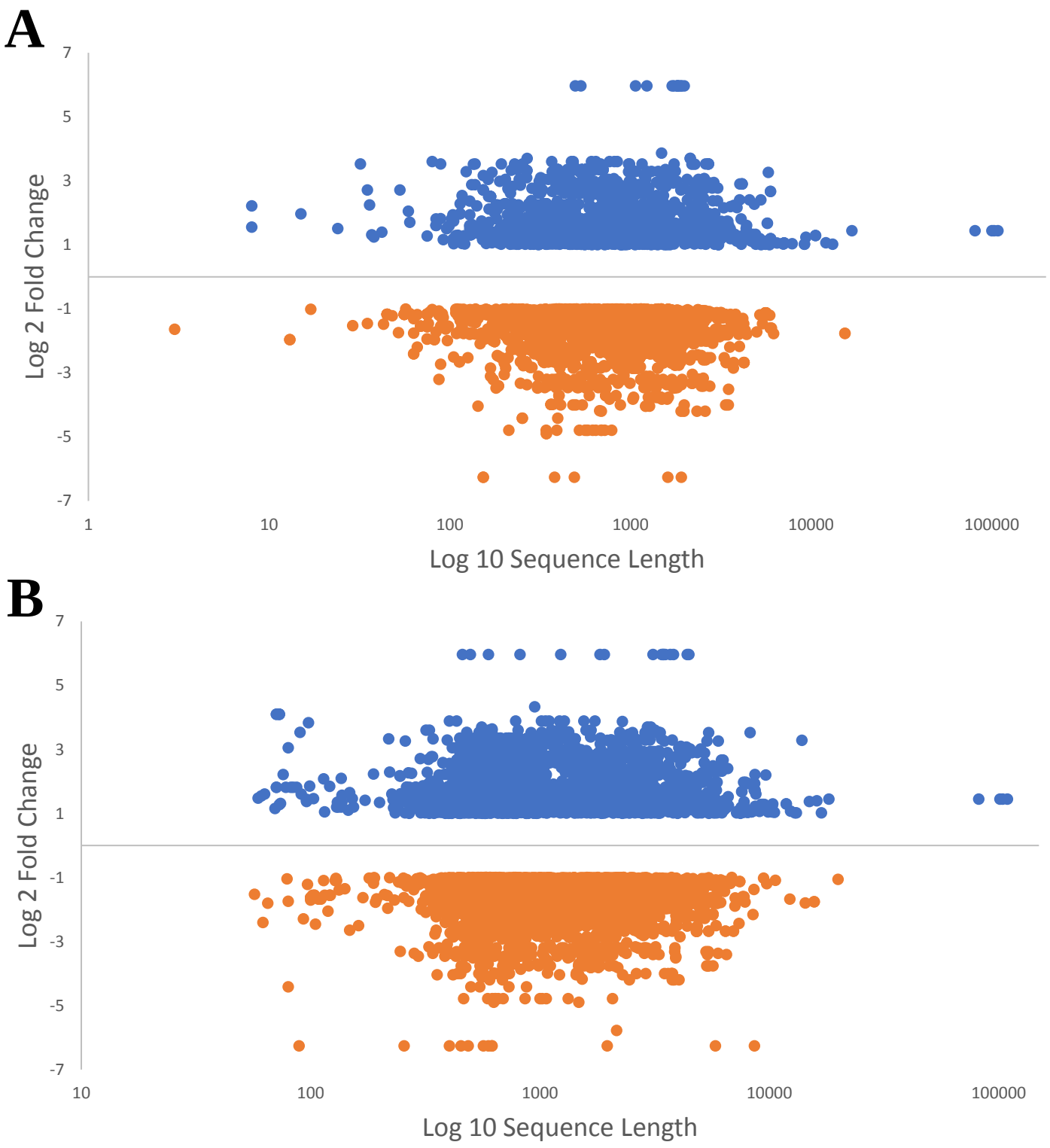

Figure 5.7. Sequence Length of Genes Upregulated and Down Regulated by EGF Stimulation. Blue dots represent genes upregulated by EGF, orange dots those that are downregulated. **(A)** coding region length, **(B)** cDNA length.

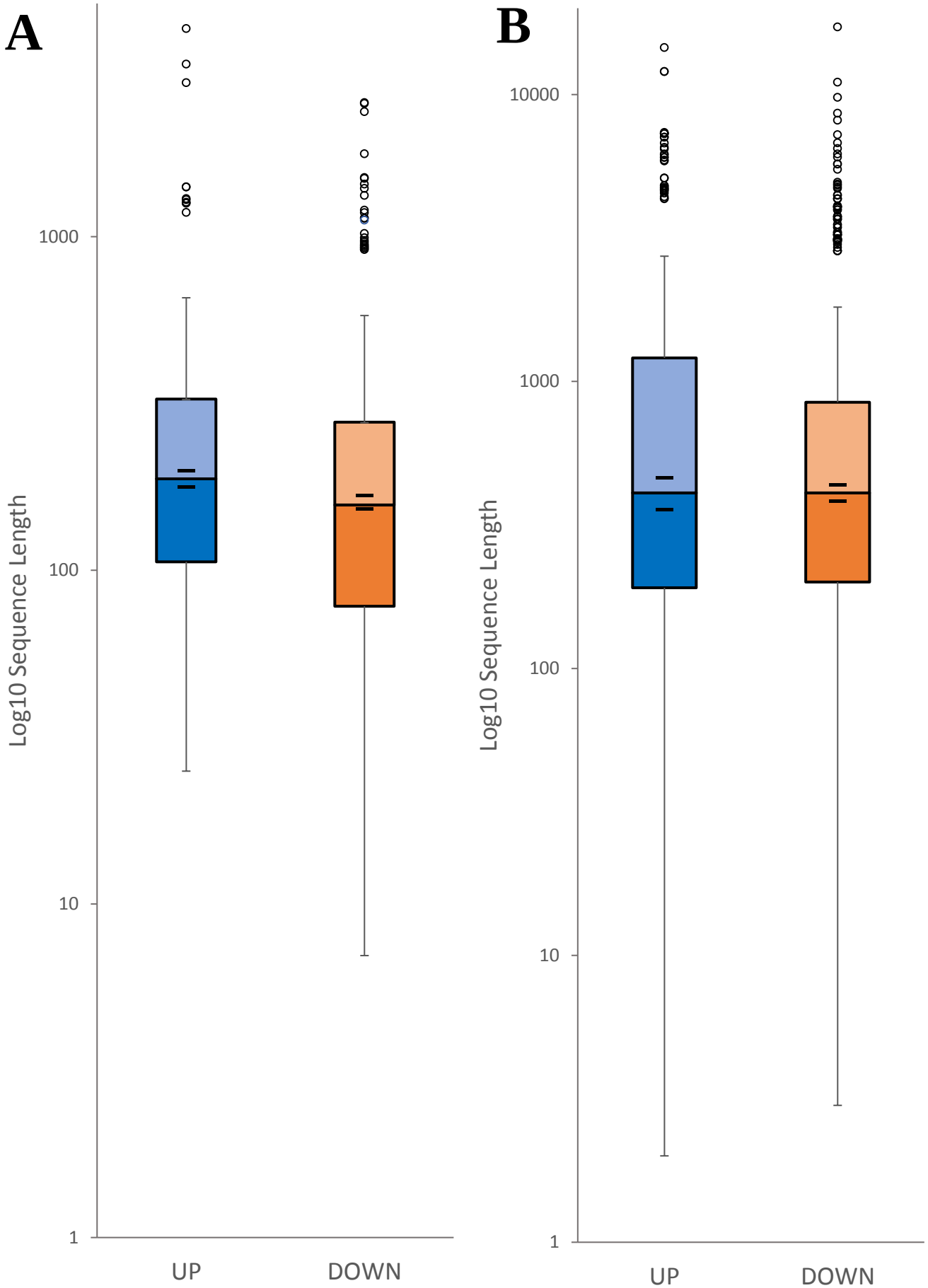

Figure 5.8. UTR Sequence Length of Genes Upregulated and Downregulated by EGF Stimulation, Represented by Boxplot. (A) 5'UTR length, **(B)** 3'UTR length. Boxplot represents 1st quartile, median and 3rd quartile. Error bars show the inner fence, representing 1.5 x interquartile distance (IQR). Dots represent outliers > 3x IQR. Dashes within the boxplot represent 95% confidence intervals of the median.

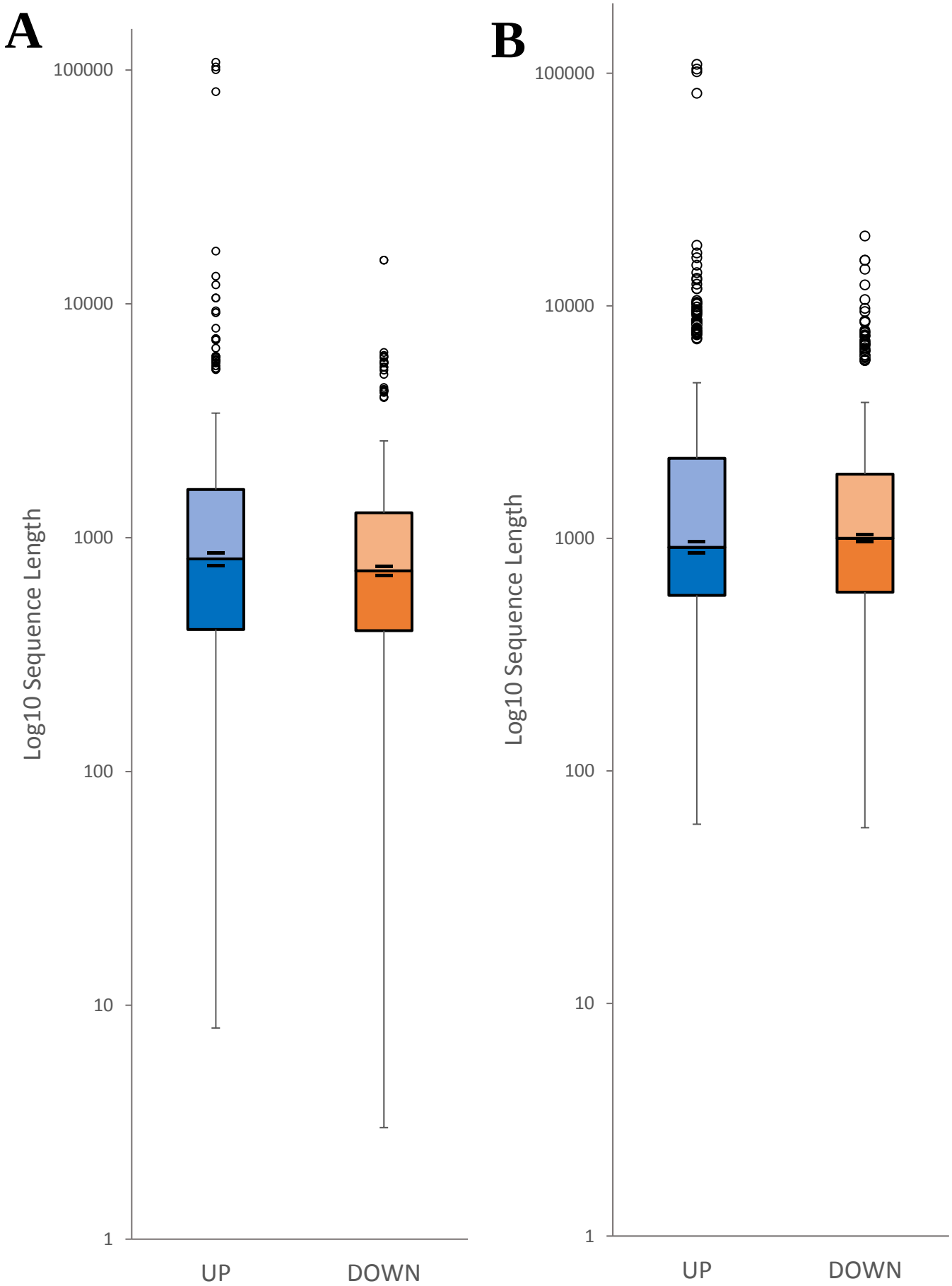

Figure 5.9. Sequence Length of Genes Upregulated and Downregulated by EGF Stimulation, Represented by Boxplot. (A) coding region, **(B)** cDNA. Boxplot represents 1st quartile, median and 3rd quartile. Error bars show the inner fence, representing 1.5 x interquartile distance (IQR). Dots represent outliers > 3x IQR. Dashes within the boxplot represent 95% confidence intervals of the median.

5.5 Discussion

The results presented here demonstrate that EGF stimulation increases the translation of a network of genes associated with Alzheimer's disease. EGF signalling activates a group of transcripts which are associated with the increased production and oligomerisation of Aβ, aggregation of tau and conditions thought to exacerbate AD progression – inflammation, increased intracellular calcium and insulin resistance. Analysing the sequence composition of these upregulated transcripts showed that on average they had longer 5'UTRs, suggesting that they would be inefficiently translated in resting conditions, but that EGF stimulation removes the inhibitory effect. Long 5'UTRs are usually associated with a greater degree of secondary structure. However, greater secondary structure usually requires a higher GC content which, as has been discussed, is not the case. Long 5'UTRs may also contain upstream AUGs and uORFs and are particularly common in growth factors and their receptors and DNA binding proteins (Davuluri et al. 2000). Thus these mRNAs may have poor translational efficiency under resting conditions, but growth signals increase their efficiency. A model of the transcripts differentially translated by EGF stimulation and their roles in AD can be seen in figure 5.10.

An important question is whether EGF levels are increased in AD or not. Wang *et al* showed that inhibition of EGFR removes memory loss in mice, but their findings suggest that oligomeric Aβ was responsible for EGFR activation in AD conditions (Wang et al. 2012). The transgenic mice used in the study however were overexpressing the Swedish mutant of APP, APPswe and PS1dE9

producing Aβ plaques within 4 months of age. Although regarded as a good model for studying AD, it is unlikely to exhibit the effects seen in the early phases of the disease. If inflammation occurs early in the disease then it is quite likely that EGF secretion occurs as part of the innate immune response. However, there is a lack of reports of high EGF levels in the disease. It is possible that EGF is secreted at a high level at the very early stage of the disease,

The next step in studying this pathway is to validate the upregulation in expression of these transcripts through quantitative PCR. Further analysis could investigate how inhibiting the activity of each of these proteins affects Aβ production.

6. Discussion

The objectives of this thesis were three-fold; to characterise the structure and the activation of the EGFR IRES and its potential as a therapeutic target, to analyse the translational profile of EGF stimulation and to create a 3-dimensional cell culture model for studying delivery systems for anti-sense oligonucleotides.

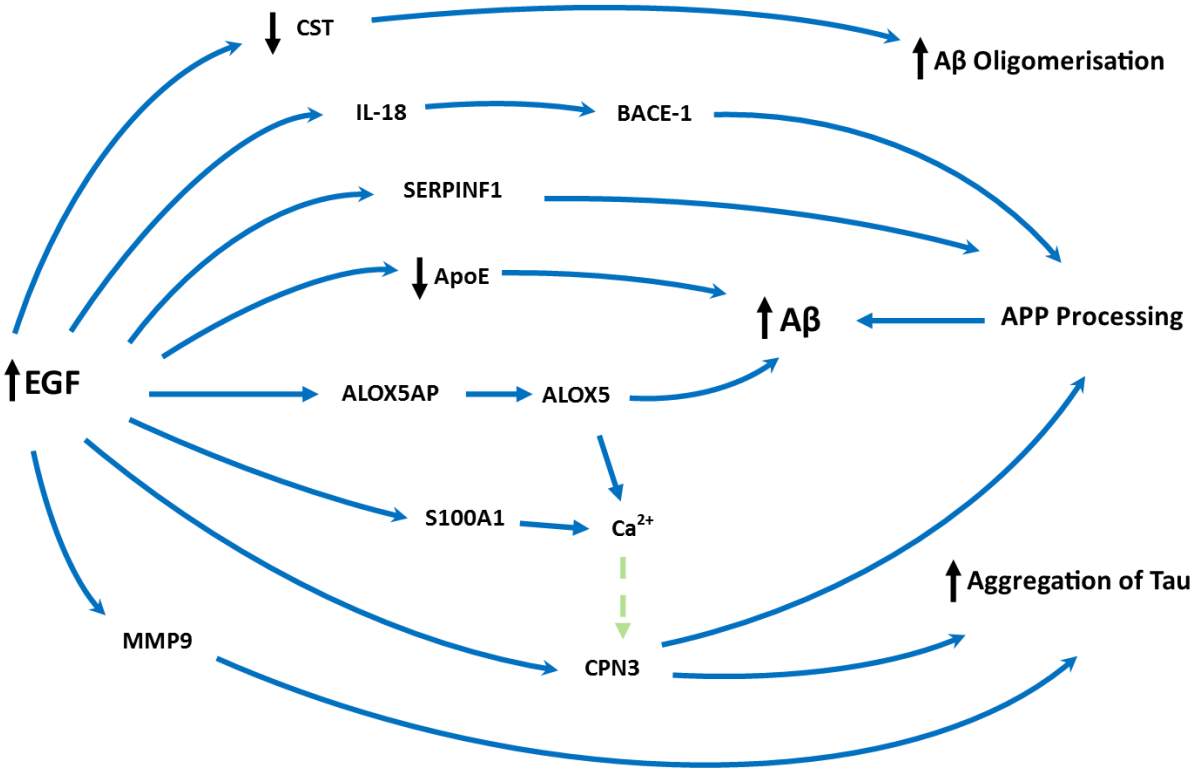

Figure 5.10. Model of EGF's Role in Alzheimer's Disease. Green line depicts activation of protein.

6.1 The characteristics and secondary structure of the EGFR IRES

In order to investigate the EGFR IRES, it was inserted into a bicistronic vector, which allows the expression of two luciferase genes from a single promoter. Insertion of the EGFR IRES between the two ORFs meant that the latter gene could only be expressed from the mRNA through ribosome binding to the IRES. The EGFR IRES was found to be active under serum starvation stress in U87MG cells but not MCF7, suggesting that IRES activation is tissue specific. Differential ITAF expression between the cell lines could affect IRES effectiveness, in a similar manner to the HIV-1 IRES (Plank, Whitehurst, and Kieft 2013), where ITAF binding modulates the IRES structure, allowing it to adopt a conformation favourable to ribosome binding. Further evidence that IRES activity differs among cell types was found through deletion analysis, where the first 57 nts of the EGFR 5'UTR had 20% of the activity of full length, whereas in MCF7 the fragment had only 7% the activity. Yet it was concluded that the IRES is not a modular IRES, as removal of small sequences from the 5' or 3' ends of the 5'UTR reducing IRES activity significantly. In this regard, the EGFR IRES is similar to the L-myc IRES (Jopling et al. 2004)

Anti-sense oligonucleotides have been utilised to block ribosomal access to the IRES of the hepatitis C virus (Tallet-Lopez et al. 2003) and have potential as a means of reducing overexpression of EGFR in disease. Targeting the EGFR IRES with 2'OMe oligonucleotides was found to be moderately successful, with a 50% reduction in expression when oligonucleotides were targeted to the

ribosome entry site. Unexpectedly, an oligonucleotide targeted upstream of this region also reduced expression, leading to the hypothesis that binding of oligonucleotides to any region of the 5'UTR disrupts structural arrangements necessary for ribosomal binding. Further tests are necessary to verify this and in order to rule out disruption of cap-dependent initiation. Resolving the structure of an IRES is important for determining its overall function and regulation and can be exploited to create new therapeutics. Using SHAPE, nucleotides in double stranded or single stranded conformations were identified and the data used to improve structure prediction models. A potential regulatory loop close to the start codon was identified, as well as a possible structural switch that may be regulated by binding proteins. Future experiments should evaluate the function of these structures, any regulatory proteins that bind to them and their role in IRES-mediated translation.

6.2 A 3D model for studying translational control

Three dimensional cell culture can bridge the gap between traditional 2d cell culture and animal models. Many features found *in vivo,* such as extracellular matrices and cell to matrix interactions, are lost in 2d cell culture but can be better replicated using 3d cell culture systems (Pampaloni, Reynaud, and Stelzer 2007; Mazzoleni, Di Lorenzo, and Steimberg 2009). 3d systems are also better models for observing the effectiveness of drug delivery systems (Marx 2006).

Stable cell lines expressing fluorescent transcripts with the EGFR 5'UTR inserted were successfully created, although only as polyclonal lines. Initial experiments appeared to show spherical cultures were created using ultra-low attachment plates but analysis revealed that cells conformed into a 'bowl' shaped culture, which appeared to consist primarily of monolayers. Studies had previously shown that ultra-low attachment plates could create spheroid cultures from U87-MG cells (Vinci et al. 2012). Characteristically, U87-MG cells are highly invasive and disperse from aggregates at a rapid rate, which may explain the inability to create spheroids with them in this study (Sabari et al. 2011). An ECM analogue, such as Matrigel, may improve cell-cell cohesion and aid in future attempts in creating spheroids. Despite this, it was found that a stress gradient existed between the top and the bottom of the cell mass, with the cells at the bottom of the mass having less access to nutrients or oxygen, leading to higher EGFR IRES activity. This could make the model developed useful for future experiments investigating stress gradients.

6.3 The translational profile of EGF stimulation

High-throughput mRNA sequencing RNA-seq, allows for the quantification of the entire transcriptome for a given condition. By fractionating the mRNA according to their sub-polysomal or polysomal location through polysome profiling, differentially expressed genes could be identified. These pools of RNA were used as a template for reverse transcription before sequencing. There is little information on the effects of EGF stimulation on translational efficiency. The transcriptional effects of EGF stimulation have been well studied, but the

effects on translation have received little attention. Identifying genes that are translationally upregulated by EGF will aid in understanding the role of EGF in disease. Polysome fractionation allows for the separation of transcripts according to their ribosome association and can be used as a measure of translational activity. The functional groups enriched by EGF were identified through ontological clustering. EGF signalling increased the ribosomal association of transcripts associated with Alzheimer's disease, as well as transcripts associated with conditions thought to exacerbate AD progression, namely: inflammation, high intracellular calcium levels and insulin resistance. Some of these genes have been directly connected to the production and oligomerisation of Aβ, and aggregation of tau. Thus our data suggests EGF stimulation can cause a number of the conditions associated with AD. Studies on whether EGF levels are increased in AD is inconclusive. (Marksteiner et al. 2011), (Chen-Plotkin et al. 2011; Bjorkqvist et al. 2012), but oligomers of Aβ can activate EGFR (Wang et al. 2012) and the activation could in theory generate similar translational effects as EGF stimulation. If inflammation occurs early in the disease then EGF secretion may occur as part of the innate immune response (Sorensen et al. 2006). EGF stimulation may lead to overproduction of Aβ which could continue the signalling through EGFR binding and activation. Validation of this data through quantitative PCR will be necessary before further analysis can begin.

7. References

Afanador, L., E. A. Roltsch, L. Holcomb, K. S. Campbell, D. A. Keeling, Y. Zhang, and D. B. Zimmer. 2014. 'The Ca2+ sensor S100A1 modulates neuroinflammation, histopathology and Akt activity in the PSAPP Alzheimer's disease mouse model', *Cell Calcium*, 56: 68-80.

Akiyama, H., K. Ikeda, H. Kondo, and P. L. McGeer. 1992. 'Thrombin accumulation in brains of patients with Alzheimer's disease', *Neurosci Lett*, 146: 152-4.

Allen, G. S., A. Zavialov, R. Gursky, M. Ehrenberg, and J. Frank. 2005. 'The cryo-EM structure of a translation initiation complex from Escherichia coli', *Cell*, 121: 703-12.

Alzheimer's, Association. 2015. '2015 Alzheimer's disease facts and figures', *Alzheimers Dement*, 11: 332-84.

Anand, N., S. Murthy, G. Amann, M. Wernick, L. A. Porter, I. H. Cukier, C. Collins, J. W. Gray, J. Diebold, D. J. Demetrick, and J. M. Lee. 2002. 'Protein elongation factor EEF1A2 is a putative oncogene in ovarian cancer', *Nature Genetics*, 31: 301-5.

Andrews, S. 2010. "FastQC: a quality control tool for high throughput sequence data. Available online at: http://www.bioinformatics.babraham.ac.uk/projects/fastqc." In.

Araujo, Patricia R., Kihoon Yoon, Daijin Ko, Andrew D. Smith, Mei Qiao, Uthra Suresh, Suzanne C. Burns, and Luiz O. F. Penalva. 2012. 'Before It Gets Started: Regulating Translation at the 5 ' UTR', *Comparative and Functional Genomics*.

Arispe, N., E. Rojas, and H. B. Pollard. 1993. 'Alzheimer disease amyloid beta protein forms calcium channels in bilayer membranes: blockade by tromethamine and aluminum', *Proc Natl Acad Sci U S A*, 90: 567-71.

Atherton, J., K. Kurbatskaya, M. Bondulich, C. L. Croft, C. J. Garwood, R. Chhabra, S. Wray, A. Jeromin, D. P. Hanger, and W. Noble. 2014. 'Calpain cleavage and inactivation of the sodium calcium exchanger-3 occur downstream of Abeta in Alzheimer's disease', *Aging Cell*, 13: 49-59.

Atwood, C. S., R. D. Moir, X. Huang, R. C. Scarpa, N. M. Bacarra, D. M. Romano, M. A. Hartshorn, R. E. Tanzi, and A. I. Bush. 1998. 'Dramatic aggregation of Alzheimer abeta by Cu(II) is induced by conditions representing physiological acidosis', *J Biol Chem*, 273: 12817-26.

Atwood, C. S., R. C. Scarpa, X. Huang, R. D. Moir, W. D. Jones, D. P. Fairlie, R. E. Tanzi, and A. I. Bush. 2000. 'Characterization of copper interactions with

alzheimer amyloid beta peptides: identification of an attomolar-affinity copper binding site on amyloid beta1-42', *J Neurochem*, 75: 1219-33.

Austin, P. C., and J. E. Hux. 2002. 'A brief note on overlapping confidence intervals', *J Vasc Surg*, 36: 194-5.

Baeyens, L., M. Lemper, G. Leuckx, S. De Groef, P. Bonfanti, G. Stange, R. Shemer, C. Nord, D. W. Scheel, F. C. Pan, U. Ahlgren, G. Gu, D. A. Stoffers, Y. Dor, J. Ferrer, G. Gradwohl, C. V. Wright, M. Van de Casteele, M. S. German, L. Bouwens, and H. Heimberg. 2014. 'Transient cytokine treatment induces acinar cell reprogramming and regenerates functional beta cell mass in diabetic mice', *Nat Biotechnol*, 32: 76-83.

Baird, S. D., S. M. Lewis, M. Turcotte, and M. Holcik. 2007. 'A search for structurally similar cellular internal ribosome entry sites', *Nucleic Acids Res*, 35: 4664-77.

Banerjee, AK. 1980. '5' Terminal Cap Structure in Eucaryotic Messenger Ribonucleic Acids', *Microbiology Review*, **44**: 175-205.

Bartolome, S., N. K. Dhillon, S. Buch, A. J. Casillan, J. G. Wood, and A. R. O'Brien-Ladner. 2009. 'Deferoxamine mimics the pattern of hypoxia-related injury at the microvasculature', *Shock*, 31: 481-85.

Baskin, F., G. M. Smith, J. A. Fosmire, and R. N. Rosenberg. 1997. 'Altered apolipoprotein E secretion in cytokine treated human astrocyte cultures', *J Neurol Sci*, 148: 15-8.

Batzer, A. G., D. Rotin, J. M. Urena, E. Y. Skolnik, and J. Schlessinger. 1994. 'Hierarchy of binding sites for Grb2 and Shc on the epidermal growth factor receptor', *Mol Cell Biol*, 14: 5192-201.

Beaudoin, M. E., V. J. Poirel, and L. A. Krushel. 2008. 'Regulating amyloid precursor protein synthesis through an internal ribosomal entry site', *Nucleic Acids Res*, 36: 6835-47.

Befani, Christina, Ilias Mylonis, Ioanna-Maria Gkotinakou, Panagiotis Georgoulias, Cheng-Jun Hu, George Simos, and Panagiotis Liakos. 2013. 'Cobalt stimulates HIF-1-dependent but inhibits HIF-2-dependent gene expression in liver cancer cells', *The international journal of biochemistry & cell biology*, 45: 2359-68.

Benne, R., and J. W. B. Hershey. 1978. 'Mechanism of action of protein-synthesis initiation-factors from rabbit reticulocytes', *Journal of Biological Chemistry*, 253: 3078-87.

Benussi, L., R. Ghidoni, T. Steinhoff, A. Alberici, A. Villa, F. Mazzoli, F. Nicosia, L. Barbiero, L. Broglio, E. Feudatari, S. Signorini, U. Finckh, R. M. Nitsch, and G. Binetti. 2003. 'Alzheimer disease-associated cystatin C variant undergoes impaired secretion', *Neurobiol Dis*, 13: 15-21.

Berasain, C., M. J. Perugorria, M. U. Latasa, J. Castillo, S. Goni, M. Santamaria, J. Prieto, and M. A. Avila. 2009. 'The epidermal growth factor receptor: a link between inflammation and liver cancer', *Exp Biol Med (Maywood)*, 234: 713-25.

Bergamini, G., T. Preiss, and M. W. Hentze. 2000. 'Picornavirus IRESes and the poly(A) tail jointly promote cap-independent translation in a mammalian cell-free system', *RNA*, 6: 1781-90.

Berthois Y., J. A. Katzenellenbogen, and B. S. Katzenellenbogen. 1986. ' Phenol red in tissue culture media is a weak estrogen: implications concerning the study of estrogen-responsive cells in culture.', *PNAS*, 83:2496-2500.

Beyer, K., J. I. Lao, M. Gomez, N. Riutort, P. Latorre, J. L. Mate, and A. Ariza. 2001. 'Alzheimer's disease and the cystatin C gene polymorphism: an association study', *Neurosci Lett*, 315: 17-20.

Bien-Ly, N., A. K. Gillespie, D. Walker, S. Y. Yoon, and Y. Huang. 2012. 'Reducing human apolipoprotein E levels attenuates age-dependent Abeta accumulation in mutant human amyloid precursor protein transgenic mice', *J Neurosci*, 32: 4803-11.

Biessels, G. J., L. P. van der Heide, A. Kamal, R. L. Bleys, and W. H. Gispen. 2002. 'Ageing and diabetes: implications for brain function', *Eur J Pharmacol*, 441: 1-14.

Birecree, E., W. O. Whetsell, Jr., C. Stoscheck, L. E. King, Jr., and L. B. Nanney. 1988. 'Immunoreactive epidermal growth factor receptors in neuritic plaques from patients with Alzheimer's disease', *J Neuropathol Exp Neurol*, 47: 549-60.

Bissell, M. J., H. G. Hall, and G. Parry. 1982. 'How does the extracellular matrix direct gene expression?', *J Theor Biol*, 99: 31-68.

Bjorkqvist, M., M. Ohlsson, L. Minthon, and O. Hansson. 2012. 'Evaluation of a previously suggested plasma biomarker panel to identify Alzheimer's disease', *Plos One*, 7: e29868.

Blehm, K. N., P. E. Spiess, J. E. Bondaruk, M. E. Dujka, G. J. Villares, Y. J. Zhao, O. Bogler, K. D. Aldape, H. B. Grossman, L. Adam, D. J. McConkey, B. A. Czerniak, C. P. Dinney, and M. Bar-Eli. 2006. 'Mutations within the kinase domain and truncations of the epidermal growth factor receptor are rare events in bladder cancer: implications for therapy', *Clin Cancer Res*, 12: 4671-7.

Bolger, A. M., M. Lohse, and B. Usadel. 2014. 'Trimmomatic: a flexible trimmer for Illumina sequence data', *Bioinformatics*, 30: 2114-20.

Bondarenko, A., N. Svichar, and M. Chesler. 2005. 'Role of Na+-H+ and Na+-Ca2+ exchange in hypoxia-related acute astrocyte death', *Glia*, 49: 143-52.

Botella, J. A., D. Kretzschmar, C. Kiermayer, P. Feldmann, D. A. Hughes, and S. Schneuwly. 2003. 'Deregulation of the Egfr/Ras signaling pathway induces

age-related brain degeneration in the Drosophila mutant vap', *Mol Biol Cell*, 14: 241-50.

Bottley, A., N. M. Phillips, T. E. Webb, A. E. Willis, and K. A. Spriggs. 2010. 'eIF4A inhibition allows translational regulation of mRNAs encoding proteins involved in Alzheimer's disease', *PLoS One*, 5.

Breslin, S., and L. O'Driscoll. 2013. 'Three-dimensional cell culture: the missing link in drug discovery', *Drug Discov Today*, 18: 240-9.

Brook, M., G. Sully, A. R. Clark, and J. Saklatvala. 2000. 'Regulation of tumour necrosis factor alpha mRNA stability by the mitogen-activated protein kinase p38 signalling cascade', *FEBS Lett*, 483: 57-61.

Brosseron, F., M. Krauthausen, M. Kummer, and M. T. Heneka. 2014. 'Body fluid cytokine levels in mild cognitive impairment and Alzheimer's disease: a comparative overview', *Mol Neurobiol*, 50: 534-44.

Brown, E. A., H. Zhang, L. H. Ping, and S. M. Lemon. 1992. 'Secondary structure of the 5' nontranslated regions of hepatitis C virus and pestivirus genomic RNAs', *Nucleic Acids Res*, 20: 5041-5.

Bryant, J. A., R. S. Finn, D. J. Slamon, T. F. Cloughesy, and A. C. Charles. 2004. 'EGF activates intracellular and intercellular calcium signaling by distinct pathways in tumor cells', *Cancer Biol Ther*, 3: 1243-9.

Bush, A. I., W. H. Pettingell, G. Multhaup, M. d Paradis, J. P. Vonsattel, J. F. Gusella, K. Beyreuther, C. L. Masters, and R. E. Tanzi. 1994. 'Rapid induction of Alzheimer A beta amyloid formation by zinc', *Science*, 265: 1464-7.

Buxbaum, J. D., A. A. Ruefli, C. A. Parker, A. M. Cypess, and P. Greengard. 1994. 'Calcium regulates processing of the Alzheimer amyloid protein precursor in a protein kinase C-independent manner', *Proc Natl Acad Sci U S A*, 91: 4489-93.

Calvo, S. E., D. J. Pagliarini, and V. K. Mootha. 2009. 'Upstream open reading frames cause widespread reduction of protein expression and are polymorphic among humans', *Proceedings of the National Academy of Sciences of the United States of America*, 106: 7507-12.

Cathcart, H. M., R. Huang, I. S. Lanham, E. H. Corder, and S. E. Poduslo. 2005. 'Cystatin C as a risk factor for Alzheimer disease', *Neurology*, 64: 755-7.

Cencig, S., C. Nanbru, S. Y. Le, C. Gueydan, G. Huez, and V. Kruys. 2004. 'Mapping and characterization of the minimal internal ribosome entry segment in the human c-myc mRNA 5' untranslated region', *Oncogene*, 23: 267-77.

Chachami, G., G. Simos, A. Hatziefthimiou, S. Bonanou, P. A. Molyvdas, and E. Paraskeva. 2004. 'Cobalt induces hypoxia-inducible factor-1alpha expression in airway smooth muscle cells by a reactive oxygen species- and PI3K-dependent mechanism', *Am J Respir Cell Mol Biol*, 31: 544-51.

Chamberlin, S. I., E. J. Merino, and K. M. Weeks. 2002. 'Catalysis of amide synthesis by RNA phosphodiester and hydroxyl groups', *Proc Natl Acad Sci U S A*, 99: 14688-93.

Chang, R. C., A. K. Wong, H. K. Ng, and J. Hugon. 2002. 'Phosphorylation of eukaryotic initiation factor-2alpha (eIF2alpha) is associated with neuronal degeneration in Alzheimer's disease', *Neuroreport*, 13: 2429-32.

Chantry, A. 1995. 'The kinase domain and membrane localization determine intracellular interactions between epidermal growth factor receptors', *J Biol Chem*, 270: 3068-73.

Chappell, S. A., G. M. Edelman, and V. P. Mauro. 2000. 'A 9-nt segment of a cellular mRNA can function as an internal ribosome entry site (IRES) and when present in linked multiple copies greatly enhances IRES activity', *Proc Natl Acad Sci U S A*, 97: 1536-41.

Chappell, S. A., J. P. LeQuesne, F. E. Paulin, M. L. deSchoolmeester, M. Stoneley, R. L. Soutar, S. H. Ralston, M. H. Helfrich, and A. E. Willis. 2000. 'A mutation in the c-myc-IRES leads to enhanced internal ribosome entry in multiple myeloma: a novel mechanism of oncogene de-regulation', *Oncogene*, 19: 4437-40.

Chaudhuri, J., D. Chowdhury, and U. Maitra. 1999. 'Distinct functions of eukaryotic translation initiation factors eIF1A and eIF3 in the formation of the 40 S ribosomal preinitiation complex', *Journal of Biological Chemistry*, 274: 17975-80.

Chen-Plotkin, A. S., W. T. Hu, A. Siderowf, D. Weintraub, R. Goldmann Gross, H. I. Hurtig, S. X. Xie, S. E. Arnold, M. Grossman, C. M. Clark, L. M. Shaw, L. McCluskey, L. Elman, V. M. Van Deerlin, V. M. Lee, H. Soares, and J. Q. Trojanowski. 2011. 'Plasma epidermal growth factor levels predict cognitive decline in Parkinson disease', *Annals of Neurology*, 69: 655-63.

Chen, J., J. K. Chen, and R. C. Harris. 2015. 'EGF receptor deletion in podocytes attenuates diabetic nephropathy', *J Am Soc Nephrol*, 26: 1115-25.

Chen, J., and M. B. Kastan. 2010. '5'-3'-UTR interactions regulate p53 mRNA translation and provide a target for modulating p53 induction after DNA damage', *Genes Dev*, 24: 2146-56.

Cheyette, T. E., and D. J. Gross. 1991. 'Epidermal growth factor-stimulated calcium ion transients in individual A431 cells: initiation kinetics and ligand concentration dependence', *Cell Regul*, 2: 827-40.

Cho, H. H., C. M. Cahill, C. R. Vanderburg, C. R. Scherzer, B. Wang, X. Huang, and J. T. Rogers. 2010. 'Selective translational control of the Alzheimer amyloid precursor protein transcript by iron regulatory protein-1', *J Biol Chem*, 285: 31217-32.

Choi, S. H., Y. H. Kim, M. Hebisch, C. Sliwinski, S. Lee, C. D'Avanzo, H. Chen, B. Hooli, C. Asselin, J. Muffat, J. B. Klee, C. Zhang, B. J. Wainger, M. Peitz,

D. M. Kovacs, C. J. Woolf, S. L. Wagner, R. E. Tanzi, and D. Y. Kim. 2014. 'A three-dimensional human neural cell culture model of Alzheimer's disease', *Nature*, 515: 274-8.

Christen, Y. 2000. 'Oxidative stress and Alzheimer disease', *Am J Clin Nutr*, 71: 621S-29S.

Cigan, A. M., L. Feng, and T. F. Donahue. 1988. 'Transfer RNA(iMET) functions in directing the scanning ribosome to the start site of translation', *Science*, 242: 93-97.

Clark, A., J. Dean, C. Tudor, and J. Saklatvala. 2009. 'Post-transcriptional gene regulation by MAP kinases via AU-rich elements', *Front Biosci (Landmark Ed)*, 14: 847-71.

Clark, A. T., M. E. Robertson, G. L. Conn, and G. J. Belsham. 2003. 'Conserved nucleotides within the J domain of the encephalomyocarditis virus internal ribosome entry site are required for activity and for interaction with eIF4G', *J Virol*, 77: 12441-9.

Clayton, A. H. A., S. G. Orchard, E. C. Nice, R. G. Posner, and A. W. Burgess. 2008. 'Predominance of activated EGFR higher-order oligomers on the cell surface', *Growth Factors*, 26: 316-24.

Cobbold, L. C., L. A. Wilson, K. Sawicka, H. A. King, A. V. Kondrashov, K. A. Spriggs, M. Bushell, and A. E. Willis. 2010. 'Upregulated c-myc expression in multiple myeloma by internal ribosome entry results from increased interactions with and expression of PTB-1 and YB-1', *Oncogene*, 29: 2884-91.

Cochet, C. 1988. 'Epidermal Growth-Factor Receptor - Its Impact on Normal and Tumoral Proliferation', *Bulletin Du Cancer*, 75: 326-27.

Cole, S. L., A. Grudzien, I. O. Manhart, B. L. Kelly, H. Oakley, and R. Vassar. 2005. 'Statins cause intracellular accumulation of amyloid precursor protein, beta-secretase-cleaved fragments, and amyloid beta-peptide via an isoprenoid-dependent mechanism', *J Biol Chem*, 280: 18755-70.

Compernolle, V., K. Brusselmans, T. Acker, P. Hoet, M. Tjwa, H. Beck, S. Plaisance, Y. Dor, E. Keshet, F. Lupu, B. Nemery, M. Dewerchin, P. Van Veldhoven, K. Plate, L. Moons, D. Collen, and P. Carmeliet. 2002. 'Loss of HIF-2 and inhibition of VEGF impair fetal lung maturation, whereas treatment with VEGF prevents fatal respiratory distress in premature mice', *Nature Medicine*, 8: 702-10.

Conejero-Goldberg, C., T. M. Hyde, S. Chen, U. Dreses-Werringloer, M. M. Herman, J. E. Kleinman, P. Davies, and T. E. Goldberg. 2011. 'Molecular signatures in post-mortem brain tissue of younger individuals at high risk for Alzheimer's disease as based on APOE genotype', *Mol Psychiatry*, 16: 836-47.

Cox, G., J. L. Jones, and K. J. O'Byrne. 2000. 'Matrix metalloproteinase 9 and the epidermal growth factor signal pathway in operable non-small cell lung cancer', *Clin Cancer Res*, 6: 2349-55.

Crooke, S. T. 1992. 'Therapeutic applications of oligonucleotides', *Biotechnology (N Y)*, 10: 882-6.

Crooke, S. T., and C.K. Mirabelli. 1992. 'Application of Oligonucleotide Drugs For Cancer Prevention.' in V.E. Steele, G.D. Stoner, C.W. Boone and G.J. Kelloff (eds.), *Cellular and Molecular Targets for Chemoprevention* (CRC Press, Inc: Florida, United States of America).

Cui, P. J., L. Zheng, L. Cao, Y. Wang, Y. L. Deng, G. Wang, W. Xu, H. D. Tang, J. F. Ma, T. Zhang, J. Q. Ding, Q. Cheng, and S. D. Chen. 2010. 'CALHM1 P86L polymorphism is a risk factor for Alzheimer's disease in the Chinese population', *J Alzheimers Dis*, 19: 31-5.

Dagle, J. M., and D. L. Weeks. 2001. 'Oligonucleotide-based strategies to reduce gene expression', *Differentiation*, 69: 75-82.

Damiano, F., S. Alemanno, G. V. Gnoni, and L. Siculella. 2010. 'Translational control of the sterol-regulatory transcription factor SREBP-1 mRNA in response to serum starvation or ER stress is mediated by an internal ribosome entry site', *Biochem J*, 429: 603-12.

Damiano, F., A. Rochira, R. Tocci, S. Alemanno, A. Gnoni, and L. Siculella. 2013. 'hnRNP A1 mediates the activation of the IRES-dependent SREBP-1a mRNA translation in response to endoplasmic reticulum stress', *Biochem J*, 449: 543-53.

Das, S., and U. Maitra. 2001. 'Functional significance and mechanism of eIF5-promoted GTP hydrolysis in eukaryotic translation initiation', *Progress in Nucleic Acid Research and Molecular Biology, Vol 70*, 70: 207-31.

Dasgupta, A., S. Das, R. Izumi, A. Venkatesan, and B. Barat. 2004. 'Targeting internal ribosome entry site (IRES)-mediated translation to block hepatitis C and other RNA viruses', *FEMS Microbiol Lett*, 234: 189-99.

Davidson, S. D., R. Passmore, and J. F. Brock. 1973. *Human nutrition and dietics*, 5th Edition. Churchill Livingstone, London, United Kingdom.

Davuluri, R. V., Y. Suzuki, S. Sugano, and M. Q. Zhang. 2000. 'CART classification of human 5 ' UTR sequences', *Genome Research*, 10: 1807-16.

De Jager, P. L., G. Srivastava, K. Lunnon, J. Burgess, L. C. Schalkwyk, L. Yu, M. L. Eaton, B. T. Keenan, J. Ernst, C. McCabe, A. Tang, T. Raj, J. Replogle, W. Brodeur, S. Gabriel, H. S. Chai, C. Younkin, S. G. Younkin, F. Zou, M. Szyf, C. B. Epstein, J. A. Schneider, B. E. Bernstein, A. Meissner, N. Ertekin-Taner, L. B. Chibnik, M. Kellis, J. Mill, and D. A. Bennett. 2014. 'Alzheimer's disease: early alterations in brain DNA methylation at ANK1, BIN1, RHBDF2 and other loci', *Nat Neurosci*, 17: 1156-63.

de la Monte, S. M., and J. R. Wands. 2005. 'Review of insulin and insulin-like growth factor expression, signaling, and malfunction in the central nervous system: relevance to Alzheimer's disease', *J Alzheimers Dis*, 7: 45-61.

Deigan, K. E., T. W. Li, D. H. Mathews, and K. M. Weeks. 2009. 'Accurate SHAPE-directed RNA structure determination', *Proc Natl Acad Sci U S A*, 106: 97-102.

Del Duca, D., T. Werbowetski, and R. F. Del Maestro. 2004. 'Spheroid preparation from hanging drops: characterization of a model of brain tumor invasion', *J Neurooncol*, 67: 295-303.

Dever, T. E., and R. Green. 2012. 'The elongation, termination, and recycling phases of translation in eukaryotes', *Cold Spring Harb Perspect Biol*, 4: a013706.

Dias, N., and C. A. Stein. 2002a. 'Antisense oligonucleotides: basic concepts and mechanisms', *Mol Cancer Ther*, 1: 347-55.

Dias, N., and C.A. Stein. 2002b. 'Potential roles of antisense oligonucleotides in cancer therapy. The example of Bcl-2 antisense oligonucleotides', *Eur J Pharm Biopharm*, 54: 263-9.

Ding, Y., A. Kantarci, J. A. Badwey, H. Hasturk, A. Malabanan, and T. E. Van Dyke. 2007. 'Phosphorylation of pleckstrin increases proinflammatory cytokine secretion by mononuclear phagocytes in diabetes mellitus', *J Immunol*, 179: 647-54.

Doudna, Jennifer A., and P Sarnow. 2007. 'Translation initiation by viral internal ribosome entry sites.', *Translational Control in Biology and Medicine (Mathews, M.B., Sonenberg, N., Hershey, J.W.B., Eds.)*, 48: 129-53.

Dreses-Werringloer, U., J. C. Lambert, V. Vingtdeux, H. Zhao, H. Vais, A. Siebert, A. Jain, J. Koppel, A. Rovelet-Lecrux, D. Hannequin, F. Pasquier, D. Galimberti, E. Scarpini, D. Mann, C. Lendon, D. Campion, P. Amouyel, P. Davies, J. K. Foskett, F. Campagne, and P. Marambaud. 2008. 'A polymorphism in CALHM1 influences Ca2+ homeostasis, Abeta levels, and Alzheimer's disease risk', *Cell*, 133: 1149-61.

Durinck, S., Y. Moreau, A. Kasprzyk, S. Davis, B. De Moor, A. Brazma, and W. Huber. 2005. 'BioMart and Bioconductor: a powerful link between biological databases and microarray data analysis', *Bioinformatics*, 21: 3439-40.

Edbauer, D., E. Winkler, J. T. Regula, B. Pesold, H. Steiner, and C. Haass. 2003. 'Reconstitution of gamma-secretase activity', *Nature Cell Biology*, 5: 486-88.

El-Lebedy, D., H. M. Raslan, and A. M. Mohammed. 2016. 'Apolipoprotein E gene polymorphism and risk of type 2 diabetes and cardiovascular disease', *Cardiovasc Diabetol*, 15: 12.

Etcheberrigaray, R., N. Hirashima, L. Nee, J. Prince, S. Govoni, M. Racchi, R. E. Tanzi, and D. L. Alkon. 1998. 'Calcium responses in fibroblasts from asymptomatic members of Alzheimer's disease families', *Neurobiol Dis*, 5: 37-45.

Etminan, M., S. Gill, and A. Samii. 2003. 'Effect of non-steroidal anti-inflammatory drugs on risk of Alzheimer's disease: systematic review and meta-analysis of observational studies', *BMJ*, 327: 128.

Evans, J. L., I. D. Goldfine, B. A. Maddux, and G. M. Grodsky. 2002. 'Oxidative stress and stress-activated signaling pathways: a unifying hypothesis of type 2 diabetes', *Endocr Rev*, 23: 599-622.

Fagan, A. M., D. M. Holtzman, G. Munson, T. Mathur, D. Schneider, L. K. Chang, G. S. Getz, C. A. Reardon, J. Lukens, J. A. Shah, and M. J. LaDu. 1999. 'Unique lipoproteins secreted by primary astrocytes from wild type, apoE (-/-), and human apoE transgenic mice', *J Biol Chem*, 274: 30001-7.

Faghihi, M. A., F. Modarresi, A. M. Khalil, D. E. Wood, B. G. Sahagan, T. E. Morgan, C. E. Finch, G. St Laurent, 3rd, P. J. Kenny, and C. Wahlestedt. 2008. 'Expression of a noncoding RNA is elevated in Alzheimer's disease and drives rapid feed-forward regulation of beta-secretase', *Nat Med*, 14: 723-30.

Fedi, P., J. H. Pierce, P. P. di Fiore, and M. H. Kraus. 1994. 'Efficient coupling with phosphatidylinositol 3-kinase, but not phospholipase C gamma or GTPase-activating protein, distinguishes ErbB-3 signaling from that of other ErbB/EGFR family members', *Mol Cell Biol*, 14: 492-500.

Fernandez, J., B. Bode, A. Koromilas, J. A. Diehl, I. Krukovets, M. D. Snider, and M. Hatzoglou. 2002. 'Translation mediated by the internal ribosome entry site of the cat-1 mRNA is regulated by glucose availability in a PERK kinase-dependent manner', *J Biol Chem*, 277: 11780-7.

Fernandez, J., I. Yaman, W. C. Merrick, A. Koromilas, R. C. Wek, R. Sood, J. Hensold, and M. Hatzoglou. 2002. 'Regulation of internal ribosome entry site-mediated translation by eukaryotic initiation factor-2alpha phosphorylation and translation of a small upstream open reading frame', *J Biol Chem*, 277: 2050-8.

Ferreira, S. T., M. N. N. Vieira, and F. G. De Felice. 2007. 'Soluble protein oligomers as emerging toxins in Alzheimer's and other amyloid diseases', *Iubmb Life*, 59: 332-45.

Ferreira, Sergio T., and William L. Klein. 2011. 'The A beta oligomer hypothesis for synapse failure and memory loss in Alzheimer's disease', *Neurobiology of Learning and Memory*, 96: 529-43.

Ferrer, I., S. Alcantara, J. Ballabriga, M. Olive, R. Blanco, R. Rivera, M. Carmona, M. Berruezo, S. Pitarch, and A. M. Planas. 1996. 'Transforming growth factor-alpha (TGF-alpha) and epidermal growth factor-receptor (EGF-R) immunoreactivity in normal and pathologic brain', *Prog Neurobiol*, 49: 99-123.

Finotello, F., E. Lavezzo, L. Bianco, L. Barzon, P. Mazzon, P. Fontana, S. Toppo, and B. Di Camillo. 2014. 'Reducing bias in RNA sequencing data: a novel approach to compute counts', *BMC Bioinformatics*, 15 Suppl 1: S7.

Firuzi, O., J. Zhuo, C. M. Chinnici, T. Wisniewski, and D. Pratico. 2008. '5-Lipoxygenase gene disruption reduces amyloid-beta pathology in a mouse model of Alzheimer's disease', *Federation Proceedings*, 22: 1169-78.

Fitz, N. F., A. A. Cronican, M. Saleem, A. H. Fauq, R. Chapman, I. Lefterov, and R. Koldamova. 2012. 'Abca1 deficiency affects Alzheimer's disease-like phenotype in human ApoE4 but not in ApoE3-targeted replacement mice', *J Neurosci*, 32: 13125-36.

Floyel, T., C. Brorsson, L. B. Nielsen, M. Miani, C. H. Bang-Berthelsen, M. Friedrichsen, A. J. Overgaard, L. A. Berchtold, A. Wiberg, P. Poulsen, L. Hansen, S. Rosinger, B. O. Boehm, R. Ram, Q. Nguyen, M. Mehta, G. Morahan, P. Concannon, R. Bergholdt, J. H. Nielsen, T. Reinheckel, M. von Herrath, A. Vaag, D. L. Eizirik, H. B. Mortensen, J. Storling, and F. Pociot. 2014. 'CTSH regulates beta-cell function and disease progression in newly diagnosed type 1 diabetes patients', *Proc Natl Acad Sci U S A*, 111: 10305-10.

Frackowiak, J., H. M. Wisniewski, J. Wegiel, G. S. Merz, K. Iqbal, and K. C. Wang. 1992. 'Ultrastructure of the microglia that phagocytose amyloid and the microglia that produce beta-amyloid fibrils', *Acta Neuropathol*, 84: 225-33.

Franovic, A., L. Gunaratnam, K. Smith, I. Robert, D. Patten, and S. Lee. 2007. 'Translational up-regulation of the EGFR by tumor hypoxia provides a nonmutational explanation for its overexpression in human cancer', *Proceedings of the National Academy of Sciences of the United States of America*, 104: 13092-97.

Freienstein, C., and G. Blobel. 1975. 'Nonribosomal proteins associated with eukaryotic native small ribosomal-subunits', *Proceedings of the National Academy of Sciences of the United States of America*, 72: 3392-96.

Fukazawa, T., S. Miyake, V. Band, and H. Band. 1996. 'Tyrosine phosphorylation of Cbl upon epidermal growth factor (EGF) stimulation and its association with EGF receptor and downstream signaling proteins', *J Biol Chem*, 271: 14554-9.

Galicia-Vazquez, G., R. Cencic, F. Robert, A. Q. Agenor, and J. Pelletier. 2012. 'A cellular response linking eIF4AI activity to eIF4AII transcription', *RNA*, 18: 1373-84.

Gan, H. K., A. N. Cvrlijevic, and T. G. Johns. 2013. 'The epidermal growth factor receptor variant III (EGFRvIII): where wild things are altered', *FEBS Journal*, 280:5350-70.

Garrett, T. P., N. M. McKern, M. Lou, T. C. Elleman, T. E. Adams, G. O. Lovrecz, H. J. Zhu, F. Walker, M. J. Frenkel, P. A. Hoyne, R. N. Jorissen, E. C. Nice, A. W. Burgess, and C. W. Ward. 2002. 'Crystal structure of a truncated epidermal growth factor receptor extracellular domain bound to transforming growth factor alpha', *Cell*, 110: 763-73.

Ge, H., X. Gong, and C. K. Tang. 2002. 'Evidence of high incidence of EGFRvIII expression and coexpression with EGFR in human invasive breast cancer by laser capture microdissection and immunohistochemical analysis', *Int J Cancer*, 98: 357-61.

Gerlitz, G., R. Jagus, and O. Elroy-Stein. 2002. 'Phosphorylation of initiation factor-2 alpha is required for activation of internal translation initiation during cell differentiation', *Eur J Biochem*, 269: 2810-9.

Gingras, A. C., Y. Svitkin, G. J. Belsham, A. Pause, and N. Sonenberg. 1996. 'Activation of the translational suppressor 4E-BP1 following infection with encephalomyocarditis virus and poliovirus', *Proc Natl Acad Sci U S A*, 93: 5578-83.

Glading, A., R. J. Bodnar, I. J. Reynolds, H. Shiraha, L. Satish, D. A. Potter, H. C. Blair, and A. Wells. 2004. 'Epidermal growth factor activates m-calpain (calpain II), at least in part, by extracellular signal-regulated kinase-mediated phosphorylation', *Mol Cell Biol*, 24: 2499-512.

Glading, A., P. Chang, D. A. Lauffenburger, and A. Wells. 2000. 'Epidermal growth factor receptor activation of calpain is required for fibroblast motility and occurs via an ERK/MAP kinase signaling pathway', *J Biol Chem*, 275: 2390-8.

Glenner, G. G., and C. W. Wong. 1984. 'Alzheimers-Disease - Initial Report of the Purification and Characterization of a Novel Cerebrovascular Amyloid Protein', *Biochemical and Biophysical Research Communications*, 120: 885-90.

Goate, A., M. C. Chartierharlin, M. Mullan, J. Brown, F. Crawford, L. Fidani, L. Giuffra, A. Haynes, N. Irving, L. James, R. Mant, P. Newton, K. Rooke, P. Roques, C. Talbot, M. Pericakvance, A. Roses, R. Williamson, M. Rossor, M. Owen, and J. Hardy. 1991. 'Segregation of a Missense Mutation in the Amyloid Precursor Protein Gene with Familial Alzheimers-Disease', *Nature*, 349: 704-06.

Goldberg, M. A., S. P. Dunning, and H. F. Bunn. 1988. 'Regulation of the erythropoietin gene: evidence that the oxygen sensor is a heme protein', *Science*, 242: 1412-5.

Goodman, T. T., C. P. Ng, and S. H. Pun. 2008. '3-D tissue culture systems for the evaluation and optimization of nanoparticle-based drug carriers', *Bioconjug Chem*, 19: 1951-9.

Goossen, B., S. W. Caughman, J. B. Harford, R. D. Klausner, and M. W. Hentze. 1990. 'Translational repression by a complex between the iron-responsive element of ferritin messenger-RNA and its specific cytoplasmic-binding protein is position-dependent invivo', *Embo Journal*, 9: 4127-33.

Gordan, J. D., J. A. Bertout, C. J. Hu, J. A. Diehl, and M. C. Simon. 2007. 'HIF-2 alpha promotes hypoxic cell proliferation by enhancing c-Myc transcriptional activity', *Cancer Cell*, 11: 335-47.

Graus-Porta, D., R. R. Beerli, J. M. Daly, and N. E. Hynes. 1997. 'ErbB-2, the preferred heterodimerization partner of all ErbB receptors, is a mediator of lateral signaling', *EMBO J*, 16: 1647-55.

Gray, N. K., and M. W. Hentze. 1994. 'Iron regulatory protein prevents binding of the 43S translation pre-initiation complex to ferritin and ealas messenger-RNAS', *Embo Journal*, 13: 3882-91.

Grehan, S., E. Tse, and J. M. Taylor. 2001. 'Two distal downstream enhancers direct expression of the human apolipoprotein E gene to astrocytes in the brain', *J Neurosci*, 21: 812-22.

Griffin, D. E., B. Levine, W. R. Tyor, and D. N. Irani. 1992. 'The immune response in viral encephalitis', *Semin Immunol*, 4: 111-9.

Grundkeiqbal, I., K. Iqbal, M. Quinlan, Y. C. Tung, M. S. Zaidi, and H. M. Wisniewski. 1986. 'Microtubule-Associated Protein-Tau - a Component of Alzheimer Paired Helical Filaments', *Journal of Biological Chemistry*, 261: 6084-89.

Guo, H., N. T. Ingolia, J. S. Weissman, and D. P. Bartel. 2010. 'Mammalian microRNAs predominantly act to decrease target mRNA levels', *Nature*, 466: 835-40.

Guy, P. M., J. V. Platko, L. C. Cantley, R. A. Cerione, and K. L. Carraway, 3rd. 1994. 'Insect cell-expressed p180erbB3 possesses an impaired tyrosine kinase activity', *Proc Natl Acad Sci U S A*, 91: 8132-6.

Hajdin, C. E., S. Bellaousov, W. Huggins, C. W. Leonard, D. H. Mathews, and K. M. Weeks. 2013. 'Accurate SHAPE-directed RNA secondary structure modeling, including pseudoknots', *Proc Natl Acad Sci U S A*, 110: 5498-503.

Halaby, M. J., B. R. Harris, W. K. Miskimins, M. P. Cleary, and D. Q. Yang. 2015. 'Deregulation of Internal Ribosome Entry Site-Mediated p53 Translation in Cancer Cells with Defective p53 Response to DNA Damage', *Mol Cell Biol*, 35: 4006-17.

Halaby, M. J., Y. Li, B. R. Harris, S. Jiang, W. K. Miskimins, M. P. Cleary, and D. Q. Yang. 2015. 'Translational Control Protein 80 Stimulates IRES-Mediated Translation of p53 mRNA in Response to DNA Damage', *Biomed Res Int*, 2015: 708158.

Halatsch, M. E., U. Schmidt, J. Behnke-Mursch, A. Unterberg, and C. R. Wirtz. 2006. 'Epidermal growth factor receptor inhibition for the treatment of glioblastoma multiforme and other malignant brain tumours', *Cancer Treat Rev*, 32: 74-89.

Hardy, J. 1997. 'Amyloid, the presenilins and Alzheimer's disease', *Trends in Neurosciences*, 20: 154-59.

Hardy, J., and D. J. Selkoe. 2002. 'The amyloid hypothesis of Alzheimer's disease: progress and problems on the road to therapeutics', *Science*, 297: 353-6.

Hellen, C. U., and P. Sarnow. 2001. 'Internal ribosome entry sites in eukaryotic mRNA molecules', *Genes Dev*, 15: 1593-612.

Hellyer, N. J., K. Cheng, and J. G. Koland. 1998. 'ErbB3 (HER3) interaction with the p85 regulatory subunit of phosphoinositide 3-kinase', *Biochem J*, 333 (Pt 3): 757-63.

Henis-Korenblit, S., N. L. Strumpf, D. Goldstaub, and A. Kimchi. 2000. 'A novel form of DAP5 protein accumulates in apoptotic cells as a result of caspase cleavage and internal ribosome entry site-mediated translation', *Mol Cell Biol*, 20: 496-506.

Heppner, F. L., R. M. Ransohoff, and B. Becher. 2015. 'Immune attack: the role of inflammation in Alzheimer disease', *Nat Rev Neurosci*, 16: 358-72.

Hernandez, G. 2008. 'Was the initiation of translation in early eukaryotes IRES-driven?', *Trends in Biochemical Sciences*, 33: 58-64.

Hick, M., U. Herrmann, S. W. Weyer, J. P. Mallm, J. A. Tschape, M. Borgers, M. Mercken, F. C. Roth, A. Draguhn, L. Slomianka, D. P. Wolfer, M. Korte, and U. C. Muller. 2015. 'Acute function of secreted amyloid precursor protein fragment APPsalpha in synaptic plasticity', *Acta Neuropathol*, 129: 21-37.

Hinnebusch, A. G. 2005. 'Translational regulation of GCN4 and the general amino acid control of yeast.' in, *Annual Review of Microbiology*.

Hiramatsu, M., M. Kashimata, A. Sato, M. Murayama, and N. Minami. 1988. 'Influence of age on epidermal growth factor receptor level in the rat brain', *Experientia*, 44: 23-5.

Hirsch-Reinshagen, V., S. Zhou, B. L. Burgess, L. Bernier, S. A. McIsaac, J. Y. Chan, G. H. Tansley, J. S. Cohn, M. R. Hayden, and C. L. Wellington. 2004. 'Deficiency of ABCA1 impairs apolipoprotein E metabolism in brain', *J Biol Chem*, 279: 41197-207.

Ho, Y. S., X. Yang, J. C. Lau, C. H. Hung, S. Wuwongse, Q. Zhang, J. Wang, L. Baum, K. F. So, and R. C. Chang. 2012. 'Endoplasmic reticulum stress induces tau pathology and forms a vicious cycle: implication in Alzheimer's disease pathogenesis', *J Alzheimers Dis*, 28: 839-54.

Hofman, E. G., A. N. Bader, J. Voortman, D. J. van den Heuvel, S. Sigismund, A. J. Verkleij, H. C. Gerritsen, and Pmpve Henegouwen. 2010. 'Ligand-induced EGF Receptor Oligomerization Is Kinase-dependent and Enhances Internalization', *Journal of Biological Chemistry*, 285: 39481-89.

Hoglund, R. A., and A. A. Maghazachi. 2014. 'Multiple sclerosis and the role of immune cells', *World J Exp Med*, 4: 27-37.

Holcik, M., C. Lefebvre, C. Yeh, T. Chow, and R. G. Korneluk. 1999. 'A new internal-ribosome-entry-site motif potentiates XIAP-mediated cytoprotection', *Nat Cell Biol*, 1: 190-2.

Hornbak, M., K. Banasik, J. M. Justesen, N. T. Krarup, C. H. Sandholt, A. Andersson, A. Sandbaek, T. Lauritzen, C. Pisinger, D. R. Witte, T. A. Sorensen, O. Pedersen, and T. Hansen. 2011. 'The minor C-allele of rs2014355 in ACADS is associated with reduced insulin release following an oral glucose load', *BMC Med Genet*, 12: 4.

Hotamisligil, G. S., N. S. Shargill, and B. M. Spiegelman. 1993. 'Adipose expression of tumor necrosis factor-alpha: direct role in obesity-linked insulin resistance', *Science*, 259: 87-91.

Howes, A. L., G. G. Chiang, E. S. Lang, C. B. Ho, G. Powis, K. Vuori, and R. T. Abraham. 2007. 'The phosphatidylinositol 3-kinase inhibitor, PX-866, is a potent inhibitor of cancer cell motility and growth in three-dimensional cultures', *Mol Cancer Ther*, 6: 2505-14.

Huang, P., X. Xu, L. Wang, B. Zhu, X. Wang, and J. Xia. 2014. 'The role of EGF-EGFR signalling pathway in hepatocellular carcinoma inflammatory microenvironment', *J Cell Mol Med*, 18: 218-30.

Hubbard, S. R., M. Mohammadi, and J. Schlessinger. 1998. 'Autoregulatory mechanisms in protein-tyrosine kinases', *J Biol Chem*, 273: 11987-90.

Huebbe, P., A. Nebel, S. Siegert, J. Moehring, C. Boesch-Saadatmandi, E. Most, J. Pallauf, S. Egert, M. J. Muller, S. Schreiber, U. Nothlings, and G. Rimbach. 2011. 'APOE epsilon4 is associated with higher vitamin D levels in targeted replacement mice and humans', *Federation Proceedings*, 25: 3262-70.

Hunter, R. C., and T. J. Beveridge. 2005. 'Application of a pH-sensitive fluoroprobe (C-SNARF-4) for pH microenvironment analysis in Pseudomonas aeruginosa biofilms', *Appl Environ Microbiol*, 71: 2501-10.

Hussain, I., D. Powell, D. R. Howlett, D. G. Tew, T. D. Week, C. Chapman, I. S. Gloger, K. E. Murphy, C. D. Southan, D. M. Ryan, T. S. Smith, D. L. Simmons, F. S. Walsh, C. Dingwall, and G. Christie. 1999. 'Identification of a novel aspartic protease (Asp 2) as beta-secretase', *Molecular and Cellular Neuroscience*, 14: 419-27.

Hutton, M., C. L. Lendon, P. Rizzu, M. Baker, S. Froelich, H. Houlden, S. Pickering-Brown, S. Chakraverty, A. Isaacs, A. Grover, J. Hackett, J. Adamson, S. Lincoln, D. Dickson, P. Davies, R. C. Petersen, M. Stevens, E. de Graaff, E. Wauters, J. van Baren, M. Hillebrand, M. Joosse, J. M. Kwon, P. Nowotny, L. K. Che, J. Norton, J. C. Morris, L. A. Reed, J. Trojanowski, H. Basun, L. Lannfelt, M. Neystat, S. Fahn, F. Dark, T. Tannenberg, P. R. Dodd, N. Hayward, J. B. J. Kwok, P. R. Schofield, A. Andreadis, J. Snowden, D. Craufurd, D. Neary, F. Owen, B. A. Oostra, J. Hardy, A. Goate, J. van Swieten, D. Mann, T. Lynch, and P. Heutink. 1998. 'Association of missense and 5 '-splice-site mutations in tau with the inherited dementia FTDP-17', *Nature*, 393: 702-05.

Hyman, B. T., K. Marzloff, and P. V. Arriagada. 1993. 'The lack of accumulation of senile plaques or amyloid burden in Alzheimer's disease suggests a dynamic balance between amyloid deposition and resolution', *J Neuropathol Exp Neurol*, 52: 594-600.

Ikonomovic, M. D., E. E. Abrahamson, T. Uz, H. Manev, and S. T. Dekosky. 2008. 'Increased 5-lipoxygenase immunoreactivity in the hippocampus of patients with Alzheimer's disease', *J Histochem Cytochem*, 56: 1065-73.

Irving, J. A., R. N. Pike, A. M. Lesk, and J. C. Whisstock. 2000. 'Phylogeny of the serpin superfamily: implications of patterns of amino acid conservation for structure and function', *Genome Res*, 10: 1845-64.

Ivanov, S., S. Y. Liao, A. Ivanova, A. Danilkovitch-Miagkova, N. Tarasova, G. Weirich, M. J. Merrill, M. A. Proescholdt, E. H. Oldfield, J. Lee, J. Zavada, A. Waheed, W. Sly, M. I. Lerman, and E. J. Stanbridge. 2001. 'Expression of hypoxia-inducible cell-surface transmembrane carbonic anhydrases in human cancer', *Am J Pathol*, 158: 905-19.

Ivascu, A., and M. Kubbies. 2006. 'Rapid generation of single-tumor spheroids for high-throughput cell function and toxicity analysis', *J Biomol Screen*, 11: 922-32.

Jackson, R. J. 2013. 'The current status of vertebrate cellular mRNA IRESs', *Cold Spring Harb Perspect Biol*, 5.

Jackson, R. J., M. T. Howell, and A. Kaminski. 1990. 'The novel mechanism of initiation of picornavirus RNA translation', *Trends Biochem Sci*, 15: 477-83.

Jakobsen, M. R., J. Haasnoot, J. Wengel, B. Berkhout, and J. Kjems. 2007. 'Efficient inhibition of HIV-1 expression by LNA modified antisense oligonucleotides and DNAzymes targeted to functionally selected binding sites', *Retrovirology*, 4: 29.

Jang, C. J., and E. Jan. 2010. 'Modular domains of the Dicistroviridae intergenic internal ribosome entry site', *RNA*, 16: 1182-95.

Jang, S. K. 2006. 'Internal initiation: IRES elements of picornaviruses and hepatitis c virus', *Virus Res*, 119: 2-15.

Jang, S. K., H. G. Krausslich, M. J. Nicklin, G. M. Duke, A. C. Palmenberg, and E. Wimmer. 1988. 'A segment of the 5' nontranslated region of encephalomyocarditis virus RNA directs internal entry of ribosomes during in vitro translation', *J Virol*, 62: 2636-43.

Jiang, L., J. Zhong, X. Dou, C. Cheng, Z. Huang, and X. Sun. 2015. 'Effects of ApoE on intracellular calcium levels and apoptosis of neurons after mechanical injury', *Neuroscience*, 301: 375-83.

Jiang, Q., C. Y. Lee, S. Mandrekar, B. Wilkinson, P. Cramer, N. Zelcer, K. Mann, B. Lamb, T. M. Willson, J. L. Collins, J. C. Richardson, J. D. Smith, T.

A. Comery, D. Riddell, D. M. Holtzman, P. Tontonoz, and G. E. Landreth. 2008. 'ApoE promotes the proteolytic degradation of Abeta', *Neuron*, 58: 681-93.

Jin, N., X. Yin, J. Gu, X. Zhang, J. Shi, W. Qian, Y. Ji, M. Cao, X. Gu, F. Ding, K. Iqbal, C. X. Gong, and F. Liu. 2015. 'Truncation and Activation of Dual Specificity Tyrosine Phosphorylation-regulated Kinase 1A by Calpain I: A molecular mechanism linked to tau pathology in Alzheimer disease', *J Biol Chem*, 290: 15219-37.

Johannes, G., M. S. Carter, M. B. Eisen, P. O. Brown, and P. Sarnow. 1999. 'Identification of eukaryotic mRNAs that are translated at reduced cap binding complex eIF4F concentrations using a cDNA microarray', *Proc Natl Acad Sci U S A*, 96: 13118-23.

Jones, J. T., R. W. Akita, and M. X. Sliwkowski. 1999. 'Binding specificities and affinities of egf domains for ErbB receptors', *FEBS Lett*, 447: 227-31.

Jopling, C. L., K. A. Spriggs, S. A. Mitchell, M. Stoneley, and A. E. Willis. 2004. 'L-Myc protein synthesis is initiated by internal ribosome entry', *Rna-a Publication of the Rna Society*, 10: 287-98.

Jopling, C. L., and A. E. Willis. 2001. 'N-myc translation is initiated via an internal ribosome entry segment that displays enhanced activity in neuronal cells', *Oncogene*, 20: 2664-70.

Kafasla, P., N. Morgner, T. A. Poyry, S. Curry, C. V. Robinson, and R. J. Jackson. 2009. 'Polypyrimidine tract binding protein stabilizes the encephalomyocarditis virus IRES structure via binding multiple sites in a unique orientation', *Mol Cell*, 34: 556-68.

Kalaria, R. N., T. Golde, S. N. Kroon, and G. Perry. 1993. 'Serine protease inhibitor antithrombin III and its messenger RNA in the pathogenesis of Alzheimer's disease', *Am J Pathol*, 143: 886-93.

Kaminski, A., G. J. Belsham, and R. J. Jackson. 1994. 'Translation of encephalomyocarditis virus RNA: parameters influencing the selection of the internal initiation site', *EMBO J*, 13: 1673-81.

Kang, D. E., C. U. Pietrzik, L. Baum, N. Chevallier, D. E. Merriam, M. Z. Kounnas, S. L. Wagner, J. C. Troncoso, C. H. Kawas, R. Katzman, and E. H. Koo. 2000. 'Modulation of amyloid beta-protein clearance and Alzheimer's disease susceptibility by the LDL receptor-related protein pathway', *J Clin Invest*, 106: 1159-66.

Kasayama, S., Y. Ohba, and T. Oka. 1989. 'Epidermal growth factor deficiency associated with diabetes mellitus', *Proc Natl Acad Sci U S A*, 86: 7644-8.

Kelliher, M., J. Fastbom, R. F. Cowburn, W. Bonkale, T. G. Ohm, R. Ravid, V. Sorrentino, and C. O'Neill. 1999. 'Alterations in the ryanodine receptor calcium release channel correlate with Alzheimer's disease neurofibrillary and beta-amyloid pathologies', *Neuroscience*, 92: 499-513.

Kenyon, J. C., S. J. Tanner, M. Legiewicz, P. S. Phillip, T. A. Rizvi, S. F. Le Grice, and A. M. Lever. 2011. 'SHAPE analysis of the FIV Leader RNA reveals a structural switch potentially controlling viral packaging and genome dimerization', *Nucleic Acids Res*, 39: 6692-704.

Kersting, C., N. Tidow, H. Schmidt, C. Liedtke, J. Neumann, W. Boecker, P. J. van Diest, B. Brandt, and H. Buerger. 2004. 'Gene dosage PCR and fluorescence in situ hybridization reveal low frequency of egfr amplifications despite protein overexpression in invasive breast carcinoma', *Lab Invest*, 84: 582-7.

Khachaturian, Z. S. 1987. 'Hypothesis on the regulation of cytosol calcium concentration and the aging brain', *Neurobiol Aging*, 8: 345-6.

Kieft, J. S., K. Zhou, A. Grech, R. Jubin, and J. A. Doudna. 2002. 'Crystal structure of an RNA tertiary domain essential to HCV IRES-mediated translation initiation', *Nat Struct Biol*, 9: 370-4.

Kim, J. B., R. Stein, and M. J. O'Hare. 2004. 'Three-dimensional in vitro tissue culture models of breast cancer-- a review', *Breast Cancer Res Treat*, 85: 281-91.

Kim, J., H. Jiang, S. Park, A. E. Eltorai, F. R. Stewart, H. Yoon, J. M. Basak, M. B. Finn, and D. M. Holtzman. 2011. 'Haploinsufficiency of human APOE reduces amyloid deposition in a mouse model of amyloid-beta amyloidosis', *J Neurosci*, 31: 18007-12.

Kim, S., J. H. Choi, H. I. Lim, S. K. Lee, W. W. Kim, S. Cho, J. S. Kim, J. H. Kim, J. H. Choe, S. J. Nam, J. E. Lee, and J. H. Yang. 2009. 'EGF-induced MMP-9 expression is mediated by the JAK3/ERK pathway, but not by the JAK3/STAT-3 pathway in a SKBR3 breast cancer cell line', *Cell Signal*, 21: 892-8.

Kim, S. K., H. J. Park, H. S. Hong, E. J. Baik, M. W. Jung, and I. Mook-Jung. 2006. 'ERK1/2 is an endogenous negative regulator of the gamma-secretase activity', *Federation Proceedings*, 20: 157-9.

Kim, Y. K., B. Hahm, and S. K. Jang. 2000. 'Polypyrimidine tract-binding protein inhibits translation of Bip mRNA', *Journal of Molecular Biology*, 304: 119-33.

Kimball, S. R. 1999. 'Eukaryotic initiation factor eIF2', *Int J Biochem Cell Biol*, 31: 25-9.

Kiyota, T., H. E. Gendelman, R. A. Weir, E. E. Higgins, G. Zhang, and M. Jain. 2013. 'CCL2 affects beta-amyloidosis and progressive neurocognitive dysfunction in a mouse model of Alzheimer's disease', *Neurobiol Aging*, 34: 1060-8.

Klapper, L. N., S. Glathe, N. Vaisman, N. E. Hynes, G. C. Andrews, M. Sela, and Y. Yarden. 1999. 'The ErbB-2/HER2 oncoprotein of human carcinomas may function solely as a shared coreceptor for multiple stroma-derived growth factors', *Proc Natl Acad Sci U S A*, 96: 4995-5000.

Kloth, M. T., K. K. Laughlin, J. S. Biscardi, J. L. Boerner, S. J. Parsons, and C. M. Silva. 2003. 'STAT5b, a Mediator of Synergism between c-Src and the Epidermal Growth Factor Receptor', *J Biol Chem*, 278: 1671-9.

Knauer, M. F., R. A. Orlando, and C. G. Glabe. 1996. 'Cell surface APP751 forms complexes with protease nexin 2 ligands and is internalized via the low density lipoprotein receptor-related protein (LRP)', *Brain Res*, 740: 6-14.

Knouff, C., M. E. Hinsdale, H. Mezdour, M. K. Altenburg, M. Watanabe, S. H. Quarfordt, P. M. Sullivan, and N. Maeda. 1999. 'Apo E structure determines VLDL clearance and atherosclerosis risk in mice', *J Clin Invest*, 103: 1579-86.

Kolupaeva, V. G., I. B. Lomakin, T. V. Pestova, and C. U. Hellen. 2003. 'Eukaryotic initiation factors 4G and 4A mediate conformational changes downstream of the initiation codon of the encephalomyocarditis virus internal ribosomal entry site', *Mol Cell Biol*, 23: 687-98.

Kolupaeva, V. G., T. V. Pestova, C. U. Hellen, and I. N. Shatsky. 1998. 'Translation eukaryotic initiation factor 4G recognizes a specific structural element within the internal ribosome entry site of encephalomyocarditis virus RNA', *J Biol Chem*, 273: 18599-604.

Kolupaeva, V. G., A. Unbehaun, I. B. Lomakin, C. U. T. Hellen, and T. V. Pestova. 2005. 'Binding of eukaryotic initiation factor 3 to ribosomal 40S subunits and its role in ribosomal dissociation and anti-association', *Rna-a Publication of the Rna Society*, 11: 470-86.

Komori, T., M. Tanaka, E. Senba, A. Miyajima, and Y. Morikawa. 2014. 'Deficiency of oncostatin M receptor beta (OSMRbeta) exacerbates high-fat diet-induced obesity and related metabolic disorders in mice', *J Biol Chem*, 289: 13821-37.

Kotch, L. E., N. V. Iyer, E. Laughner, and G. L. Semenza. 1999. 'Defective vascularization of HIF-1 alpha-null embryos is not associated with VEGF deficiency but with mesenchymal cell death', *Developmental Biology*, 209: 254-67.

Kounnas, M. Z., R. D. Moir, G. W. Rebeck, A. I. Bush, W. S. Argraves, R. E. Tanzi, B. T. Hyman, and D. K. Strickland. 1995. 'LDL receptor-related protein, a multifunctional ApoE receptor, binds secreted beta-amyloid precursor protein and mediates its degradation', *Cell*, 82: 331-40.

Kozak, M. 1983. 'Translation of insulin-related polypeptides from messenger-RNAs with tandemly reiterated copies of the ribosome binding-site', *Cell*, 34: 971-78.

Kozak, M. 1989. 'Circumstances and mechanisms of inhibition of translation by secondary structure in eukaryotic messenger-RNAs', *Molecular and Cellular Biology*, 9: 5134-42.

Kozak, M. 1991. 'A short leader sequence impairs the fidelity of initiation by eukaryotic ribosomes', *Gene Expr*, 1: 111-5.

Kozak, M. 2001. 'Constraints on reinitiation of translation in mammals', *Nucleic Acids Research*, 29: 5226-32.

Kozak, M. 2005. 'A second look at cellular mRNA sequences said to function as internal ribosome entry sites', *Nucleic Acids Res*, 33: 6593-602.

Kuruppu, A. 2016. 'The role of HER family signalling in breast cancer', University of Nottingham.

Lai, C. H., J. T. Tseng, Y. C. Lee, Y. J. Chen, J. C. Lee, B. W. Lin, T. C. Huang, Y. W. Liu, T. H. Leu, Y. W. Liu, Y. P. Chen, W. C. Chang, and L. Y. Hung. 2010. 'Translational up-regulation of Aurora-A in EGFR-overexpressed cancer', *J Cell Mol Med*, 14: 1520-31.

Lambert, M. P., A. K. Barlow, B. A. Chromy, C. Edwards, R. Freed, M. Liosatos, T. E. Morgan, I. Rozovsky, B. Trommer, K. L. Viola, P. Wals, C. Zhang, C. E. Finch, G. A. Krafft, and W. L. Klein. 1998. 'Diffusible, nonfibrillar ligands derived from Abeta1-42 are potent central nervous system neurotoxins', *Proc Natl Acad Sci U S A*, 95: 6448-53.

Langan, L. M., N. J. Dodd, S. F. Owen, W. M. Purcell, S. K. Jackson, and A. N. Jha. 2016. 'Direct Measurements of Oxygen Gradients in Spheroid Culture System Using Electron Parametric Resonance Oximetry', *Plos One*, 11: e0149492.

Langmead, B., C. Trapnell, M. Pop, and S. L. Salzberg. 2009. 'Ultrafast and memory-efficient alignment of short DNA sequences to the human genome', *Genome Biol*, 10: R25.

Larson, J., G. Lynch, D. Games, and P. Seubert. 1999. 'Alterations in synaptic transmission and long-term potentiation in hippocampal slices from young and aged PDAPP mice', *Brain Res*, 840: 23-35.

Le Quesne, J. P., M. Stoneley, G. A. Fraser, and A. E. Willis. 2001. 'Derivation of a structural model for the c-myc IRES', *J Mol Biol*, 310: 111-26.

Lee, H. K., C. Velazquez Sanchez, M. Chen, P. J. Morin, J. M. Wells, E. B. Hanlon, and W. Xia. 2016. 'Three Dimensional Human Neuro-Spheroid Model of Alzheimer's Disease Based on Differentiated Induced Pluripotent Stem Cells', *Plos One*, 11: e0163072.

Lee, S. J., C. E. Kim, K. W. Seo, and C. D. Kim. 2010. 'HNE-induced 5-LO expression is regulated by NF-{kappa}B/ERK and Sp1/p38 MAPK pathways via EGF receptor in murine macrophages', *Cardiovasc Res*, 88: 352-9.

Leissring, M. A., Y. Akbari, C. M. Fanger, M. D. Cahalan, M. P. Mattson, and F. M. LaFerla. 2000. 'Capacitative calcium entry deficits and elevated luminal calcium content in mutant presenilin-1 knockin mice', *J Cell Biol*, 149: 793-8.

Lemp, N. A., K. Hiraoka, N. Kasahara, and C. R. Logg. 2012. 'Cryptic transcripts from a ubiquitous plasmid origin of replication confound tests for cis-regulatory function', *Nucleic Acids Res*, 40: 7280-90.

Lewis, S. M., A. Veyrier, N. Hosszu Ungureanu, S. Bonnal, S. Vagner, and M. Holcik. 2007. 'Subcellular relocalization of a trans-acting factor regulates XIAP IRES-dependent translation', *Mol Biol Cell*, 18: 1302-11.

Li, A. R., D. Chitale, G. J. Riely, W. Pao, V. A. Miller, M. F. Zakowski, V. Rusch, M. G. Kris, and M. Ladanyi. 2008. 'EGFR mutations in lung adenocarcinomas: clinical testing experience and relationship to EGFR gene copy number and immunohistochemical expression', *J Mol Diagn*, 10: 242-8.

Li, X., D. Song, and S. X. Leng. 2015. 'Link between type 2 diabetes and Alzheimer's disease: from epidemiology to mechanism and treatment', *Clin Interv Aging*, 10: 549-60.

Li, Z. W., J. J. Li, L. Wang, J. P. Zhang, J. J. Wu, X. Q. Mao, G. F. Shi, Q. Wang, F. Wang, and J. Zou. 2014. 'Epidermal growth factor receptor inhibitor ameliorates excessive astrogliosis and improves the regeneration microenvironment and functional recovery in adult rats following spinal cord injury', *J Neuroinflammation*, 11: 71.

Liang, W. S., T. Dunckley, T. G. Beach, A. Grover, D. Mastroeni, D. G. Walker, R. J. Caselli, W. A. Kukull, D. McKeel, J. C. Morris, C. Hulette, D. Schmechel, G. E. Alexander, E. M. Reiman, J. Rogers, and D. A. Stephan. 2007. 'Gene expression profiles in anatomically and functionally distinct regions of the normal aged human brain', *Physiol Genomics*, 28: 311-22.

Liang, X. H., W. Shen, H. Sun, M. T. Migawa, T. A. Vickers, and S. T. Crooke. 2016. 'Translation efficiency of mRNAs is increased by antisense oligonucleotides targeting upstream open reading frames', *Nat Biotechnol*, 34: 875-80.

Liberman, N., V. Gandin, Y. V. Svitkin, M. David, G. Virgili, M. Jaramillo, M. Holcik, B. Nagar, A. Kimchi, and N. Sonenberg. 2015. 'DAP5 associates with eIF2beta and eIF4AI to promote Internal Ribosome Entry Site driven translation', *Nucleic Acids Res*, 43: 3764-75.

Lin, J. C., M. Hsu, and W. Y. Tarn. 2007. 'Cell stress modulates the function of splicing regulatory protein RBM4 in translation control', *Proc Natl Acad Sci U S A*, 104: 2235-40.

Lin, W., N. L. Wadlington, L. Chen, X. Zhuang, J. R. Brorson, and U. J. Kang. 2014. 'Loss of PINK1 attenuates HIF-1alpha induction by preventing 4E-BP1-dependent switch in protein translation under hypoxia', *J Neurosci*, 34: 3079-89.

Lipton, P. 1999. 'Ischemic cell death in brain neurons', *Physiol Rev*, 79: 1431-568.

Liu, F., I. Grundke-Iqbal, K. Iqbal, Y. Oda, K. Tomizawa, and C. X. Gong. 2005. 'Truncation and activation of calcineurin A by calpain I in Alzheimer disease brain', *J Biol Chem*, 280: 37755-62.

Liu, L. X., X. Y. Shao, W. Gao, Z. Zhang, P. Liu, R. S. Wang, P. W. Huang, Y. M. Yin, and Y. Q. Shu. 2012. 'MicroRNA-133b inhibits the growth of non-

small-cell lung cancer by targeting the epidermal growth factor receptor', *Febs Journal*, 279: 3800-12.

Liu, Q.Y. 2015. 'Blocking IRES-mediated translation pathway as a new method to treat Alzheimer's disease', *Journal of Medical Hypotheses and Ideas*, 9: 57-60.

Liu, S. J., A. H. Zhang, H. L. Li, Q. Wang, H. M. Deng, W. J. Netzer, H. Xu, and J. Z. Wang. 2003. 'Overactivation of glycogen synthase kinase-3 by inhibition of phosphoinositol-3 kinase and protein kinase C leads to hyperphosphorylation of tau and impairment of spatial memory', *J Neurochem*, 87: 1333-44.

Lloyd, M. A., J. C. Osborne, B. Safer, G. M. Powell, and W. C. Merrick. 1980. 'Characteristics of eukaryotic initiation factor-II and its subunits', *Journal of Biological Chemistry*, 255: 1189-93.

Lomakin, I. B., C. U. Hellen, and T. V. Pestova. 2000. 'Physical association of eukaryotic initiation factor 4G (eIF4G) with eIF4A strongly enhances binding of eIF4G to the internal ribosomal entry site of encephalomyocarditis virus and is required for internal initiation of translation', *Mol Cell Biol*, 20: 6019-29.

Lomakin, I. B., V. G. Kolupaeva, A. Marintchev, G. Wagner, and T. V. Pestova. 2003. 'Position of eukaryotic initiation factor eIF1 on the 40S ribosomal subunit determined by directed hydroxyl radical probing', *Genes & Development*, 17: 2786-97.

Lopez de Quinto, S., and E. Martinez-Salas. 1997. 'Conserved structural motifs located in distal loops of aphthovirus internal ribosome entry site domain 3 are required for internal initiation of translation', *J Virol*, 71: 4171-5.

Lopez de Quinto, S., and E. Martinez-Salas. 2000. 'Interaction of the eIF4G initiation factor with the aphthovirus IRES is essential for internal translation initiation in vivo', *RNA*, 6: 1380-92.

Lorenz, R., S. H. Bernhart, C. Honer Zu Siederdissen, H. Tafer, C. Flamm, P. F. Stadler, and I. L. Hofacker. 2011. 'ViennaRNA Package 2.0', *Algorithms Mol Biol*, 6: 26.

Lorenzl, S., D. S. Albers, N. Relkin, T. Ngyuen, S. L. Hilgenberg, J. Chirichigno, M. E. Cudkowicz, and M. F. Beal. 2003. 'Increased plasma levels of matrix metalloproteinase-9 in patients with Alzheimer's disease', *Neurochem Int*, 43: 191-6.

Lu, Z. J., J. W. Gloor, and D. H. Mathews. 2009. 'Improved RNA secondary structure prediction by maximizing expected pair accuracy', *RNA*, 15: 1805-13.

Luukkonen, B. G., W. Tan, and S. Schwartz. 1995. 'Efficiency of reinitiation of translation on human immunodeficiency virus type 1 mRNAs is determined by the length of the upstream open reading frame and by intercistronic distance', *J Virol*, 69: 4086-94.

Ma, T., M. A. Trinh, A. J. Wexler, C. Bourbon, E. Gatti, P. Pierre, D. R. Cavener, and E. Klann. 2013. 'Suppression of eIF2alpha kinases alleviates Alzheimer's disease-related plasticity and memory deficits', *Nat Neurosci*, 16: 1299-305.

Maag, D., M. A. Algire, and J. R. Lorsch. 2006. 'Communication between eukaryotic translation initiation factors 5 and 1A within the ribosomal pre-initiation complex plays a role in start site selection', *Journal of Molecular Biology*, 356: 724-37.

MacGregor-Fors, I., and M. E. Payton. 2013. 'Contrasting diversity values: statistical inferences based on overlapping confidence intervals', *Plos One*, 8: e56794.

Madden, J. A., D. E. Ray, P. A. Keller, and J. G. Kleinman. 2001. 'Ion exchange activity in pulmonary artery smooth muscle cells: the response to hypoxia', *Am J Physiol Lung Cell Mol Physiol*, 280: L264-71.

Mahley, R. W., K. H. Weisgraber, and Y. Huang. 2006. 'Apolipoprotein E4: a causative factor and therapeutic target in neuropathology, including Alzheimer's disease', *Proc Natl Acad Sci U S A*, 103: 5644-51.

Majumder, M., I. Yaman, F. Gaccioli, V. V. Zeenko, C. Wang, M. G. Caprara, R. C. Venema, A. A. Komar, M. D. Snider, and M. Hatzoglou. 2009. 'The hnRNA-binding proteins hnRNP L and PTB are required for efficient translation of the Cat-1 arginine/lysine transporter mRNA during amino acid starvation', *Mol Cell Biol*, 29: 2899-912.

Manev, H., and R. Manev. 2006. '5-Lipoxygenase (ALOX5) and FLAP (ALOX5AP) gene polymorphisms as factors in vascular pathology and Alzheimer's disease', *Med Hypotheses*, 66: 501-3.

Marash, L., and A. Kimchi. 2005. 'DAP5 and IRES-mediated translation during programmed cell death', *Cell Death Differ*, 12: 554-62.

Markesbery, W. R. 1997. 'Oxidative stress hypothesis in Alzheimer's disease', *Free Radic Biol Med*, 23: 134-47.

Marksteiner, J., G. Kemmler, E. M. Weiss, G. Knaus, C. Ullrich, S. Mechtcheriakov, H. Oberbauer, S. Auffinger, J. Hinterholzl, H. Hinterhuber, and C. Humpel. 2011. 'Five out of 16 plasma signaling proteins are enhanced in plasma of patients with mild cognitive impairment and Alzheimer's disease', *Neurobiol Aging*, 32: 539-40.

Martin, S. A., and B. Moss. 1975. 'Modification of RNA by messenger-RNA guanylyltransferase and messenger-RNA(guanine-7-)methyltransferase from vaccinia virions', *Journal of Biological Chemistry*, 250: 9330-35.

Marx, U. & Sandig, V. 2006. *Drug Testing in vitro: Breakthrough and Trends in Cell Culture Technology* (Wiley-VCH: Weinheim).

Mathews, D. H., M. D. Disney, J. L. Childs, S. J. Schroeder, M. Zuker, and D. H. Turner. 2004. 'Incorporating chemical modification constraints into a

dynamic programming algorithm for prediction of RNA secondary structure', *Proc Natl Acad Sci U S A*, 101: 7287-92.

Mathews, D. H., J. Sabina, M. Zuker, and D. H. Turner. 1999. 'Expanded sequence dependence of thermodynamic parameters improves prediction of RNA secondary structure', *J Mol Biol*, 288: 911-40.

Matoulkova, E., E. Michalova, B. Vojtesek, and R. Hrstka. 2012. 'The role of the 3' untranslated region in post-transcriptional regulation of protein expression in mammalian cells', *RNA Biol*, 9: 563-76.

Matsumura, T., Y. Takamura, T. Tomomatsu, S. Arimura, M. Gozawa, Y. Takihara, and M. Inatani. 2015. 'Changes in Matrix Metalloproteinases in Diabetes Patients' Tears After Vitrectomy and the Relationship With Corneal Epithelial Disorder', *Invest Ophthalmol Vis Sci*, 56: 3559-64.

Maynard, C. J., A. I. Bush, C. L. Masters, R. Cappai, and Q. X. Li. 2005. 'Metals and amyloid-beta in Alzheimer's disease', *Int J Exp Pathol*, 86: 147-59.

Mazzoleni, G., D. Di Lorenzo, and N. Steimberg. 2009. 'Modelling tissues in 3D: the next future of pharmaco-toxicology and food research?', *Genes Nutr*, 4: 13-22.

McCaskill, J. S. 1990. 'The equilibrium partition function and base pair binding probabilities for RNA secondary structure', *Biopolymers*, 29: 1105-19.

Merino, E. J., K. A. Wilkinson, J. L. Coughlan, and K. M. Weeks. 2005. 'RNA structure analysis at single nucleotide resolution by selective 2'-hydroxyl acylation and primer extension (SHAPE)', *J Am Chem Soc*, 127: 4223-31.

Minopoli, G., F. Passaro, L. Aloia, F. Carlomagno, R. M. Melillo, M. Santoro, F. Forzati, N. Zambrano, and T. Russo. 2007. 'Receptor- and non-receptor tyrosine kinases induce processing of the amyloid precursor protein: role of the low-density lipoprotein receptor-related protein', *Neurodegener Dis*, 4: 94-100.

Miskimins, W. K., G. Wang, M. Hawkinson, and R. Miskimins. 2001. 'Control of cyclin-dependent kinase inhibitor p27 expression by cap-independent translation', *Mol Cell Biol*, 21: 4960-7.

Mitchell, S. A., E. C. Brown, M. J. Coldwell, R. J. Jackson, and A. E. Willis. 2001. 'Protein factor requirements of the Apaf-1 internal ribosome entry segment: Roles of polypyrimidine tract binding protein and upstream of N-ras', *Molecular and Cellular Biology*, 21: 3364-74.

Mitchell, S. A., K. A. Spriggs, M. J. Coldwell, R. J. Jackson, and A. E. Willis. 2003. 'The Apaf-1 internal ribosome entry segment attains the correct structural conformation for function via interactions with PTB and unr', *Mol Cell*, 11: 757-71.

Miura, T., K. Suzuki, N. Kohata, and H. Takeuchi. 2000. 'Metal binding modes of Alzheimer's amyloid beta-peptide in insoluble aggregates and soluble complexes', *Biochemistry*, 39: 7024-31.

Mizoguchi, H., K. Takuma, E. Fukuzaki, D. Ibi, E. Someya, K. H. Akazawa, T. Alkam, H. Tsunekawa, A. Mouri, Y. Noda, T. Nabeshima, and K. Yamada. 2009. 'Matrix metalloprotease-9 inhibition improves amyloid beta-mediated cognitive impairment and neurotoxicity in mice', *J Pharmacol Exp Ther*, 331: 14-22.

Mohamed, N. V., V. Plouffe, G. Remillard-Labrosse, E. Planel, and N. Leclerc. 2014. 'Starvation and inhibition of lysosomal function increased tau secretion by primary cortical neurons', *Sci Rep*, 4: 5715.

Mok, T. S., Y. L. Wu, S. Thongprasert, C. H. Yang, D. T. Chu, N. Saijo, P. Sunpaweravong, B. Han, B. Margono, Y. Ichinose, Y. Nishiwaki, Y. Ohe, J. J. Yang, B. Chewaskulyong, H. Jiang, E. L. Duffield, C. L. Watkins, A. A. Armour, and M. Fukuoka. 2009. 'Gefitinib or carboplatin-paclitaxel in pulmonary adenocarcinoma', *N Engl J Med*, 361: 947-57.

Moriki, T., H. Maruyama, and I. N. Maruyama. 2001. 'Activation of preformed EGF receptor dimers by ligand-induced rotation of the transmembrane domain', *Journal of Molecular Biology*, 311: 1011-26.

Nielsen, P. J., and H. Trachsel. 1988. 'The mouse protein synthesis initiation factor 4A gene family includes two related functional genes which are differentially expressed', *EMBO J*, 7: 2097-105.

Nomoto, A., Y. F. Lee, and E. Wimmer. 1976. 'The 5' end of poliovirus mRNA is not capped with m7G(5')ppp(5')Np', *Proc Natl Acad Sci U S A*, 73: 375-80.

Nubling, G., J. Levin, B. Bader, L. Israel, K. Botzel, S. Lorenzl, and A. Giese. 2012. 'Limited cleavage of tau with matrix-metalloproteinase MMP-9, but not MMP-3, enhances tau oligomer formation', *Exp Neurol*, 237: 470-6.

O'Connor, T., K. R. Sadleir, E. Maus, R. A. Velliquette, J. Zhao, S. L. Cole, W. A. Eimer, B. Hitt, L. A. Bembinster, S. Lammich, S. F. Lichtenthaler, S. S. Hebert, B. De Strooper, C. Haass, D. A. Bennett, and R. Vassar. 2008. 'Phosphorylation of the translation initiation factor eIF2alpha increases BACE1 levels and promotes amyloidogenesis', *Neuron*, 60: 988-1009.

Oberer, M., A. Marintchev, and G. Wagner. 2005. 'Structural basis for the enhancement of eIF4A helicase activity by eIF4G', *Genes & Development*, 19: 2212-23.

Ochs, K., A. Zeller, L. Saleh, G. Bassili, Y. Song, A. Sonntag, and M. Niepmann. 2003. 'Impaired binding of standard initiation factors mediates poliovirus translation attenuation', *J Virol*, 77: 115-22.

Ogiso, H., R. Ishitani, O. Nureki, S. Fukai, M. Yamanaka, J. H. Kim, K. Saito, A. Sakamoto, M. Inoue, M. Shirouzu, and S. Yokoyama. 2002. 'Crystal structure of the complex of human epidermal growth factor and receptor extracellular domains', *Cell*, 110: 775-87.

Ojala, J., I. Alafuzoff, S. K. Herukka, T. van Groen, H. Tanila, and T. Pirttila. 2009. 'Expression of interleukin-18 is increased in the brains of Alzheimer's disease patients', *Neurobiol Aging*, 30: 198-209.

Olayioye, M. A., D. Graus-Porta, R. R. Beerli, J. Rohrer, B. Gay, and N. E. Hynes. 1998. 'ErbB-1 and ErbB-2 acquire distinct signaling properties dependent upon their dimerization partner', *Mol Cell Biol*, 18: 5042-51.

Otto, G. A., and J. D. Puglisi. 2004. 'The pathway of HCV IRES-mediated translation initiation', *Cell*, 119: 369-80.

Page, G., A. Rioux Bilan, S. Ingrand, C. Lafay-Chebassier, S. Pain, M. C. Perault Pochat, C. Bouras, T. Bayer, and J. Hugon. 2006. 'Activated double-stranded RNA-dependent protein kinase and neuronal death in models of Alzheimer's disease', *Neuroscience*, 139: 1343-54.

Pampaloni, F., E. G. Reynaud, and E. H. Stelzer. 2007. 'The third dimension bridges the gap between cell culture and live tissue', *Nat Rev Mol Cell Biol*, 8: 839-45.

Parmer, T. G., M. D. Ward, E. J. Yurkow, V. H. Vyas, T. J. Kearney, and W. N. Hait. 1999. 'Activity and regulation by growth factors of calmodulin-dependent protein kinase III (elongation factor 2-kinase) in human breast cancer', *Br J Cancer*, 79: 59-64.

Passmore, L. A., T. M. Schmeing, D. Maag, D. J. Applefield, M. G. Acker, M. A. Algire, J. R. Lorsch, and V. Ramakrishnan. 2007. 'The eukaryotic translation initiation factors eIF1 and eIF1A induce an open conformation of the 40S ribosome', *Molecular Cell*, 26: 41-50.

Pastore, S., F. Mascia, V. Mariani, and G. Girolomoni. 2008. 'The epidermal growth factor receptor system in skin repair and inflammation', *J Invest Dermatol*, 128: 1365-74.

Paulin, F. E., M. J. West, N. F. Sullivan, R. L. Whitney, L. Lyne, and A. E. Willis. 1996. 'Aberrant translational control of the c-myc gene in multiple myeloma', *Oncogene*, 13: 505-13.

Pawlik, M., M. Sastre, M. Calero, P. M. Mathews, S. D. Schmidt, R. A. Nixon, and E. Levy. 2004. 'Overexpression of human cystatin C in transgenic mice does not affect levels of endogenous brain amyloid Beta Peptide', *Journal of Molecular Neuroscience*, 22: 13-8.

Pelletier, J., and N. Sonenberg. 1988. 'Internal initiation of translation of eukaryotic mRNA directed by a sequence derived from poliovirus RNA', *Nature*, 334: 320-5.

Peppelenbosch, M. P., L. G. Tertoolen, J. den Hertog, and S. W. de Laat. 1992. 'Epidermal growth factor activates calcium channels by phospholipase A2/5-lipoxygenase-mediated leukotriene C4 production', *Cell*, 69: 295-303.

Pesole, G., F. Mignone, C. Gissi, G. Grillo, F. Licciulli, and S. Liuni. 2001. 'Structural and functional features of eukaryotic mRNA untranslated regions', *Gene*, 276: 73-81.

Pestova, T. V., S. I. Borukhov, and C. U. T. Hellen. 1998. 'Eukaryotic ribosomes require initiation factors 1 and 1A to locate initiation codons', *Nature*, 394: 854-59.

Pestova, T. V., S. de Breyne, A. V. Pisarev, I. S. Abaeva, and C. U. Hellen. 2008. 'eIF2-dependent and eIF2-independent modes of initiation on the CSFV IRES: a common role of domain II', *EMBO J*, 27: 1060-72.

Pestova, T. V., C. U. Hellen, and I. N. Shatsky. 1996. 'Canonical eukaryotic initiation factors determine initiation of translation by internal ribosomal entry', *Mol Cell Biol*, 16: 6859-69.

Pestova, T. V., and V. G. Kolupaeva. 2002. 'The roles of individual eukaryotic translation initiation factors in ribosomal scanning and initiation codon selection', *Genes & Development*, 16: 2906-22.

Pestova, T. V., I. B. Lomakin, J. H. Lee, S. K. Choi, T. E. Dever, and C. U. T. Hellen. 2000. 'The joining of ribosomal subunits in eukaryotes requires eIF5B', *Nature*, 403: 332-35.

Pestova, T. V., I. N. Shatsky, S. P. Fletcher, R. T. Jackson, and C. U. T. Hellen. 1998. 'A prokaryotic-like mode of cytoplasmic eukaryotic ribosome binding to the initiation codon during internal translation initiation of hepatitis C and classical swine fever virus RNAs', *Genes & Development*, 12: 67-83.

Pfrieger, F. W. 2003. 'Cholesterol homeostasis and function in neurons of the central nervous system', *Cell Mol Life Sci*, 60: 1158-71.

Piao, Y., H. Jiang, R. Alemany, V. Krasnykh, F. C. Marini, J. Xu, M. M. Alonso, C. A. Conrad, K. D. Aldape, C. Gomez-Manzano, and J. Fueyo. 2009. 'Oncolytic adenovirus retargeted to Delta-EGFR induces selective antiglioma activity', *Cancer Gene Ther*, 16: 256-65.

Pickering, B. M., S. A. Mitchell, J. R. Evans, and A. E. Willis. 2003. 'Polypyrimidine tract binding protein and poly r(C) binding protein 1 interact with the BAG-1 IRES and stimulate its activity in vitro and in vivo', *Nucleic Acids Research*, 31: 639-46.

Pickering, B. M., S. A. Mitchell, K. A. Spriggs, M. Stoneley, and A. E. Willis. 2004. 'Bag-1 internal ribosome entry segment activity is promoted by structural changes mediated by poly(rC) binding protein 1 and recruitment of polypyrimidine tract binding protein 1', *Mol Cell Biol*, 24: 5595-605.

Pickering, B. M., and A. E. Willis. 2005. 'The implications of structured 5 ' untranslated regions on translation and disease', *Seminars in Cell & Developmental Biology*, 16: 39-47.

Pierrot, N., P. Ghisdal, A. S. Caumont, and J. N. Octave. 2004. 'Intraneuronal amyloid-beta1-42 production triggered by sustained increase of cytosolic calcium concentration induces neuronal death', *J Neurochem*, 88: 1140-50.

Pilipenko, E. V., V. M. Blinov, B. K. Chernov, T. M. Dmitrieva, and V. I. Agol. 1989. 'Conservation of the secondary structure elements of the 5'-untranslated region of cardio- and aphthovirus RNAs', *Nucleic Acids Res*, 17: 5701-11.

Pilipenko, E. V., A. P. Gmyl, S. V. Maslova, Y. V. Svitkin, A. N. Sinyakov, and V. I. Agol. 1992. 'Prokaryotic-like cis elements in the cap-independent internal initiation of translation on picornavirus RNA', *Cell*, 68: 119-31.

Pitas, R. E., J. K. Boyles, S. H. Lee, D. Hui, and K. H. Weisgraber. 1987. 'Lipoproteins and their receptors in the central nervous system. Characterization of the lipoproteins in cerebrospinal fluid and identification of apolipoprotein B,E(LDL) receptors in the brain', *J Biol Chem*, 262: 14352-60.

Plank, T. D., J. T. Whitehurst, and J. S. Kieft. 2013. 'Cell type specificity and structural determinants of IRES activity from the 5' leaders of different HIV-1 transcripts', *Nucleic Acids Res*, 41: 6698-714.

Plant, L. D., J. P. Boyle, I. F. Smith, C. Peers, and H. A. Pearson. 2003. 'The production of amyloid beta peptide is a critical requirement for the viability of central neurons', *J Neurosci*, 23: 5531-5.

Prinz, M., J. Priller, S. S. Sisodia, and R. M. Ransohoff. 2011. 'Heterogeneity of CNS myeloid cells and their roles in neurodegeneration', *Nat Neurosci*, 14: 1227-35.

Proudfoot, N. J., A. Furger, and M. J. Dye. 2002. 'Integrating rnRNA processing with transcription', *Cell*, 108: 501-12.

Qiu, Z., D. K. Strickland, B. T. Hyman, and G. W. Rebeck. 1999. 'Alpha2-macroglobulin enhances the clearance of endogenous soluble beta-amyloid peptide via low-density lipoprotein receptor-related protein in cortical neurons', *J Neurochem*, 73: 1393-8.

Qu, T., R. Manev, and H. Manev. 2001. '5-Lipoxygenase (5-LOX) promoter polymorphism in patients with early-onset and late-onset Alzheimer's disease', *J Neuropsychiatry Clin Neurosci*, 13: 304-5.

Qu, W. S., D. S. Tian, Z. B. Guo, J. Fang, Q. Zhang, Z. Y. Yu, M. J. Xie, H. Q. Zhang, J. G. Lu, and W. Wang. 2012. 'Inhibition of EGFR/MAPK signaling reduces microglial inflammatory response and the associated secondary damage in rats after spinal cord injury', *J Neuroinflammation*, 9: 178.

Querfurth, H. W., J. Jiang, J. D. Geiger, and D. J. Selkoe. 1997. 'Caffeine stimulates amyloid beta-peptide release from beta-amyloid precursor protein-transfected HEK293 cells', *J Neurochem*, 69: 1580-91.

Querfurth, H. W., and D. J. Selkoe. 1994. 'Calcium ionophore increases amyloid beta peptide production by cultured cells', *Biochemistry*, 33: 4550-61.

Rami, B. K. 2012. 'Direct thrombin inhibitors' potential efficacy in Alzheimer's disease', *Am J Alzheimers Dis Other Demen*, 27: 564-7.

Ray, B. K., T. G. Lawson, J. C. Kramer, M. H. Cladaras, J. A. Grifo, R. D. Abramson, W. C. Merrick, and R. E. Thach. 1985. 'ATP-dependent unwinding of messenger-RNA structure by eukaryotic initiation-factors', *Journal of Biological Chemistry*, 260: 7651-58.

Rebeck, G. W., J. S. Reiter, D. K. Strickland, and B. T. Hyman. 1993. 'Apolipoprotein E in sporadic Alzheimer's disease: allelic variation and receptor interactions', *Neuron*, 11: 575-80.

Reddy, R., T. S. Rochoi, D. Henning, and H. Busch. 1974. 'primary sequence of u-1 nuclear ribonucleic-acid of novikoff hepatoma ascites-cells', *Journal of Biological Chemistry*, 249: 6486-94.

Richter, J. D., and J. Coller. 2015. 'Pausing on Polyribosomes: Make Way for Elongation in Translational Control', *Cell*, 163: 292-300.

Rios, E. J., M. Fallon, J. Wang, and L. A. Shimoda. 2005. 'Chronic hypoxia elevates intracellular pH and activates Na+/H+ exchange in pulmonary arterial smooth muscle cells', *Am J Physiol Lung Cell Mol Physiol*, 289: L867-74.

Robakis, N. K., K. Sambamurti, J. P. Anderson, P. Mehta, and L. M. Refolo. 1991. 'Effects of Neurotrophic Factors on the Secretion and Metabolism of the Alzheimer Amyloid Precursor.' in Franz Hefti, Philippe Brachet, Bruno Will and Yves Christen (eds.), *Growth Factors and Alzheimer's Disease* (Springer Berlin Heidelberg: Berlin, Heidelberg).

Roberts, A., C. Trapnell, J. Donaghey, J. L. Rinn, and L. Pachter. 2011. 'Improving RNA-Seq expression estimates by correcting for fragment bias', *Genome Biol*, 12: R22.

Rodriguez, M. S., C. Dargemont, and F. Stutz. 2004. 'Nuclear export of RNA', *Biol Cell*, 96: 639-55.

Rogers, J., R. Strohmeyer, C. J. Kovelowski, and R. Li. 2002. 'Microglia and inflammatory mechanisms in the clearance of amyloid beta peptide', *Glia*, 40: 260-9.

Rosenbloom, K. R., J. Armstrong, G. P. Barber, J. Casper, H. Clawson, M. Diekhans, T. R. Dreszer, P. A. Fujita, L. Guruvadoo, M. Haeussler, R. A. Harte, S. Heitner, G. Hickey, A. S. Hinrichs, R. Hubley, D. Karolchik, K. Learned, B. T. Lee, C. H. Li, K. H. Miga, N. Nguyen, B. Paten, B. J. Raney, A. F. Smit, M. L. Speir, A. S. Zweig, D. Haussler, R. M. Kuhn, and W. J. Kent. 2015. 'The UCSC Genome Browser database: 2015 update', *Nucleic Acids Res*, 43: D670-81.

Roses, A. D. 1996. 'Apolipoprotein E alleles as risk factors in Alzheimer's disease', *Annu Rev Med*, 47: 387-400.

Rozen, F., I. Edery, K. Meerovitch, T. E. Dever, W. C. Merrick, and N. Sonenberg. 1990. 'bidirectional RNA helicase activity of eukaryotic translation initiation factor-4A and factor-4F', *Molecular and Cellular Biology*, 10: 1134-44.

Sabari, J., D. Lax, D. Connors, I. Brotman, E. Mindrebo, C. Butler, I. Entersz, D. Jia, and R. A. Foty. 2011. 'Fibronectin matrix assembly suppresses dispersal of glioblastoma cells', *Plos One*, 6: e24810.

Saghizadeh, M., D. J. Brown, R. Castellon, M. Chwa, G. H. Huang, J. Y. Ljubimova, S. Rosenberg, K. S. Spirin, R. B. Stolitenko, W. Adachi, S. Kinoshita, G. Murphy, L. J. Windsor, M. C. Kenney, and A. V. Ljubimov. 2001. 'Overexpression of matrix metalloproteinase-10 and matrix metalloproteinase-3 in human diabetic corneas: a possible mechanism of basement membrane and integrin alterations', *Am J Pathol*, 158: 723-34.

Saikali, S., T. Avril, B. Collet, A. Hamlat, J. Y. Bansard, B. Drenou, Y. Guegan, and V. Quillien. 2007. 'Expression of nine tumour antigens in a series of human glioblastoma multiforme: interest of EGFRvIII, IL-13Ralpha2, gp100 and TRP-2 for immunotherapy', *J Neurooncol*, 81: 139-48.

Salnikow, K., M. V. Blagosklonny, H. Ryan, R. Johnson, and M. Costa. 2000. 'Carcinogenic nickel induces genes involved with hypoxic stress', *Cancer Res*, 60: 38-41.

Sarkar, N. 1997. 'Polyadenylation of mRNA in prokaryotes', *Annual Review of Biochemistry*, 66: 173-97.

Sasaoka, T., W. J. Langlois, J. W. Leitner, B. Draznin, and J. M. Olefsky. 1994. 'The signaling pathway coupling epidermal growth factor receptors to activation of p21ras', *J Biol Chem*, 269: 32621-5.

Sastre, M., M. Calero, M. Pawlik, P. M. Mathews, A. Kumar, V. Danilov, S. D. Schmidt, R. A. Nixon, B. Frangione, and E. Levy. 2004. 'Binding of cystatin C to Alzheimer's amyloid beta inhibits in vitro amyloid fibril formation', *Neurobiol Aging*, 25: 1033-43.

Sato, N., K. Imaizumi, T. Manabe, M. Taniguchi, J. Hitomi, T. Katayama, T. Yoneda, T. Morihara, Y. Yasuda, T. Takagi, T. Kudo, T. Tsuda, Y. Itoyama, T. Makifuchi, P. E. Fraser, P. St George-Hyslop, and M. Tohyama. 2001. 'Increased production of beta-amyloid and vulnerability to endoplasmic reticulum stress by an aberrant spliced form of presenilin 2', *J Biol Chem*, 276: 2108-14.

Savage, M. J., Y. G. Lin, J. R. Ciallella, D. G. Flood, and R. W. Scott. 2002. 'Activation of c-Jun N-terminal kinase and p38 in an Alzheimer's disease model is associated with amyloid deposition', *J Neurosci*, 22: 3376-85.

Scheibel, M. E., R. D. Lindsay, U. Tomiyasu, and A. B. Scheibel. 1975. 'Progressive Dendritic Changes in Aging Human Cortex', *Experimental Neurology*, 47: 392-403.

Schmid, B., J. Schindelin, A. Cardona, M. Longair, and M. Heisenberg. 2010. 'A high-level 3D visualization API for Java and ImageJ', *BMC Bioinformatics*, 11: 274.

Schneider, R., V. I. Agol, R. Andino, F. Bayard, D. R. Cavener, S. A. Chappell, J. J. Chen, J. L. Darlix, A. Dasgupta, O. Donze, R. Duncan, O. Elroy-Stein, P. J. Farabaugh, W. Filipowicz, M. Gale, Jr., L. Gehrke, E. Goldman, Y. Groner, J. B. Harford, M. Hatzglou, B. He, C. U. Hellen, M. W. Hentze, J. Hershey, P. Hershey, T. Hohn, M. Holcik, C. P. Hunter, K. Igarashi, R. Jackson, R. Jagus, L. S. Jefferson, B. Joshi, R. Kaempfer, M. Katze, R. J. Kaufman, M. Kiledjian, S. R. Kimball, A. Kimchi, K. Kirkegaard, A. E. Koromilas, R. M. Krug, V. Kruys, B. J. Lamphear, S. Lemon, R. E. Lloyd, L. E. Maquat, E. Martinez-Salas, M. B. Mathews, V. P. Mauro, S. Miyamoto, I. Mohr, D. R. Morris, E. G. Moss, N. Nakashima, A. Palmenberg, N. T. Parkin, T. Pe'ery, J. Pelletier, S. Peltz, T. V. Pestova, E. V. Pilipenko, A. C. Prats, V. Racaniello, G. S. Read, R. E. Rhoads, J. D. Richter, R. Rivera-Pomar, T. Rouault, A. Sachs, P. Sarnow, G. C. Scheper, L. Schiff, D. R. Schoenberg, B. L. Semler, A. Siddiqui, T. Skern, N. Sonenberg, W. Sossin, N. Standart, S. M. Tahara, A. A. Thomas, J. J. Toulme, J. Wilusz, E. Wimmer, G. Witherell, and M. Wormington. 2001. 'New ways of initiating translation in eukaryotes', *Mol Cell Biol*, 21: 8238-46.

Sharma, S. V., D. W. Bell, J. Settleman, and D. A. Haber. 2007. 'Epidermal growth factor receptor mutations in lung cancer', *Nat Rev Cancer*, 7: 169-81.

Shen, L., A. Siwkowski, E. V. Wancewicz, E. Lesnik, M. Butler, D. Witchell, G. Vasquez, B. Ross, O. Acevedo, G. Inamati, H. Sasmor, M. Manoharan, and B. P. Monia. 2003. 'Evaluation of C-5 propynyl pyrimidine-containing oligonucleotides in vitro and in vivo', *Antisense Nucleic Acid Drug Dev*, 13: 129-42.

Sheng, J. G., R. A. Jones, X. Q. Zhou, J. M. McGinness, L. J. Van Eldik, R. E. Mrak, and W. S. Griffin. 2001. 'Interleukin-1 promotion of MAPK-p38 overexpression in experimental animals and in Alzheimer's disease: potential significance for tau protein phosphorylation', *Neurochem Int*, 39: 341-8.

Sherrill, K. W., M. P. Byrd, M. E. Van Eden, and R. E. Lloyd. 2004. 'BCL-2 translation is mediated via internal ribosome entry during cell stress', *J Biol Chem*, 279: 29066-74.

Shin, E. S., C. M. Sorenson, and N. Sheibani. 2014. 'PEDF expression regulates the proangiogenic and proinflammatory phenotype of the lung endothelium', *Am J Physiol Lung Cell Mol Physiol*, 306: L620-34.

Slack, B. E., J. Breu, L. Muchnicki, and R. J. Wurtman. 1997. 'Rapid stimulation of amyloid precursor protein release by epidermal growth factor: role of protein kinase C', *Biochem J*, 327 (Pt 1): 245-9.

Slieker, L. J., and M. D. Lane. 1986. 'Biosynthesis of the Epidermal Growth-Factor Receptor - Acquisition of Ligand-Binding Capacity Occurs Posttranslationally in the Endoplasmic-Reticulum', *Federation Proceedings*, 45: 1736-36.

Small, Scott A., and Karen Duff. 2008. 'Linking A beta and Tau in Late-Onset Alzheimer's Disease: A Dual Pathway Hypothesis', *Neuron*, 60: 534-42.

Soltoff, S. P., and L. C. Cantley. 1996. 'p120cbl is a cytosolic adapter protein that associates with phosphoinositide 3-kinase in response to epidermal growth factor in PC12 and other cells', *J Biol Chem*, 271: 563-7.

Sonenberg, N., M. A. Morgan, W. C. Merrick, and A. J. Shatkin. 1978. 'Polypeptide in eukaryotic initiation-factors that crosslinks specifically to 5'-terminal cap in messenger-RNA', *Proceedings of the National Academy of Sciences of the United States of America*, 75: 4843-47.

Sorensen, O. E., D. R. Thapa, K. M. Roupe, E. V. Valore, U. Sjobring, A. A. Roberts, A. Schmidtchen, and T. Ganz. 2006. 'Injury-induced innate immune response in human skin mediated by transactivation of the epidermal growth factor receptor', *J Clin Invest*, 116: 1878-85.

Spahn, C. M., J. S. Kieft, R. A. Grassucci, P. A. Penczek, K. Zhou, J. A. Doudna, and J. Frank. 2001. 'Hepatitis C virus IRES RNA-induced changes in the conformation of the 40s ribosomal subunit', *Science*, 291: 1959-62.

Spahn, C. M. T., M. G. Gomez-Lorenzo, R. A. Grassucci, R. Jorgenson, G. R. Andersen, R. Beckmann, P. A. Penczek, J. P. G. Ballesta, and J. Frank. 2004. 'Domain movements of elongation factor eEF2 and the eukaryotic 80S ribosome facilitate tRNA translocation', *Embo Journal*, 23: 1008-19.

Spindler, K. L., D. A. Olsen, J. N. Nielsen, I. Brandslund, H. S. Poulsen, M. Villingshoj, and A. Jakobsen. 2006. 'Lack of the type III epidermal growth factor receptor mutation in colorectal cancer', *Anticancer Res*, 26: 4889-93.

Spitale, R. C., R. A. Flynn, Q. C. Zhang, P. Crisalli, B. Lee, J. W. Jung, H. Y. Kuchelmeister, P. J. Batista, E. A. Torre, E. T. Kool, and H. Y. Chang. 2015. 'Structural imprints in vivo decode RNA regulatory mechanisms', *Nature*, 519: 486-90.

Spriggs, K. A., M. Bushell, S. A. Mitchell, and A. E. Willis. 2005. 'Internal ribosome entry segment-mediated translation during apoptosis: the role of IRES-trans-acting factors', *Cell Death Differ*, 12: 585-91.

Spriggs, Keith A., Laura C. Cobbold, Catherine L. Jopling, Rebecca E. Cooper, Lindsay A. Wilson, Mark Stoneley, Mark J. Coldwell, Didier Poncet, Ya-Ching Shen, Simon J. Morley, Martin Bushell, and Anne E. Willis. 2009. 'Canonical Initiation Factor Requirements of the Myc Family of Internal Ribosome Entry Segments', *Molecular and Cellular Biology*, 29: 1565-74.

Stebbins-Boaz, B., Q. P. Cao, C. H. de Moor, R. Mendez, and J. D. Richter. 1999. 'Maskin is a CPEB-associated factor that transiently interacts with eIF-4E', *Molecular Cell*, 4: 1017-27.

Steinhoff, T., E. Moritz, M. A. Wollmer, M. H. Mohajeri, S. Kins, and R. M. Nitsch. 2001. 'Increased cystatin C in astrocytes of transgenic mice expressing

the K670N-M671L mutation of the amyloid precursor protein and deposition in brain amyloid plaques', *Neurobiol Dis*, 8: 647-54.

Stern, S., D. Moazed, and H. F. Noller. 1988. 'Structural-Analysis of Rna Using Chemical and Enzymatic Probing Monitored by Primer Extension', *Methods in Enzymology*, 164: 481-89.

Stoneley, M., F. E. M. Paulin, J. P. C. Le Quesne, S. A. Chappell, and A. E. Willis. 1998. 'C-Myc 5 ' untranslated region contains an internal ribosome entry segment', *Oncogene*, 16: 423-28.

Stoneley, M., and A. E. Willis. 2004. 'Cellular internal ribosome entry segments: structures, trans-acting factors and regulation of gene expression', *Oncogene*, 23: 3200-07.

Strittmatter, W. J., A. M. Saunders, D. Schmechel, M. Pericak-Vance, J. Enghild, G. S. Salvesen, and A. D. Roses. 1993. 'Apolipoprotein E: high-avidity binding to beta-amyloid and increased frequency of type 4 allele in late-onset familial Alzheimer disease', *Proc Natl Acad Sci U S A*, 90: 1977-81.

Stutzmann, G. E., A. Caccamo, F. M. LaFerla, and I. Parker. 2004. 'Dysregulated IP3 signaling in cortical neurons of knock-in mice expressing an Alzheimer's-linked mutation in presenilin1 results in exaggerated Ca2+ signals and altered membrane excitability', *J Neurosci*, 24: 508-13.

Summerton, J. 1999. 'Morpholino antisense oligomers: the case for an RNase H-independent structural type', *Biochim Biophys Acta*, 1489: 141-58.

Sundelof, J., J. Arnlov, E. Ingelsson, J. Sundstrom, S. Basu, B. Zethelius, A. Larsson, M. C. Irizarry, V. Giedraitis, E. Ronnemaa, M. Degerman-Gunnarsson, B. T. Hyman, H. Basun, L. Kilander, and L. Lannfelt. 2008. 'Serum cystatin C and the risk of Alzheimer disease in elderly men', *Neurology*, 71: 1072-9.

Sutherland, R. M., B. Sordat, J. Bamat, H. Gabbert, B. Bourrat, and W. Mueller-Klieser. 1986. 'Oxygenation and differentiation in multicellular spheroids of human colon carcinoma', *Cancer Research*, 46: 5320-9.

Sutinen, E. M., T. Pirttila, G. Anderson, A. Salminen, and J. O. Ojala. 2012. 'Pro-inflammatory interleukin-18 increases Alzheimer's disease-associated amyloid-beta production in human neuron-like cells', *J Neuroinflammation*, 9: 199.

Svitkin, Y. V., A. Pause, A. Haghighat, S. Pyronnet, G. Witherell, G. J. Belsham, and N. Sonenberg. 2001. 'The requirement for eukaryotic initiation factor 4A (eIF4A) in translation is in direct proportion to the degree of mRNA 5 ' secondary structure', *Rna-a Publication of the Rna Society*, 7: 382-94.

Takasugi, N., T. Tomita, I. Hayashi, M. Tsuruoka, M. Niimura, Y. Takahashi, G. Thinakaran, and T. Iwatsubo. 2003. 'The role of presenilin cofactors in the gamma-secretase complex', *Nature*, 422: 438-41.

Takayanagi, T., T. Kawai, S. J. Forrester, T. Obama, T. Tsuji, Y. Fukuda, K. J. Elliott, D. G. Tilley, R. L. Davisson, J. Y. Park, and S. Eguchi. 2015. 'Role of epidermal growth factor receptor and endoplasmic reticulum stress in vascular remodeling induced by angiotensin II', *Hypertension*, 65: 1349-55.

Tallet-Lopez, B., L. Aldaz-Carroll, S. Chabas, E. Dausse, C. Staedel, and J. J. Toulme. 2003. 'Antisense oligonucleotides targeted to the domain IIId of the hepatitis C virus IRES compete with 40S ribosomal subunit binding and prevent in vitro translation', *Nucleic Acids Res*, 31: 734-42.

Tang, C. E., Y. J. Guan, B. Yi, X. H. Li, K. Liang, H. Y. Zou, H. Yi, M. Y. Li, P. F. Zhang, C. Li, F. Peng, Z. C. Chen, K. T. Yao, and Z. Q. Xiao. 2010. 'Identification of the amyloid beta-protein precursor and cystatin C as novel epidermal growth factor receptor regulated secretory proteins in nasopharyngeal carcinoma by proteomics', *J Proteome Res*, 9: 6101-11.

Tang, C., J. E. Kanter, K. E. Bornfeldt, R. C. Leboeuf, and J. F. Oram. 2010. 'Diabetes reduces the cholesterol exporter ABCA1 in mouse macrophages and kidneys', *J Lipid Res*, 51: 1719-28.

Tanguay, R. L., and D. R. Gallie. 1996. 'Translational efficiency is regulated by the length of the 3' untranslated region', *Mol Cell Biol*, 16: 146-56.

Tanner, K. G., and J. Kyte. 1999. 'Dimerization of the extracellular domain of the receptor for epidermal growth factor containing the membrane-spanning segment in response to treatment with epidermal growth factor', *Journal of Biological Chemistry*, 274: 35985-90.

Tasi, Y. C., T. Y. Chin, Y. J. Chen, C. C. Huang, S. L. Lee, and T. Y. Wu. 2015. 'Potential natural products for Alzheimer's disease: targeted search using the internal ribosome entry site of tau and amyloid-beta precursor protein', *Int J Mol Sci*, 16: 8789-810.

Tebaldi, T., A. Re, G. Viero, I. Pegoretti, A. Passerini, E. Blanzieri, and A. Quattrone. 2012. 'Widespread uncoupling between transcriptome and translatome variations after a stimulus in mammalian cells', *BMC Genomics*, 13: 220.

Terenin, I. M., S. E. Dmitriev, D. E. Andreev, and I. N. Shatsky. 2008. 'Eukaryotic translation initiation machinery can operate in a bacterial-like mode without eIF2', *Nat Struct Mol Biol*, 15: 836-41.

Terry, R. D., E. Masliah, D. P. Salmon, N. Butters, R. Deteresa, R. Hill, L. A. Hansen, and R. Katzman. 1991. 'Physical Basis of Cognitive Alterations in Alzheimers-Disease - Synapse Loss Is the Major Correlate of Cognitive Impairment', *Annals of Neurology*, 30: 572-80.

Terry, Robert D., Robert Katzman, and Katherine L. Bick. 1994. *Alzheimer disease* (Raven Press: New York).

Thakor, N., and M. Holcik. 2012. 'IRES-mediated translation of cellular messenger RNA operates in eIF2alpha- independent manner during stress', *Nucleic Acids Res*, 40: 541-52.

Thambisetty, M., A. Simmons, L. Velayudhan, A. Hye, J. Campbell, Y. Zhang, L. O. Wahlund, E. Westman, A. Kinsey, A. Guntert, P. Proitsi, J. Powell, M. Causevic, R. Killick, K. Lunnon, S. Lynham, M. Broadstock, F. Choudhry, D. R. Howlett, R. J. Williams, S. I. Sharp, C. Mitchelmore, C. Tunnard, R. Leung, C. Foy, D. O'Brien, G. Breen, S. J. Furney, M. Ward, I. Kloszewska, P. Mecocci, H. Soininen, M. Tsolaki, B. Vellas, A. Hodges, D. G. M. Murphy, S. Parkins, J. C. Richardson, S. M. Resnick, L. Ferrucci, D. F. Wong, Y. Zhou, S. Muehlboeck, A. Evans, P. T. Francis, C. Spenger, and S. Lovestone. 2010. 'Association of Plasma Clusterin Concentration With Severity, Pathology, and Progression in Alzheimer Disease', *Archives of General Psychiatry*, 67: 739-48.

Thomas, A., W. Spaan, H. Vansteeg, H. O. Voorma, and R. Benne. 1980. 'Mode of action of protein-synthesis initiation-factor EIF-1 from rabbit reticulocytes', *Febs Letters*, 116: 67-71.

Thomason, L. A., L. J. Smithson, L. N. Hazrati, J. McLaurin, and M. D. Kawaja. 2013. 'Reactive astrocytes associated with plaques in TgCRND8 mouse brain and in human Alzheimer brain express phosphoprotein enriched in astrocytes (PEA-15)', *FEBS Lett*, 587: 2448-54.

Thorand, B., H. Kolb, J. Baumert, W. Koenig, L. Chambless, C. Meisinger, T. Illig, S. Martin, and C. Herder. 2005. 'Elevated levels of interleukin-18 predict the development of type 2 diabetes: results from the MONICA/KORA Augsburg Study, 1984-2002', *Diabetes*, 54: 2932-8.

Tice, D. A., J. S. Biscardi, A. L. Nickles, and S. J. Parsons. 1999. 'Mechanism of biological synergy between cellular Src and epidermal growth factor receptor', *Proc Natl Acad Sci U S A*, 96: 1415-20.

Tizon, B., E. M. Ribe, W. Mi, C. M. Troy, and E. Levy. 2010. 'Cystatin C protects neuronal cells from amyloid-beta-induced toxicity', *J Alzheimers Dis*, 19: 885-94.

Toda, S., K. Watanabe, F. Yokoi, S. Matsumura, K. Suzuki, A. Ootani, S. Aoki, N. Koike, and H. Sugihara. 2002. 'A new organotypic culture of thyroid tissue maintains three-dimensional follicles with C cells for a long term', *Biochem Biophys Res Commun*, 294: 906-11.

Toescu, E. C., and A. Verkhratsky. 2007. 'The importance of being subtle: small changes in calcium homeostasis control cognitive decline in normal aging', *Aging Cell*, 6: 267-73.

Tolnay, M., and A. Probst. 1999. 'REVIEW: tau protein pathology in Alzheimer's disease and related disorders', *Neuropathology and Applied Neurobiology*, 25: 171-87.

Toni, M., J. Hermida, M. J. Goni, P. Fernandez, W. C. Parks, E. Toledo, R. Montes, and N. Diez. 2013. 'Matrix metalloproteinase-10 plays an active role in microvascular complications in type 1 diabetic patients', *Diabetologia*, 56: 2743-52.

Trapnell, C., D. G. Hendrickson, M. Sauvageau, L. Goff, J. L. Rinn, and L. Pachter. 2013. 'Differential analysis of gene regulation at transcript resolution with RNA-seq', *Nat Biotechnol*, 31: 46-53.

Trapnell, C., L. Pachter, and S. L. Salzberg. 2009. 'TopHat: discovering splice junctions with RNA-Seq', *Bioinformatics*, 25: 1105-11.

Trapnell, C., B. A. Williams, G. Pertea, A. Mortazavi, G. Kwan, M. J. van Baren, S. L. Salzberg, B. J. Wold, and L. Pachter. 2010. 'Transcript assembly and quantification by RNA-Seq reveals unannotated transcripts and isoform switching during cell differentiation', *Nat Biotechnol*, 28: 511-5.

Triantafyllou, A., P. Liakos, A. Tsakalof, E. Georgatsou, G. Simos, and S. Bonanou. 2006. 'Cobalt induces hypoxia-inducible factor-1alpha (HIF-1alpha) in HeLa cells by an iron-independent, but ROS-, PI-3K- and MAPK-dependent mechanism', *Free Radic Res*, 40: 847-56.

Tripathy, D., A. Sanchez, X. Yin, J. Luo, J. Martinez, and P. Grammas. 2013. 'Thrombin, a mediator of cerebrovascular inflammation in AD and hypoxia', *Front Aging Neurosci*, 5: 19.

Truitt, M. L., and D. Ruggero. 2016. 'New frontiers in translational control of the cancer genome', *Nat Rev Cancer*, 16: 288-304.

Tsukimoto, A., R. Sugiyama, M. Abe, H. Nishitsuji, Y. Shimizu, K. Shimotohno, G. Kawai, and H. Takaku. 2015. 'A new role for PGA1 in inhibiting hepatitis C virus-IRES-mediated translation by targeting viral translation factors', *Antiviral Res*, 117: 1-9.

Ulery, P. G., J. Beers, I. Mikhailenko, R. E. Tanzi, G. W. Rebeck, B. T. Hyman, and D. K. Strickland. 2000. 'Modulation of beta-amyloid precursor protein processing by the low density lipoprotein receptor-related protein (LRP). Evidence that LRP contributes to the pathogenesis of Alzheimer's disease', *J Biol Chem*, 275: 7410-5.

Ullrich, A., L. Coussens, J. S. Hayflick, T. J. Dull, A. Gray, A. W. Tam, J. Lee, Y. Yarden, T. A. Libermann, J. Schlessinger, J. Downward, E. L. V. Mayes, N. Whittle, M. D. Waterfield, and P. H. Seeburg. 1984. 'Human Epidermal Growth-Factor Receptor Cdna Sequence and Aberrant Expression of the Amplified Gene in A431 Epidermoid Carcinoma-Cells', *Nature*, 309: 418-25.

Uniacke, J., C. E. Holterman, G. Lachance, A. Franovic, M. D. Jacob, M. R. Fabian, J. Payette, M. Holcik, A. Pause, and S. Lee. 2012. 'An oxygen-regulated switch in the protein synthesis machinery', *Nature*, 486: 126-U54.

Unsworth, B. R., and P. I. Lelkes. 1998. 'Growing tissues in microgravity', *Nat Med*, 4: 901-7.

Vassar, R. 2004. 'BACE1 - The beta-secretase enzyme in Alzheimer's disease', *Journal of Molecular Neuroscience*, 23: 105-13.

Vassar, R., B. D. Bennett, S. Babu-Khan, S. Kahn, E. A. Mendiaz, P. Denis, D. B. Teplow, S. Ross, P. Amarante, R. Loeloff, Y. Luo, S. Fisher, L. Fuller, S. Edenson, J. Lile, M. A. Jarosinski, A. L. Biere, E. Curran, T. Burgess, J. C. Louis, F. Collins, J. Treanor, G. Rogers, and M. Citron. 1999. 'beta-secretase cleavage of Alzheimer's amyloid precursor protein by the transmembrane aspartic protease BACE', *Science*, 286: 735-41.

Vasudevan, S., Y. Tong, and J. A. Steitz. 2007. 'Switching from repression to activation: microRNAs can up-regulate translation', *Science*, 318: 1931-4.

Vende, P., M. Piron, N. Castagne, and D. Poncet. 2000. 'Efficient translation of rotavirus mRNA requires simultaneous interaction of NSP3 with the eukaryotic translation initiation factor eIF4G and the mRNA 3' end', *J Virol*, 74: 7064-71.

Vengellur, A., J. M. Phillips, J. B. Hogenesch, and J. J. LaPres. 2005. 'Gene expression profiling of hypoxia signaling in human hepatocellular carcinoma cells', *Physiological Genomics*, 22: 308-18.

Venkatesan, S., A. Gershowitz, and B. Moss. 1980. 'Modification of the 5' end of messenger-RNA - Association of rna triphosphatase with the RNA guanylyltransferase RNA (guanine-7-)methyltransferase complex from vaccinia virus', *Journal of Biological Chemistry*, 255: 903-08.

Veo, B. L., and L. A. Krushel. 2009. 'Translation initiation of the human tau mRNA through an internal ribosomal entry site', *J Alzheimers Dis*, 16: 271-5.

Verghese, P. B., J. M. Castellano, K. Garai, Y. Wang, H. Jiang, A. Shah, G. Bu, C. Frieden, and D. M. Holtzman. 2013. 'ApoE influences amyloid-beta (Abeta) clearance despite minimal apoE/Abeta association in physiological conditions', *Proc Natl Acad Sci U S A*, 110: E1807-16.

Vickers, T., B. F. Baker, P. D. Cook, M. Zounes, R. W. Buckheit, Jr., J. Germany, and D. J. Ecker. 1991. 'Inhibition of HIV-LTR gene expression by oligonucleotides targeted to the TAR element', *Nucleic Acids Res*, 19: 3359-68.

Vinci, M., S. Gowan, F. Boxall, L. Patterson, M. Zimmermann, W. Court, C. Lomas, M. Mendiola, D. Hardisson, and S. A. Eccles. 2012. 'Advances in establishment and analysis of three-dimensional tumor spheroid-based functional assays for target validation and drug evaluation', *BMC Biol*, 10: 29.

Walker, K., S. A. Elela, and R. N. Nazar. 1990. 'Inhibition of protein synthesis by anti-5.8 S rRNA oligodeoxyribonucleotides', *J Biol Chem*, 265: 2428-30.

Walton, G. M., and G. N. Gill. 1975. 'Nucleotide regulation of a eukaryotic protein-synthesis initiation complex', *Biochimica Et Biophysica Acta*, 390: 231-45.

Wang, G. L., and G. L. Semenza. 1993. 'Desferrioxamine induces erythropoietin gene expression and hypoxia-inducible factor 1 DNA-binding activity: implications for models of hypoxia signal transduction', *Blood*, 82: 3610-5.

Wang, L., H. C. Chiang, W. Wu, B. Liang, Z. Xie, X. Yao, W. Ma, S. Du, and Y. Zhong. 2012. 'Epidermal growth factor receptor is a preferred target for treating amyloid-beta-induced memory loss', *Proc Natl Acad Sci U S A*, 109: 16743-8.

Wang, V., D. A. Davis, M. Haque, L. E. Huang, and R. Yarchoan. 2005. 'Differential gene up-regulation by hypoxia-inducible factor-1 alpha and hypoxia-inducible factor-2 alpha in HEK293T cells', *Cancer Research*, 65: 3299-306.

Wang, X., W. Zheng, J. W. Xie, T. Wang, S. L. Wang, W. P. Teng, and Z. Y. Wang. 2010. 'Insulin deficiency exacerbates cerebral amyloidosis and behavioral deficits in an Alzheimer transgenic mouse model', *Mol Neurodegener*, 5: 46.

Wartenberg, M., F. Donmez, F. C. Ling, H. Acker, J. Hescheler, and H. Sauer. 2001. 'Tumor-induced angiogenesis studied in confrontation cultures of multicellular tumor spheroids and embryoid bodies grown from pluripotent embryonic stem cells', *Federation Proceedings*, 15: 995-1005.

Wassef, L., D. J. Kelly, and R. E. Gilbert. 2004. 'Epidermal growth factor receptor inhibition attenuates early kidney enlargement in experimental diabetes', *Kidney Int*, 66: 1805-14.

Webb, T. E., A. Hughes, D. S. Smalley, and K. A. Spriggs. 2015. 'An internal ribosome entry site in the 5' untranslated region of epidermal growth factor receptor allows hypoxic expression', *Oncogenesis*, 4: e134.

Wheeler, M., and J. Domin. 2001. 'Recruitment of the class II phosphoinositide 3-kinase C2beta to the epidermal growth factor receptor: role of Grb2', *Mol Cell Biol*, 21: 6660-7.

Wilson, J. E., M. J. Powell, S. E. Hoover, and P. Sarnow. 2000. 'Naturally occurring dicistronic cricket paralysis virus RNA is regulated by two internal ribosome entry sites', *Mol Cell Biol*, 20: 4990-9.

Wimmer, E., C. U. Hellen, and X. Cao. 1993. 'Genetics of poliovirus', *Annu Rev Genet*, 27: 353-436.

Winzen, R., M. Kracht, B. Ritter, A. Wilhelm, C. Y. Chen, A. B. Shyu, M. Muller, M. Gaestel, K. Resch, and H. Holtmann. 1999. 'The p38 MAP kinase pathway signals for cytokine-induced mRNA stabilization via MAP kinase-activated protein kinase 2 and an AU-rich region-targeted mechanism', *EMBO J*, 18: 4969-80.

Wu, T. Y., and C. P. Chen. 2009. 'Dual action of memantine in Alzheimer disease: a hypothesis', *Taiwan J Obstet Gynecol*, 48: 273-7.

Wu, W., J. M. Samet, R. Silbajoris, L. A. Dailey, D. Sheppard, P. A. Bromberg, and L. M. Graves. 2004. 'Heparin-binding epidermal growth factor cleavage mediates zinc-induced epidermal growth factor receptor phosphorylation', *Am J Respir Cell Mol Biol*, 30: 540-7.

Wuchty, S., W. Fontana, I. L. Hofacker, and P. Schuster. 1999. 'Complete suboptimal folding of RNA and the stability of secondary structures', *Biopolymers*, 49: 145-65.

Xia, X., and M. Holcik. 2009. 'Strong eukaryotic IRESs have weak secondary structure', *PLoS One*, 4: e4136.

Xu, Q., A. Bernardo, D. Walker, T. Kanegawa, R. W. Mahley, and Y. Huang. 2006. 'Profile and regulation of apolipoprotein E (ApoE) expression in the CNS in mice with targeting of green fluorescent protein gene to the ApoE locus', *J Neurosci*, 26: 4985-94.

Yamada, M., T. Ikeuchi, and H. Hatanaka. 1997. 'The neurotrophic action and signalling of epidermal growth factor', *Prog Neurobiol*, 51: 19-37.

Yamamoto, N., Y. Fukata, M. Fukata, and K. Yanagisawa. 2007. 'GM1-ganglioside-induced Abeta assembly on synaptic membranes of cultured neurons', *Biochim Biophys Acta*, 1768: 1128-37.

Yamamoto, N., T. Matsubara, K. Sobue, M. Tanida, R. Kasahara, K. Naruse, H. Taniura, T. Sato, and K. Suzuki. 2012. 'Brain insulin resistance accelerates Abeta fibrillogenesis by inducing GM1 ganglioside clustering in the presynaptic membranes', *J Neurochem*, 121: 619-28.

Yamauchi, T., K. Ueki, K. Tobe, H. Tamemoto, N. Sekine, M. Wada, M. Honjo, M. Takahashi, T. Takahashi, H. Hirai, T. Tushima, Y. Akanuma, T. Fujita, I. Komuro, Y. Yazaki, and T. Kadowaki. 1997. 'Tyrosine phosphorylation of the EGF receptor by the kinase Jak2 is induced by growth hormone', *Nature*, 390: 91-6.

Yan, L., A. C. Nairn, H. C. Palfrey, and M. J. Brady. 2003. 'Glucose regulates EF-2 phosphorylation and protein translation by a protein phosphatase-2A-dependent mechanism in INS-1-derived 832/13 cells', *J Biol Chem*, 278: 18177-83.

Yang, D. S., D. H. Small, U. Seydel, J. D. Smith, J. Hallmayer, S. E. Gandy, and R. N. Martins. 1999. 'Apolipoprotein E promotes the binding and uptake of beta-amyloid into Chinese hamster ovary cells in an isoform-specific manner', *Neuroscience*, 90: 1217-26.

Yang, L. S., and H. Ksiezak-Reding. 1995. 'Calpain-induced proteolysis of normal human tau and tau associated with paired helical filaments', *Eur J Biochem*, 233: 9-17.

Yanofsky, C. 1981. 'Attenuation in the control of expression of bacterial operons', *Nature*, 289: 751-58.

Yarden, Y., and M. X. Sliwkowski. 2001. 'Untangling the ErbB signalling network', *Nature Reviews Molecular Cell Biology*, 2: 127-37.

Yatime, L., Y. Mechulam, S. Blanquet, and E. Schmitt. 2006. 'Structural switch of the gamma subunit in an archaeal alF2 alpha y heterodimer', *Structure*, 14: 119-28.

Yin, X., J. Wright, T. Wall, and P. Grammas. 2010. 'Brain endothelial cells synthesize neurotoxic thrombin in Alzheimer's disease', *Am J Pathol*, 176: 1600-6.

Yoo, B. H., E. Bochkareva, A. Bochkarev, T. C. Mou, and D. M. Gray. 2004. '2'-O-methyl-modified phosphorothioate antisense oligonucleotides have reduced non-specific effects in vitro', *Nucleic Acids Res*, 32: 2008-16.

Yu, S. P. 2003. 'Regulation and critical role of potassium homeostasis in apoptosis', *Prog Neurobiol*, 70: 363-86.

Yuan, Y., G. Hilliard, T. Ferguson, and D. E. Millhorn. 2003. 'Cobalt inhibits the interaction between hypoxia-inducible factor-alpha and von Hippel-Lindau protein by direct binding to hypoxia-inducible factor-alpha', *J Biol Chem*, 278: 15911-6.

Zarrinkar, P. P., and J. R. Williamson. 1994. 'Kinetic intermediates in RNA folding', *Science*, 265: 918-24.

Zhang, X., J. Gureasko, K. Shen, P. A. Cole, and J. Kuriyan. 2006. 'An allosteric mechanism for activation of the kinase domain of epidermal growth factor receptor', *Cell*, 125: 1137-49.

Zhang, Xin, and Weidong Le. 2010. 'Pathological role of hypoxia in Alzheimer's disease', *Experimental Neurology*, 223: 299-303.

Zhang, Y. W., R. Wang, Q. Liu, H. Zhang, F. F. Liao, and H. Xu. 2007. 'Presenilin/gamma-secretase-dependent processing of beta-amyloid precursor protein regulates EGF receptor expression', *Proc Natl Acad Sci U S A*, 104: 10613-8.

Zheng, X. Y., S. P. Zhao, and H. Yan. 2013. 'The role of apolipoprotein A5 in obesity and the metabolic syndrome', *Biol Rev Camb Philos Soc*, 88: 490-8.

Zhou, X., F. Li, L. Kong, J. Chodosh, and W. Cao. 2009. 'Anti-inflammatory effect of pigment epithelium-derived factor in DBA/2J mice', *Mol Vis*, 15: 438-50.

Zimmer, D. B., J. Chaplin, A. Baldwin, and M. Rast. 2005. 'S100-mediated signal transduction in the nervous system and neurological diseases', *Cell Mol Biol (Noisy-le-grand)*, 51: 201-14.

Zlokovic, B. V., R. Deane, A. P. Sagare, R. D. Bell, and E. A. Winkler. 2010. 'Low-density lipoprotein receptor-related protein-1: a serial clearance homeostatic mechanism controlling Alzheimer's amyloid beta-peptide elimination from the brain', *J Neurochem*, 115: 1077-89.